Enhanced reforming of methane to synthesis gas by co-doped perovskite catalysts

---

A thesis submitted to Keele University in partial fulfilment of the requirements for the degree of Doctor of Philosophy

Majida Hameed Khazaal

March 2019

Abstract

Greenhouse gases conversion have become an environmentally friendly way of producing H_2 and CO that can be used as a fuel to power solid oxide fuel cells as well as wider industrial applications. The direct conversion of CH_4 and CO_2 into synthesis gas will reduce the impact of global warming as well as help avoid an energy crisis. This dissertation presents a comprehensive review of the design, preparation and catalytic activity of a variety of catalysts with a specific focus on the stability and ability to suppress coke formation.

Dry reforming, biogas reforming and partial oxidation of methane were performed over hydrothermally synthesised co-doped perovskite nanomaterial, and the results compared to a conventional 10% Ni/Al_2O_3 catalyst at different temperatures and reaction times. $SrZrO_3$ perovskite catalysts were modified by doping with 4% Ni and either 1% Al or Ru or Fe, aiming to increase the activity, stability and resistance to carbon deposition for reforming of methane reactions. The results have shown that all the pervoskites are catalytically active towards methane conversion reactions with a good resistance to carbon formation.

Isothermal temperature programmed reaction studies were conducted to determine the operating conditions needed to inhibit carbon deposition, whilst still giving high activity and stability, as well as to study the potential of hydrothermally synthesised perovskite catalysts for methane reforming with different quantities and types of oxidant (CO_2 and O_2). The results show that elevated temperatures of more than 800 °C are required to achieve maximum reactant conversions and product yields for all catalysts with all three reforming methods used in this study.

Acknowledgements

“Forget the good you do, but never forget the good that was done to you”

First and foremost, I would like to express my sincere gratitude to my supervisor Dr Richard Darton for the years of guidance and invaluable knowledge, for his expertise, support and motivation. His training and guidance helped me in all the time of research and writing of this thesis. I would also like to thank my co-supervisor Prof. Mark Ormerod for his helpful suggestions.

In this regard, I owe my gratitude to Dr John Staniforth for his excellent guidance on experimental technique and data analysis, to him I owe too much, his knowledge helped me throughout my time in the laboratory.

I owe a huge thanks to The University of Kufa, Ministry of Higher Education and Scientific Research in Iraq for giving me this wonderful opportunity to study my PhD in the United Kingdom and for the financial support. Special thanks go to all staff at the Iraqi Cultural Attaché for their responses to my questions and queries.

In addition to that, I am grateful to all staff at Keele University, School of Chemical and Physical Sciences, staff in the Lennard-Jones building and a special thanks to Ann Billington, Lisa Cartlidge, Dave Evans and Lisa Blackburn.

I would also like to add a very special thanks to my colleagues (Catalysis and Sustainable Material Group) for their wonderful friendship and scientific support during the project work. To all my fellow PhD students who have shared this experience with me.

And finally thank you to Mum, sisters, brothers. Big thanks to my husband for all his patience and help throughout this crucial time of my life. Thank you to my wonderful Kids (Mohammed, Mustafa and Ghadah) for their endless love. Thank you all for bearing me even with my mood swings and being my greatest supporters.

"Do not let your difficulties fill you with anxiety. After all, it is only in the darkest nights that the stars shine more brilliantly"

Contents

Contents

Contents

Contents

Contents

List of Abbreviations

POX	Partial oxidation of methane reforming
DRM	Dry reforming of methane
BIO	Biogas reforming of methane
SRM	Steam reforming of methane
RWGS	Reverse Water Gas Shift
XRD	X-ray powder diffraction
QMS	Quadrupole mass spectrometer
TPR	Temperature-programmed reduction
TPCR	Temperature-programmed conversion reaction
TPO	Temperature-programmed oxidation
BET	Brunauer-Emmett-Teller surface area analysis
SOFC	Solid oxide fuel cell
SEM	Scanning electron microscopy
EDS	Energy dispersive X-ray spectroscopy
HR-SEM	High resolution scanning electron microscopy
RGA	Residual Gas Analysis

List of figures and tables

List of figures and tables

List of figures and tables

List of figures and tables

List of figures and tables

List of figures and tables

****

****

****

****

****

Chapter 1

Introduction, Literature Review and Aims of Research

1. Introduction and Literature Review

1.1 Introduction

During the past few decades, fossil fuels have contributed significantly to the improvement of our industry. However, the huge use of such non-renewable combustion resources has also introduced serious problems, such as increasing atmospheric pollution [1, 2]. Currently, increasing demand for economically environmentally friendly energy has led to extensive efforts being made to convert greenhouse gasses into a useful gas called synthesis gas (H_2+CO). Recycling carbon dioxide could have a significant impact on global CO_2 emission. Using natural gas (methane), the simplest hydrocarbon instead of petroleum fuel as an alternative energy source has attracted significant attention of researchers in the last few years.

Methane is considered a renewable energy resource that can be generated by the fermentation of organic materials, including wastewater sludge, landfill waste or any other biodegradable feedstock, under anaerobic conditions [3, 4]. Methane has a high hydrogen-to-carbon ratio in its molecular composition so it is cleaner than any other fossil fuel such as coal and oil.

Historical and current energy systems are dominated by fossil fuels (coal, oil and gas) which create carbon dioxide and other greenhouse gases. The data available for 1965 indicates that energy consumption by source across the world's regions was 40000 TWh while by 2016; the global energy consumption was 140000 TWh [5].

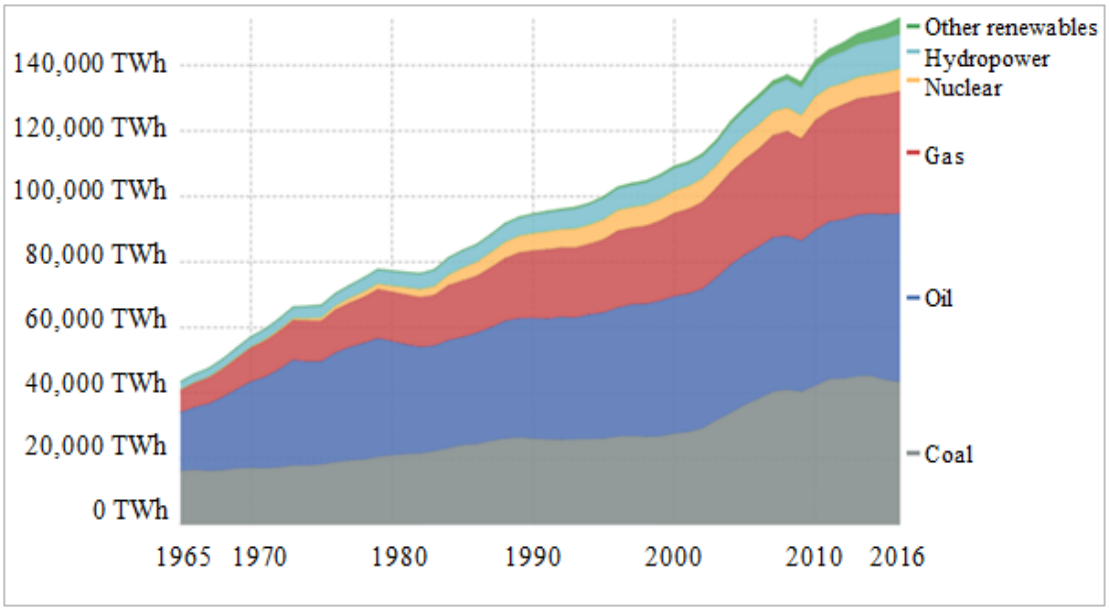

Figure 1.1: Energy consumption by source across the world's regions, measured in terawatt- hours (TWh). Note that 'Other renewables' includes renewable sources including wind, geothermal, solar, biomass and waste [5].

Methane reforming can be used to produce a wide range of important products as well as used as fuel in solid oxide fuel cells. Syngas is a mixture of H_2 and CO, which is utilized in the Fischer–Tropsch Synthesis process as a feedstock in several chemical industries for the production of higher hydrocarbons, alcohols, acetic acid, ammonia, olefin, gasoline and kerosene.

The best utilization of hydrogen energy is in fuel cells, which are now considered as a solution for reducing our dependence on imported oil, increasing demand for electricity and worries about climate changes [6]. Solid Oxide Fuel Cells (SOFCs) have a high operation temperature (700-1000 ^{0}C) that efficiently and directly generates power by converting the chemical energy of a fuel such as methane into electrical power through an internal reforming anode catalyst [7, 8]. The direct utilization of hydrocarbons as fuel with internal reforming can help to increase system efficiency and reduce the cell costs, which

could accelerate commercial use of SOFCs in different services like residential, transportation, and distributed energy applications [9].

Since a great portion of the world's hydrogen is produced by catalytic processes, involving multiple steps with different types of catalyst, it is clear that the catalyst structure plays a critical role in the dissociation of C-H bonds, hence the rate of hydrogen generation. The catalyst must therefore, be thermally stable, active, have a high surface area and coke resistance, in addition to being economically advantageous.

Metals that have shown to have a good activity for reforming reactions are Ni, Pt, Rh, and Ru [10-12]. The best catalyst suited in terms of cost and availability for widespread commercialized applications is nickel, so most research has focused on preparing novel Ni catalyst formulations. Nevertheless, Ni has drawbacks of being susceptible to coke accumulation by methane decomposition and Boudard reactions which are favoured over Ni catalysts [13-15]. Despite noble metals being much more active, selective to synthesis (H_2, CO) and having a high resistance to carbon deposition than Ni catalysts, but commercially unfavourable due to their high prices.

Academic and industrial research is focused on the development and optimisation of the catalyst used during the different reforming process to increase the hydrogen yield. Hence, researchers try to manipulate different catalyst preparation conditions such as changing the type of the active metal within the catalyst and its ratio, the type of the support, the type of promoter, the catalyst preparation method and the calcination conditions to find a highly stable, active catalyst with less degree of deleterious coke formation and sintering.

As a result, there are a large number of publications in the literature mentioning practical results for a variety of catalyst preparation and operating conditions. Therefore, specific

attention has been devoted in this study to the catalysts prepared in particular sample composition, reaction temperature, calcination temperature, pH and influence of different reforming methods in order to get excellent performance and more carbon resistant catalysts.

1.2 Summary of the known reforming technologies for H_2 production

Hydrogen is a promising alternative fuel source that can be used to power many devices such as fuel cells and combustion engines. When non-fossil fuels are used for producing energy this offers an important reduction in NOx, CO, and CO_2 contaminants. The future world energy industries require using renewable sources of H_2 in order to satisfy the expected future energy needs of users and industries. Therefore, the attention on hydrogen production technology has been steadily increasing in the last few years.

Hydrogen can be produced by a variety of methods such as partial oxidation of methane, dry reforming, steam reforming, photolysis (splitting of water) [16], electrolysis [17, 18], thermal plasma reforming [19-21], solar reforming [22, 23], dry oxidation reforming [24, 25], autothermal reforming [26, 27], tri-reforming of methane [28] and other hydrocarbons or alcohols [29, 30].

Biogas reforming has also been proposed as a viable fuel source for the production of hydrogen; it is a mixture of methane, carbon dioxide, and other gases in which the concentration can vary with time. Staniforth et al. have focused on the development of catalysts for converting biogas to syngas, which is used as a fuel within solid oxide fuel cells [31-34].

Carbon dioxide reforming of methane [35, 36] has attracted attention in the last decades as an alternative method using a mixture of biogas consisting mainly of CO_2 and CH_4 as reactants to produce syngas with molar ratio H_2 /CO of 1. However, this approach hardly finds its way for industrial use due to the high level of deleterious coke deposition.

Currently, large-scale production of the world's hydrogen (~80%) is mainly by steam reforming of natural gas [37]. Other approaches for hydrogen production are from electrolysis of water which is used industrially due to the cost reductions in the main process [38]. The real opportunities in the generation of H_2 with regard to concerns about the environment is that if we could improve methods to produce H_2 from water and then be able to combust it back to water while generating power, this would provide environmentally attractive technology.

The reforming reaction remains a conventional method for hydrogen production. However, one of the important factors that contribute to the success of hydrogen production process by low-temperature reforming methods is the modification or development of catalysts that can activate the conversion of methane with high rates as well as prohibited carbon formation reactions. The most dominant CH_4 reforming processes are explained below:

1.2.1 Partial oxidation of methane reforming (POX)

The production of syngas by burning methane in air by mildly exothermic partial oxidation of methane was first investigated in the middle of the 20th century [39]. The earliest work on methane partial oxidation was done by Prettre et al. [40] They found that for the reaction to occur, the mixture needed to be heated over 700 $^{\circ}$C in the absence of a catalyst, and synthesis gas with the product ratio of 2:1 H_2 /CO could be produced above 850 $^{\circ}$C in

addition to other gasses such as CO_2 and H_2O over the catalyst, which contained 10% metallic Ni.

In this technique, synthesis gas depends on several factors: reaction temperature, feed gas ratio, pressure and the type of catalyst. Carbon formation occurred on the catalyst surface, leading to deactivation and cannot be avoided by changing the oxygen to methane ratio or by changing the operating temperature. For instance, partial oxidation (POX) is an exothermic reaction that is favored at low temperatures and thus lowers the formation of carbon that results from the pyrolysis of methane which is favored at high temperature as observed in another kind of reforming. However, with decreasing reaction temperatures the total oxidation (equ.1.2) becomes progressively more favored over partial oxidation (equ.1.1).

The sample selectivity of methane oxidation is greatly dependent on the availability of oxide ions on the catalyst surface. Weng et. al [41] have observed that there is a significant difference in the methane partial oxidation mechanisms by using a mixture of CH_4 /O_2 /Ar (2 /1 /45, molar ratio) upon Rh/SiO_2 and Ru/SiO_2 catalysts, suggesting that this is related to the difference in the concentration of O_2 species over the catalysts due to the difference in oxygen affinity of the two active metals. In the presence of a high concentration of O_2 species on the catalyst surface, methane will be totally oxidized to CO_2. In contrast, if the concentration of O_2 species is low enough, CH_4 can be selectively converted to just CO.

Similar findings from another study show that the pyrolysis-oxidation mechanism has played a major role in the partial oxidation of CH_4 (CD_4) to synthesis gas over Rh/Al_2O_3 catalysts. The experiments revealed that the mechanism of oxidation is dependent on the metal loading within the catalyst and reaction temperature. It is likely that at high loadings

(1.0 wt% Rh) with high temperatures the amounts of carbon deposited were much higher due to a combination of the combustion-reforming and pyrolysis-oxidation mechanisms, while at low loadings (0.05 wt% Rh) and with low temperatures a combustion-reforming mechanism is responsible for the reaction because no carbon was deposited over the 0.05 wt % catalyst [42].

Other work was on the perovskite-based $La_{0.75}Sr_{0.25}Cr_{1-x}Mn_xO_{3-\delta}$ catalyst demonstrated the important roles lattice oxygen and anode morphology play in the rate of formation of products and selectivity of methane oxidation. Total oxidation is favoured by the presence of low levels of oxygen vacancies and raising the concentration of reducible B-site cations [43]. It should be noted that the catalytic activity of perovskites is primarily affected by the nature of the B-site cations.

The POX reaction produces a H_2 /CO ratio close to 2, making it a more practical industrial reaction then dry and steam reforming, which suffer from limitations, such as intensive energy requirements, and in the case of steam reforming produce a higher ratio of H_2 /CO ratio (which is not appropriate for Fischer–Tropsch or methanol synthesis) [44]. However, the POX reaction suffers from easily turning into total oxidation and catalyst deactivation. So, In order to overcome these problems, the catalyst is required to have greater selectivity towards synthesis gas (H_2 and CO) than (CO_2 and H_2O) [45]. The most important reactions occurring are shown in the following equations.

$$CH_4 + ½O_2 \rightleftharpoons CO + 2H_2 \qquad \Delta H^{\circ}_{298K} = -36\ kJ.mol^{-1} \qquad [1.1]$$

$$CH_4 + O_2 \rightleftharpoons CO_2 + 2H_2 \qquad \Delta H^{\circ}_{298K} = -319\ kJ.mol^{-1} \qquad [1.2]$$

$$CH_4 + 2O_2 \rightleftharpoons CO_2 + 2H_2O \qquad \Delta H^{\circ}_{298K} = -802\ kJ.mol^{-1} \qquad [1.3]$$

$$CO + H_2O \rightleftharpoons CO_2 + H_2 \qquad \Delta H^{\circ}_{298K} = -41\ kJ.mol^{-1} \qquad [1.4]$$

$CO + ½O_2 \rightleftharpoons CO_2$ $\Delta H^{\circ}_{298K} = -41\ kJ.mol^{-1}$ [1.5]

$C + H_2O \rightleftharpoons CO + H_2$ $\Delta H^{\circ}_{298K} = +131\ kJ.mol^{-1}$ [1.6]

$C + O_2 \rightleftharpoons CO_2$ $\Delta H^{\circ}_{298K} = -393\ kJ.mol^{-1}$ [1.7]

One of the most industrial important reactions that combined with methane partial oxidation is Water-Gas Shift Reaction. It is employed for removing CO from H_2 in the presence of water during catalytic processes as shown in equation (1.4).

1.2.2 Dry reforming of methane (DRM)

Dry reforming is one of the most promising techniques for future catalysis and energy technologies in sustainable systems, which converts two greenhouse gasses (CH_4 and CO_2) into syngas as shown in equation1.8. The production of synthesis gas over a heterogeneous catalyst from a highly endothermic process like dry reforming of methane is affected by the simultaneous occurrence of a side reaction called Reverse Water Gas-Shift (RWGS) shown in equation (1.9). RWGS is a reversible, slightly endothermic chemical reaction, usually assisted by a catalyst, resulting in the decrease in syngas production. Under typical operating conditions this results in a H_2 /CO ratio less than one. Therefore, a stable catalyst at high temperatures is required for successful DRM [46].

$CH_4 + CO_2 \rightleftharpoons 2CO + 2H_2$ $\Delta H^{\circ}_{298K} = +247\ kJ.mol^{-1}$ [1.8]

$CO_2 + H_2 \rightleftharpoons CO + H_2O$ $\Delta H^{\circ}_{298K} = +41\ kJ.mol^{-1}$ [1.9]

Dry reforming of methane is an environmentally friendly way for hydrogen production, but at the same time it has a high propensity for unfavorable carbon deposition on the catalytic

active sites, which can be produced by several reaction pathways depending on pressure, temperature and feed gas ratio:

$CO + H_2 \rightleftharpoons H_2O + C$ $\Delta H^{\circ}_{298K} = -131$ kJ.mol^{-1} [1.10]

$CH_4 \rightleftharpoons 2H_2 + C$ $\Delta H^{\circ}_{298K} = +75$ kJ.mol^{-1} [1.11]

$2CO \rightleftharpoons CO_2 + C$ $\Delta H^{\circ}_{298K} = -172$ kJ.mol^{-1} [1.12]

These reactions participate in deactivation of the available active sites by the accumulation of solid carbon on the catalyst surface as well as, the size and shape of the active metal crystallites can change through physical migration or sintering and agglomerate into larger clusters thereby decreasing the catalyst surface area and consequently the number of available active sites [47].

The proportion of oxygen to carbon and hydrogen to carbon in the feed gases can be used to estimate the propensity to form coke on the catalyst surface. For example, dry reforming ($CH_4 + CO_2$) has a low ratio (O /C = 1 and H /C = 2) compared to partial oxidation and steam reforming, so has the higher propensity to carbon accumulation. Thermodynamic studies on the dry reforming of methane reaction have observed that spontaneous reaction cannot be achieved below 700 $^{\circ}$C [48]. However, the major advantage of DRM is that it consumes two low-cost reactants (greenhouse gases) simultaneously and it is more suitable for producing a variety of chemicals such as alkanes, dimethyl ether and alcohols due to equimolar hydrogen and carbon monoxide [49].

1.2.3 Steam reforming of methane (SRM)

Steam reforming involves the high-temperature reaction of a hydrocarbon with steam in the presence of a catalyst to produce syngas (a mixture of H_2 + CO) with a ratio H_2 /CO = 3 and a small amount of carbon dioxide, often with the carbon monoxide further reacted with water to produce additional hydrogen. It is usually operated in a temperature range of 700–900 °C to obtain an acceptable conversion level. Commonly, this reaction is performed in fixed bed reactors and used for almost 50% of the world's hydrogen production industrially [50]. The main disadvantage of steam reforming is the high cost due to it being an endothermic process, equation (1.13). However, the advantage of SRM is that it the most efficient method of inhibiting coke formation. The main reactions are:

$$CH_4 + H_2O \rightleftharpoons CO + 3H_2 \qquad \Delta H^{\circ}_{298K} = + 206\ kJ.mol^{-1} \qquad [1.13]$$

$$CH_4 + 2H_2O \rightleftharpoons CO_2 + 4H_2 \qquad \Delta H^{\circ}_{298K} = + 165\ kJ.mol^{-1} \qquad [1.14]$$

As can be seen from the equations above, hydrogen production generates large quantities of CO_2 as a by-product that is dependent on the technology used and the ratio of the feedstock selection for reactants. Steam reforming is considered one of the oldest and the most feasible technology for the production of hydrogen by converting methane, however it also suffers from the water gas shift reaction, equation 1.4.

1.3 Catalyst definition and its importance

A catalyst is a substance that in a small amount causes a large change which helps accelerate chemical reactions and steer the reaction towards a desired valuable product by forming chemical bonds with reactants and generating intermediates that react more easily to give products without being appreciably consumed during the reaction. Most

heterogeneous catalysts are solids, provide accurate control of chemical conversions, increase the rate of the desired reaction and hence play a vital role in modern industry and environmental protection by pollution control. The easiest way to understand how the catalyst works is that they decrease the activation energy required to begin a reaction. Activation energy is the energy barrier that must be overcome in order to begin a chemical reaction and shows a new path for the reaction to occur. From an energy profile diagram the difference between a catalysed and an uncatalyzed reaction can be seen.

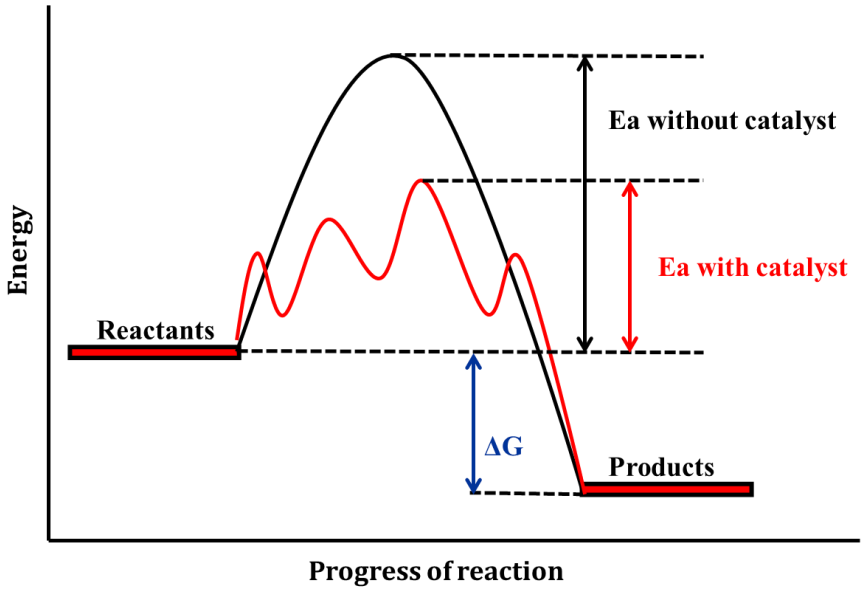

Figure 1.2: Activation energy profile with and without catalyst.

1.3.1 Heterogeneous catalyst

Heterogeneous catalysis refers to the form of catalysis using reactants in the phase that differs from the phase of catalysts in reaction atmosphere, it means that more than one phase exists in the reactor, usually gaseous reactants over solid catalyst material at high temperature. For example, there is gas or liquid in contact with catalytically active solid components (i.e. metals, metal oxides), typically in a low concentration. A solid catalyst is

an important material which is used to increase the rate of a reaction to produce fuels and chemicals. Consequently; considerations such as activity, durability, and selectivity should be taken into account when preparing a new catalyst or optimizing the performance of an existing one. The catalyst must be able to sustain the chosen reaction over long periods of time while the rate of side reactions be minimal. The catalytic reaction involves adsorption of reactants from a gas phase onto a solid surface, a reaction of adsorbed species, and desorption of products into the gas phase. Significant enhancements can be realized to accomplish the desired chemical reaction in the presence of a catalyst.

Heterogeneous catalysis has many advantages as it can be separated from the reaction mixture in an easy way such as by filtration; however, one limitation of heterogeneous catalysis is the availability of the active sites on the surface. Once the surface of the catalyst is completely saturated with reactant molecules, the reaction cannot proceed until products leave the surface site, recycling has to be done in order to allow some space to open up for a new reactant molecule to adsorb.

There are three mechanisms that describe heterogeneous catalytic reactions that often occur on the surface and the Langmuir-Hinshelwood mechanism is considered the most commonly utilized to explain heterogeneous catalysis [51].

- Langmuir-Hinshelwood mechanism. The two molecules of reactant species adsorb and settle onto the active site of the catalyst surface which can limit the rate of heterogeneous reactions. Rearrangement of electrons takes place due to the molecules reacting with each other, and then the new molecules desorb as the product, this is described in the following schematic.

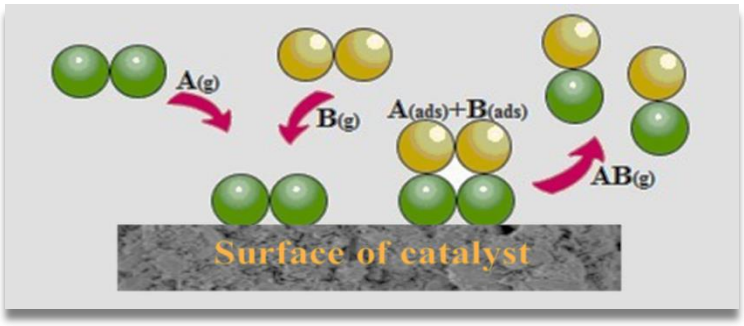

Figure 1.3: Schematic representation of Langmuir-Hinshelwood mechanism.

- Rideal-Eley mechanism. One of the two reactants molecules is adsorbed to the available reaction sites which exist on the surface, whilst the second molecule still in the gas phase reacts with the adsorbed species to form a product that is then released from the surface [52]. This can be observed using the following schematic.

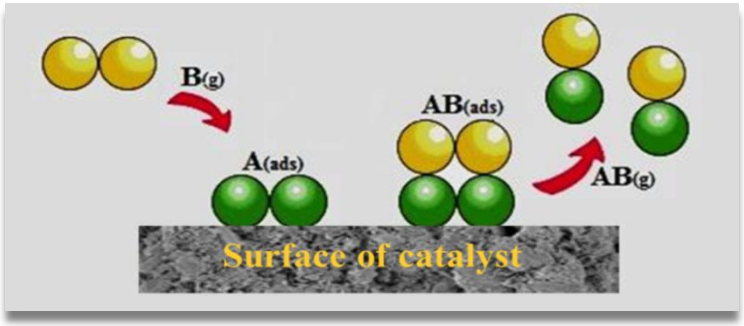

Figure 1.4: Schematic representation of Rideal-Eley mechanism.

- Precursor mechanism. One of the two molecules species is adsorbed on to the surface while the second molecule species collides with the surface, forming a mobile precursor state that then collides with the correct orientation to the first molecule on the surface, thereby, reacting and binding to each other to liberate the new product molecules [53].

1.4 Perovskite based catalysts: structure, properties and uses

Perovskite is represented by the general formula ABO_3 as shown in figure 1.5. A is a large cation such as an alkaline earth metal, a rare earth or an alkali metal which occupy the dodecahedral site of the framework. The B site is often a transition metal cation that occupies the octahedral site. About 90% of elements from the periodic table can be used in the formation of the perovskite structure. The formation of the perovskite structure needs to meet specific restrictions determined by the Goldschmidt tolerance factor (as shown in equa.1.15). This states that for a cubic structure t must be 1 and always within the range $0.75 \leq t \leq 1.00$. Deviation of unity ($t = 1$) leads to structural distortion. For a small deviation ($t < 1$), the crystal structure changes from cubic to tetragonal or orthorhombic due to a decrease in the bond angle [54].

$$t = (R_A+R_O) / \sqrt{2}\ (R_B+R_O) \qquad [1.15]$$

(R is the ionic radius; O is an anion such as oxide or halide).

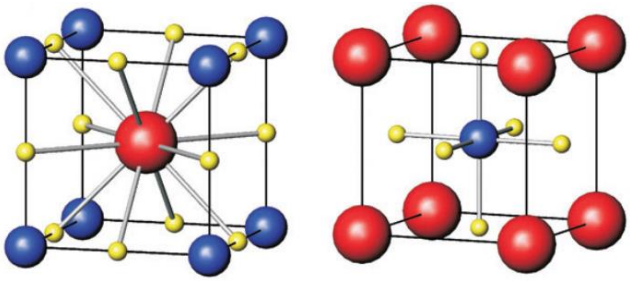

Figure1.5: Cubic perovskite structure (**ABO_3**), **(A)** site cations, **(B)** site cations and **(O)** site anions [55].

Perovskite-type oxides can tolerate partial replacement of the cationic sites one or both with foreign metal ions while maintaining their original crystal structures, thereby modifying their physicochemical properties. These physicochemical properties are dependent on the lattice defects, crystal structure, surface morphology, particle size, specific surface area and the pore structure. A large number of perovskite-type oxides have

been synthesized and investigated for their properties. Several works have been published as books and reviews related to the fabrication, characterization, and catalytic applications of perovskites.

The first catalytic studies on perovskite compounds were published at the beginning of the 1970s, suggesting the possibility of substituting Pt metal by a Pt based perovskite for the oxidation of CO, and it was found that this enhanced the catalytic activity as well as increased the sulphur resistance with no deactivation observed in the presence of 50 ppm SO_2 with a Pt loading as low as 200 ppm [56]. Since then a considerable number of researches have published new synthesis routes and applications of perovskites, which will be described later.

Perovskite material can tolerate partial substitution of A or B sites with other metals having different valence while still maintaining it's structure, however this creates an oxygen vacancy. The effect of the degree of substitution (x) on the catalytic activity and stability was studied by Valderrama et al. They found that the combination of well dispersed Ni particles and availability of oxygen throughout the La_2O_3 phase in a $La_{1-x}Sr_xNiO_3$ perovskite greatly improved the catalyst performance including resistance to carbon deposition and stability for long periods in the dry reforming reaction. [57].

1.4.1 Bimetallic catalysts

Since traditional Ni catalysts often lose activity due to the accumulation of carbon on the surface active sites, bimetallic systems have been studied where Ni is diluted with another active metal to improve the activity of the catalysts toward the hydrocarbon cracking reactions, reduce sintering by increasing the dispersion of the Ni, and prohibit coking. The

role of bimetallic catalysts has been shown to modify the electronic properties of the active metal and increase its stability [58].

Shah et al. have reported the use of a series of bimetallic catalysts 4.5%Fe – 0.5%M/Al_2O_3 (where M = Pd, Mo, Ni) for H_2 production by catalytic methane decomposition. All samples of bimetallic Fe-M/Al_2O_3 catalysts were stable at elevated temperature and exhibited significantly higher activity than monometallic or any metals supported on alumina alone. The H_2 production was nearly 90% for all the catalyst samples at 800 °C. While at 700 °C, Pd-Fe /Al_2O_3 appears to be the most effective, yielding 80% of hydrogen concentration compared to approximately 75% and 65% for Mo-Fe and Ni-Fe respectively. At temperatures above 900 °C, hydrogen production decreases and carbon is deposited on the catalyst in the form of amorphous carbon, carbon flakes, and carbon fibres [59].

Briefly, it can be concluded that most of the bimetallic catalysts materials proposed in the literature show excellent catalytic activity and resistance to carbon and sulphur poisoning compared to their individual counterparts. Several reasons lead to these positive results obtained with the bimetallic compound; a change in the number of active sites, cooperative effect between two active metals resulting in less sensitive materials toward sulphur poisoning. However, even in the best bimetallic catalysts there are still there a number of constraints or problems that need to be tackled.

1.5 Parameters that affect catalytic performance

1.5.1 The effect of active metal and metal loading on catalytic performance

The nickel-based catalyst is still the most preferred material for reforming reactions due to it's low cost, availability, good activity, and relatively simple preparation. However, Ni sintering and carbon deposition are common problems, which lead to deactivation. [60].

Active metals including noble metals [61] and transition metals [62] have been used in the reforming process to enhance catalytic performance. Noble metals were reported to have higher coking resistance in comparison to transition metals. However, the high price and the low availability of noble metals have limited their applications for industrial purposes. Typically, nickel is used instead of noble metals in reforming processes; however, nickel is highly susceptible to carbon deposition because carbon can react with Ni surface layer and produce nickel carbide.

Therefore, it is believed that the synthesis of highly dispersed, active and stable metallic Ni-based catalyst can decrease the coke selectivity which is closely related to nickel loading and nickel particle sizes [63]. A balance between optimum active metal loading and stability is necessary, as a high loading amount of active metal may result in a greater activity in the reaction but at the same time reduce stability over time.

Thus, the presence of small amounts of noble metals can improve reducibility and performance of the main metal. In principle, to obtain high activity, selectivity to desired products, extended longevity, high resistance to sintering and poisoning (coke or sulphur) can be strongly affected by the interaction between metals in a bimetallic catalyst due to the difference in electronic affinity. For example metal M (1) can suffer an electronic

density increase or a decrease depending on whether metal M (2) has a lower or higher electronic affinity [64].

1.5.2 The effect of promoter on catalytic performance

The catalyst promoter is a non-active material that is suggested to improve the catalytic performance through surface structural effects. The most common catalyst promoters for reforming processes are the basic oxides and rare earth metal oxide which are considered as a promising material due to their high oxygen storage capacities. It is well-known from the literature that the addition of promoters can enhance catalytic activity, resistance against carbon deposition and decrease sintering by enhancing the active metal dispersion on the surface of the catalyst.

A promoter may also be required to improve the reducibility at lower temperatures. ZrO_2 is a metal oxide has been used as a promoter to investigate the improvement of Ni/Al_2O_3 catalyst stability as well as the efficiency to produce H_2 under dry reforming of methane. In this reaction, Ni/Al_2O_3 is deactivated quickly due to coke deposition. This deactivation was evidently inhibited by using ZrO_2 because it enhances dissociation of CO_2 forming oxygen intermediates which help in the gasification of coke that deposited during reforming reaction. Therefore, ZrO_2 has received the highest interest among the other metal oxide promoters [65].

1.5.3 The effect of calcination temperature on catalytic performance

Calcination is usually necessary to obtain an interaction between the support and precursors and often leads to an improvement in thermal stability. An enhanced control of

this interaction can be achieved by optimizing the choice of the precursors to achieve higher dispersion and the formation of the new compound. Smolakova et al. [66] studied the effect of calcination temperature on Ni/Al_2O_3 and $Ni{-}Ce\ /Al_2O_3$ catalysts on the activity, selectivity, ratio of pore volume, and specific surface area. They found that calcination temperature played a significant role on the activity and selectivity of both catalysts, an increase the value of the calcination temperature of $Ni{-}Ce\ /Al_2O_3$ and Ni/Al_2O_3 catalysts led to decrease of the productivity to ethane as well as a decrease in the specific surface area and pore volume. The $Ni{-}Ce\ /Al_2O_3$ catalysts calcined at 900 °C and 1000 °C showed a sharp decrease in the catalytic performance in terms of selectivity and activity, due to the formation of $NiAl_2O_4$ spinel.

Another paper was reported by Chen et al. [67] showed the relationship between calcination temperature and surface area for Ni/Al_2O_3. The average NiO crystallite size increased from (2.4 nm to 6.3 nm) and surface area decreased from 170 m^2/g to 105 m^2/g with the increase of calcination temperature (573-873 °C), which suggested that higher calcination temperatures result in segregated phases of NiO and $NiAl_2O_4$ spinel. The catalyst showed higher catalytic activity when calcined at lower temperatures (300 and 450 °C), compared to the catalyst calcined at more than 600 °C. The low catalytic activity for Ni/Al_2O_3 was shown to be as a result of inactive Ni sites due to the formation of $NiAl_2O_4$ spinel at high calcination temperatures.

1.6 Deactivation of catalysts

Catalyst deactivation is an important topic as it is very strongly correlated to performance. The main deactivating effect is that the catalyst reacts and forms other, less or non-

catalytically active compounds. Deactivation can be caused by physical or chemical effect and is one of the most serious problems that need to be taken into consideration in the design and operation of the catalytic process. There are several reasons for losing catalytic activity and degradation:

(i) The catalyst can be poisoned via the strong chemisorption as a monolayer or physical adsorption in multilayers of contaminants such as sulphur, which are naturally contained within biogas feed and block access of the reactants to the active metal surface sites. Although it is possible to remove sulphur from biogas fuel this is considered a costly process as well as being difficult to achieve 100% removal [69].

(ii) Coke formed as a product by methane cracking and encapsulating the metal particles thereby deactivating them completely.

(iii) Thermal sintering of the catalyst leads to loss of surface area and hence reduces the performance. These take place at an elevated reaction temperature (e.g. > 500 °C) and are enhanced by the presence of water vapour.

(iv) Loss of metal particles that were pulled out from the support due to the formation of carbon filaments [68], it can also destroy the structure of the anode in the fuel cell or push the metal particles away from the support.

Typical catalysts should maintain a high activity over time. But it is observed that the activity of catalysts is always lost due to deactivation over variable time scales. Different types of deactivation are already known and can be classified into thermal, chemical, and mechanical. Catalyst deactivation can influence the reactant conversions and the amount of product, for these reasons different models should be considered. For example, adding to

the catalyst a promoter, bimetallic or different active metals in order to combine their properties to enhance the performance and stability of the catalyst's active particles [70].

Poisoning with carbon can reduce the performance of catalysts, especially when using materials such as nickel which catalyse carbon deposition. The rate of deactivation is related to the balance between the rates of formation and gasification /oxidation of the carbon, which is strongly influenced by the reaction conditions and the type of active metals that catalysts involved [71]. However, carbon deposition can be removed by catalysis with oxygen at moderate temperatures (e.g, 400 – 600 °C), industrial processes typically regenerate catalysts deactivated by coke in air [72].

Another observation reported about the carbon formation is that the inactive carbon in reformation reactions reactors takes the form of carbon nanotubes (whiskers) or encapsulating carbon. Whisker carbon is the most destructive shape of carbon formed over nickel catalysts. In this situation, many layers grow by addition of carbon atoms to the surface nickel particles [73]. Carbon accumulation occurs gradually on the catalyst leading to lower catalyst activity. When carbon is deposited in a large amount this can blocking the reactor tube preventing gas flow.

Deactivation of catalysts used in fuel reforming also can be caused by sulphur poisoning which reduces catalytic activity. Therefore, Considerable work has been directed to the development of catalysts that can maintain great levels of catalytic activity in the presence of low level of sulphur. The thermodynamics reaction of sulphur poisoning can be qualitatively testing by considering the reaction of H_2S with various reduced metals as shown in the equation.

$$H_2S + Me^0 \rightarrow MeS + H_2 \qquad [1.16]$$

Poisoning involves strong chemisorption of an impurity such as different sulfur species H_2S, SO_2, CS_2 or NOX and coke deposition, bonded to the active surface sites of the catalyst and consequently lowering the effectiveness of the catalyst. In addition, the adsorbed poison blocks access of adsorbed reactants and finally prevents diffusion. Although, different sulphur-containing species are present within biogas, they will be converted to H_2S in a high temperature reforming environment [74].

Some researchers have studied the surface de- sulphurization process (by O_2 and H_2O) for a sulfur-poisoned nickel surface and examined the effects of the partial pressures of O_2 [pO_2] and H_2O [pH_2O], as well as the ratio of pO_2 /pH_2O on the regeneration of a sulphur-covered Ni surface at different temperatures to identify the best conditions for regeneration of Ni under practical conditions. They observed that H_2O is less effective than O_2 in removing the sulphur atoms that are adsorbed onto the nickel surface. However, both O_2 and H_2O may be present under fuel cell operating conditions [75].

The most extensive studies to improve the resistance of catalysts to deactivation by sulphur are to add oxygen mobility to the catalyst that helps limit sulphur poisoning by avoiding the formation of inactive metal sulphides. Moreover, increasing temperatures from 700 °C to 900 °C can be minimised sulphur poisoning and limit the thermodynamic driving force for the deactivation as noticed by Ashrafi et al.[76].

In General, there are two ways for suppressing or at least decreasing the level of coke formation: changing reaction conditions, such as increasing oxidant to carbon ratio or using different temperature. Despite the large progress and improvements made in catalytic materials, it is clear that there is still a need for developing catalytically more superior, non-coking and deactivated anode materials that were used in SOFCs especially for direct

dry reforming of methane. While high operating temperatures increase carbon deposition problems due to methane decomposition, lowering the cell temperature leads to poor cell performance [77].

1.6.1 Coke forming reactions and ways to minimize it

In the production of hydrogen by using methane reforming, carbon accumulation usually the main problem takes place under reaction conditions in the form of fibres or filaments. Carbon reacts directly with the catalyst to form metal carbide and that leads to reduce the number of active sites by deposition within the porous structure [78]. Coke formation is one of the most important problems which especially associated with dry reforming, and closely related to other problem (sintering and poisoning). Toxicity by the carbon is increased with increasing the particle size of the catalyst, and decrease if the adsorbed poison can be gasified by oxidant agent like O_2, H_2O, CO present in the reactant stream to CO or CO_2.

The most commonly used catalysis material is Ni/YSZ, despite certain disadvantages when hydrocarbon is used as fuels, the active site will be blocked due to the deposition of carbon. Therefore, there is a need to develop alternative materials that have tolerance to carbon and sulphur. The carbon deposition over Ni- catalysts for POX, DRM, and SRM has been extremely investigated during the past decades [79, 80].

Four types of carbon have been identified on the surface of the catalyst, encapsulating, amorphous, whisker, and graphite [81]. These different types of carbon have different influence on catalytic activity, some lead to catalyst deactivation, whereas others have little impact on reforming activity [82].

Wisker carbon is one of the most destructive forms produced on Ni-catalyst; graphitic carbon is oxidized at high temperature, while the oxidation of amorphous carbon occurs at low temperature [83, 84]. The catalyst deactivation was found to be closely related to the accumulation of encapsulating carbon. Suggesting the development of a new catalyst that minimizes the carbon formation is a key research priority.

1.6.1.1 Surface modification by introducing foreign metals

The most useable metal in industry is nickel as it is relatively cheap and highly active toward syngas production, but it has problems relating to volume expansions because it easily absorbs both carbon and sulphur, meaning that carbon filaments can be formed and deactivated the catalyst by destroying the structure as well as blocking system gas diffusion pathways. Since nickel is known as an active catalyst, many studies have been focused on replacing some other active material for some of the nickel rather than replacing the nickel entirely.

In a series of studies of testing iron, it was found that iron could reduce carbon deposition to the low level on both bimetal Ni-Fe /$La_{0.9}Sr_{0.1}Ga_{0.8}Mg_{0.2}O_3$ [85] which has a high surface activity to CH_4 oxidation, and Ni-Fe /Gadolinium-Doped Ceria [86] which showed no degradation over 50 h.

The loss of cell performance after a short operating time can be an extreme problem in hydrocarbon reforming processes. Therefore, to suppress coke formation over nickel based catalysts another metal needs to be introduced in order to modify the surface of the nickel particles. For example, ceria is well known for its ability to store oxygen under an oxidative condition and release it under reducing conditions. For example, novel Ni-based

catalysts containing small amounts of (Sn) have promise as commercial catalysts that promote steam reforming with low level of coke formation [87-89].

Rare earth metals with high basicity when added to the support appear to favour gasification of carbon [90, 91]. Several catalysts that use noble metals have been reported to be effective for the dry reforming reaction without exhibiting the serious problems of coke formation that is found with the conventional catalysts such as Ni supported catalysts [92-95].

The best coking resistance and catalytic activity is achieved to when there is a high dispersion of active metal over the support and therefore limiting the active metals content needed. For example, catalysts with nickel contents higher than 15% suffer from carbon accumulation for the oxy- steam reforming of methane (OSRM) [96].

Wang et.al have found that the catalysts 3-7 wt.% Ru/Al_2O_3 have excellent catalytic activity and operational stability compared to 1 wt.% Ru/Al_2O_3, which showed insufficient activity for the conversion of methane under partial oxidation, steam reforming and CO_2 reforming reactions. This was combined with their TPO results that showed that the 3 wt% Ru/Al_2O_3 also had excellent coking resistance [97].

Ceria-based oxides have been found to be very good supports for metals in steam reforming reactions, as they enable the dissociation of water molecule to produce hydrogen directly through a redox process, as shown below. [98].

$$H_2O + Ce_2O_3 \rightarrow 2CeO_2 + H_2 \quad [1.17]$$

$$CH_4 + 2CeO_2 \rightarrow CO + Ce_2O_3 + 2H_2 \quad [1.18]$$

1.6.1.2 Increasing dispersion ways to control deactivation

It is often found that the dispersion of active metals plays an important role in a catalyst's resistance to sintering and hence increased catalytic longevity. Avoiding deleterious carbon accumulation can be increased by maintaining high metal dispersion, so introducing another metal was a good way to suppress the sintering of Ni due to increased dispersion of Ni particles, hence preventing coke formation [99].

In general, the support provides a surface for dispersing the catalytically active metal and the strong interaction between the metal and support can make a catalyst more resistant to carbon deposition and sintering. Most common supports for methane reforming are Al_2O_3, SiO_2, ZrO_2 and MgO.

Maximal dispersion of active metal on the catalyst surface by using specific preparation methods leads to greater resistance to deactivation and thereby limits carbon deposition [100- 102]. Wu et al [103] have used an incipient wetness method to load different ratios of bimetal Rh/Ni on boron nitride and γ-Al_2O_3 supports. They found that large metal particles were formed on the boron nitride surface during the reaction and the dispersion of $Rh_{0.1}Ni_1$ on BN (1.9%) is significantly lower than that on γ-Al_2O_3 (11.9%).

1.6.1.3 Coupling the DRM with various reforming reactions

The concept of mixed reforming is a technique used to integrate reforming methods for producing the desired ratio of syngas using less energy. For example, coupling SRM or POM with CO_2 and CH_4 can potentially reduce carbon accumulation on the surface of the catalyst due to the oxidation of carbonaceous species [104]. This indicates that the presence of O_2 containing species makes coke formation thermodynamically unfavourable.

Factors that increase thermodynamic favourability of deleterious carbon include lower temperature and higher C /O_2 ratio.

The dry and steam reforming reactions are strongly endothermic, so both of them have similar thermodynamic characteristics except that the carbon formation in dry reforming is more serious than in the steam reforming due to the lower H /C ratio of this reaction. Coupling O_2 in the dry reforming reaction is thermodynamically favourable as it generates heat in situ that can be used to increase energy efficiency.

Choudhary et.al [105] have observed that methane conversion and H_2 selectivity increase when using two strong oxidants (CO_2 and O_2) in the CH_4 reforming reaction. Nickel supported catalysts for tri-reforming of methane at 800–850 °C have achieved 97% CH_4 conversion and 80% CO_2 conversion for producing synthesis gas without coke formation due to the presence of O_2 [106]

The addition of small amounts of water to CO_2 reforming can help to adjust the H_2 /CO ratio through the water gas shift reaction. Furthermore, the gasification rate of carbonaceous species on the catalyst surface can be enhanced by the addition of water as shown in the following equations.

$$C + H_2O \rightleftharpoons CO + H_2 \quad [1.19]$$

$$C + ½O_2 \rightleftharpoons CO \quad [1.20]$$

$$C + CO_2 \rightleftharpoons 2CO \quad [1.21]$$

$$C + O_2 \rightleftharpoons CO_2 \quad [1.22]$$

Although the addition of steam into fuel can minimize coke formation thermodynamically, it can also contribute to the sintering of nickel particles and thus reduce the overall active

surface area. The feed composition also has a strong influence on coke deposition as detailed in the following section.

1.6.1.4 Effects of pressure, temperature and oxidant feed ratio

To achieve the optimization of processes, and control deactivation, incorporation of additional oxidants like H_2O or O_2 in the reactant stream can improve the resistance of the catalyst to deactivation depending on the thermodynamic equilibria. The influence of temperature, pressure and feed ratio of a composition all highly influence the thermodynamic equilibrium of a reforming reaction. As expected, higher temperatures lead to increased syngas production, up to an almost complete conversion of methane.

The easiest way to avoid coke formation over catalyst materials is via a thermodynamic approach that requires the addition of oxygen or steam to the fuel gas mixture to increase the O/C ratio. For example, the thermodynamic calculation for autothermal steam and CO_2 reforming of methane was performed by Yunhua et al. [107]. The H_2 yield and carbon formation as a function of reforming temperature, the ratio of H_2O /CH_4, CO_2 /CH_4, O_2 /CH_4, and the pressure were all examined.

Coke elimination was observed to be easier in steam reforming than in CO_2 reforming under the same conditions. These results showed that the optimal CH_4 /CO_2 /O_2 feed ratios was 1:0.8 /1.0:0.1 /0.2 and the coke formation inhibited by increasing steam content and decreasing the pressure, whereas in CO_2 reforming it was by increasing the reaction temperatures up to 800 $^{\circ}$C.

A similar concept using multiple oxidants has been reported by other authors [108] in which the addition of small amounts of steam along with CH_4 and CO_2 over bimetallic Rh–

Ni/Al_2O_3 catalysts was shown to improve the gasification of the coke accumulated during methane dry reforming compared to the gasification carried out by CO_2 alone.

Another approach to the oxidative CO_2 reforming of methane with an equal amount of CH_4 and CO_2 was reported in 2011 by Nikoo and Amin [109]. They reported that reactant conversion and syngas yields were above 90% with no carbon formation, and they attributed this to the optimal operating temperature and feed ratio of 1073 K and CO_2 /CH_4 /O_2 equal to 1 /1 /0.1, respectively. Their study also showed that higher pressures inhibited the effect of temperature on reactant conversion and hence decreased CO and H_2 production to less than unity due to methane decomposition reactions, and increased carbon accumulation.

1.6.1.5 Alloying effect

Noble metals are known to be the best for resistant to coke than any other metals. Among noble metals, Rh is the most commonly used in the bimetallic catalyst with Ni, which enriches the Ni surface, forming a surface alloy Ni-Rh, rather than a bulk alloy. Preparation conditions can affect the carbon inhibition of a bimetallic system; if the catalyst is calcined at high temperatures, metal segregation can occur and reduce the resistance to carbon.

The activity and stability of silica supported monometallic Ni, Rh and bimetallic Ni–Rh catalysts have been investigated for methane CO_2 reforming. It has been reported that SiO_2 supported monometallic and bimetallic catalysts are both good catalysts for CO_2 reforming of methane and the resistivity toward coke formation and catalytic deactivation are increased with increasing Rh within the catalyst structure. It has been shown that there is

an effective process of Ni–Rh alloy formation taking place in the case of bimetallic Ni–Rh /SiO_2 catalysts at high calcination temperatures. [110].

The conventional Ni-YSZ anodes are prone to uncontrolled carbon deposition during reforming reactions with hydrocarbons as fuels. Foreign metals such as chromium act as inhibitors by forming alloys with Ni and prohibiting small particles growing into larger ones, which are prone to carbon deposition [111].

Linic et al.[112] have identified that carbon tolerance of Ni can be improved by synthesizing Sn /Ni surface alloys for steam reforming catalysts compared to monometallic Ni, suggesting that the oxidization of C atoms rather than forming C–C bonds has a lower thermodynamic driving force, which is associated with the nucleation of carbon atoms on low-coordinated Ni sites.

In other studies the alloy formation and structure of Ni-Au nanoparticle catalysts supported on SiO_2 and on $MgAl_2O_4$ have been described. The simulations and results give evidence for the formation of active catalysts of Ni-Au surface alloys for steam reforming, which showed more resistance to carbon than the pure Ni catalyst, and this was attributed to Au atoms appearing to block the high reactivity sites on the small Ni particles, thereby lowering the probability of adsorbed carbon to form graphite and carbon whiskers [113].

To conclude, the rate of coke accumulation is a function of the metal's type, the promoter, the crystal size, calcination temperature and the interaction between the metal- metal and metal- support [114].

1.6.2 Thermal degradation

There are many paths for heterogeneous catalyst decay and deactivation. High temperatures is one of these paths can enhance thermal deactivation when applied to the catalyst to achieve a higher activity. Thermal degradation of heterogeneous catalyst is a major cause of irreversible catalyst deactivation as a result of overheating, a large number of DRM catalysts have been published with varying activities, and the main problem usually highlighted is catalyst thermal deactivation which lowers the surface area [115] hence the overall catalytic efficiency in terms of activity, selectivity, durability and longevity. Since the catalytic activity depends on the available surface area. Although sintering rates of catalysts are strongly affected by temperature, another factor can be used to limit sintering such as increase dispersion of active metals.

Recently, it has been reported that methane decomposition occurring at high temperature during the dry reforming reaction has high effect on both the type and amount of coke formation hence affect the activity and stability of the catalyst. Also, it is reported that amorphous carbon is the most active, being consumed rapidly by the Boudard reaction, whereas filamentous and graphitic are less active than amorphous carbon [116]. Thus selecting an appropriate catalyst, temperature is very vital in prohibiting carbon formation hence deactivation and maintains stable performance of the catalyst for DRM.

1.7 The latest catalytic studies for metals Fe, Ru, Al, and Ni

Perovskite oxides have received a lot of attention as promising catalysts for syngas production because of their reasonable reactivity and impurity tolerance. Challenges still exist for advancing perovskite catalyst materials, which normally suffer from deactivation

due to several reasons mentioned in section 1.6. The introduction of other transition elements into the *A*-site (Ca, Sr, and Mg) and *B*-site (Mn, Fe, Co, Ni) of $LaCrO_3$ lattice showed three different catalytic behaviours, depending on the metal substituents. Among these various dopants, nickel seems to be the most successful substituent due to having the highest activity toward CH_4, H_2O, and CO_2 reforming. While in the case of Fe-substituted $LaCrO_3$, only a small amount of coke was detected on the surface. Sr and Ni were found to be the most active and the most suitable substituents for the $LaCrO_3$. On the other hand, the accommodation of active species in the perovskite lattice is a good way to overcome stability problems and form stable structures [117].

Significant progress in different aspects of catalysis has been made recently; these include approaches to synthesis, characterization and evaluation of catalysts. Mg /Ni /Al catalyst which showed good stability with a conversion of methane in excess of 90% compared to large amounts of coke formed over Ni/Al catalyst, causing deactivation with a decrease in the conversion from 75% to 30% in just over 5 h [118].

A study has shown through the comparison between mono- and bi-metallic catalysts; Ni-Co/Al_2O_3-ZrO_2 catalyst could provide more active site for methane reforming reaction hence shows good catalytic activity and better resistance to carbon deposition than Ni/Al_2O_3-ZrO_2, Co/Al_2O_3-ZrO_2 [119].

Another study used bimetallic Fe-Ni /$MgAl_2O_4$ catalysts for methane dry reforming. It was found during H_2-TPR, Fe_2O_3 and NiO are reduced to Fe and Ni and then Fe could be oxidized by CO_2 to FeOx which acted as an oxygen carrier and involved in the oxidation of surface carbon resulting in a reduction of coke formations as described by the following equations [120]:

$$CH_4 \xrightarrow{Ni} 2H_2 + C_{Ni} \quad [1.23]$$

$$Fe + xCO_2 \rightleftharpoons FeO_x + xCO \quad [1.24]$$

$$FeO_x + C_{Ni} \rightleftharpoons xCO + Ni + Fe \quad [1.25]$$

$$FeO_x + H_2 \rightleftharpoons Fe + H_2O \quad [1.26]$$

Highly active and stable Ru-doped lanthanide chromate ($LaCr_{0.8}Ru_{0.2}O_3$) perovskite catalyst was tested by Jeon et al. [121] for the application to methane reforming at reaction environments such as partial oxidation, steam and autothermal conditions. The reaction conditions at autothermal reforming were obviously found as the most effective conditions in terms of both CH_4 conversion and H_2 production of over 95%, and 70% respectively, which was comparable to the theoretical calculations.

Both conversion and selectivity increase with increasing temperature and the activation of the catalyst are accelerated. The conversion of CH_4 and the production of H_2 increases in the order of autothermal reforming > steam reforming > partial oxidation. Therefore, the most proper process in utilizing Ru-doped lanthanide chromate perovskite catalyst was the autothermal operating condition.

1.8 The project aim and objectives

The motivation of this dissertation is to develop and/or modify catalysts by incorporating small amount of bimetallic noble and non-noble metals into perovskite materials and compare with conventional nickel supported alumina catalysts and suggest further focus in catalyst development. Several methods for reforming of hydrocarbons or oxygenated natural gas to synthesis gas are presented in this dissertation (Chapter 4: Biogas reforming, Chapter 5: Dry reforming and Chapter 6: Partial Oxidation).

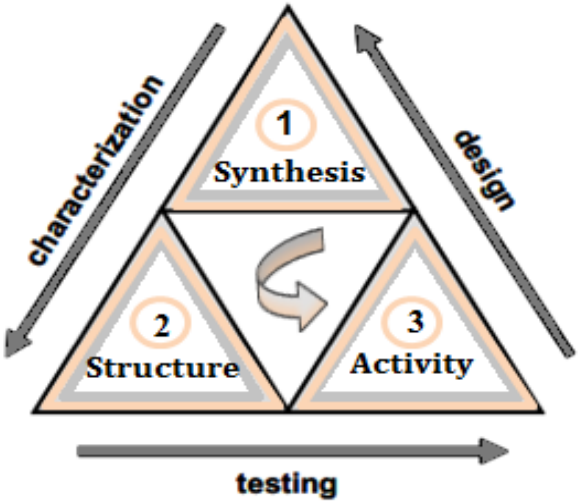

Figure 1.6: Schematic shows the practical stages for this study.

The aims of this project are as follows:

- To provide essential information relevant to the future development of catalysts for reforming applications.
- To assess the influence of active metal addition on the activity and selectivity of strontium zirconate for the catalytic reforming of simulated biogas, dry reforming, and partial oxidation.
- To prepare perovskite catalytic materials by hydrothermal technique under pH control of 12-14.
- To compare three methods of reforming activity over co-doped perovskite catalysts under comprehensive catalyst testing.
- To understand the variation in physicochemical properties and the morphological features for the co-doped perovskite catalysts, that may offer the chance to highlight potential synergies.

- Investigate the effect of incorporating different active metals into the perovskite catalyst for synthesis gas production by using three routes of reforming reactions and compare the results with a conventional catalyst.
- To identify the effect of reaction temperature and time on methane conversion, syngas production, H_2 /CO ratio and ability in supressing coke formation.
- Further characterization of post reaction catalysts to confirm the stability after 20 hours aging.

1.9 References

[1] W. Wang, C. Su, Y. Wu, R. Ran, and Z. Shao, *Chem. Rev*., 2013, **113**, 8104−8151.

[2] Y. Shiratori, T. Ijichi, T. Oshima, and K. Sasaki, *Int. J. Hydrogen Energy*, 2010, **35**, 7905–7912.

[3] R. Kothari, V. Kumar, V. V. Pathak, and V.V. Tyagi, *Int. J. Hydrogen Energy*, 2017, **42**, 4870-4879.

[4] P. Kaparaju, I. Buendia, L. Ellegaard, and I. Angelidakia, *Bioresour. Techn*., 2008, **99**, 4919-4928.

[5] H. Ritchie and M. Roser, (2018), OurWorldInData.org/energy-production-and-changing-energy-sources/.

[6] A. W. Palumbo, J. C. Sorli, and A. W. Weimer, *Appl. Energy*, 2015, **157**, 13–24.

[7] K. Girona, J. Laurencin, J. Fouletier, F. L. Joud, *J. Power Sources*, 2012, **210**, 381-391.

[8] R. M. Ormerod, Chem. *Soc. Reviews*, 2003, **32**, 17–28.

[9] C. Sun, and U. Stimming, *J. Power Sources*, 2007, **171**, 247–260.

[10] H. E. Figen, and S. Z. Baykara, *Int. J. Hydrogen Energy*, 2015, **40**, 7439–7451.

[11] Y. Khani, Z. Shariatinia, and F. Bahadoran, *Chem. Eng. J*., 2016, **299**, 353–366.

[12] F. Frusteri, S. Freni, L. Spadaro, V. Chiodo, G. Bonura, S. Donato, and S. Cavallaro, *Cata. Communi*., 2004, **5**, 611–615.

[13] S. Corthals, J. Nederkassel, J. Geboers, H. Winne, J. Noyen, B. Moens, B. Sels, and P. Jacobs, *Catal. Today*, 2008, **138**, 28–32.

[14] J. H. Kim, D. J. Suh, T.J. Park, and K.L. Kim, *Appl. Catal. A: Gen.*, 2000, **197**, 191–200.

[15] J. Guo , H. Lou , H. Zhao, D. Chai, X. Zheng, *Appl. Catal. A: Gen.*, 2004, **273**, 75–82.

[16] J. Deng, X. Lv, J. Gao, A. Pu, M. Li, X. Sun and J. Zhong, *Ene. Environ. Sci*., 2013, **6**, 1965-1970.

[17] J. Rossmeisl, A. Logadottir, and J.K. Nørskov, *Chem. Physics*, 2005, **319**, 178–184.

[18] J. Rossmeisla, Z.W. Qu, H. Zhu, G.J. Kroes, and J.K. Nørskov, *J. Elect. Chem*., 2007, **607**, 83–89.

[19] B. Zhu, X.S. Li, C. Shi, J.L. Liu, T.L. Zhao, and A. M. Zhu, *Int. J. Hydrogen Energy*, 2012, **37**, 4945–4954.

[20] Y. N. Chun,Y. C. Yang, and K. Yoshikawa, *Catal. Today*, 2009, **148**, 283–289.

[21] H. Zhang, X. Li, F. Zhu, K. Cen, C. Du, and X. Tu, *Chem. Engineering J*., 2017, **310**, 114–119.

[22] S. A. M. Said, M. Waseeuddin, and D. S. A. Simakov, *Renew. Sustain. Energy Reviews*, 2016, **59**, 149–159.

[23] M.D. Dolan, A.C. Beath, S.S. Hla, J.D. Way, and H.W. A. El Hawa, *Int. J. Hydrogen Energy*, 2016, **41**, 14583–14595.

[24] B. Nematollahi, M. Rezaei, and M. Khajenoori, *Int. J. Hydrogen Energy*, 2011, **36**, 2969–2978.

[25] U. Izquierdo, V.L. Barrio, N. Lago, J. Requies, J.F. Cambra, M.B. Güemez, and P.L. Arias, *Int. J. Hydrogen Energy*, 2012, **37**, 13829–13842.

[26] M. Akri, T. Chafik, P. Granger, P. Ayrault, and C. Dupeyrat, *Fuel*, 2016, **178**, 139–147.

[27] J. Gao, Z. Hou, X. Liu, Y. Zeng, M. Luo, and X. Zheng, *Int. J. Hydrogen Energy*, 2009, **34**, 3734–3742.

[28] H. Jiang, H. Li and Y. Zhang, *J. Fuel Chem Technol.*, 2007, **35**, 72-78.

[29] R. Siriwardane, H. Tian, and J. Fisher, *Int. J. Hydrogen Energy*, 2015, **40**, 1698–1708.

[30] S. M. Lima, I. O. Cruz, G. Jacobs, B. H. Davis, L. V. Mattos, and F.B. Noronha, *J. Catalysis*, 2008, **257**, 356–368.

[31] J. Staniforth and R. M. Ormerod, *Catal. Letters*, 2002, **81**, 19-23.

[32] J. Staniforth, and K. Kendall, *J. Power Sources*, 1998, **71**, 275-277.

[33] C. J. Laycock, J. Z. Staniforth and R. M. Ormerod, *Dalton Trans.*, 2011, **40**, 5494-5504.

[34] C. J. Laycock, J. Z. Staniforth and R. M. Ormerod, *Electro. Chem. Soc. Trans.*, 2009, **16**, 177–188.

[35] D. Li, R. Li, M. Lu, X. Lin, Y. Zhan, and L. Jiang, *Appl. Catal. B Environ*., 2017, **200**, 566-577.

[36] W. Hou,Y. Wang,Y. Bai, W. Sun, W. Yuan, L. Zheng, X. Han and L. Zhou, *Int. J. Hydrogen Energy*, 2017, **42**, 16459-16475.

[37] A.P. Simpson and A.E. Lutz, *Int. J. Hydrogen Energy*, 2007, **32**, 4811-4820.

[38] S.D. Angeli, G. Monteleone, A. Giaconia, and A.A Lemonidou, *Int. J. Hydrogen Energy*, 2014, **39**, 1979–1997.

[39] Andrew P. E. York , Tian-cun Xiao , Malcolm L. H. Green and John B. Claridge, *Catal. Reviews*, 2007, **49**, 511–560.

[40] M. Prettre, C. Eichner and M. Perrin, *Trans. Faraday Soc*., 1946, **42**, 335-339.

[41] W. Z. Weng, Q. G. Yan, C. R. Luo, Y. Y. Liao, and H. L. Wan, *Catal. Letters*., 2001, **74**, 37–43.

[42] H. Y. Wang and E. Ruckenstein, *J. Phys. Chem. B*, 1999, **103**, 11327-11331.

[43] S. McIntosh, and M. Bossche, *Solid State Ionics*, 2011, **192**, 453-457.

[44] W. Chu, W. Yang and L. Lin, *Catal. Letters*., 2001, **74**, 139-144.

[45] S. Evans, O. Good, J. Staniforth, M. Ormerod and R. Darton, *RSC Adv*., 2014, **4**, 30816–30819.

[46] T. Johansson, D. Pakhare, D. Haynes, V. Abdelsayed, D. Shekhawat, and J. Spivey, *Chem. Pap*., 2014, **68**, 1240–1247.

[47] C. Wang, N. Sun, N. Zhao, W. Wei, Y. Sun, C. Sun, H. Liu, and C. E. Snape, *Fuel*, 2015, **143**, 527–535.

[48] M. Usman, W. W. Daud, and H. F.Abbas, *Renew. Sustain. Energy Reviews*, 2015, **45**, 710-744.

[49] P. Gangadharan, K. C. Kanchi and H. H. Lou, *Chem. Eng. Res. Des*., 2012, **90**, 1956–1968.

[50] A. Iulianelli, S. Liguori, J. Wilcox and A. Basile, *Catal. Reviews*, 2016, **58**, 1-35.

[51] K. V. Kumar, K. Porkodi and F. Rocha, *Catal. Commun*., 2008, **9**, 82–84.

[52] R. J. Willey, *J. Thermophysics. Heat transfer*, 1993, **7**, 55-62.

[53] P. Granger, V. I. Parvulescu, S. Kaliaguine, W. Prellier, Perovskites and Related Mixed Oxides: Concepts and Applications, books.google.com,2015,volum**1**.

[54] J. Zhu, H. Li, L. Zhong, P. Xiao, X. Xu, X. Yang, Z. Zhao and J. Li, *ACS Catal*., 2014, **4**, 2917–2940.

[55] D. R. Modeshia and R. I. Walton, *Chem. Soc. Rev.*, 2010, **39**, 4303–4325.

[56] P.K.Gallagher, D.W.Johnson, Jr.J.P.Remeika, F.Schrey, L.E.Trimble, E.M.Vogel, and R.J.H.Voorhoeve, *Mater. Res. Bull*., 1975, **10**, 529-538.

[57] G. Valderrama, M. R. Goldwasser, C. U. de Navarro, J. M. Tatiboue¨t, J.¨l Barrault, C. Batiot-Dupeyrat, and F. Martı´nez, *Catal. Today*, 2005, **108**, 785–791.

[58] L.´ Guczi, *Catal. Today*, 2005. **101**, 53-64.

[59] N. Shah, D. Panjala and G.P. Huffman, *Ene. Fuels*, 2001, **15**, 1528–1534.

[60] L. F.Bobadilla, A. Penkova, A. Álvarez, M. I. Domínguez, F. Romero-Sarria, M. A. Centeno and J. A. Odriozola, *Appl. Catal. A : Gen.*, 2015, **492**, 38−47.

[61] D. KLiguras, D. IKondarides and X. EVerykios, *Appl. Catal. B: Enviro.*, 2003, **43**, 345-354.

[62] S. Li and J. Gong, *Chem. Soc. Rev*., 2014, **43**, 7245-7256.

[63] Z. Li, X. Hu, L. Zhang, S. Liu, and G. Lu, *Appl. Catal*. A: Gen., 2012, **417**, 281–289.

[64] Vladimiro Dal Santo, Alessandro Gallo, Alberto Naldoni, Matteo Guidotti, and Rinaldo Psaro, *Catal. Today*, 2012, **197**, 190–205.

[65] S. Therdthianwong, C. Siangchin , and A. Therdthianwong, *Fuel Proc. Technology*, 2008, **89**, 160-168.

[66] L. Smoláková, M. Kout, E. Koudelková, and L. Čapek, *Ind. Eng. Chem. Res*., 2015, **54**, 12730–12740.

[67] J. Chen, Q. Ma, T. E. Rufford and Y. Li, Z. Zhu, *Appl. Catal. A: Gen.*, 2009, **362**, 1-7.

[68] M. Gong, X. Liu, J. Trembly and C. Johnson, *J. Power Sources*, 2007, **168**, 289–298.

[69] M. D. Argyle and C. H. Bartholomew, *Catalysts*, 2015, **5**, 145−269.

[70] C. H. Bartholomew, *Appl. Catal. A: Gen*., 2001, **212**, 17–60.

[71] J. J. Spivey, *Fuel Cells: Technologies for Fuel Processing*, 2011, 285−315.

[72] C. Bartholomew and Kirk-Othmer, *Encyclopedia of Chemical Technology*, 2003, **5.**

[73] J. Sehested, *Catal. Today*, 2006, **111**, 103–110.

[74] D. J. Nixon, PhD Thesis, Keele University, 2013.

[75] J. H. Wang and M. L. Liu, *J. Power Sources*, 2008, **176**, 23-30.

[76] M. Ashrafi, C. Pfeifer, T. Pröll and H. Hofbauer, *Energy Fuels*, 2008, **22**, 4190–4195.

[77] T. M. Gür, *Progress in Energy and Combustion Science*, 2016, **54**, 1–64.

[78] S. E. Evans, J. Z. Staniforth, M. R. Ormerod and R. J. Darton, *Green Chem*., 2014, **16**, 4587-4594.

[79] J.Z. Luo, Z.L. Yu, C.F. Ng and C.T. Au, *J. Catal.*, 2000, **194**, 198–210.

[80] S. Xu, R. Zhao and X. Wang, *Fuel Process. Technol*., 2004, **86**, 123–133.

[81] J. Guo, H. Lou and X. Zheng, *Carbon*, 2007, **45**, 1314–1321.

[82] A.L. Alberton, M.V.M. Souza, and M. Schmal, *Catal. Today*, 2007. **123**, 257-264.

[83] K.Young Koo, H. Roh, Y. Seo, D. Joo Seo, W. Yoon and S. Park, *Appl. Catal. A:Gen.*, 2008, **340**, 183–190.

[84] C. Liu, J.Ye, J. Jiang, and Y. Pan, *Chem.Cat.Chem*., 2011, **3**, 529 – 541.

[85] H. Zhong, H. Matsumoto, and T. Ishihara, *Electrochemistry*, 2009, **77**,155-157.

[86] H. Kan, and H. Lee, *Catal. Commun*., 2010, **12**, 36–39.

[87] L. Bobadilla, F. Sarria, M. Centeno and J. Odriozola, *Int. J. Hydrogen Energy*, 2016, **41** , 9234–9244.

[88] H. Kan, S. Hyun, Y. Shul and H. Lee, *Catal. Commun*., 2009, **11**, 180-183.

[89] M. Ferreira, N. Nichio and O. Ferretti, *J. Mol. Catal. A: Chemical*, 2003, **202**, 197–213.

[90] D.L. Trimm, *Catal. Today*, 1999, **49**, 3-10.

[91] R. M. Navarro, M. A. Pen, and J. L. G. Fierro, *Chem. Rev*., 2007, **107**, 3952−3991.

[92] J.Wei and E. Iglesia, *J. Catal*., 2004, **225**, 116–127.

[93] A. Yamaguchi and E. Iglesia, *J. Catal*., 2010, **274**, 52–63.

[94] C. Xie, Y. Chen,Y. Li, X. Wang, C. Song, *Appl. Catal. A: Gen*., 2011, **394**, 32– 40.

[95] W. Wang, R. Ran, C. Su, Z. Shao, D. W. Jung, S. Seo and S.M. Lee, *Int. J. Hydrogen Energy*, 2011, **36**, 10958–10967.

[96] W.S. Dong, H. Roh, K. Jun, S. Park and Y. Sam , *Appl. Catal. A: Gen*., 2002, **226**, 63–72.

[97] W. Wang, R. Ran and Z. Shao, *Int. J. Hydrogen Energy*, 2011, **36**, 755 -764.

[98] X. Wang and R. J. Gorte, *Appl. Catal. A: Gen*., 2002, **224**, 209–218.

[99] J. Sehested, J. Gelten and S. Helveg, *Appl. Catal., A: Gen*., 2006, **309,** 237–246.

[100] S.Wang and G.Q.M. Lu, *Appl. Catal. B: Environ*. 1998. **16**, 269-277.

[101] M. Garcia-Dieguez, I. S. Pieta, M. C. Herrera, M. A. Larrubia, I. Malpartida and L. J. Alemany, *Catal. Today*, 2010, **149**, 380–387.

[102] A. F. Lucredio, J. Assaf and E. M. Assaf, *Appl. Catal. A: Gen.*, 2011, **400**, 156–165.

[103] J. C. S. Wu and H. C. Chou, *Chem. Eng. J.*, 2009, **148**, 539–545.

[104] M. M. V. M. Souza, M. Schmal, *Appl. Catal. A: Gen*., 2005, 281, 19–24.

[105] V. R. Choudhary, K. C. Mondal, and T. V. Choudhary, *Fuel*, 2006, **85**, 2484 –2488.

[106] C. S. Song, and W. Pan, *Catal. Today*, 2004, **98**, 463–484.

[107] Y. Li, Y. Wang, X. Zhang and Z. Mi, *Int. J. hydrogen Energy*., 2008, **33**, 2507-2514.

[108] M. Garcia-Dieguez, I. S. Pieta, M. C. Herrera, M. A. Larrubia and L. J. Alemany, *Catal. Today*, 2011, **172**, 136–142.

[109] M. K. Nikooa, and N. A. S. Amin, *Fuel Pro. Techn*., 2011, **92**, 678-691.

[110] W. K. Jóźwiak, M. Nowosielska and J. Rynkowski, *Appl. Catal. A: Gen*., 2005, **280**, 233-244.

[111] Y. Kim, J. Um, S. Kim, T. Lim and H. Lee, *Appl. Catal. A: Gen*., 2010**, 384**, 10–17.

[112] E. Nikolla, J. Schwank, and S. Linic, *J. Catal*., 2007, **250**, 85–93.

[113] A. M. Molenbroek and J. K. Nørskov, *J. Phys. Chem. B*, 2001, **105**, 5450-5458.

[114] P. Boldrin, E. R. Trejo, J. Mermelstein, J. M. B. Menéndez, T. R. Reina, and N. P. Brandon, *Chem. Rev*., 2016, **116**, 13633–13684.

[115] A. W. Budiman, S. H. Song, T. S. Chang, C. H. Shin, and M. J. Choi, *Catal. Surv., Asia*, 2012, **16**, 183–197.

[116] J. Newnham, K. Mantri, M. Hassan Amin, J. Tardio, and S. K. Bhargava, *Int. J. Hydrogen Energy*, 2012, **37**, 1454-1464.

[117] J. Sfeir, P. A. Buffat, P. M ¨ockli, N. Xanthopoulos, R. Vasquez, H. J. Mathieu, J. V. herle, and K. R. Thamp, *J. Catal.*, 2001, **202**, 229–244.

[118] T. L. LeValley, A. R. Richard, and M. Fan, *Int. J. Hydrogen Energy*, 2014, **39**, 16983-17000.

[119] X. Li, J. Ai, W. Li and D. Li, *Front. Chem. Eng. China*, 2010, **4**, 476- 480.

[120] S. A. Theofanidis, V. V. Galvita, H. Poelman and G. B. Marin, *ACS Catal.*, 2015, **5**, 3028– 3039.

[121] Y. Jeon, H. Kim, C. Lee, S. Lee, S. Song and Y. Shul, *Fuel*, 2017, **207**, 493–502.

Chapter 2

Methodology

2. Methodology

2.1 Summary of different catalytic synthesis methods

2.1.1 Hydrothermal synthesis

Hydrothermal synthesis is a method which plays an important role in the preparation fine powders of metal oxides under hydrothermal and pressure conditions using autoclave, which consists of a closed steel pressure vessel employed to achieve the required conditions. These methods depend on the ability to dissolve materials that are often practically insoluble under normal conditions, such as some oxides and sulphides in aqueous solutions at temperatures above 100 °C.

Several advantages have been reported for the hydrothermal technique over other conventional methods, including the ability to synthesize high-quality crystals of materials in a single step process using lower synthesis temperatures. It is possible to control particle size and shapes by using different starting materials, different reaction times, alteration in pH and hydrothermal conditions [1, 2].

However, there are drawbacks of the synthesis method including the high cost of equipment, accidental explosion of the high-pressure vessel cannot be ruled out and the impossibility to monitor the crystal growth as it progresses [3]. This method is also more environmentally friendly as the product e.g. perovskites are synthesized directly from the mixed metal oxides or metal nitrates precursors without releasing toxic gases.

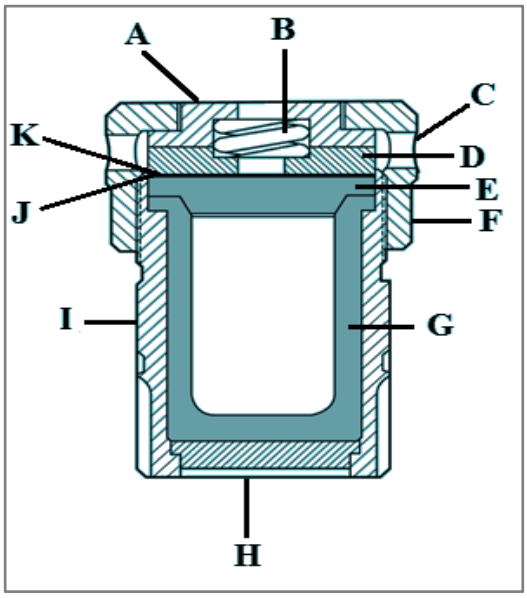

A	**Pressure plate, upper**
B	Spring
C	Relief port
D	Compressible disc
E	Teflon lid
F	Screw cap
G	Teflon cup
H	Bottom plate disc
I	Vessel body
J	Pressure plate, lower
K	Corrosion disc

Figure 2.1: Teflon-lined stainless steel autoclave adapted from [4].

The reactants are dissolved in a specific amount of solvent and placed inside at the bottom of the autoclave; they are exposed to high temperature under high vapor pressures, once the reaction ends, the autoclave was cooled in order to grow the desired crystal.

2.1.2 Sol-Gel synthesis

Sol-gel techniques have been widely applied for producing a powder of ceramic materials by using inexpensive equipment at low reaction temperatures. This synthesis method involves hydrolysis and condensation of metals precursors such as chlorides, nitrates, or acetates which are generally dissolved in aqueous solutions or metal alkoxides in organic solvents at controlled temperature [5]. The gel intermediate is then heated between 150-300 $^{\circ}$C to remove volatile organic compounds, excess water, etc., leading to dried intermediate powders. After gelation process, the gel must be calcined at a high temperature in order to remove any moisture and start crystallization. However, high

calcination temperatures can lead to sintering of the product and therefore lowering the useful surface area; this is considered one of the drawbacks for the Sol-Gel route.

2.1.3 Solid state synthesis

It is one of the simplest conventional methods for preparation of a mixed-oxide catalyst. This method is achieved by grinding or ball-milling mixed metals oxides or metal carbonates, either dry or as wet slurry. Conditions such as the rotating rate and grinding time can have a significant effect on the surface area and catalytic performances. The mixture also needs high calcination temperatures of 600 –1200 °C for many hours to obtain the final powder catalyst.

Calcination is usually necessary to obtain an interaction between reactants and to complete the reaction get a pure perovskite phase. Sometimes, impurities can be introduced from milling media and calcination boat that is used to complete reaction at high temperature. Several repeated grinding and heating cycles are required to obtain homogeneous and pure perovskites. However, it should be noted that the solid-state method can easily be achieved but that the reaction conditions often result in grain growth due to agglomeration at high calcination temperature and show a relatively low specific surface area, characteristics not suitable for catalysis applications [6, 7].

2.1.4 Co-precipitation synthesis

Another common preparation method for producing mixed-oxide catalysts is the co-precipitation method that deposits the active metals on the support by adding suitable

precipitator into the metal precursor solution, followed by drying and calcination. Mostly, nitrates, carbonates, and oxalates could be used as the metal source, in addition to sodium hydroxide solution or aqueous ammonia as a precipitant agent [8]. The process has three stages, super-saturation, nucleation, and growth. The resulting gel is filtered, washed, dried and finally calcined to give the final catalyst material. Controlling the pH value and temperature is an important factor during the precipitation process to get a well-defined nanostructured catalyst. These precipitates require low calcination temperatures to yield the final powder with desired properties.

2.1.5 Combustion synthesis

Combustion synthesis is an effective, low-cost and quick way for the preparation of various nanomaterials that are industrially useful. New materials are synthesized by this technique from self-sustained exothermic chemical reactions instead of long time heat treatment. The combustion method involves an exothermic decomposition of a metal salt and organic fuel such as urea, glycine, glycerol, etc. at relatively low temperatures.

Once the reactants are mixed together, exothermic combustion reactions occur immediately and a large quantity of heat energy is produced which lead the reaction to continue to convert all reactants into products [9]. However, contamination with a large volume of gases (mainly NH_3 or NO_x) that are emitted during the synthesis is one of the main disadvantages of this method in addition uncontrollable agglomeration of particles at high temperature [10]. Current efforts seek to control combustion in order to get final products with more desired properties.

2.1.6 Impregnation synthesis

This technique is widely used for solid-catalyst synthesis that depends on the deposition of one or more active metal or compound on a high-surface-area material. This preparation method involves a support to be placed in the solvent containing the precursor solution and then dried to remove the solvent and finally calcined to decompose the metal precursor compounds to metal oxides [11].

The total volume of liquid added during this method should be in excess of the total pore volume of the support. The purpose of a catalyst support is to provide mechanical strength and a large surface area for the dispersion of the active materials. The support is usually catalytically inactive alone, but when modified with the active phase, may participate in the reaction in a desirable way.

2.1.7 Detailed Synthesis of co-doped perovskite and 10% Ni/Al_2O_3

Bimetallic Ni-M doped $SrZrO_3$ perovskite (M= Fe, Al, Ru) were prepared by hydrothermal methods [12]. Appropriate stoichiometric amounts of precursors 3 g of $ZrOCl_2 \cdot 8H_2O$ (Alfa Aesar, 99.9%), 1.576 g of $Sr(NO_3)_2$ (Alfa Aesar, 99.97%), 0.541 g of $Ni(NO_3)_2.6H_2O$ (Sigma Aldrich, 99.99%), 0.188 g of $Fe(NO_3)_3.9H_2O$ (Aldrich, 99.95%), 0.174 g of $Al(NO_3)_3.9H_2O$ (Aldrich, 99.00%), 0.122 g of $RuCl_3.3H_2O$ (Aldrich, 99.00%), were dissolved in deionized water at room temperature within a 23ml Teflon-lined stainless steel autoclave and physically mixed. Sodium hydroxide (Sigma Aldrich, 97.0%) was then added and thoroughly mixed until a homogeneous gel was formed. After that, the Teflon liner was then sealed within the autoclave and heated for 72 hours at 180 °C for the co-doped perovskite samples. Once the reaction was complete, the autoclaves were cooled to

room temperature naturally. The product was transferred into centrifuge tubes and washed with ultra-pure water, and centrifuged at 4500 rpm for 15 minutes. The supernatant solution was poured away and the tube rewashed with ultra-pure water and centrifuged again. The samples were then dried in an oven at 60 °C for 24 hours, before using an agate mortar and pestle to form a fine powder of the perovskite specimens. Finally, the perovskite samples were then heated in ceramic combustion boats on a temperature programme of 2 °C .min^{-1} up to 300 °C to drive off any moisture or hydroxide compounds that were bound into the structure.

Nickel supported on alumina 10wt% Ni/Al_2O_3 was prepared by wet impregnated technique [13]. An aqueous solution of 14.86 g of Ni $(NO_3)_2.6H_2O$ (Fluka-Garantie, 99%) was dissolved in 50 ml of distilled water and then added to the beaker that contains the support and Stirrer bead which then placed on a stirrer hot plate. The water was gently evaporated off, with stirring, until the stirrer bead could no longer move, at which point the catalyst precursor was then transferred to an oven and left overnight at 403K. The resulting powder was then loaded into ceramic combustion boats (Fisher Scientific) and calcined on a temperature programme of 5 °C min^{-1} up to 500 °C with a dwell of 2 hours in a furnace (Carbolite furnace RHF 1600) and then reduced to room temperature at 5 °C min^{-1}. The sample formed was then milled with a mortar and pestle to form a fine powder and then passed through a 100 µm sieve, the portion which did not pass through the mesh was retaining.

2.2 Catalysts Characterization

There are many techniques for characterising catalysts, with respect to both physical and chemical properties. It has been known that the first stage in any gas-solid reactions

method is the adsorption of reactants on the catalyst surface; therefore, investigation of this surface is of interest. The keyword here is accessibility of reactants to the surface. The character of the catalyst surface can be determined by two sorts of adsorption called physisorption and chemisorption. Physisorption is utilized for total surface area and pore volume determination; molecules are adsorbed to the surface by van der Waals interactions, characterized by low heats of adsorption aproxmitly10 - 40 $kJ.mol^{-1}$. On the other hand, chemical adsorption requires higher heats between 80 - 400 $kJ.mol^{-1}$ for the breaking and forming of chemical bonds between the surface and the gas.

Essential characterization was carried out to explore and understand the textural structures and properties of the catalysts synthesized. Powder X-ray diffraction, surface area analysis BET, scanning electron microscopy with energy dispersive spectroscopy (SEM-EDS), temperature programmed reduction (TPR), temperature programmed conversion reaction (TPCR), temperature programmed oxidation (TPO) have all been used to characterize catalyst materials. Each of these techniques provides some information about the physical and chemical properties of the catalyst and further details will be discussed in the following sections.

2.2.1 Powder X-Ray Diffraction Theory

X-rays are an important non-destructive, high energy, short wavelength form of electromagnetic radiation. Powder XRD is used for structural phase identification of compounds which exist within the sample, determination of lattice parameters, provides information regarding the crystallite sizes and even full structures using Rietveld refinements.

Generally, the powder X-ray diffractometer contains three main components: the X-ray generator tube, sample holders, and detector as shown in figure (2.2). High energy electrons from a heated tungsten filament are accelerated by a high voltage to bombard a metal target which is usually copper generating X-rays that exit the tube towards a fine powder material, the strength with which an atom scatters light corresponds to the number of electrons around the atom.

The X-rays scattering from atoms produces a diffraction pattern that gives an indication about the atomic arrangement within the crystal. For example, an amorphous material does not have a periodic array of atoms with long-range order, so they do not produce the diffraction pattern. Whereas a crystalline material gives a pattern containing a series of sharp peaks due to the arrangement of atoms within the 3-D structure, whilst amorphous substances have noisy backgrounds because of the random nature of the arrangement of atoms. Diffraction occurs when the X-rays are scattered by a periodic array with a long-range order of atoms within the crystal, producing constructive interference that satisfies the Bragg equation depending on the 2θ angle as shown in figure (2.3).

This causes a signal spike at specific detector angles, and it is important to have a sufficient number of crystals to have an even distribution at all possible crystal orientations. During a scan, the detector is rotated over a range of angles to detect bands of diffracted x-ray produced by the correctly aligned crystals within the sample. The intensities of the reflected X-rays are dependent on the electron densities around the atoms.

The types of atom and interatomic distances are specific to each crystal structure, resulting in a characteristic XRD pattern, so crystalline materials have a unique XRD pattern and peak intensity which is affected by the type of atoms and their position within the unit cell.

The crystal sizes of the crystalline materials can be determined using the Scherrer equation [14], as larger crystallites give narrower peaks.

$$D = \frac{0.9\lambda}{\beta.cos\theta} \qquad [2.1]$$

D = the crystal size, λ = the wavelength of the Cu Kα radiation, β = the full width at half maximum of the diffraction peak of the sample, θ = the Bragg diffraction angle.

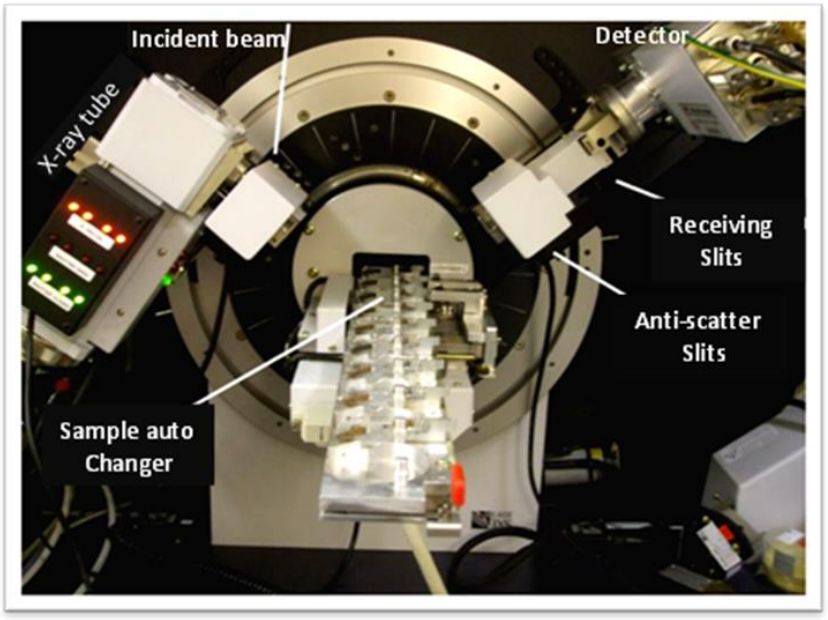

Figure 2.2: Image of a laboratory powder X-ray diffractometer (Bruker D8 Advance).

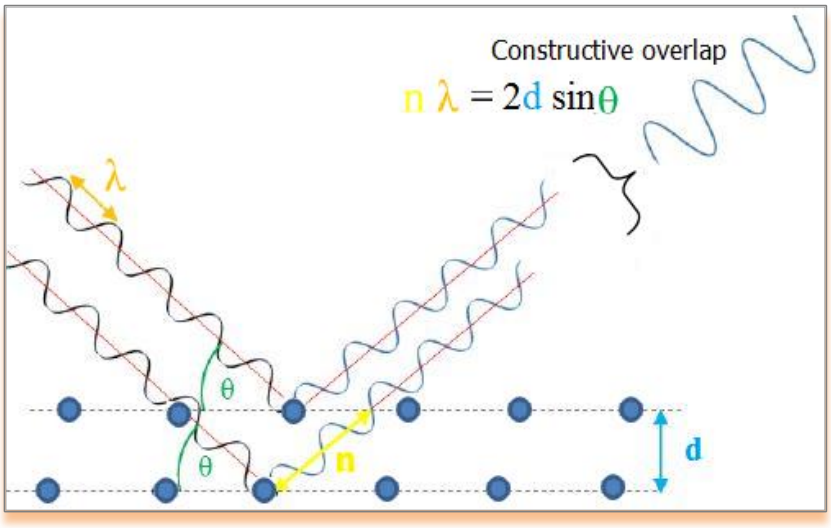

Figure 2.3: Schematic representation of Bragg's law, the XRD pattern should show a peak corresponding to this reflection.

2.2.2 XRD Measurement for all Prepared Catalysts

The powder X-ray diffraction patterns for all samples were recorded using a Bruker D8 Advance powder X-ray diffractometer using Cu Kα radiation with a wavelength of 1.5406 A° with a 2θ range of 10° to 90° scanning at 4° min^{-1} at 0.07° steps. All peaks in the X-ray patterns of perovskite materials were identified using the "Eva" software and the crystallography open database (COD) which is supplied by Bruker. The most distinct peaks relating to the crystallite were selected and crystallite size was determined via the Scherrer equation, as described in Section 2.2.1. The width of higher intensity peaks at half maximum and corresponding 2θ values for use in the Scherrer equation analysis were determined using EVA software.

2.2.3 Brunauer-Emmett-Teller (BET) Theory

Brunauer–Emmett–Teller (BET) theory is an important analysis technique for the measurement of the surface area of materials which aims to elucidate the physical adsorption of gas molecules on a solid surface. This theory applies to systems of monolayer and multilayer adsorption and usually utilizes probing gases such as nitrogen that do not chemically react with material surfaces as adsorbates to calculate the specific surface area. Therefore, standard BET analysis is most often conducted at the boiling temperature of N_2 (77 K).

The first article about the BET theory was published in 1938 by Stephen Brunauer, Paul Hugh Emmett, and Edward Teller [15]. The idea of the theory is a continuation of the Langmuir theory, which is a theory for monolayer molecular adsorption, to multilayer adsorption with the following assumptions: physical adsorption of gas molecules on a solid surface occurs in infinite layers with no lateral interactions between adsorbed species, gas molecules only interact with adjacent layers, and the Langmuir theory can be applied to each layer. Nitrogen physisorption analysis is an important way to determine the surface area, total pore volume and pore size of the catalysts. When a material is exposed to a gas, intrinsic surface energy acts to attract the gas molecules to the solid surface sites.

The result of the interaction between the exposed surface of the solid and the gas molecules is characterized as physical (or Van der Waals) adsorption, thus the amount of gas adsorbed thereby filling the surface layer by layer is dependent on the available solid surface sites and the relative vapour pressure, in contrast to the stronger chemical attractions associated with chemisorption. The type of materials whether porous or nonporous under investigation can be characterised by the type of isotherm obtained as shown following in figure 2.4 [16].

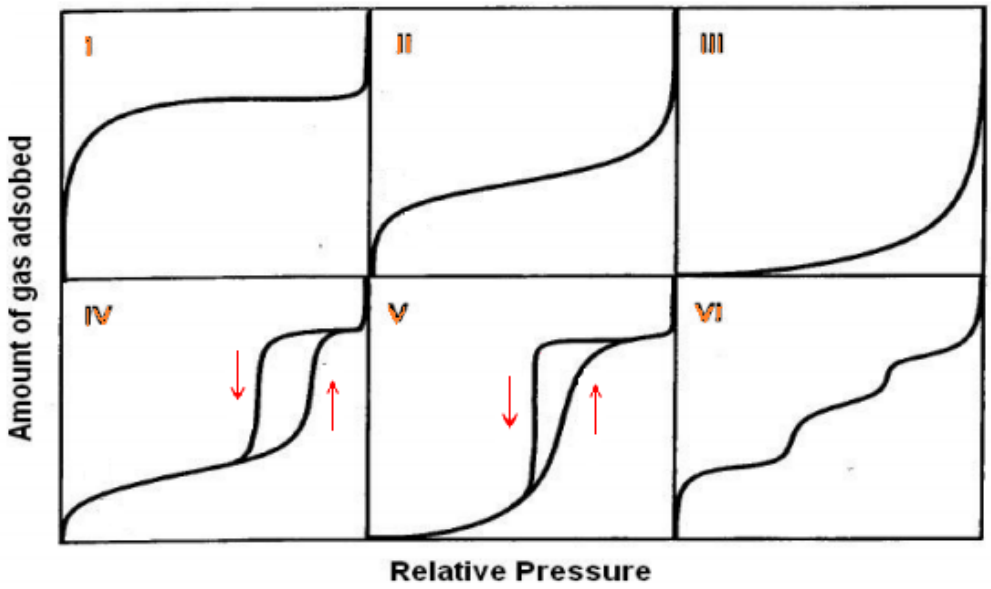

Figure 2.4: The IUPAC classification that represents the types of sorption isotherms which found due to different gas/solid interactions at relative vapour pressure $P/P_{\circ}$ [16].

Type I: isotherm is given by microporous solids materials and chemisorption isotherms e.g. charcoal. It is clearly Langmuir monolayer type.

Type II: for non-porous or macroporous solids materials.

Type III and type V: porous materials with cohesive force between adsorbate molecules greater than the adhesive force between gas adsorbate molecules and adsorbent, typical of vapour adsorption (i.e. water vapour on hydrophobic materials).

Type IV and type VI: isotherms are given by a mesoporous adsorbent which staged adsorption the first monolayer then build-up of additional layers.

2.2.4 Surface area Measurements for Perovskite Catalysts

For catalytic uses, specific surface area and crystal structure play important roles. Therefore, the syntheses of perovskite materials for catalytic applications always focus on obtaining crystalline materials with a high specific surface area. BET surface areas for the

catalytic samples were investigated using a Quantachrome Autosorb-1 apparatus, the samples of about 200 mg were outgassed at 350 °C in vacuum for 5 hours prior to analysis to ensure that all contaminants and moisture were removed.

Following this step, the catalyst material was brought to constant temperature by using an external bath containing liquid nitrogen; in addition, a small amount of N_2 gas was introduced into the sample chamber as the adsorbate upon the solids adsorbent. Finally, the surface area was calculated by the BET method (shown in equation 2.2) from the monolayer amount of adsorbed. BOC scientific high purity (> 99.99%) nitrogen gas was used as the adsorbate for the adsorption measurements.

$$\frac{P}{V(P_\circ - P)} = \frac{1}{V_m C} + \frac{C-1}{V_m C}\left(\frac{P}{P_\circ}\right) \qquad [2.2]$$

V is the amount adsorbed, P represents the equilibrium pressure at temperature of adsorption, $P_\circ$ represents the saturation pressure at temperature of adsorption and Vm is the volume of adsorbate gas forming monolayer coverage of sample. C is related exponentially to the enthalpy of the first adsorbed layer, (showed in equation 2.3).

$$C = \exp\frac{(H_1 - H_2)}{RT} \qquad [2.3]$$

The BET equation requires a linear relationship between P/V($P_\circ - P$) and $P/P_\circ$, thereby producing a BET plot.

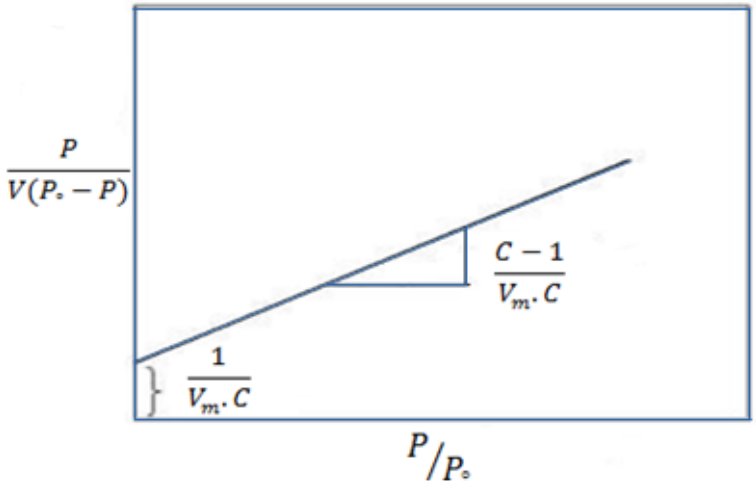

Figure 2.5: BET plot show the linear relationship between $P/\,\mathrm{V}(P_\circ - P)$ and $P\,/P_\circ$.

BET isotherm and surface area data were obtained for each catalyst sample. Integrated AUTOSORB software, on a computer interfaced to the Autosorb-1 analyser, was used for data acquisition and processing.

2.2.5 Scanning Electron Microscopy SEM and EDX Spectroscopy Theory

EDX–SEM was used to get qualitative and quantitative information about the elements that actually exist in a composition of the sample and distribution of metals in the catalyst sample. SEM provides high magnification image with tremendous resolution for surface morphology. The surface of the sample can be used to identify the surface coverage homogeneity and any surface impurities or segregation prior to a reaction. At the top of the microscope, a tungsten filament under vacuum produces an electron beam that follows through the magnetic fields and lenses towards the sample.

An objective lens focuses the beam to a fine point on the sample. As the electron beam collides with the sample, x-rays and electrons are released. Secondary electrons and backscattered electrons are detected by a backscattered electron (BSE) detector and this

provides the sample image. An adjacent x-ray detector detects the x-rays ejected from the atoms allowing compositional chemical analysis as the emitted x-rays are characteristic of each element.

The morphologies and structures of the samples were characterized by SEM, which was undertaken on a Hitachi TM3000 scanning electron microscope with a magnification of up to X 30 K and a Bruker Quantax 70 EDX system.

2.3 Catalyst Test System using Quadrupole Mass Spectrometry

Mass spectrometry is a powerful analytical technique used to quantify known materials. This process involves the conversion of the sample into gaseous ions, with or without fragmentation and then detection and quantification of ions and ion fragments. All catalysts prepared in this project were evaluated by a catalytic test system displayed schematically in Figure 2.6.

As can be seen, there are three main sections: first one is a manifold, the second is the catalytic micro reactor, and the third one is the gas analysis system. The manifold consists of a gas tight stainless steel that is fed from gas cylinders such as hydrogen, methane, oxygen, carbon dioxide and helium. Helium was used as a carrier gas, with a typical flow rate of 18 ml/ min employed. The gases were directed to a stainless-steel manifold via molecular sieve traps which were used to remove any water, where they were combined to achieve the required gas composition. These pure gases were fed to the reactor tube in which the catalysts was present within a quartz tube using 1/8 inch stainless steel piping throughout the manifold, with the ability to control the flow rate by mass flow controllers.

A bubble flow system was used to measure the flow rate of each gas. Each gas was controlled individually using a mass flow controller with the exception of a helium line that was used as a bypass gas to ensure the continuous flow of gas through the Quadrupole Mass Spectrometer (QMS) during setup of reactant gas composition. This line was controlled using a Swagelok needle valve. The temperature was varied using a ceramic furnace which contained in the centre a k-type thermocouple placed as close as possible to the reactor tube that contained the catalyst material.

The temperature was monitored via Eurotherm temperature controller. The temperature controller allows for temperatures between room temperature and more than 1000 °C to be used and also the use of temperature programs including multiple ramps and dwell periods. The product gases are transported to the quadrupole mass spectrometer (QMS) where the masses were analysed. The whole process is carried out under computer control with simultaneous monitoring of a number of possible products.

RGA (Residual Gas Analyser) software for Windows was used in order to control the analyser and display a real-time analysis of chosen masses. All data was stored using the RGA for Windows program onto the interfaced computer in a text format. Microsoft Excel was then used to format the data into Excel which is considered the standard program used to manipulate and display the data.

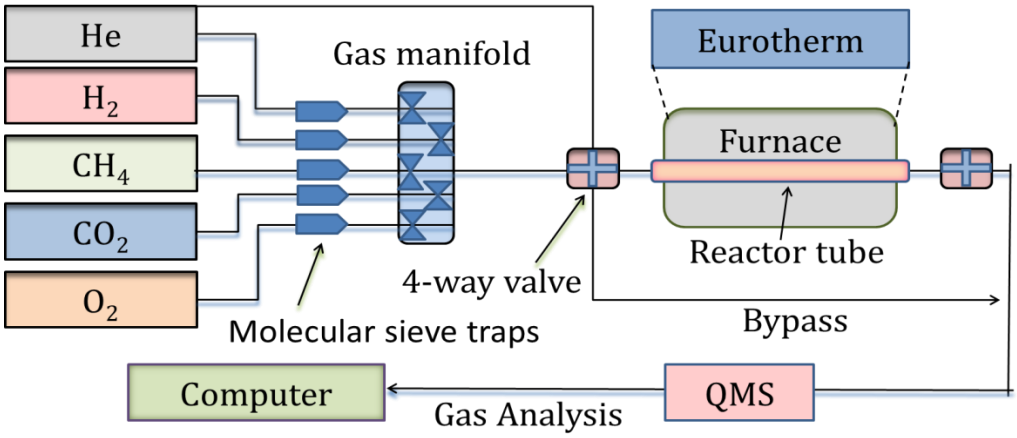

Figure 2.6: Schematic diagram representative apparatus for catalyst testing.

2.3.1 Reactor tube preparation

Catalytic investigations required 20 mg ± 0.5 mg of catalyst material be loaded into a quartz reactor tube. The quartz reactor tube of dimensions 240 mm in length with an inner diameter of 5 mm and thickness of 1 mm, containing the catalyst were placed in the centre of the furnace of dimensions 210×110×155 mm as shown in figure 2.7. This quartz tube was used to keep the catalyst in the centre of the furnace and within the tube was held in position between two quantities of quartz wool to ensure that no catalyst movement occurred during reforming reactions.

Cajon Swagelock fittings were used to connect the quartz tube to the gas flow system and to ensure a gas-tight seal. The furnace consisted of two ceramic bricks which had each been hollowed out on one side. One brick was placed on top of the other, with the hollows facing inwards to form a cavity. Each hollow of top and bottom furnace contained resistive Ni/Cr wire purchased from Advent Research Materials Ltd wrapped around 6 ceramic tubes which wired together to form a heating filament. The temperature of the furnace was

measured using a K-type thermocouple, which was inserted into the centre of the furnace cavity through a thin hole that had been drilled into the rear of the lower brick.

The thermocouple was connected to Eurotherm 818 temperature programmed controller that could achieve linear heating rates of 5-20 °C min^{-1} and furnace temperatures of up to 1000 °C. Gases from the reactor tube were passed to a four-way valve to a vent or by a direct route to the on-line Quadrupole Mass Spectrometer (QMS) for real-time analysis. This system set up allowed two flows of different gases in parallel, one flow in the reactant line which contained a premeasured mix of gases and the second line contained pure helium which could be directed over the furnace when necessary in order to provide an inert atmosphere for the pre-reaction of the catalyst.

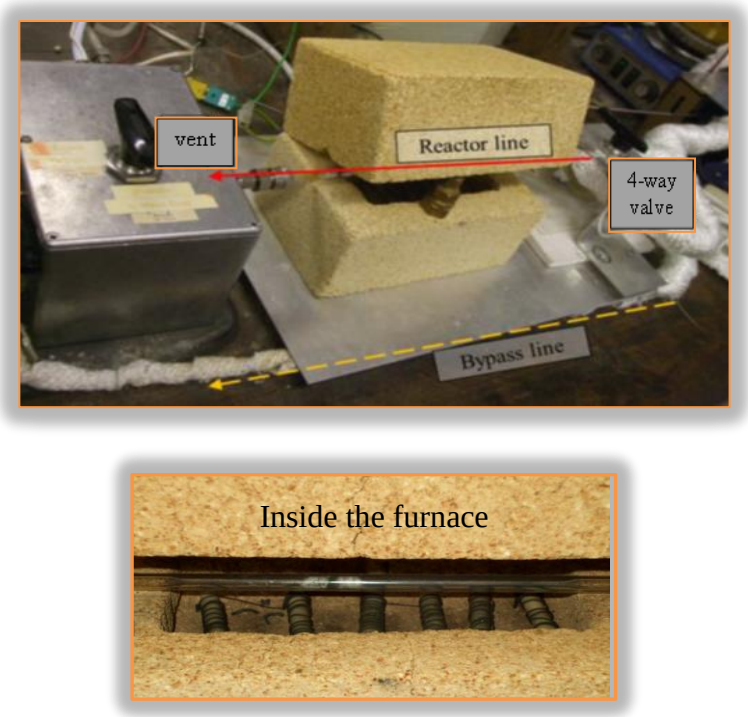

Figure 2.7: Photographs of ceramic furnace showing thermocouple, the layout of the quartz reactor tube and bypass line.

2.3.2 Gas-flow rate and Relative Sensitivity measurements

The quadrupolar mass spectrometer (MKS Spectra Satellite Model) provides signal strength for mass/charge of ion fragments based on partial pressure; gases were ionised when entering the vacuum chamber by a thoria coated iridium filament for detection. The detected signal intensities of chosen masses of gases were displayed on a computer using Residual Gas Analysis (RGA) as the software for Windows.

Different gases were not ionised equally by the QMS filament, which meant the QMS was more sensitive to the detection of some gases like CO than others such as He. Therefore, sensitivity values were corrected to determine non-uniformity in ionisation of different ion fragments. O_2 was used as a reference gas to compare the other mass fragments against because of its ability for ionisation, and was given a sensitivity value of 1 and the other gases were calculated relative to this.

To measure the relative sensitivity value of a gas, a known flow rate of the gas (e.g. 1 cm^3 min^{-1}) was sent to the QMS with a known flow rate of oxygen (e.g. 1 cm^3 min^{-1}). In this case, flow rates were measured manually using a stopwatch and bubble flow meter, which was attached to the bypass line using a three-way valve. To calculate the relative sensitivity of the QMS to a fragment an applicable fragment is chosen for each gas of interest. The signal intensity is then measured for the chosen fragment and oxygen fragment after the gases signal intensities have settled. The following formula is used to gain a sensitivity value by recording several values and the average value used:

$$Gas\ Sensitivity\ Relative\ to\ Oxygen\ = \frac{Flow\ rate\ of\ O_2}{Flow\ rate\ of\ Gas} \times \frac{Reading\ for\ Gas\ Fragment}{Reading\ for\ O_2} \quad [2.4]$$

This sensitivity needed to be taken into consideration when analysing data as well as the helium correction which was determined using the initial helium signal value divided by

each subsequent value giving an intensity correction factor. Helium was chosen to calculate this due to being chemically inert and thus unaffected by the reaction conditions. These differences were then applied to all signal values for all reactive gases as shown in equation 2.5 using CH_4 as an example of how raw partial pressures of gases were corrected for using relative sensitivity and helium correction values to give the amount of each gas present. This difference was then applied to all signal values for all reactive gases.

$$Corrected\ Signal\ Strength\ for\ CH_4 = \frac{Signal\ CH_4\ Intensity}{CH_4\ Sensitivity} \times\ He\ Correction \qquad [2.5]$$

The corrected values were then applied to give a number of moles for each gas relative to moles of methane. Finally, these obtained values were plotted against temperature or time to display the reaction profile, depending on reaction type.

2.4 Investigational Protocol for Catalytic Reforming

There are a range of techniques for studying surface reactions. All reactions were first reduced by using a temperature programmed reduction (TPR) in order to increase the activity of catalyst materials and then carried out as a function of temperature or time by temperature programmed conversion reaction (TPCR), before analysing the carbon deposition by temperature programmed oxidation reaction (TPO). More details are given in the sections below.

2.4.1Temperature Programmed Catalyst Reduction (TPR)

Temperature programmed reduction is a technique used for the characterization of solid materials such as heterogeneous catalysis to make the metals in the materials electronically

rich. So pre-treatment conditions of the catalysts is an important factor to activate and control their performance because this fact determines the nature and amount of active sites that could be present on the catalyst.

The catalyst material is usually reduced in a hydrogen atmosphere in the presence of inert gas [17, 18]. Each gas was supplied from pressurised cylinders to the gas manifold through separate gas tight stainless steel tubing lines with Swagelok fittings. A mixture of 2 ml min^{-1} of hydrogen in 18 ml min^{-1} of helium carrier were passed over the catalyst while the temperature was raised linearly from room temperature up to 900 °C at 10 °C min^{-1}. On reaching 900 °C the perovskite catalyst was quickly cooled under the same flow rate of hydrogen in helium until reaching room temperature to prevent re-oxidation.

Output gases were constantly carried to the QMS for analysis, with readings saved at 12 sec periods, corresponding to a 2 °C increase per reading. After a reaction completion, any data stored on the computer interfaced to the mass spectrometer was stored in the form of relative signal intensities for each gas monitored. Sensitivities for each gas determined during calibration (section 2.3.2), were then applied to the relative gas signal intensities in order to gain the actual amounts of each gas detected by the QMS.

TPR profiles were gained by measuring hydrogen consumption and water production as a function of temperature. The characteristics of the peak area and the reduction temperature depend on the experimental conditions, the hydrogen concentration, the nature of the oxides, and the flow rate of the reducing gas mixture. The area of the reduction peak gives an indication about the levels of the hydrogen uptake by the catalyst during reduction reaction.

2.4.2 Temperature Programmed Conversion Reaction (TPCR)

TPCR technique provides information for comparing and screening different catalyst materials for different reforming reactions under different reaction conditions. After completion of the reduction treatment and before switching the flow of gases to the catalyst material, appropriate mixtures of reactant gases were passed and monitored out through the bypass line using the QMS to ensure that no change in gas quantities had occurred during the course of the reaction.

Once the reactant gases had been adjusted, the Eurotherm was programmed to the required temperature and initial readings were recorded for 5 minutes by the QMS for the reactant gases alone. Temperature programmed surface reaction was performed by using a mixture of 1ml min^{-1} of CH_4, 0.5 ml min^{-1} of O_2 in helium carrier for methane partial oxidation reforming, 1ml min^{-1} of CH_4, 0.5 ml min^{-1} of CO_2 in helium carrier for biogas reforming and 1ml min^{-1} of CH_4, 1ml min^{-1} of CO_2 in helium carrier for dry reforming.

For each run, the stream of reactant gases was passed through the reactor tube over ~20 mg of catalyst sample. The furnace temperature was ramped from room temperature up to 900 °C at 10 °C min^{-1} and then reversed at 5 °C min^{-1} down to room temperature in order to produce a good profile of activity and observe any hysteresis across the temperature range [19].

At the end of the reaction period the product gases were diverted away from the furnace to the bypass line and a flow of pure helium was re-established to allow the furnace to cool to room temperature in preparation for temperature programmed oxidation (TPO). Finally the data is plotted against temperature to give a reaction profile which provides information about the suitable temperatures for complete, or near to complete reactant consumption.

Immediately after each TPCR run in which the catalysts were tested for the effect of using different oxidant with different feed ratio, each sample was subjected to in situ TPO technique to characterize the quantity of carbon formed during reforming reaction.

2.4.3 Temperature-Programmed Isothermal reactions

Temperature programmed isothermal reaction is an analysis method to monitor the catalytic activity over a specific period of time at a specific reaction temperature. All isothermal experiments were performed with the same quantity of gasses that mentioned in (Section 2. 4. 2) for each catalyst at three constant temperatures (700 °C, 800 °C, and 900 °C) for a period of 20 hours. These three temperatures were chosen as the reaction started to achieve acceptable conversion and reach or near to reach the equilibrium constant at which catalyst can catalyse methane for synthesis gas production.

After the reduction of the catalyst and the reactant gases had settled through the bypass line. While the furnace was heated to the required temperature, gases were passed through the bypass line and the temperature was maintained for 6 min until the measured temperature inside the catalyst bed was stabled. Then the mixture of reactant gases was passed through reactor tube over ~20 mg of the catalyst material for the 20 hours period of time. The measured reactant gases were monitored using the QMS and RGA program. At the end of 20 hours, the reactant gases were once again passed through the bypass line while the furnace cooled to room temperature in preparation for in situ carbon deposition measurement by temperature programmed oxidation reaction.

2.4.4 Temperature Programmed Oxidation-post reaction measurement

This post- measurement was used following catalytic reforming reaction (Section 2. 4. 2) and following isothermal reaction (Section 2. 4. 3) to quantify any mass of carbon that may have been deposited on the catalyst surface during reforming reaction test. This TPO reaction was carried out in the same way to the TPR reaction, with readings saved at 12 second intervals, identical to a 2 °C increase per reading. The temperature was raised from room temperature up to 900 °C at 10 °C min^{-1}, whilst 2 ml min^{-1} oxygen in 18 ml min^{-1} helium was passed through the reactor tube over the catalyst. Carbon deposited on the catalyst is gasified in the form of carbon dioxide and carbon monoxide which are then passed to the QMS for analysis.

The resulting profile for carbon dioxide and carbon monoxide were quantified by integrating the peaks and compared to pre-determined calibration, which gives some information about the mass quantity of carbon and the nature of the coke [20]. Different peaks of CO_2 production at different temperatures in a TPO profile correspond to the number of different types of carbon. The total area of the CO_2 peaks gives an indication to the level of carbon deposited on the catalyst. Samples were not removed from the reactor tube between any of the reduction or oxidation procedures.

2.4.5 Reactant Conversion and Product Analysis

Different calculations were performed to quantity the percentage of conversions of reactant (CH_4 and CO_2) and the yield of product (H_2, and CO) by using equations below respectively:

$$CH_4\ conversion\ (\%) = \frac{M_{CH_4,in} - M_{CH_4,out}}{M_{CH_4,in}} \times 100 \quad [2.6]$$

$$CO_2\ conversion\ (\%) = \frac{M_{CO_2,in} - M_{CO_2,out}}{M_{CO_2,in}} \times 100 \quad [2.7]$$

$$Y_{CO}\ (\%) = \frac{M_{CO,out}}{M_{CO_2,in} + M_{CH_4,in}} \times 100 \quad [2.8]$$

$$Y_{H_2}(\%) = \frac{M_{H_2,out}}{2M_{CH_4,in}} \times 100 \quad [2.9]$$

$$\frac{H_2}{CO}\ ratio = \frac{M_{H_2,out}}{M_{CO,out}} \quad [2.10]$$

All reactions were carried out over ~20 mg of catalyst (weighed initially in its unreduced form). Thus each catalyst material was studied with respect to methane reforming over a range of temperature started from room temperature up to 900 °C in addition to specific three temperatures 700 °C, 800 °C and 900 °C for 20 hours of reaction for methane partial oxidation ($1CH_4$: $½O_2$), dry reforming ($1CH_4$:$1CO_2$), and methane-rich ($2CH_4$:$1CO_2$) conditions.

2.5 References

[1] T. Adschiri , Y. Hakuta, and K. Arai, *Ind. Eng. Chem. Res*., 2000, **39**, 4901–4907.

[2] V. S, Hongwei Zhu, R. Vajtai, P. M. Ajayan , and B. Wei, *J. Phys. Chem. B*, 2005, **109**, 20207–20214.

[3] http://en.wikipedia.org/wiki/Hydrothermal_synthesis. This page was last modified on 20 June 2015, at 12:18.

[4]http://www.parrinst.com/wpcontent/uploads/downloads/2011/06/4700MB_Parr_Sample - Preparation-Vessels-Literature.pdf.

[5] J. Livage and D. Ganguli, *Solar Energy Materials & Solar Cells*, 2001, **68**, 365-381.

[6] S. Royer, F. Be´rube´ and S. Kaliaguine, *Appl. Catal., A: Gen.,* 2005, **282,** 273–284.

[7] S. Royer, D. Duprez, F. Can, X. Courtois, C. Batiot-Dupeyrat, S. Laassiri, and H. Alamdari, *Chem. Rev.*, 2014, **114**, 10292–10368.

[8] Z. Junwu, S. Xiaojie, W. Yanping, W. Xin, Y. Xujie, and L. Lude, *J. Rare Earths*, 2007, **25**, 601-604.

[9] S. Specchia, A. Civera and G. Saracco, *Chem. Eng. Sci.* 2004, **59**, 5091 – 5098.

[10] A. Civera, M. Pavese, G. Saracco, and V. Specchia, *Catal. Today*, 2003, **83**, 199–211.

[11] A. J. Dillen, R. J.A.M. Terörde, D. J. Lensveld, J. W. Geus, and K. P. Jong, *J. Catal.*, 2003, **216**, 257–264.

[12] C. Chen, J. Cheng, S. Yu, L. Che, Z. Meng, *J. Crystal Growth*, 2006, **291**, 135 –139.

[13] A. M. Diskin, PhD Thesis, Keele University, 2000.

[14] B. A. Josephine, A. Manikandan, V. M. Teresita, and S. A. Antony, *Korean J. Chem. Eng.*, 2016, **33**, 1590-1598.

[15] S. Brunauer, P. H. Emmett and E. Teller, *J. Am. Chem. Soc*., 1938, **60**, 309 –319.

[16] S. Lowell, J. E. Shields, M. A. Thomas and M. Thommes, *Characterization of Porous Solids and Powders: Surface Area, Pore Size and Density*, 2012, 349.

[17] C. K. Chang, Y. J. Chen and C. Yeh, *Appl. Cata. A: Gen.*, 1998, **174**, 13-23.

[18] J. Xiaoyuan, L. Guanglie, Z. Renxian, M. Jianxin, C. Yu and Z. Xiaoming, Appl. *Surface Science*, 2001, **173**, 208-220.

[19] J. Staniforth, S. E. Evans, O. J. Good, R. J. Darton and R. M. Ormerod, *Dalton Trans*., 2014, **43**, 15022–15027.

[20] R. M. Ormerod, *Studies in Surface Science and Catalysis*, 1999, **122**, 35-46.

Chapter 3

Characterisation Of Catalyst

3. Catalyst Characterisation

3.1 Introduction

Characterization is a central aspect of catalyst development and refers to the general process by which a material's structure, composition, and properties are measured. In heterogeneous catalysis studies, two principal objectives may be distinguished: (1) The characterization of the catalysts to gain information relevant to understanding the catalytic phenomenon; and (2) the testing of catalysts to get information relevant to performance in terms of activity.

These objectives provide a better understanding of the relationship between catalyst properties and catalytic performance which is essential to optimize reaction conditions to develop more active, selective, and durable catalysts. The first objective depends on determining an "identity card" for the catalyst, indicating its structure, morphology, surface area, porosity and other fundamental physicochemical data.

This information is important for a meaningful comparison of catalysts synthesized under different conditions and laboratories. The second objective concerns the catalytic reaction process and involves several steps: reagent transportation to the active site surface, chemisorption of at least one reagent, formation of the reaction intermediate, product desorption and regeneration of the catalyst [1].

Nickel-based catalysts have been shown to be one of the best catalysts for reformation of methane actively and economically. However, there are several obstacles when using nickel involving carbon formation, deactivation, sintering and poisoning with sulphur. Perovskite catalysts have been shown to have great potential as they have a wide range of desirable properties such as higher resistance to carbon formation [2, 3], sulphur

resistance [4, 5], redox stability [6]. flexibility to accept a wide range of elements into the structure via partial substitution at either the A or B site, leading to an increase in dispersion and reduction in sintering [7]. Reactions that are catalysed by mixed metal oxides as heterogeneous catalysts occur through a phenomenon called redox catalysis, which via loss and gain of surface lattice oxygen of the catalyst and the gas phase. The reoxidation will be very fast when the oxygen vacancies are located near the surface.

In the last decades, a new approach for developing catalyst performance in terms of enhancing methane conversion has been through the utilization of bi-metallic catalysts [8]. Several studies have showed that the combination of two metals can be more effective than the single metal-based catalysts in terms of increased hydrogen selectivity, resistance to coke accumulations and catalytic activity [9, 10]. This study describes perovskite catalysts consisting of co-doped strontium zirconates using various transition metals (Fe, Ru, Ni, and Al) prepared by hydrothermal methods using nitrate precursors in an effort to find active and selective catalysts for synthesis gas production at low temperatures.

3.2 XRD pattern for all prepared catalysts

XRD analysis was performed in order to evaluate the degree of crystalline materials synthesized and to identify any precursor impurities. Dense mixed metal oxide perovskite catalysts for reforming reactions have been prepared by a low-temperature synthesis hydrothermal route unlike the traditional solid state method which requires a high calcination temperature. Hydrothermal synthesis was chosen as in most cases it produces small particle size [11] and previously it has been observed that small particle size catalysts have the greatest catalytic activity towards the reforming process [12]. It also, has been

shown that using hydrothermal synthesis leads to the production of materials or phases that cannot be synthesised by other techniques [13] as shown in figure 3.1.

The characteristic peaks at 2θ = (30.2 °, 43.4°, 53.9 °, 63.5 °) assigned to the basic $SrZrO_3$ perovskite can be observed in all the patterns of the samples.

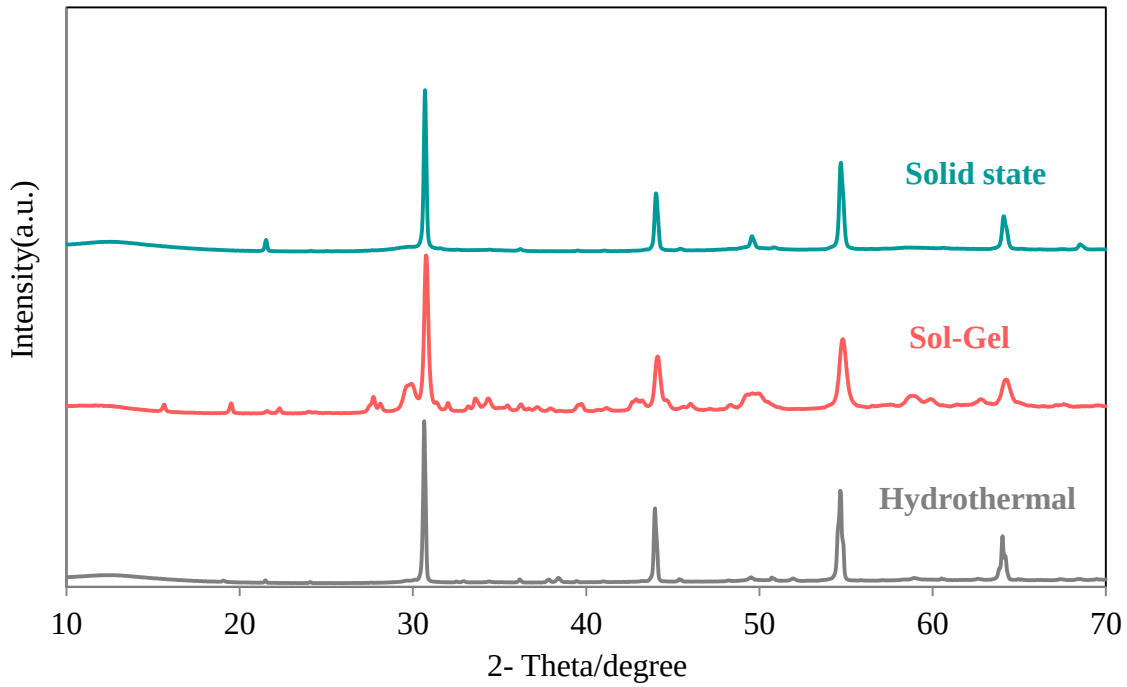

Figure 3.1: Comparison of the XRD patterns for 4 mol% Ni doped $SrZrO_3$ perovskite in different preparation methods.

These results show that the preparation method plays an important role in determining the textural properties of the prepared catalysts.

The x-ray patterns of all prepared perovskite catalysts shown in figures 3.2, and the corresponding unit cell parameters are shown in table 3.1. The patterns for each of the three catalysts (Ni- Fe, Ni- Ru, and Ni- Al) doped $SrZrO_3$ perovskite materials do not show significant differences in peak position. This suggests that a small amount (1mol %) of active metal substitution on the Zr^{4+} site does not have a significant effect on the structure.

The x-ray patterns of the perovskite materials prepared in this study illustrate the expected orthorhombic (Pbnm) unit cell structure with lattice parameters and unit cell volume shown in table 3.1. The lattice parameters for $SrZrO_3$ and Ni doped $SrZrO_3$ have been taken from the literature [14].

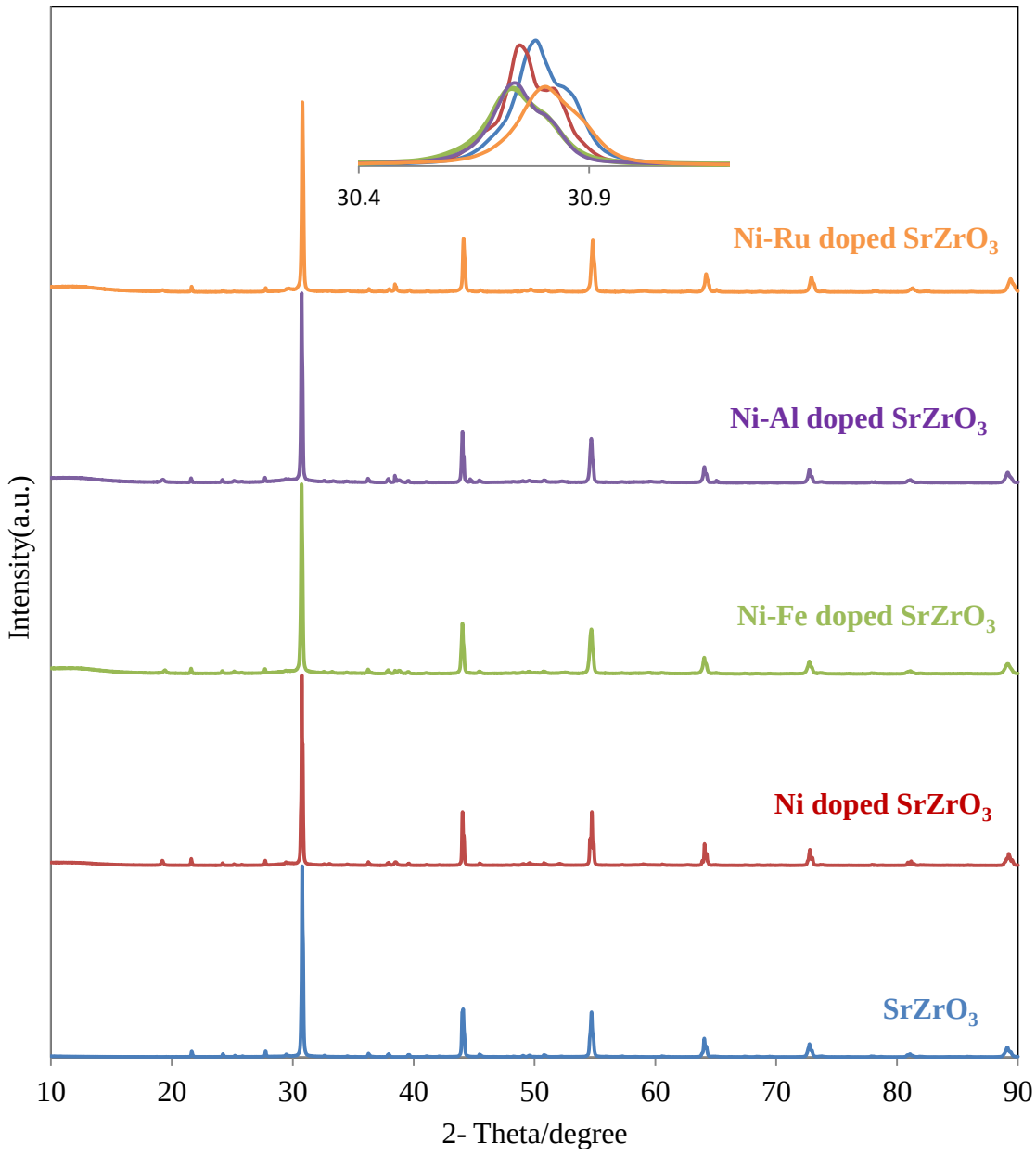

Figure 3.2: Powder X-ray diffraction patterns of (1) $SrZrO_3$, (2) Ni doped $SrZrO_3$, (3) Fe-Ni doped $SrZrO_3$, (4) Al-Ni doped $SrZrO_3$, (5) Ru-Ni doped $SrZrO_3$ from down to up.

Table 3.1: The unit cell parameters and cell volume to the perovskite catalysts.

Samples	Unit cell parameters A°			Cell volume A^3
	a	b	c	
$SrZrO_3$	5.7920	5.8130	8.1960	275.95
Ni doped $SrZrO_3$	5.7948	5.8014	8.1985	275.62
Ni-Fe doped $SrZrO_3$	5.8118	5.8067	8.2187	277.36
Ni-Al doped $SrZrO_3$	5.8034	5.8085	8.2215	277.14
Ni-Ru doped $SrZrO_3$	5.9801	5.7950	8.1929	283.92

In the current research, the pH conditions for all the perovskites formed under hydrothermal condition were investigated. It was observed that a highly alkaline medium is necessary for the production of phase pure perovskites as shown below in figures 3.3, 3.4, and 3.5.

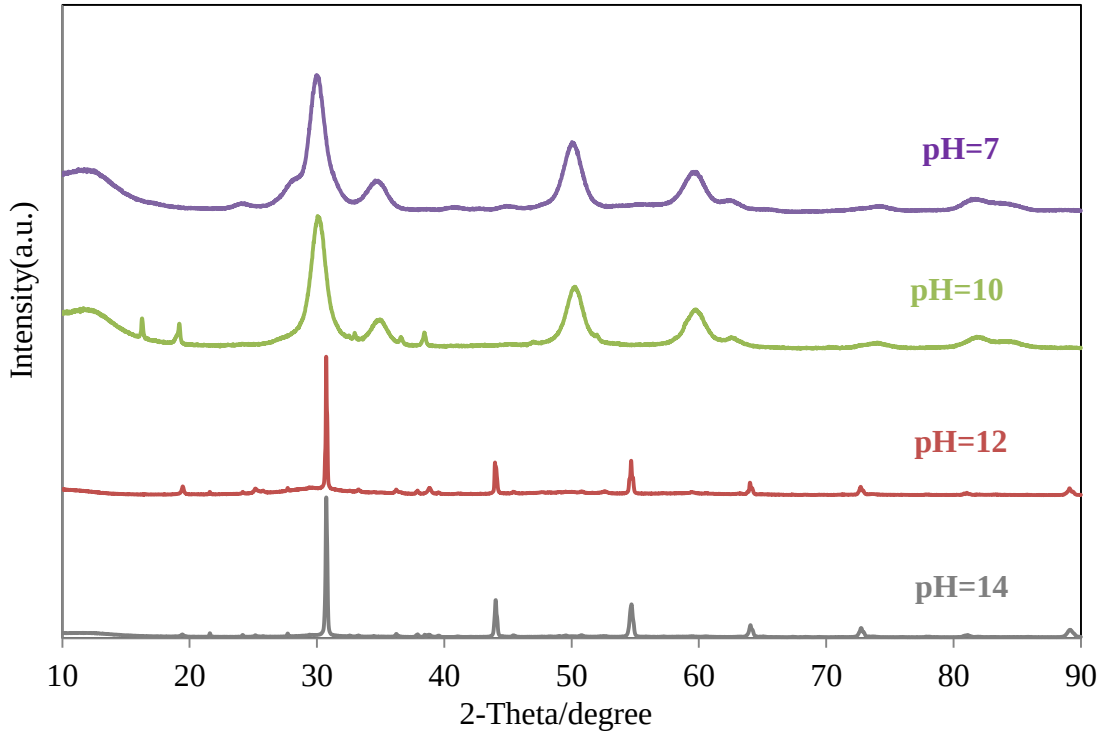

Figure 3.3: Powder XRD patterns of Ni-Fe doped $SrZrO_3$ perovskite at different pH.

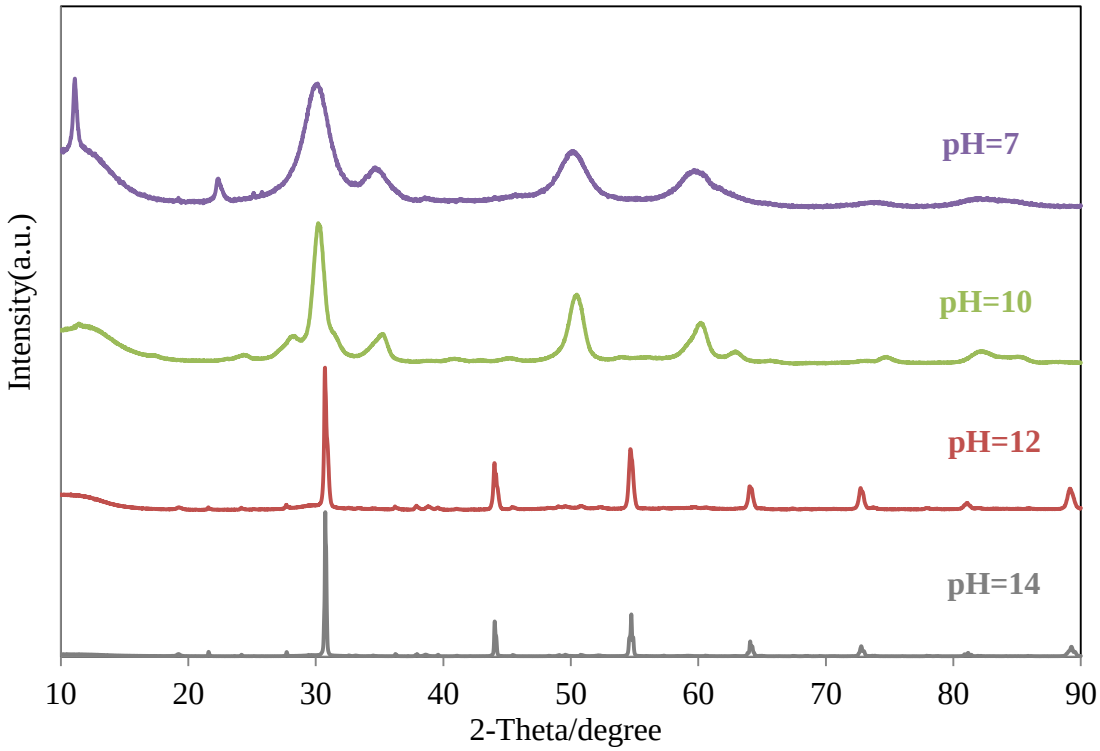

Figure 3.4: Powder XRD patterns of Ni-Al doped $SrZrO_3$ perovskite at different pH.

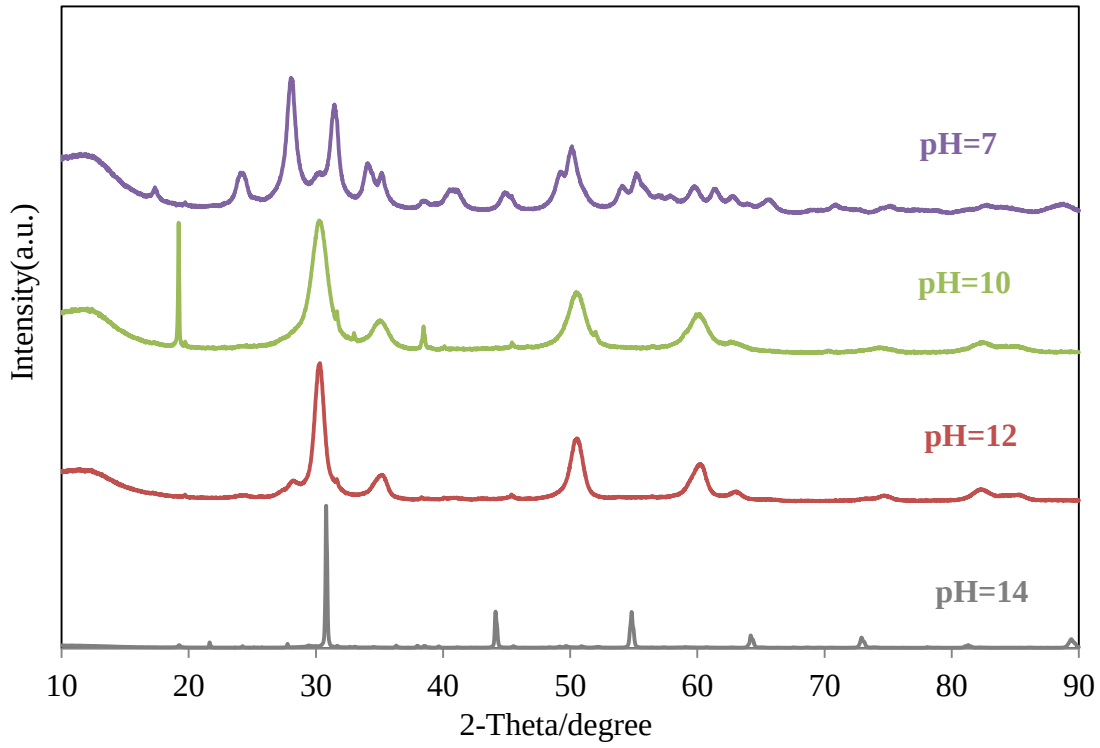

Figure 3.5: Powder XRD patterns of Ni-Ru doped $SrZrO_3$ perovskite at different pH.

From the figures above it can be observed that there is a clear decrease in crystallinity with a decrease in pH value and that accurately adjusting the solution pH can be crucial in these reactions in addition to other factors such as reaction temperature and time. The reactions at the lower pH values show that no perovskite product was formed and only metal oxides such as ZrO_2, SrO and NiO were present in the samples.

Furthermore, a range of Fe, Al, or Ru doping from 0.05 - 0.2 g was used to evaluate the optimum level of active metal doping for keeping phase purity. The results showed that the maximum amount of active metal that can be incorporated successfully within the structure without producing impurities is 0.05 g.

In situ high temperature XRD studies were carried out to investigate the effect of temperature on the crystal structure and thermal stability of the perovskite samples. As shown in figures 3.6, 3.7, 3.8 and 3.9, a heating stage allowed rising temperatures from room temperature up to 900 $^{\circ}$C to be reached over nine stages (100 - 900) $^{\circ}$C and then down to 100 $^{\circ}$C again, whilst XRD investigations were collected in situ, at these specific temperatures.

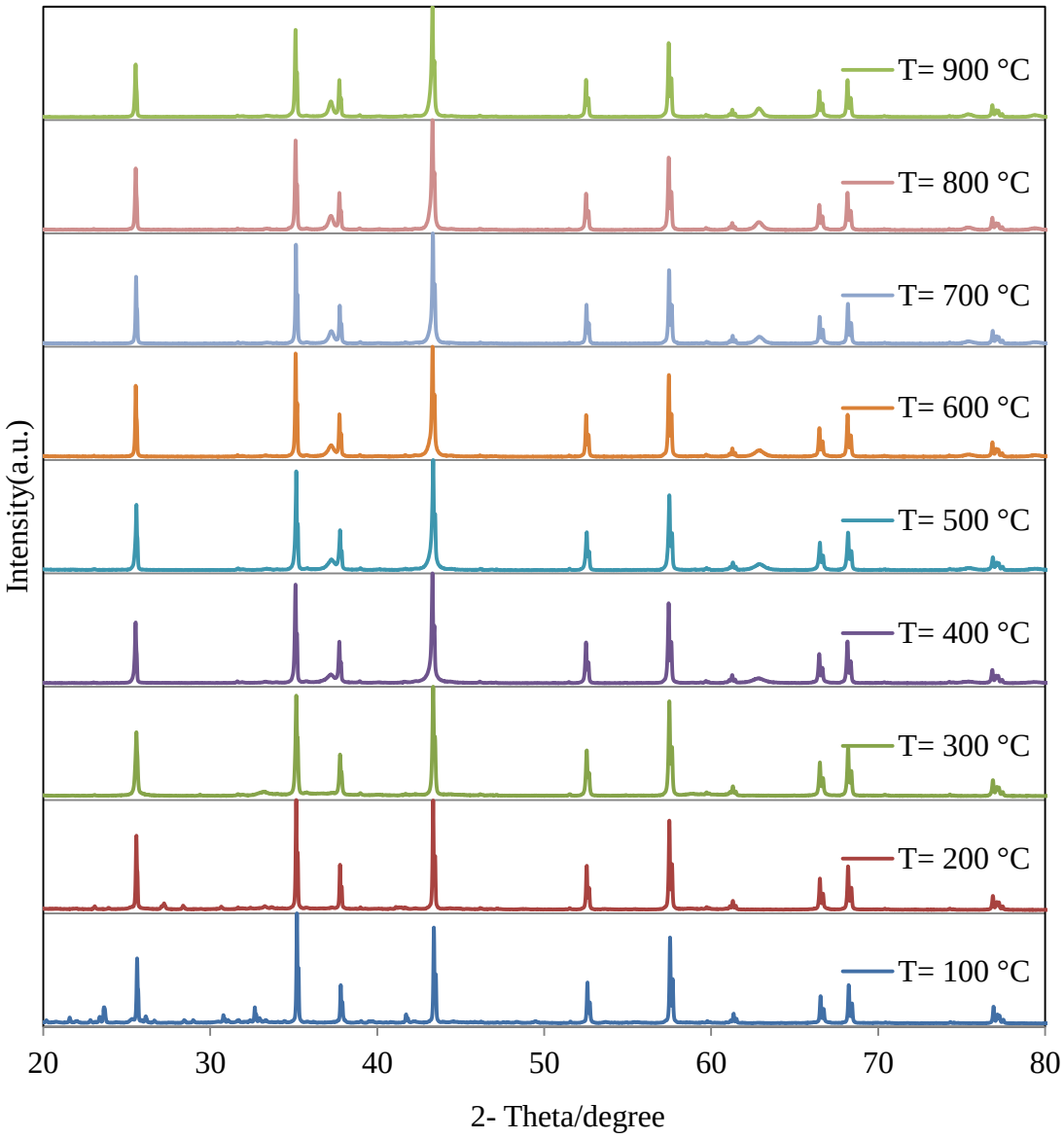

Figure 3.6: XRD pattern of 10% Ni/Al_2O_3 before reforming reaction over a temperature range from 100 °C up to 900 °C.

In the standard Ni supported catalyst 10% Ni/Al_2O_3 the peaks present at 2θ values of 25.5°, 35.1°, 37.7°, 43.3°, 52.5°, 57.4°, 66.4° and 68.2° in the x-ray profiles at all calcination temperatures are attributed to α-Al_2O_3. However, additional small peaks are observed at 36.9° and 62.1° by 400 °C, which are attributed to the formation of nickel oxide and

become greater by 900 °C due to an increase in crystallinity as the temperature is increased.

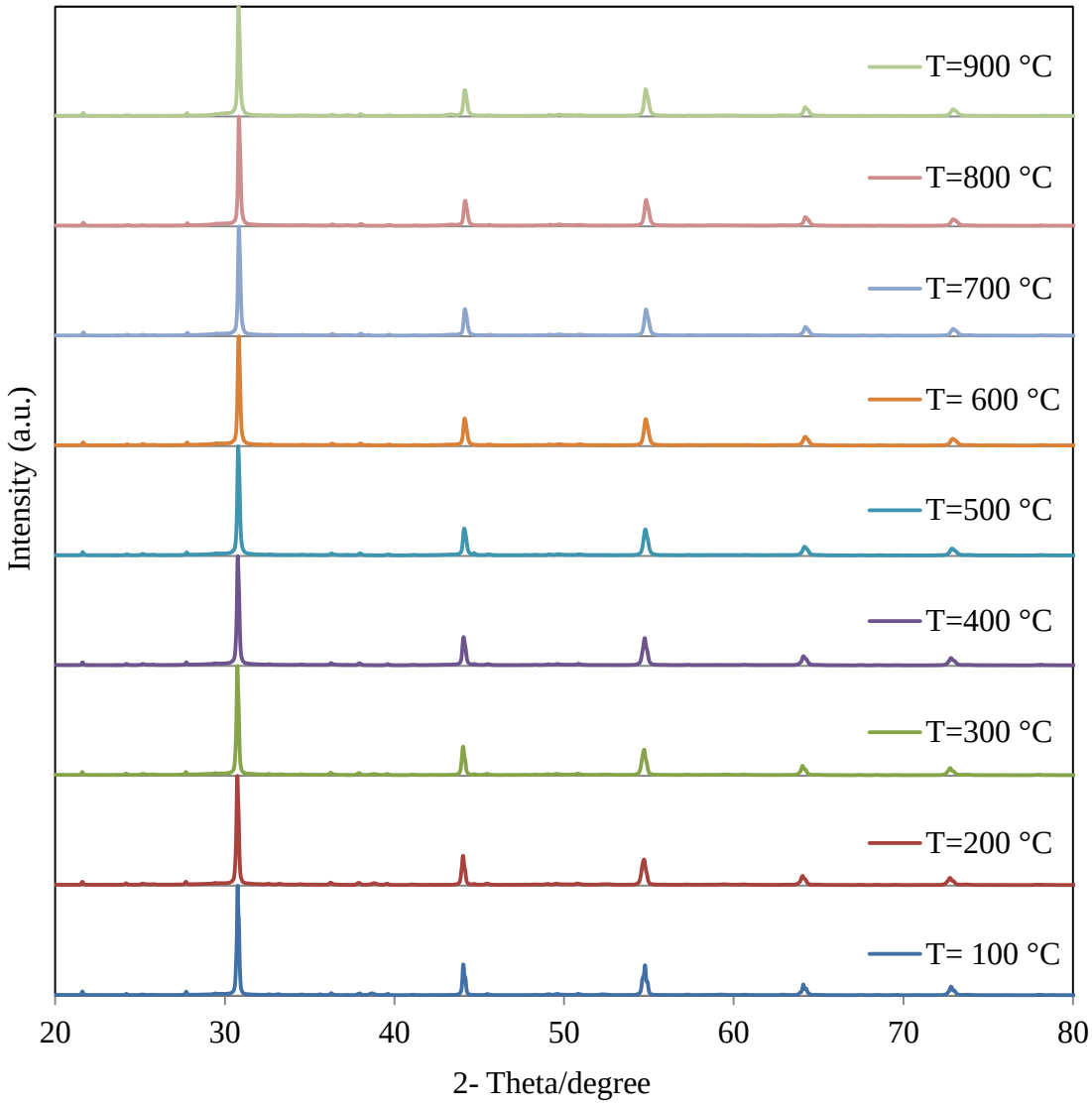

Figure 3.7: XRD pattern of Ni-Fe doped $SrZrO_3$ before reforming reaction over a temperature range from 100 °C up to 900 °C.

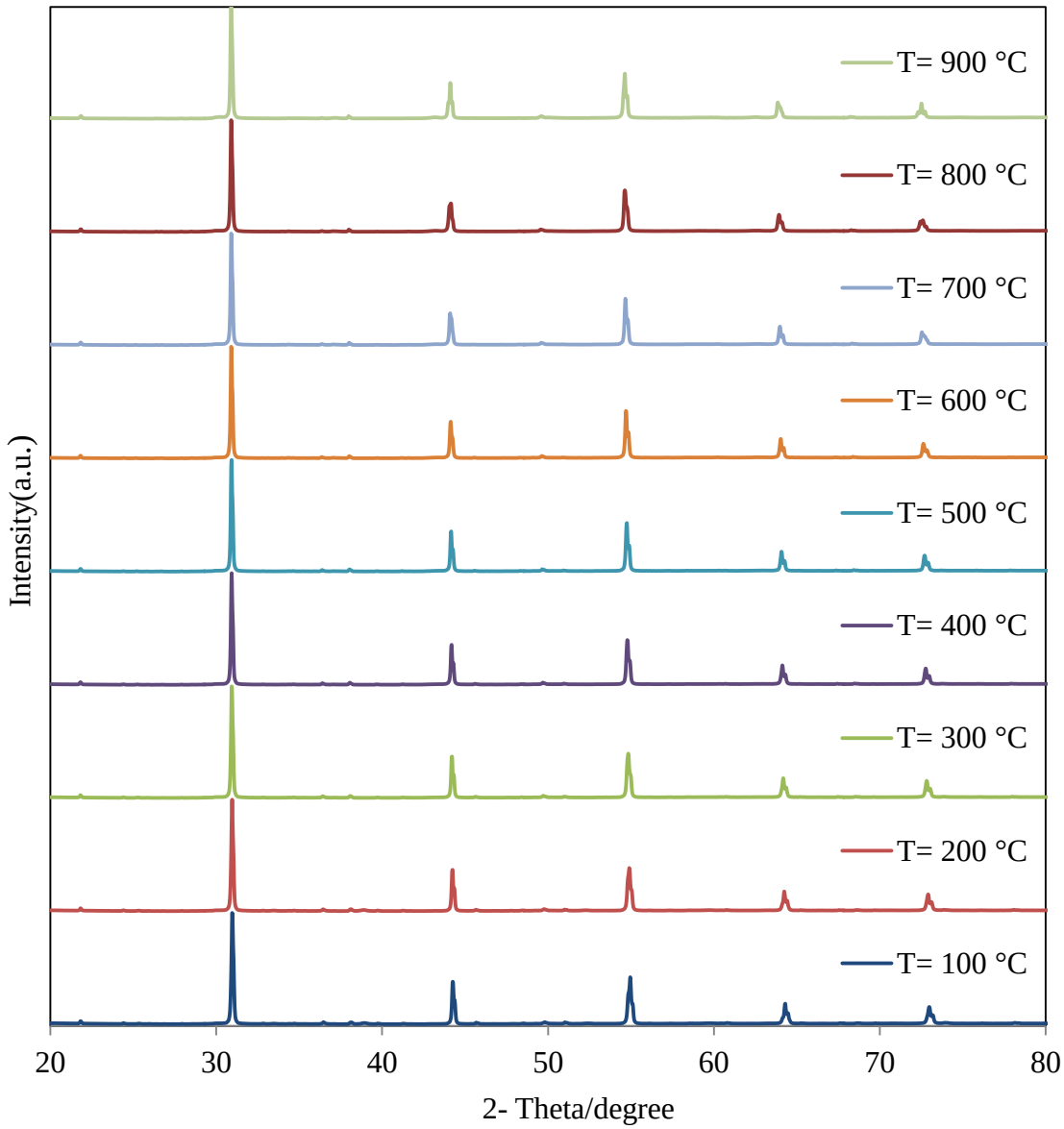

Figure 3.8: XRD pattern of Ni-Al doped $SrZrO_3$ before reforming reaction over a temperature range from 100 °C up to 900 °C.

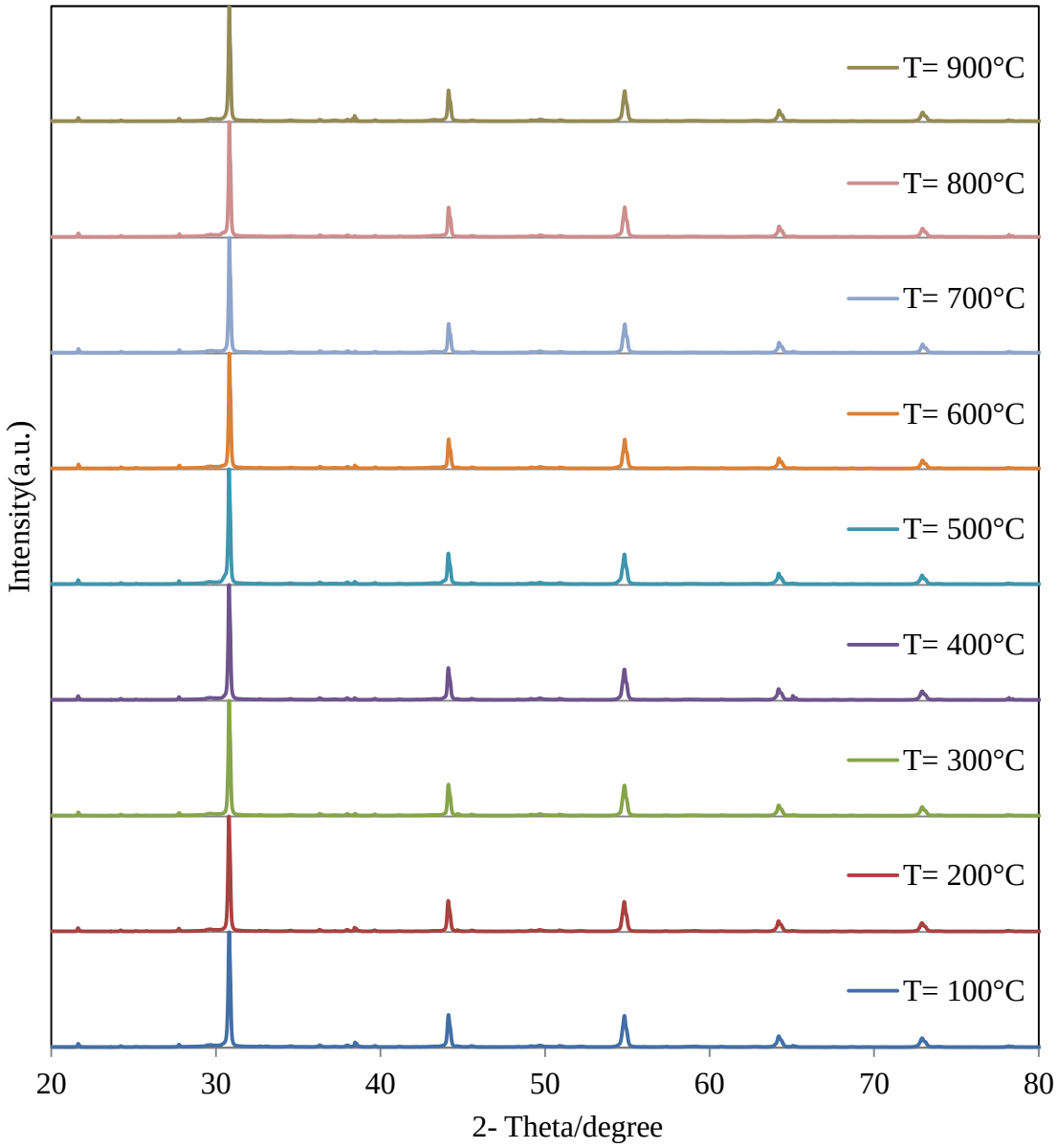

Figure 3.9: XRD pattern of Ni-Ru doped $SrZrO_3$ before reforming reaction over a temperature range from 100 °C up to 900 °C.

Figures above indicate that the co-doped $SrZrO_3$ perovskites remain stable at all calcination temperatures. On this basis, no phase transformation or separation is likely to occur under the reforming reaction temperatures employed in this study.

3.3 Crystallite size determination

Comparing the diffraction patterns for the three perovskite catalyst samples synthesised, peaks corresponding to the perovskite structure were detected in all the samples indicating that the hydrothermal technique produces a well-crystalline perovskite material. The catalyst crystallite sizes based on the sharpest peaks were calculated using Scherer's equation as 50.22, 55.93 and 50.35 nm for Ni-Fe doped, Ni-Al doped, and Ni-Ru doped $SrZrO_3$ perovskite respectively. The particle size can be an important factor for providing favourable conditions to avoid or decrease carbon formation and increase desirable catalytic activity.

3.4 Surface area measurements

BET surface areas for the catalytic samples were determined using a Quantachrome Autosorb-1 apparatus, the samples of about 200 mg were outgassed at 350 °C under vacuum for 5 hours and then nitrogen gas was used as the adsorbent. Investigation of the surface area of the perovskites was determined by using a nitrogen BET method. Among all the perovskites, Ni-Fe doped had the highest surface area (47.4 m^2/g), followed by the Ni-Al doped (42.3 m^2/g) whilst the Ni-Ru doped had the lowest surface area (37.6 m^2/g) but this was still higher than the conventional Ni/Al_2O_3 catalyst (17.8 m^2/g).

The N_2 adsorption desorption isotherms of all the perovskite catalysts in Figures 3.10, 3.11 and 3.12 show that the point of inflection at a relative pressure of ($P/P_\circ$ = 0 - 0.2) represents the completion of monolayer coverage by N_2. The uptake in N_2 adsorption from ($P/P_\circ$ = 0.2 - 1.0) corresponds to multilayer N_2 adsorption or condensation within the

macroporous materials. Nitrogen physisorption data of catalysts shows type (II) isotherm obtained with a macroporous adsorbent.

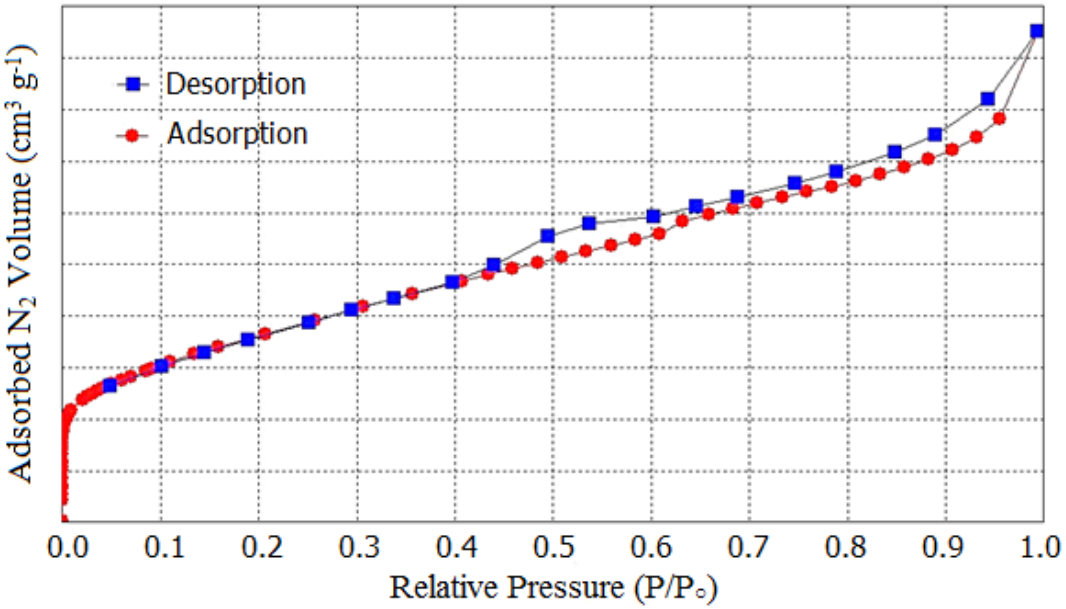

Figure 3.10: Nitrogen adsorption desorption isotherms at 77 K on a Ni-Fe doped $SrZrO_3$ catalyst.

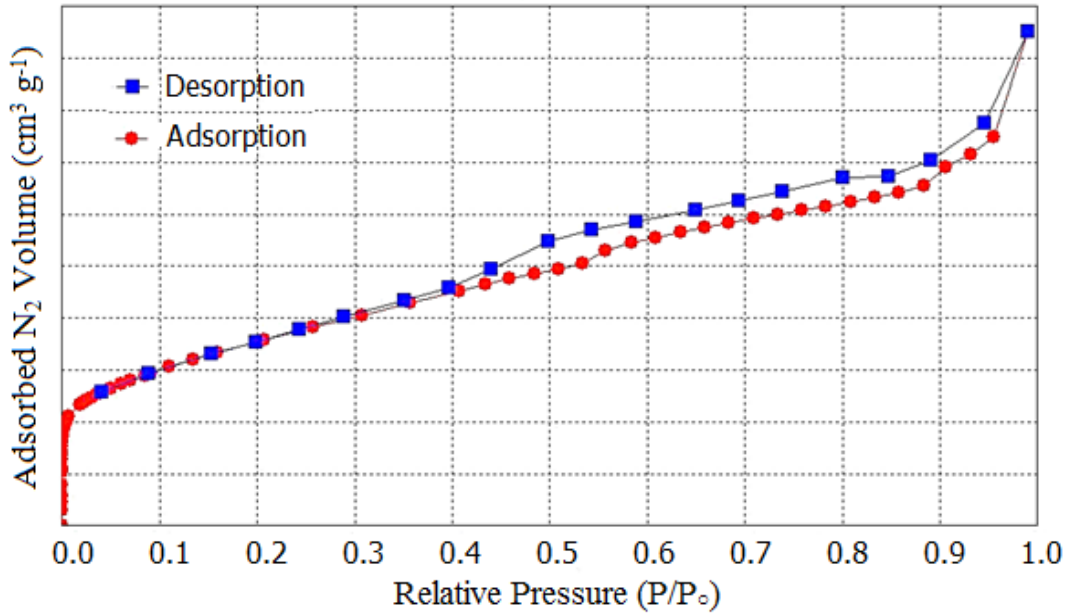

Figure 3.11: Nitrogen adsorption desorption isotherms at 77 K on a Ni-Al doped $SrZrO_3$ catalyst.

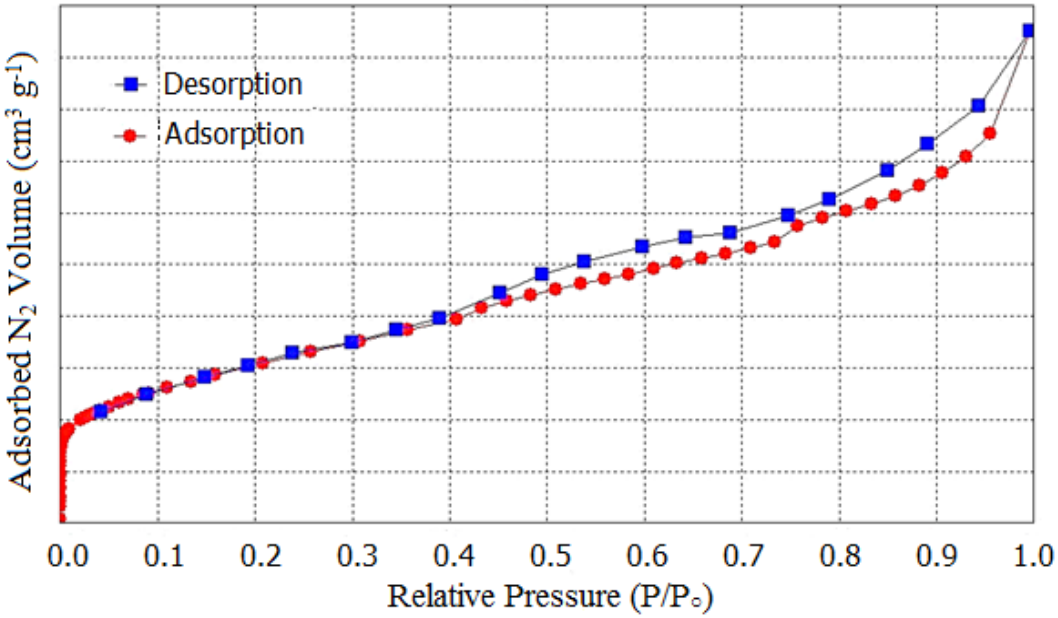

Figure 3.12: Nitrogen adsorption desorption isotherms at 77 K on a Ni-Ru doped $SrZrO_3$ catalyst.

3.5 SEM - EDX analysis before reforming

The morphologies and surface compositions of the samples were characterized by SEM and HR-SEM in which the sample was coated with a thin layer of gold. A small amount of sample was placed onto carbon tabs that were fixed to metallic stubs and then either placed directly in to the Hitachi TM3000 scanning electron microscope or coated with a thin layer of gold (sputtering) before analysis. SEM images were collected for all catalysts using a magnification range of 2,000 x to 3,000 x as shown on the images below and a Bruker Quantax 70 EDS system was used alongside SEM to complete chemical analysis in order to gain quantitative compositional information.

SEM images were obtained for all perovskite catalyst samples following preparation as shown in Figure 3.13 - Figure 3.16. SEM images show a clear difference between the

morphologies of hydrothermally synthesised perovskite catalysts in terms of the size of crystals and the shape, and a huge difference in morphology compared to the conventional 10% Ni/Al_2O_3 catalyst.

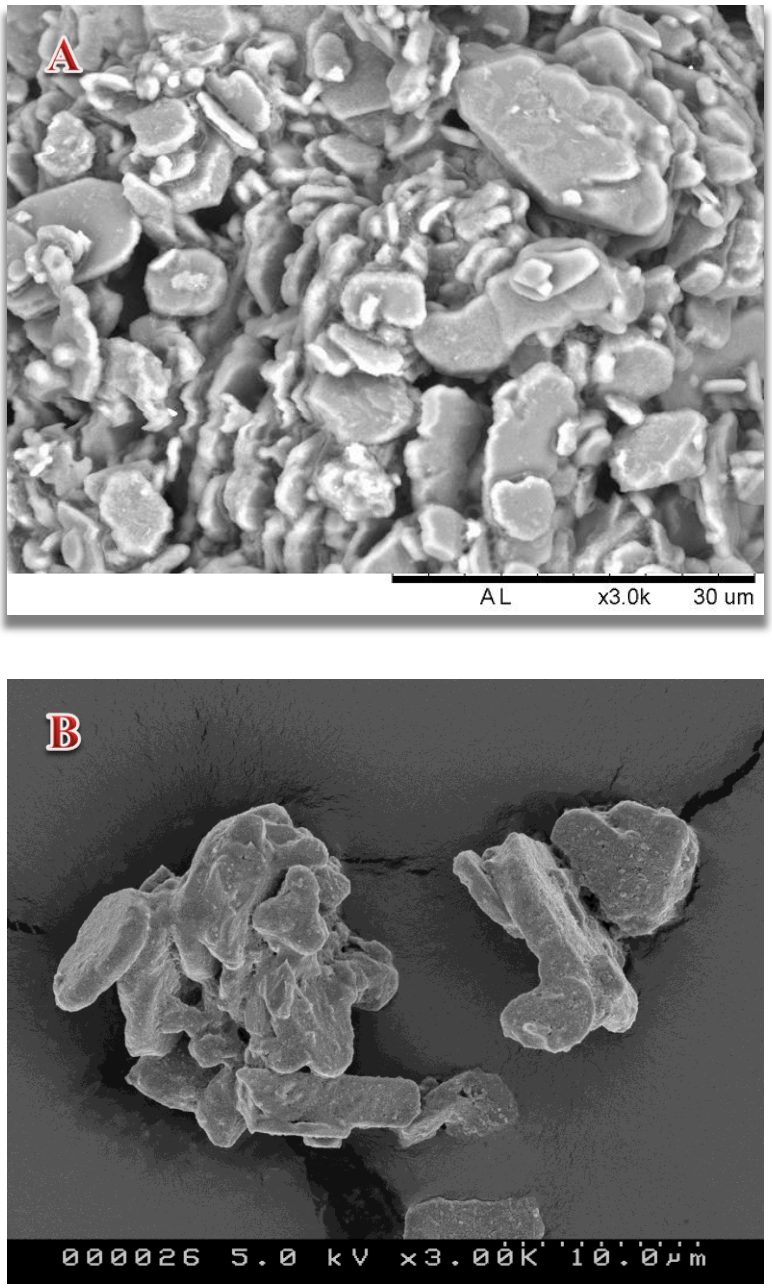

Figure 3.13: (A) SEM image and (B) HR-SEM image of standard catalyst 10% Ni/Al_2O_3 before reforming reactions at 3000 x magnification.

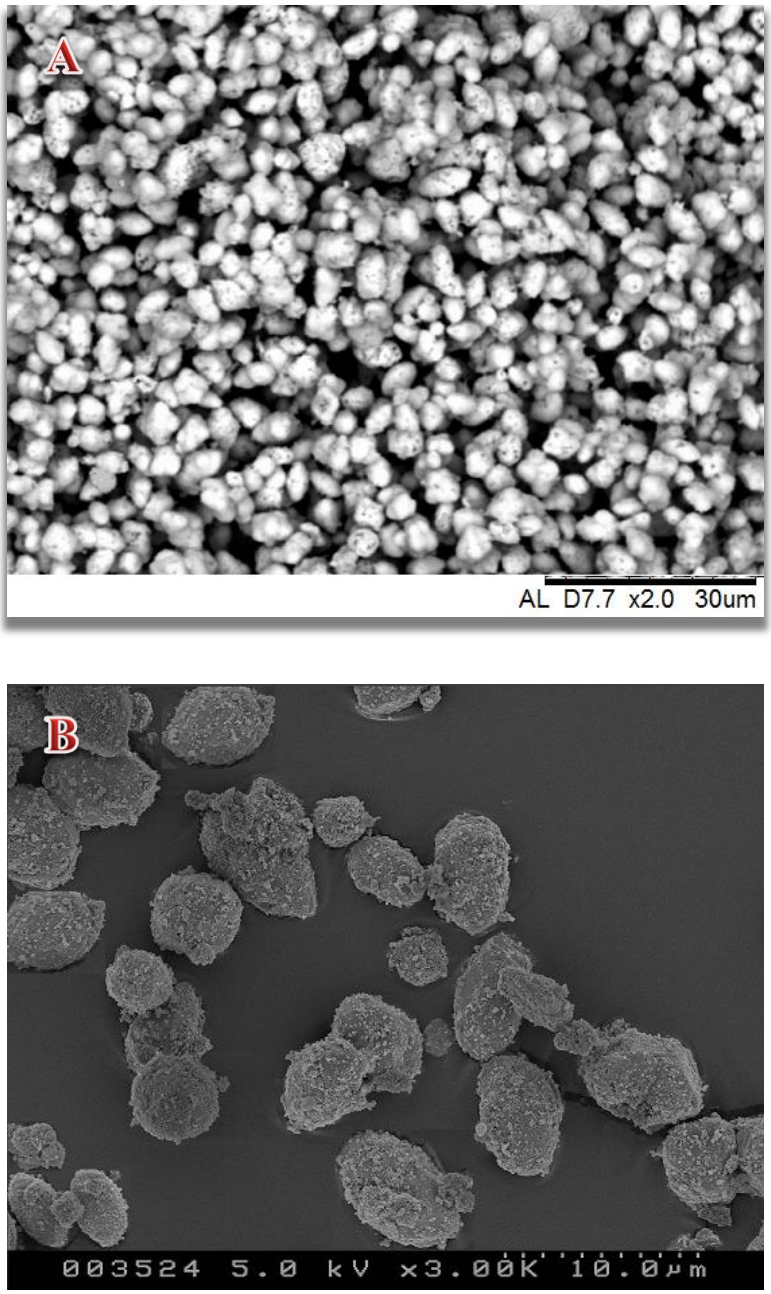

Figure 3.14: (A) SEM image and (B) HR-SEM image of Ni-Fe doped $SrZrO_3$ perovskite before reforming reactions at 2000 x and 3000 x magnification respectively.

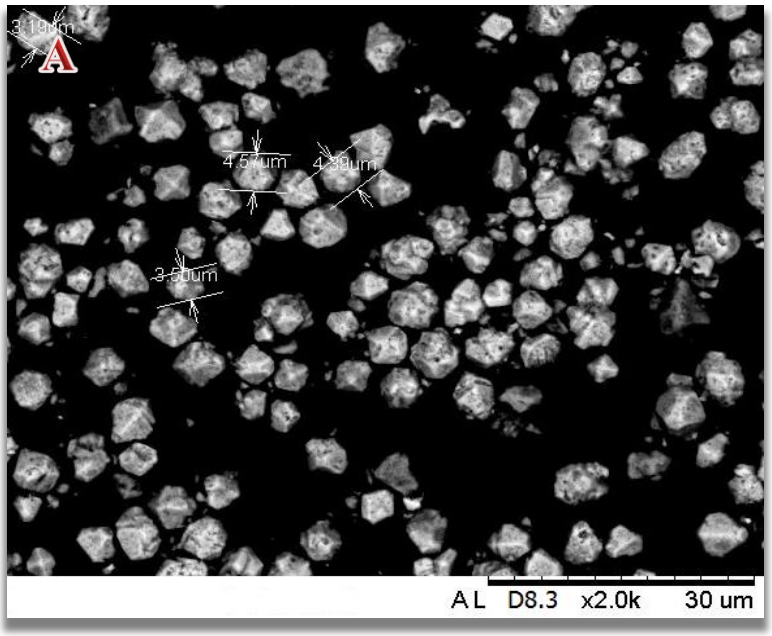

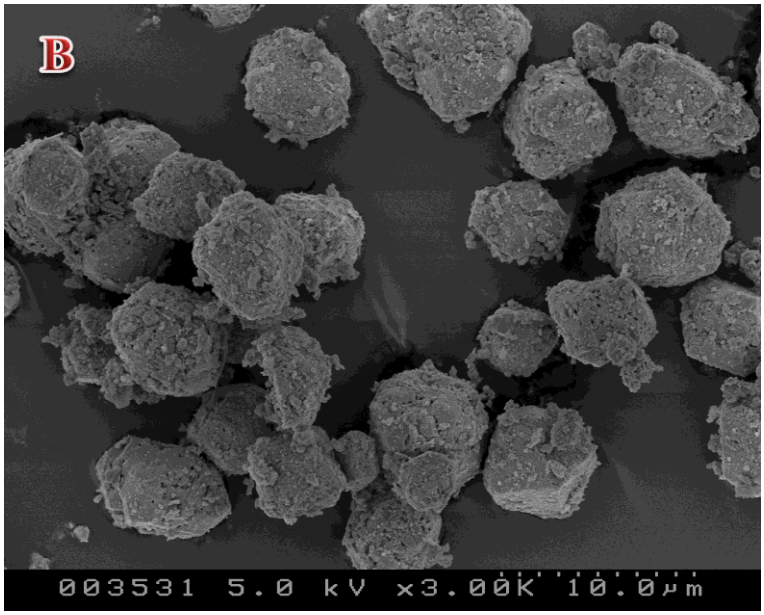

Figure 3.15: (A) SEM image and (B) HR-SEM image of Ni-Al doped $SrZrO_3$ perovskite before reforming reactions at 2000 x and 3000 x magnification respectively.

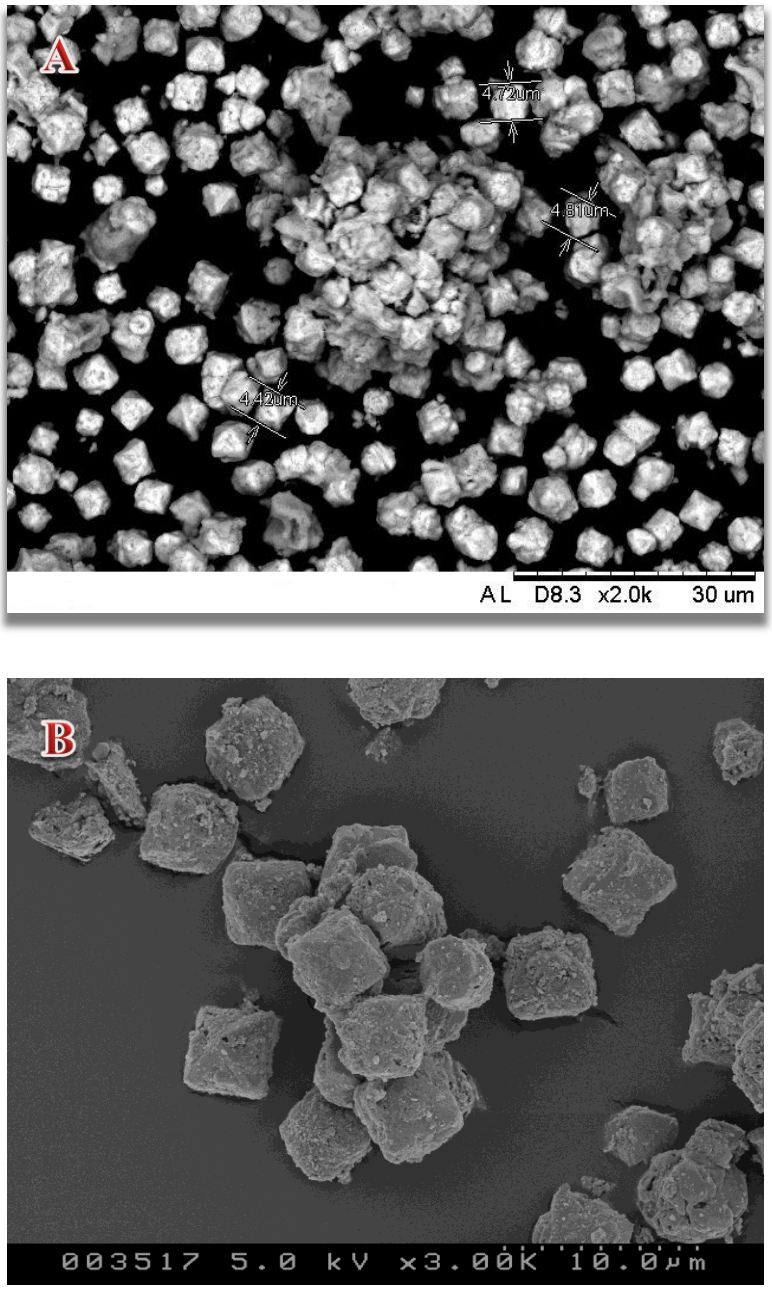

Figure 3.16: (A) SEM image and (B) HR-SEM image of Ni-Ru doped $SrZrO_3$ perovskite before reforming reactions at 2000 x and 3000 x magnification respectively.

It can be seen from these images that there is likely some small amount of impurity which appears as very thin crystallites dispersed throughout the material particles or that some of the spheres are still in the process of being formed. HR-SEM images display a porous

material consisting of irregular particles with different size spheres to the regular octahedron that has been reported for other perovskite samples.

EDX analysis measurements were completed so as to quantify the chemical composition of many hydrothermally-synthesised perovskites, shown in Table 3.2, it was found that the active metals were well distributed and present in all of the sample compositions at levels consistent with the original synthesis formulations, five repeats were taken at different points on the samples for improved accuracy of the results. In order to obtain further information on the metal doping environments and in particular to determine whether they had been incorporated into the lattice of the $SrZrO_3$ perovskite, reduction measurements were carried out, as detailed in section 3.6.1.

Table 3.2: EDS analysis of perovskite materials.

Samples	%Atom Sr	%Atom Ni	%Atom M=Fe, Al, Ru	%Atom Zr	%Atom O
Ni-Fe doped $SrZrO_3$	15.25	4.42	0.96	18.47	60.90
Ni-Al doped $SrZrO_3$	15.24	3.75	0.89	17.93	62.19
Ni-Ru doped $SrZrO_3$	16.20	4.32	1.14	17.83	60.51

3.6 Catalysts Testing

3.6.1 Temperature-Programmed Reduction (TPR)

The reduction behaviour of the catalyst materials was characterized by temperature-programmed reduction measurements, which provides semi-quantitative information about the interactions between H_2 and the surface oxides. Incorporating dopants into nickel perovskite catalysts changes the temperature effect of the reduction potential, this determined whether it had been incorporated into the lattice of the sample. Features of the

TPR profile can be characteristic of the catalyst composition and an example of this is shown in Figure 3.17 where reduction peaks for nickel and other active metals can be seen. Hydrogen consumption and water evolution were both recorded during experimental data collection. However, subsequent TPR profiles for all catalysts in this study will show only the water evolution, since the H_2 consumption mirrors the H_2O evolution.

Temperature-programmed reduction is also usually used to achieve maximum catalytic activity as well as characterize the ease of reducibility of the mixed metal oxide and evaluate the level of interactions between metals. The characteristics of the TPR profile, including the peak area and the reduction temperature depend on the nature of the oxides, the sensitivity to the experimental conditions, the hydrogen concentration and the flow rate of the reducing gas mixture, therefore the profiles for the same material could be significantly different if the measurement was done under different conditions.

Molina and Poncelet have reported an increasing resistance to reduction with increasing calcination temperature, irrespective of the type of support (silica, alumina). The reducibility of nickel in NiO/Al_2O_3 catalysts decreases with increasing calcination temperature due to a chemical interaction with the support that depends on the NiO crystallite size and the surface-area of the support. Moreover, the properties of supported metal catalysts are not uniquely determined by the combination of metal/support, but also depend on their synthesis method and reduction conditions [15].

TPR analysis can also be used for determining the interactions between species in the catalyst and the optimum reduction temperature. For example, species that are reduced at higher temperatures are often indicative of more stable catalysts due to the presence of strongly interacting components [16]. The general reduction reaction of a metal oxide can be represented in the following equation.

$$MO + H_2 \rightarrow M + H_2O \quad [3.1]$$

The flow rate of the hydrogen gas is kept constant throughout the temperature programmed reduction reaction and the outlet gas composition is measured, so that the change in H_2 concentration is proportional to the reduction of the metal oxide species to the M° element.

The reducibility of NiO is dependent on the extent of the interaction between Ni and the support. Therefore, Ni-support interactions can be characterized by the reducibility of the nickel oxide species. Chiuping et al. [17] classified the interaction between the metal oxide and the support into three types: (a) very weak interactions in which the support acts only as a dispersing agent, (b) solid solution formation, and (c) strong interactions e.g. formation of nickel aluminate spinel, which lead to a difficulty in reduction. It was found in this study that increasing the nickel loading led to an increase in the proportion of the reduction peak and a shift to lower temperatures, with reduction starting at around 250 ^{o}C. The TPR profiles for 10% Ni/Al_2O_3 are shown in figure 3.17 where a broad peak is observed at around 440 °C which can be assigned to the reduction of surface nickel aluminate and is consistent with TPR profiles studied by Chiuping of impregnated Ni supported Al_2O_3 catalysts.

Reduction peaks for all the co-doped perovskite catalysts in this study were shifted to lower temperatures by more than 50 °C compared with monometallic doped (nickel strontium zirconate) prepared by Evans [14], suggesting that bimetallic doping has increased the ease of catalyst reduction.

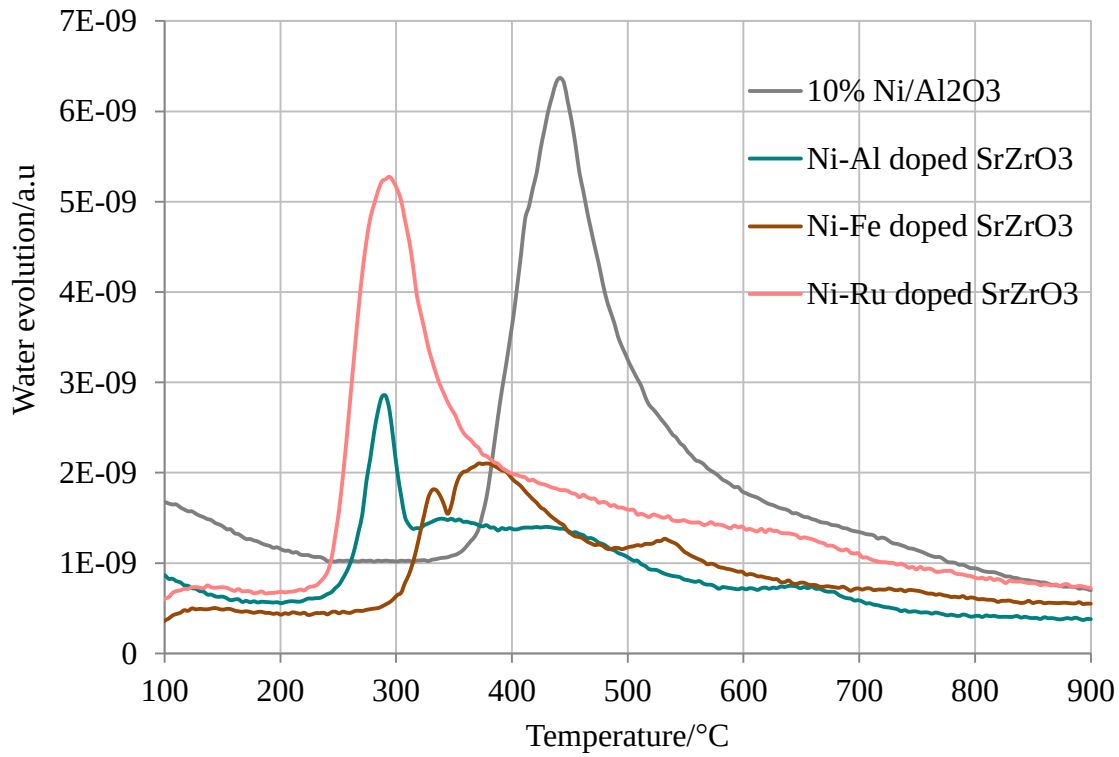

Figure 3.17: Comparison of water evolution resulting from temperature controlled reduction profiles for each catalyst material under study.

As can be seen from the reduction profiles for the three perovskite catalysts, the profile obtained for the Ni-Fe-doped $SrZrO_3$ perovskite displays more than one peak. The number of peaks in this profile is indicative of multiple reducible sites, as is expected due to the presence of multiple dopants. The propensity of Fe to occupy many oxidation states with relative flexibility would be expected to result in multiple reduction steps of Fe, resulting in multiple peaks on the TPR profile [18]. The presence of iron in the structure could make an alloy with nickel and stabilise the nickel inside the bulk, making the Ni more difficult to be reduced. The second peak in the TPR profile is related to partial reduction of Fe^{3+} to Fe^{2+} [19].

The TPR profiles of the Ni-Ru doped $SrZrO_3$ perovskite show a broad single reduction peak at approximately 295 ^{o}C due to the reduction of Ru^{3+}, Ru^{2+} and/or Ni^{2+} species to

form metallic Ru^0 and Ni^0 which located at the surface of the bimetallic particles in addition to that in the bulk structure [20, 21]. Noble metals have been known to improve the reducibility of NiO. Gaur et al. Mentioned that the peak appears at 270 ^oC was attributed to reduce Ru species which substituted into the B- site of the pyrochlore catalyst [22].

Again, the presence of iron in the perovskites may shift the reduction to higher temperatures because of a stronger interaction between Fe and surrounding lattice species and the TPR profile displays two more diffused peaks at temperatures between 330 and 700 °C, one peak corresponding to the reduction of Ni^{2+} and the other to the reduction of Fe^{3+} species [23]. While the Ni-Al doped perovskite profile exhibited a broad reduction peak from about 286-700 ^oC suggesting a range of Ni and Al-oxygen interaction strengths for these Ni and Al atoms these are more strongly associated with the lattice oxygen.

The H_2 -TPR profile results for Ni-Al doped $SrZrO_3$ show small narrow reduction peaks compared with the TPR peaks for the Ni supported alumina which has big broad reduction peaks that can be attributed to the reduction of surface nickel oxide species that are weakly interacting with the Al_2O_3 support. These results help confirm the incorporation of both metals within the bulk of the perovskite structure.

3.7 Conclusion

Three co-doped perovskite catalysts have been successfully prepared using hydrothermal synthesis. The optimum length of time for synthesis was found to be 72 hours at a temperature of just 180 °C in order to produce highly crystalline solids with minimal impurities detectable by x-ray analysis and confirmed by HR-SEM images.

It can be concluded that the catalyst preparation method and pre-treatment processes such as pH, reaction temperature, solvent concentration, and ageing time have a strong influence on the catalyst final properties such as crystal structure, morphologies and the reduction behaviour which directly affect the catalytic performance. This study has shown that perovskite synthesis requires some extra effort in tuning the fine details of the reaction conditions in order to produce the desired compound in both a pure and highly crystalline form. It has also be shown through TPR results for the conventional catalyst (10% Ni/Al_2O_3) that $NiAl_2O_4$ spinal is not formed during reaction and all Ni^{2+} species can be reduced at relatively low reduction temperatures, due to limited interactions between the nickel and the support.

3.8 Reference

[1] B. Imelik, and J. C. Vedrine, *Fundamental and Applied Catalysis*, 1st edn., 2013.

[2] K. Urasaki, Y, Sekine, S. Kawabe, E. Kikuchi, and M, Matsukata, *Appl. Catal. A: General*, 2005, **286**, 23-29.

[3] H. Li, Y. Tian, Z. Wang, F. Qie and Y. Li, *RSC Adv*., 2012, **2**, 3857-3863.

[4] Y. Bu, Q. Zhong, D. Xu, and W. Tan, *J. Alloys and Compd.*, 2013, **578**, 60-66.

[5] M. J. Koponen, T, Venäläinen, M. Suvanto, K. Kallinen, T.J.J.Kinnunen, M. Härkönen, and T. A. Pakkanen, J. Molecu. *Catal. A: Chem*., 2006, **258**, 246-250.

[6] D. M. Bastidas, S. Tao and J. T. S. Irvine, *J. Mater. Chem*., 2006, **16**, 1603-1605.

[7] X. Song, X. Dong, S. Yin, M. Wang, M. Li, and H. Wang, *Appl. Catal. A: General*, 2016, **526**, 132-138.

[8] A. Iulianelli, S. Liguori, J. Wilcox, and A. Basile, *Catal. Review*, 2016, **58**, 1–35.

[9] D. Li, K. Nishida, y. Zhan , T. Shishido , Y. Oumi , T. Sano, and K. Takehira, *Appl. Catal. A: General*, 2008, **350**, 225–236.

[10] L. Li, D. H. Anjum, H. Zhu, Y. Saih, P. V. Laveille, L. D'Souza, and J-M. Basset, *Chem. Cat. Chem.*, 2015, **7**, 427–433.

[11] B. Liu and H. C. Zeng, *J. Am. Chem. Soc*., 2003, **125**, 4430–4431.

[12] A.W. Budiman, S. H. Song, T. Chang, C. Shin, and M. Choi, *Catal. Surv Asia*, 2012, **16**,183-197.

[13] D. R. Modeshia, R. J. Darton, S. E. Ashbrook and R. I. Walton, *Chem. Commun*., 2009, 68–70.

[14] S. E. Evans, PhD Thesis, Keele University, 2016.

[15] R. Molina and G. Poncelet, *J. Catal.*, 1998, **173**, 257–267.

[16] T. Maneerung, K. Hidajat, and S. Kawi, Int. *J. Hydrogen Energ.*, 2015, **40**, 13399-13411.

[17] C. Li, and Y-W. Chen, *Thermochimica Acta*, 1995, **256**, 457 -465.

[18] E. Yang, Y. Noh, S. S. Lim, B. S. Ahn and D. J. Moon, *J. Nanosci.. Nanotechno*., 2016, **16**, 1938-1941.

[19] H. Provendier, C. Petit, C. Estourne, Ás, S. Libs, and A. Kiennemann, *Appl. Catal. A: General*, 1999, **180**, 163-173.

[20] N. Mota , I.Z. Ismagilov, E.V. Matus, V. Kuznetsov, M. Kerzhentsev , Z.R. Ismagilov, R.M. Navarro, and J.L.G. Fierro, *Int. J. Hydrogen Energ.*, 2016, **41**, 19373 - 19381.

[21] S. Gaur, D. J. Haynes, and J. J. Spivey, *Appl. Catal. A: General*, 2011, **403**, 142– 151.

[22] S.Gaur, D. Pakhare, H. Wu, D. J. Haynes, and J. J. Spivey, *Energy Fuels* 2012, **26**, 1989−1998.

[23] P. Erri, P. Dinka, and A. Varma, *Chem. Eng. Sci.*, 2006, **61**, 5328–5333.

Chapter 4

Studies for Biogas Reforming of Methane

4. Biogas reforming over 10% Ni/Al_2O_3 and three types of co-doped perovskite catalysts

4.1 Introduction

Biogas reforming has attracted considerable scientific interest due to offering the possibility of transforming two inexpensive greenhouse gases into useful chemical products. In this study a 2:1 ratio of CH_4: CO_2 mixture was used as it represents the most common composition for naturally produced biogas. DRM has several advantages in comparison to steam reforming and partial oxidation as the H_2 /CO ratio is close to one, which is the most appropriate for Fischer–Tropsch reactions and other hydrocarbon synthesis [1]. However, it has not reached commercialization due to the following reasons: (I) highly endothermic reaction which needs much energy to attain high equilibrium conversions to synthesis gas. (II) Produces a large quantity of carbon that covers the active surface sites and leads to deactivation of the catalyst.

Moral et al. [2] have suggested including different amounts of oxygen together with the biogas mixture to reduce the energy requirements of the process by partially or completely oxidizing the methane. A combination of combustion would make the overall reforming process thermodynamically neutral reaction by manipulating the $CH_4/CO_2/O_2$ ratio as well as helping alleviate coke formation, such an approach may be very attractive when carbon on the catalyst becomes significant after long times-on-stream [3].

Generally, the lowest methane conversions and greatest carbon formation are obtained from CH_4- rich conditions (2:1 CH_4 /CO_2 mixtures) due to there being insufficient CO_2 present to react with all methane molecules in the reaction atmosphere. A large quantity of carbon is often produced due to an excess of 50% methane that is thermally

decomposed. Methane decomposition becomes more prevalent with increasing reaction temperature, consequently carbon deposition increases with increasing reaction temperatures.

Most biogas reforming studies show fast deactivation caused by serious carbon accumulation. This suggests that there is a requirement for developing catalysts that are thermodynamically stable and have a limited affinity to coke formation. Based on reported research in the literature, Ni-based catalysts impregnated on various supports also show high catalytic activity with low levels of coking and have thus attracted more attention from an economic point of view.

This chapter contains a detailed study of biogas reforming over nickel supported alumina and nickel co-doped perovskite catalysts. Investigations have been done about the effects of temperature and time on stream on methane and carbon dioxide conversion, H_2 and CO production, H_2 /CO ratio, and the amount of carbon deposition.

4.2 Thermodynamics and mechanism of dry reforming reactions under CH_4-rich conditions

Hypothetically, biogas reforming of methane produces a 1:1 ratio of hydrogen and carbon monoxide at high temperature and atmospheric pressure, as shown in equation [4.1]. Experimentally, numerous side reactions simultaneously occur with the main reaction and these affect the pathway of the reaction, altering the amount of H_2 /CO production. For example, in the reverse water gas shift reaction (RWGS), this leads to lower the level of H_2 and therefore decreases the H_2 /CO ratio and produces more CO in addition to water as shown in equation [4.3]. While pyrolysis of methane and the Boudouard reaction both

increase the H_2 /CO ratio as well as producing carbon on the catalyst surface, shown in equations [4.4, 4.5].

These reactions depend on the operating temperature and partial pressure. Moreover, carbon may also be produced as a result of reaction (hydrogen and carbon monoxide) but has no effect on the H_2 /CO ratio, shown in equation [4.6]. The driving force for all side reactions at different temperatures was determined by Wang et al [4]. Syngas production is accompanied by methane cracking reactions over 640 °C, whereas reverse water-gas shift and the Boudouard reactions do not occur above 820 °C. In the temperature range of 557-700 °C coke can be deposited by methane pyrolysis or the Boudouard reaction.

$CH_4 + CO_2 \rightleftharpoons 2H_2 + 2CO$ $\Delta H^{\circ}_{298K} = +247\ kJ.mol^{-1}$ [4.1]

$2CH_4 + CO_2 \rightleftharpoons C_2H_6 + CO + H_2O$ $\Delta H^{\circ}_{298K} = +106\ kJ.mol^{-1}$ [4.2]

$CO + H_2O \rightleftharpoons CO_2 + H_2$ $\Delta H^{\circ}_{298K} = -41\ kJ.mol^{-1}$ [4.3]

$CH_4 \rightleftharpoons C + 2H_2$ $\Delta H^{\circ}_{298K} = +75\ kJ.mol^{-1}$ [4.4]

$2CO \rightleftharpoons C + CO_2$ $\Delta H^{\circ}_{298K} = -172\ kJ.mol^{-1}$ [4.5]

$H_2 + CO \rightleftharpoons C + H_2O$ $\Delta H^{\circ}_{298K} = -131\ kJ.mol^{-1}$ [4.6]

$CO_2 + 2H_2 \rightleftharpoons C + 2H_2O$ $\Delta H^{\circ}_{298K} = -90\ kJ.mol^{-1}$ [4.7]

The reaction mechanism of biogas reforming was proposed by Bobadilla et al. In the first step methane is adsorbed and dissociates on the metal sites to produces hydrogen and CH_x species, whereas CO_2 is also adsorbed dissociatively on the metallic particles to form carbon monoxide and oxygen. These oxygen adsorbed species reacts with CH_x to produce CH_xO species. Finally, the CH_xO species then dissociate to form synthesis gas CO and H_2 in a fast step. This adsorbed hydrogen can also interact with surface bound

species derived from CO_2 to yield additional CO and water via the reverse water gas shift (RWGS) reaction [5].

$$CH_4\,(g) \rightleftharpoons CH_3{}^a + H^a \quad [4.8]$$

$$CO_2\,(g) \rightleftharpoons CO^a + O^a \quad [4.9]$$

$$CH_3{}^a \rightleftharpoons CH_2{}^a + H^a \quad [4.10]$$

$$CH_2{}^a \rightleftharpoons CH^a + H^a \quad [4.11]$$

$$CH^a \rightleftharpoons C^a + H^a \quad [4.12]$$

$$H^a + H^a \rightleftharpoons H_2\,(g) \quad [4.13]$$

$$CH^a + O^a \rightleftharpoons CHO^a \quad [4.14]$$

$$CHO^a \rightleftharpoons CO(g) + H^a \quad [4.15]$$

$$CO_2^a + H^a \rightleftharpoons COOH^a \quad [4.16]$$

$$COOH^a \rightleftharpoons CO^a + OH^a \quad [4.17]$$

$$OH^a + H^a \rightleftharpoons H_2O(g) \quad [4.18]$$

$$CO^a + O^a \rightleftharpoons CO_2\,(g) \quad [4.19]$$

Schuurman et al. have illustrated that the choice of catalyst has an important role in the dry reforming of methane mechanism. They found that when using nickel catalysts, dissociation of methane was fast, resulting in the production of H_2 gas and the accumulation of surface carbon species as well as dissociation of CO_2 leading to adsorbed oxygen and CO. However, in the case of ruthenium catalysts, the methane decomposition on the catalyst surface was slower and therefore other reactions take place, such as CO_2 reacts with adsorbed carbon giving CO. This paper also elucidated that the support can also strongly influence the dry reforming mechanism [6], as can various other parameters that are mentioned in chapter one such as the morphology of the metal surface, the reaction temperature, the pressures, the surface area and particles size of the catalyst.

According to the suggested mechanisms, the dry reforming reaction requires breaking down both of reactant CH_4 and CO_2 producing two carbon atoms and hence increasing the possibility of undesirable carbon being deposited, which deactivates the catalyst by blocking the active sites on the surface as well as damaging fuel inlets inside the reactor [7]. Unlike in other reforming methods that have higher levels of oxidants and lower amounts of carbon atoms. Carbon formation is shown more on nickel supported catalysts such as nickel supported on yttria stabilised zirconia [8]. Perovskites have been observed to be catalytically active materials for methane conversion and show a lower propensity to form carbon.

4.3 Catalytic characterizations for biogas reforming

4.3.1Temperature programmed conversion reaction (TPCR)

Dry reforming of 2:1 CH_4 /CO_2 was carried out at atmospheric pressure over all catalysts at the same conditions. Figures 4.1-4.4 show the reaction profiles for gases passed over each catalyst as a function of temperature. As can be seen from these figures a sharp drop in methane and carbon dioxide coincide with production of carbon monoxide and hydrogen in addition to low levels of water, caused by reverse water gas shift reaction. The occurrence of the RWGS reaction is confirmed by existence of water [9, 10]. By 550 °C the products H_2 /CO ratio start to rise and stabilise at ~1 by about 900 °C. After approximately 800 °C the CO_2 level becomes depleted, and the amount of H_2 becomes more than the CO, due to decomposition of methane reaction occurring, which increases with increasing reaction temperature. In the final stages of the reaction, thermal decomposition of excess methane becomes favourable as the CO_2 conversion approaches

100% and the temperature increases above 850 °C, however, this is not observed with the Fe-doped perovskite where the conversion of methane remains at ~50% with no signs of methane decomposition occurring.

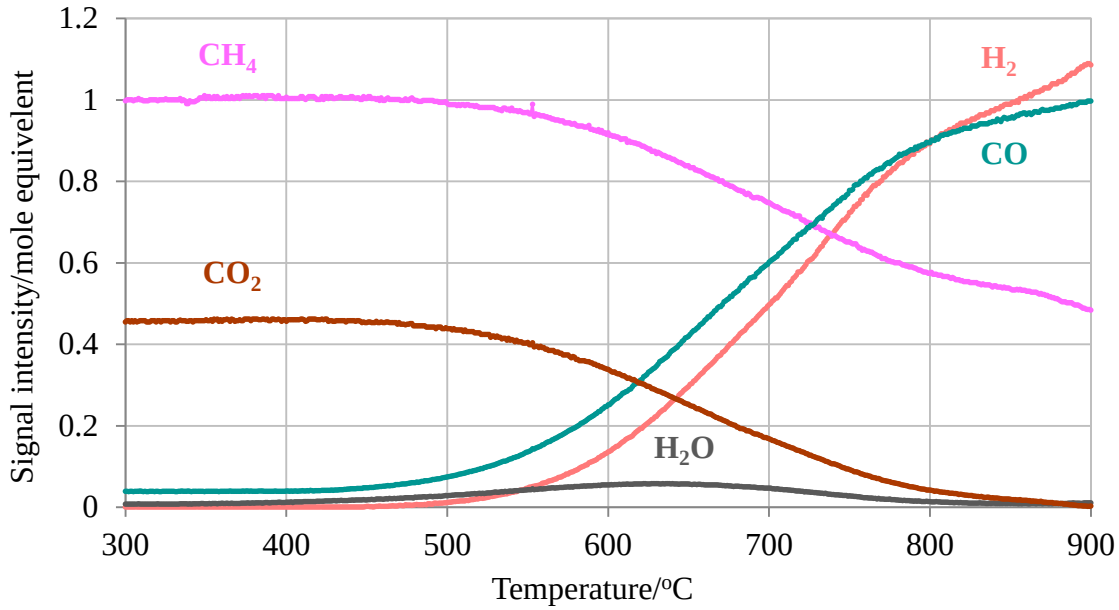

Figure 4.1: Temperature programmed conversion reaction profiles for mixture of 2:1 CH_4 /CO_2 over 10% Ni/Al_2O_3

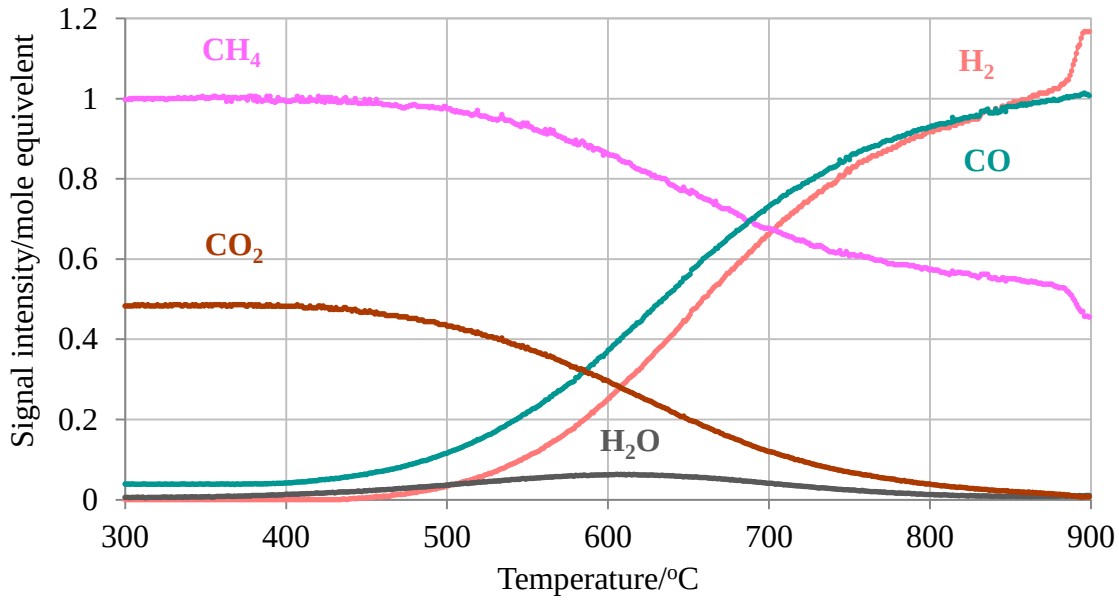

Figure 4.2: Temperature programmed conversion reaction profiles for mixture of 2:1 CH_4 /CO_2 over Ni-Al doped $SrZrO_3$ perovskite.

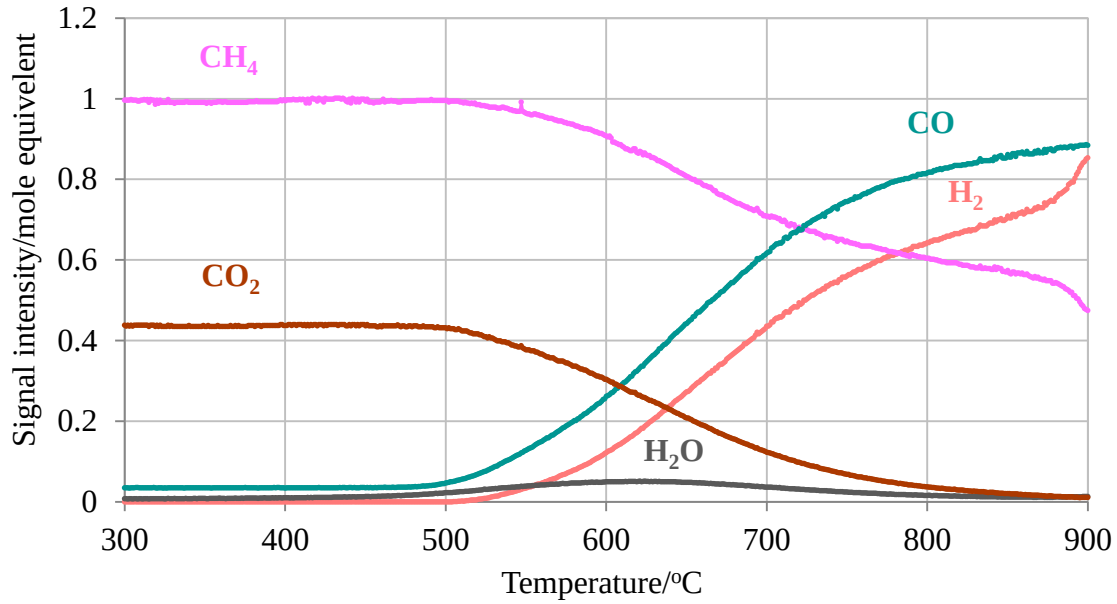

Figure 4.3: Temperature programmed conversion reaction profiles for mixture of 2:1 CH_4 /CO_2 over Ni-Fe doped $SrZrO_3$ perovskite.

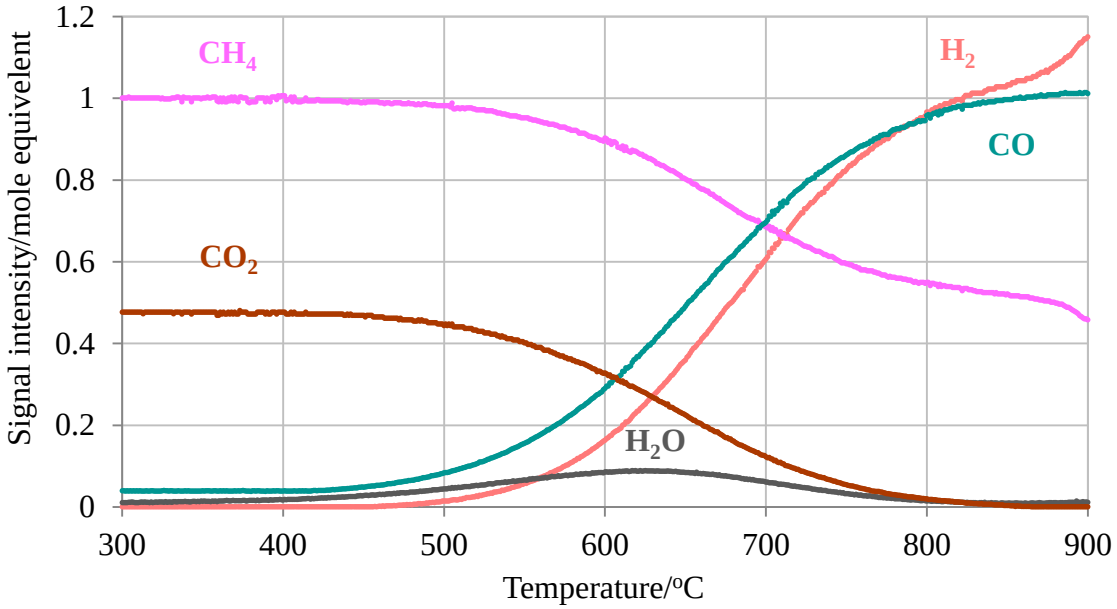

Figure 4.4: Temperature programmed conversion reaction profiles for mixture of 2:1 CH_4 /CO_2 over Ni-Ru doped $SrZrO_3$ perovskite.

Figure 4.3 for the Ni-Fe doped perovskite shows that the syngas production occurs at slightly higher light off temperature than for the other doped samples and increases linearly with higher amounts of carbon monoxide than H_2 production, suggesting that

RWGS is occurring at lower temperatures, but then after 800 ^{o}C becomes slow and unfavourable due to depleting CO_2

The percentage of methane and carbon dioxide conversion is shown in figures 4.5 and 4.6. It should be noted that CH_4 and CO_2 conversions increase steadily with increasing reaction temperature and the CO yields are always higher than that of H_2 until 800 °C, these behaviours could be explained by the fact that the consumption of some hydrogen occurs via the reverse water gas shift reaction which is the predominant reactions at low temperatures. The H_2 /CO ratio reaches the theoretical value of 1 at ~ 850 °C and continues to increase with reaction temperature then quickly exceeds 1 due to thermal decomposition of excess methane occurring over all the catalysts except the iron doped sample. The addition of 1% iron to the perovskite material lowers the H_2 /CO ratio for the full extent of the reaction and this may be due to the Fe not being as active as Ru and Al.

Roughly the same trend is observed for all co-doped perovskite catalysts including the supported alumina catalyst, which means all samples prepared have approximately the same activity even with doping different metals, probably due to the very small amount (1%) of dopant metals. At nearby 900 °C, carbon dioxide is almost fully consumed and this coincides with 50% methane conversion. Above this temperature, the increase in methane conversion is then attributed to an increase in the rate of thermal cracking of excess methane, which becomes more favourable at higher temperatures [11].

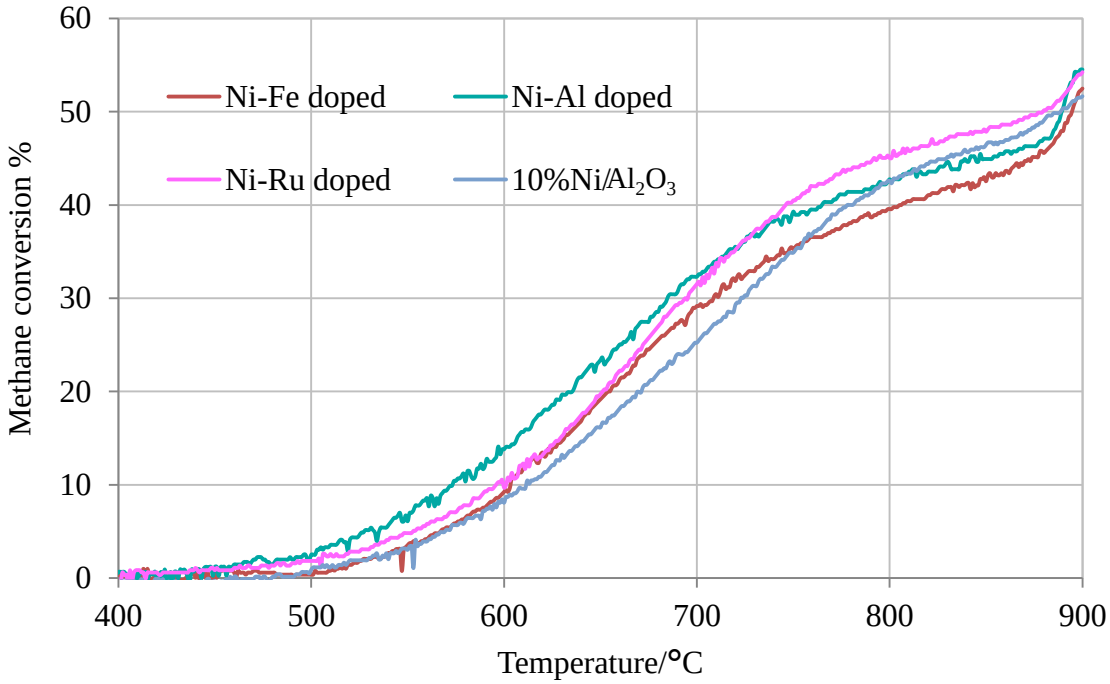

Figure 4.5: Methane conversion profiles during TPCR of 2:1 CH_4 /CO_2 mixture over each catalyst material studied.

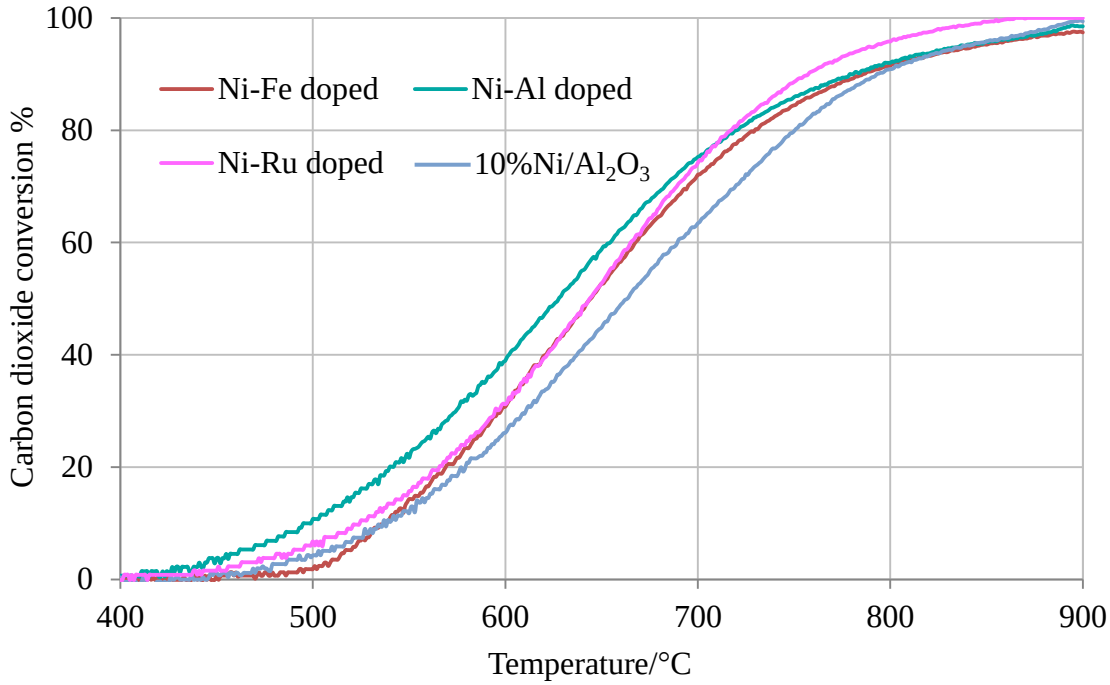

Figure 4.6: Carbon dioxide conversion profiles during TPCR of 2:1 CH_4 /CO_2 mixture over each catalyst material studied.

Once the reaction start at ~500 °C the conversion of methane and carbon dioxide increases at approximately the same rate for all catalysts until completely consumed. Methane cracking is thermodynamically more favourable at elevated temperatures and a methane conversion for the ruthenium doped sample was 53% at 900 °C causing an increase in the hydrogen level and resulting in a H_2 /CO ratio of 1.14.

4.3.2 Catalytic performance investigations (isothermal testing)

To study the effect of temperature in the presence of both the three co-doped perovskites and the nickel supported catalyst on reactant conversion and product yield, a conventional reaction of temperature programmed conversion reaction under methane rich conditions was performed in fixed bed reactor for 20 hours at different reaction temperatures of 700 °C, 800 °C and 900 °C. These temperatures were chosen as the reaction temperature of interest as it represents the temperature where the majority of the reforming reaction occurs. Before starting the experiment, all catalysts were reduced with a mixture of H_2 and He (section 2.4.1). This was done to ensure that the catalyst was activated prior to the reforming process.

As shown from figures 4.7- 4.10, all reactions on all catalyst started with the fast production of hydrogen unlike the production of carbon monoxide; probably due to methane decomposition occurring during the first half an hour of reforming reaction. Then syngas products were predominant suggesting that an efficient biogas reforming reaction was taking place over all catalysts especially at 800 °C and 900 °C with no loss of reforming activity seen. All of the carbon dioxide was consumed and as a result was unavailable for the reverse water gas shift reaction to occur.

At 900 °C methane and carbon dioxide conversions was stable producing an approximately 1: 1 ratio of H_2 /CO, indicating that an effective reaction was taking place on all catalysts. Graphs B and C (800 and 900 °C) in all of the figures show that during 20 hours of biogas reforming all the co-doped catalysts exhibited ~50% CH_4 conversion with no significant deactivation. However, the 10% Ni/Al_2O_3 catalyst showed a steady deactivation under reaction conditions.

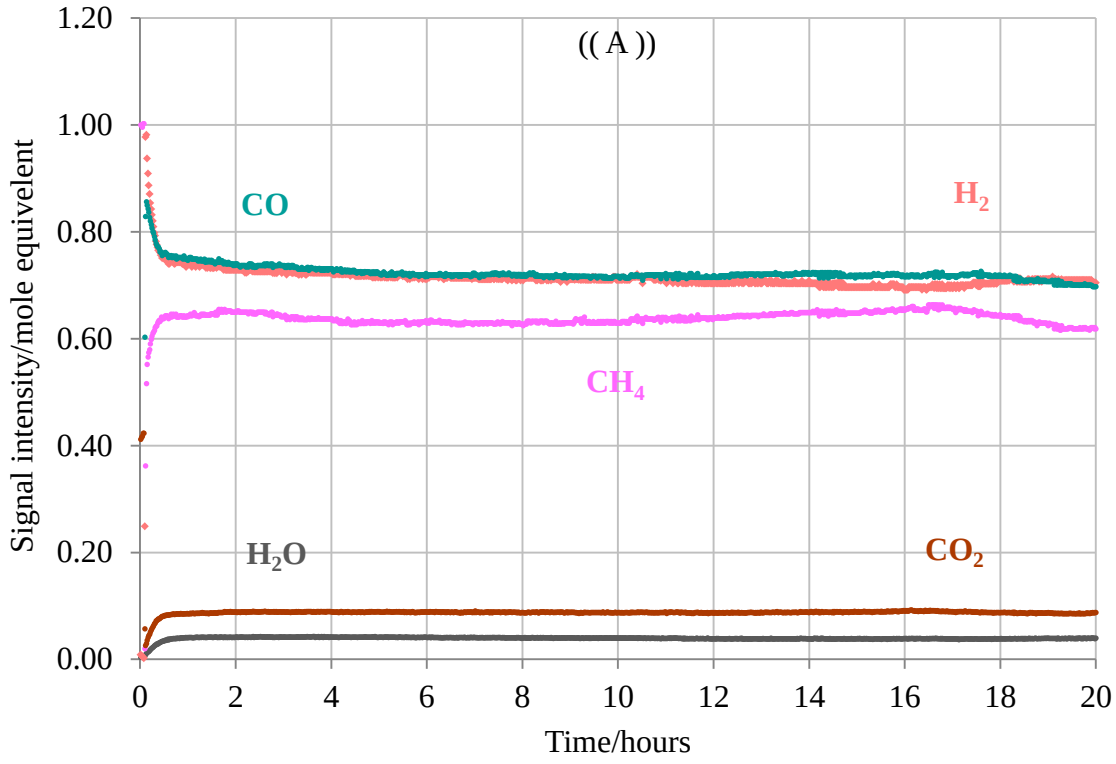

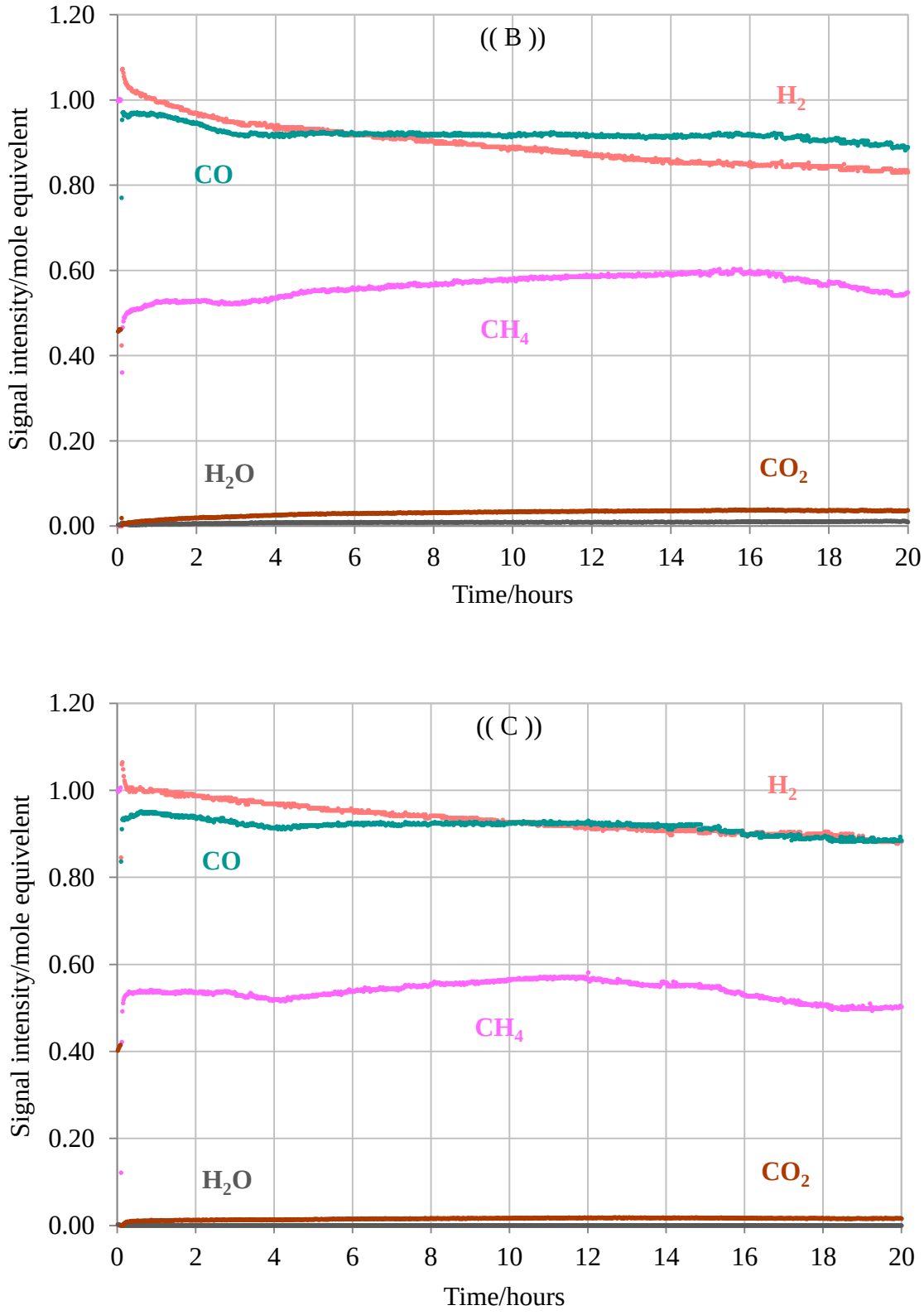

Figure 4.7: Biogas reforming profiles of 2:1 CH_4 /CO_2 mixture over 10% Ni/Al_2O_3 catalyst for 20 hours of reaction at (A) 700 °C, (B) 800 °C and (C) 900 °C.

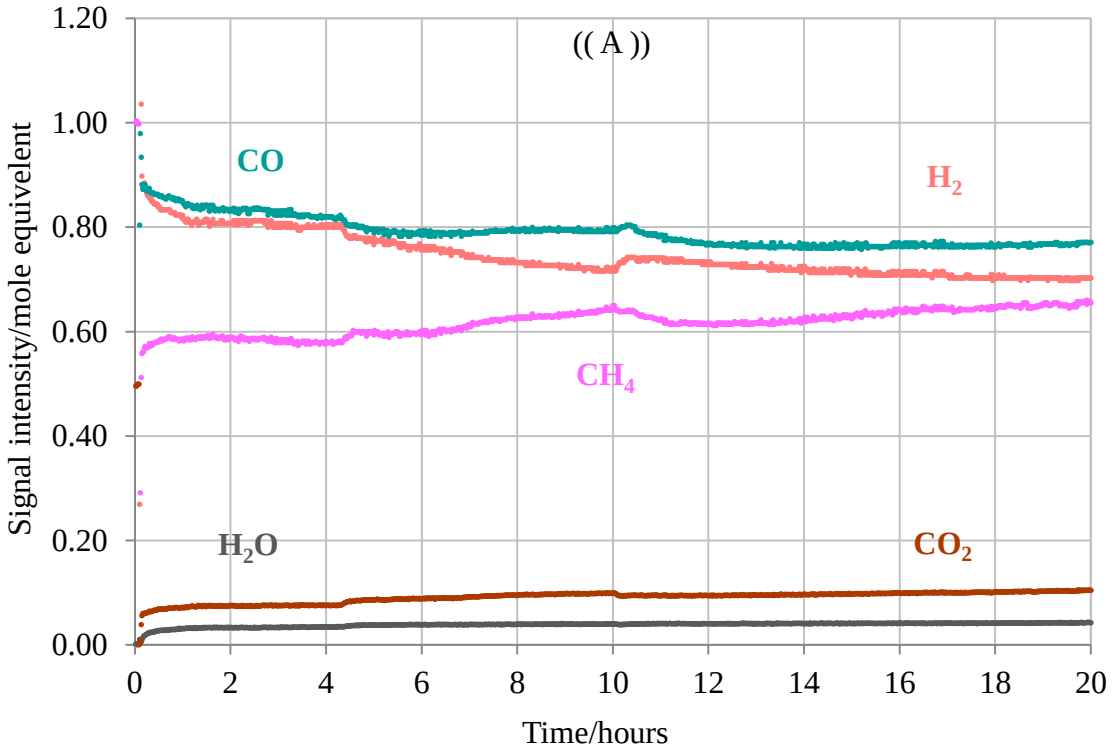
((A))
Signal intensity/mole equivelent
Time/hours
CO
H2
CH4
H2O
CO2
1.20
1.00
0.80
0.60
0.40
0.20
0.00
0
2
4
6
8
10
12
14
16
18
20

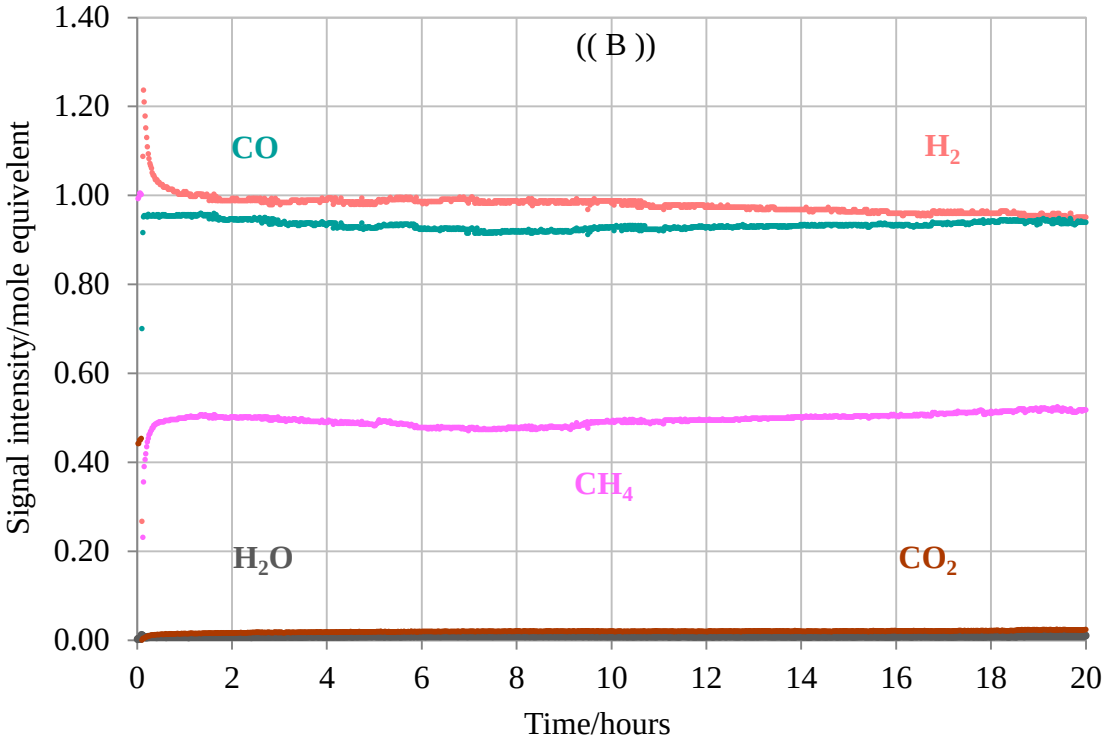
((B))
Signal intensity/mole equivelent
Time/hours
CO
H2
CH4
H2O
CO2
1.40
1.20
1.00
0.80
0.60
0.40
0.20
0.00
0
2
4
6
8
10
12
14
16
18
20

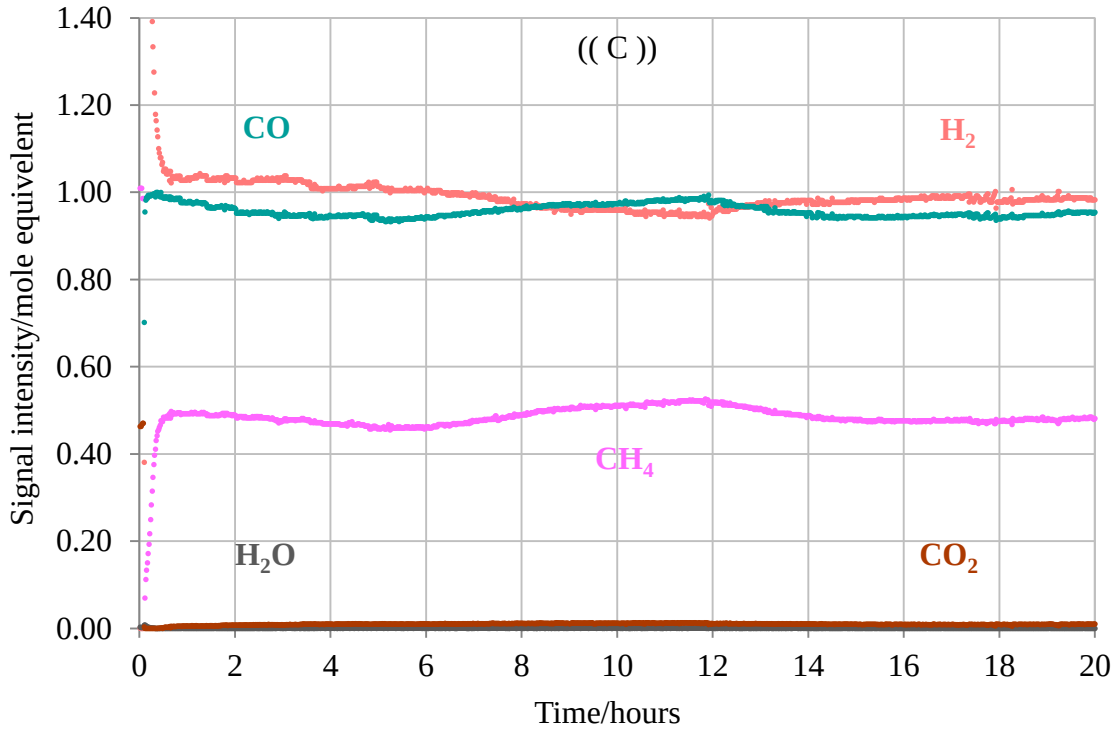

Figure 4.8: Biogas reforming profiles of 2:1 CH_4 /CO_2 mixture over Ni-Al doped $SrZrO_3$ catalyst for 20 hours of reaction at (A) 700 °C, (B) 800 °C and (C) 900 °C.

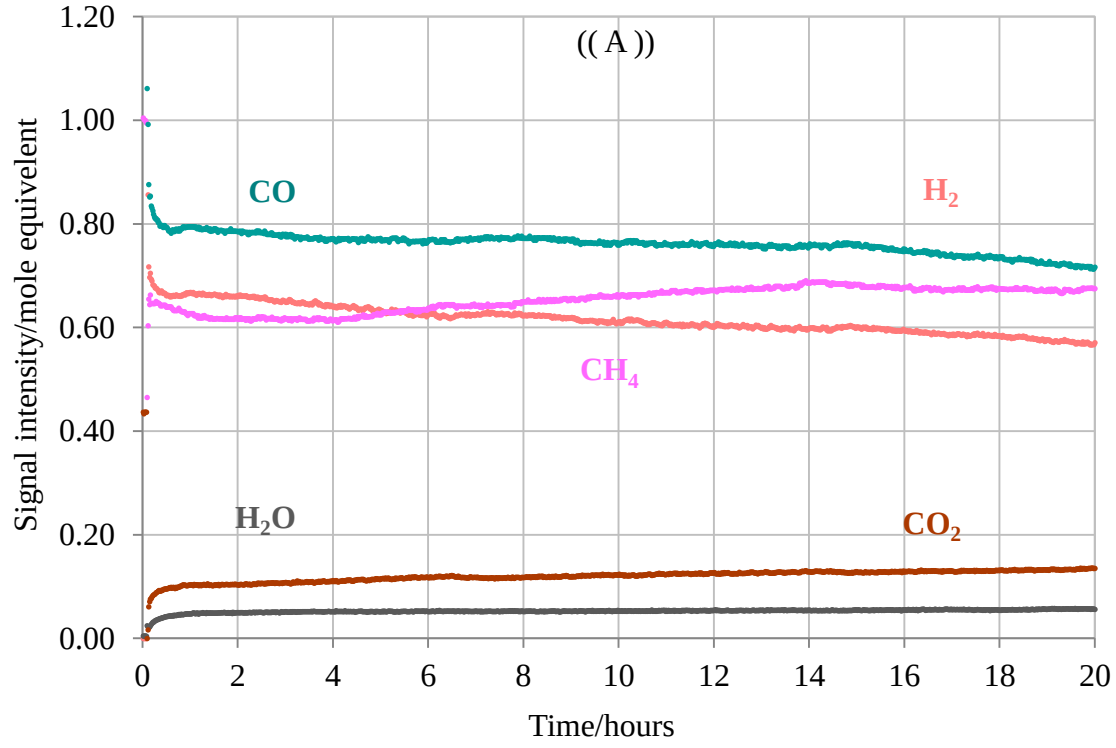

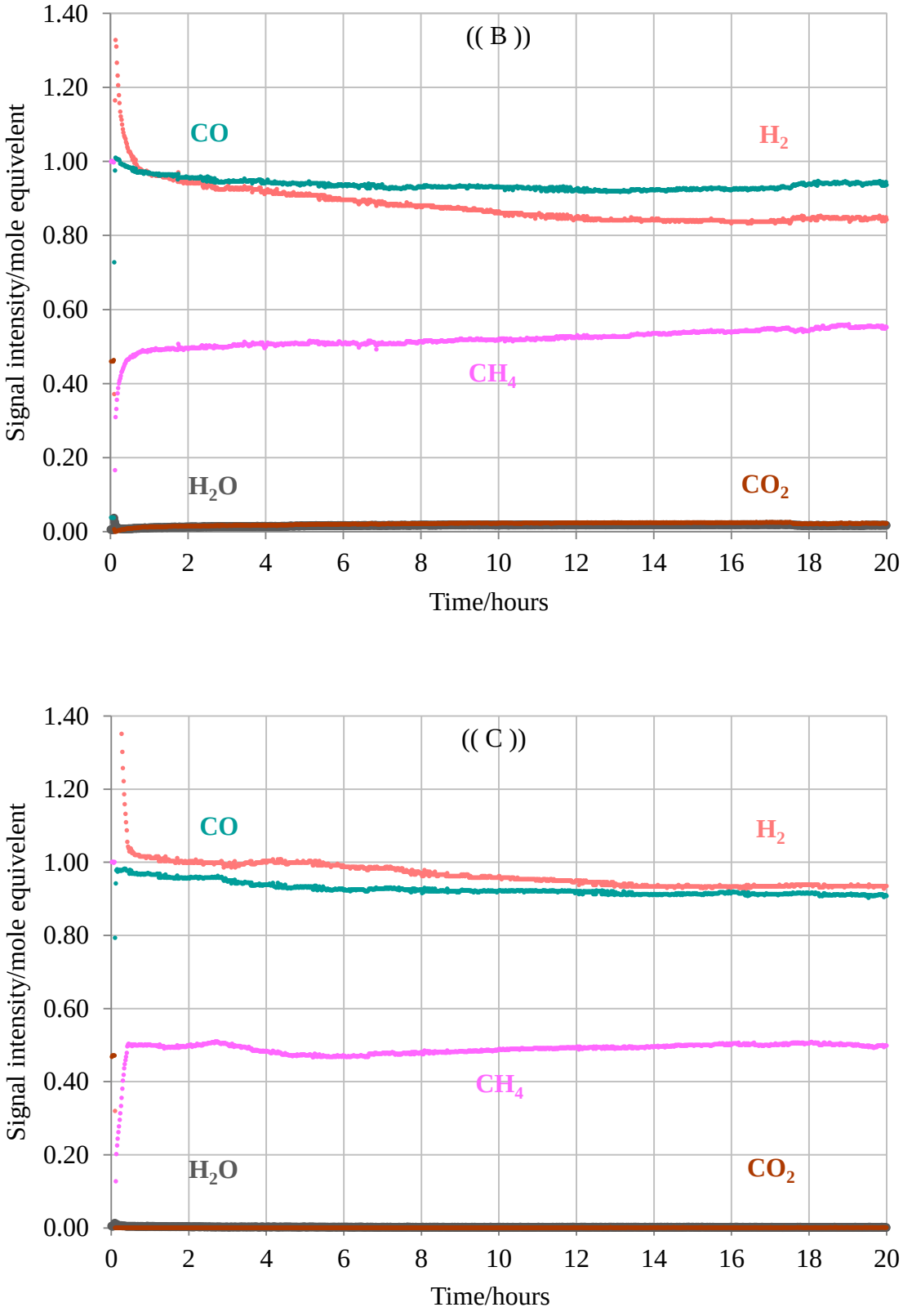

Figure 4.9: Biogas reforming profiles of 2:1 CH_4 /CO_2 mixture over Ni-Fe doped $SrZrO_3$ for 20 hours of reaction at (A) 700 °C, (B) 800 °C and (C) 900 °C.

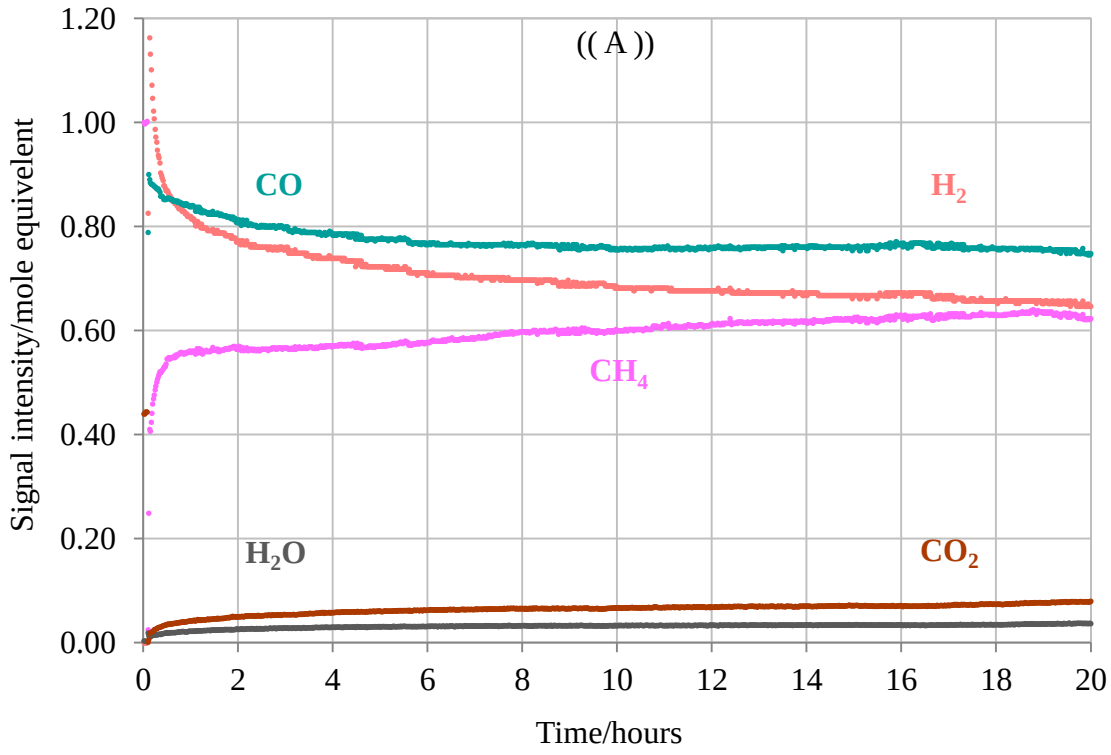
((A))
Signal intensity/mole equivelent
Time/hours
CO
H2
CH4
H2O
CO2
1.20
1.00
0.80
0.60
0.40
0.20
0.00
0
2
4
6
8
10
12
14
16
18
20

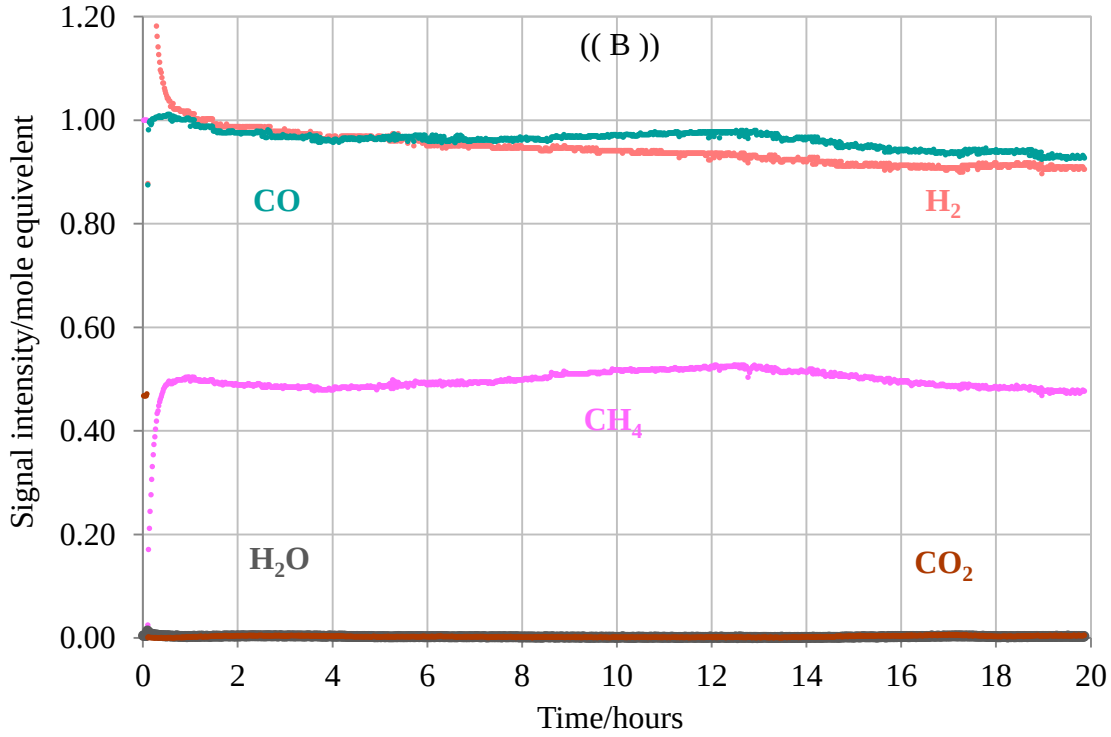
((B))
Signal intensity/mole equivelent
Time/hours
CO
H2
CH4
H2O
CO2
1.20
1.00
0.80
0.60
0.40
0.20
0.00
0
2
4
6
8
10
12
14
16
18
20

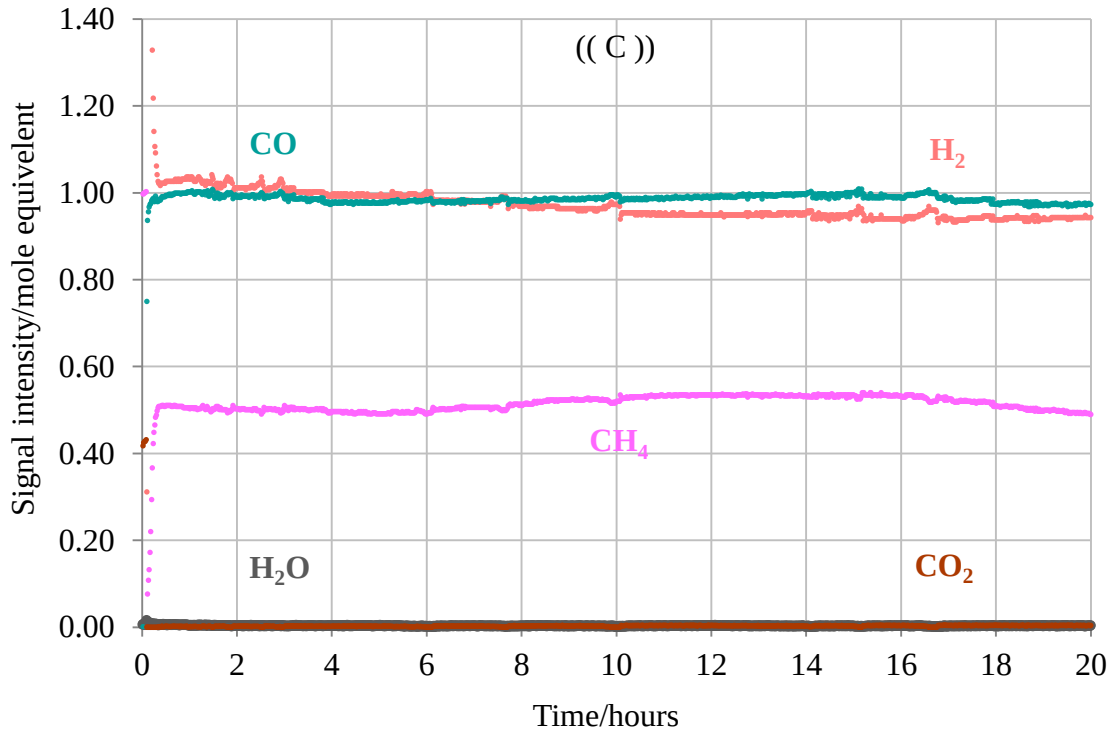

Figure 4.10: Biogas reforming profiles of 2:1 CH_4 /CO_2 mixture over Ni-Ru doped $SrZrO_3$ for 20 hours of reaction at (A) 700 °C, (B) 800 °C and (C) 900 °C.

It has been noted that there is potential for the RWGS reaction to occur and this coincides with the presence of a high concentration of CO_2, resulting in the formation of steam and carbon monoxide and a reduction in the H_2 yield as seen in figures A for all catalysts. In this section all catalysts were shown to be reasonably stable under the reaction conditions with no catalytic deactivation seen and the syngas products predominating over water. The inclusion of a low level of Fe in the perovskite structure resulted in a greater stability to catalyst deactivation [12].

4.3.2.1 Methane and carbon dioxide conversions

Figures 4.11 and 4.12 show the average methane and carbon dioxide conversion for methane-rich reactions over three co-doped catalysts and the Ni supported catalyst,

during 20 hours of testing at three temperatures. Methane conversion is observed to be higher for the doped perovskite materials than for the nickel supported catalyst and this increase with increasing reactor temperature. And at 900 °C reaches 51% CH_4 conversion for the Ni-Fe doped and Ni-Al doped $SrZrO_3$ catalysts. This suggests the formation of a small amount of solid carbon on the surface of the catalysts due to decomposition of excess methane.

All of the co-doped perovskites maintain a greater CO_2 and CH_4 conversion than that of the Ni supported alumina catalyst especially at 900 °C and 800 °C, indicating that the perovskites have better performance toward reactant conversion than the Ni/Al_2O_3. Whereas at 700 °C, a difference in activity is observed where the 10% Ni supported Al_2O_3 converts roughly 6% more of the CO_2 than the Ni-Fe doped perovskite. However the Ni-Ru doped perovskite shows an 86% CO_2 conversion.

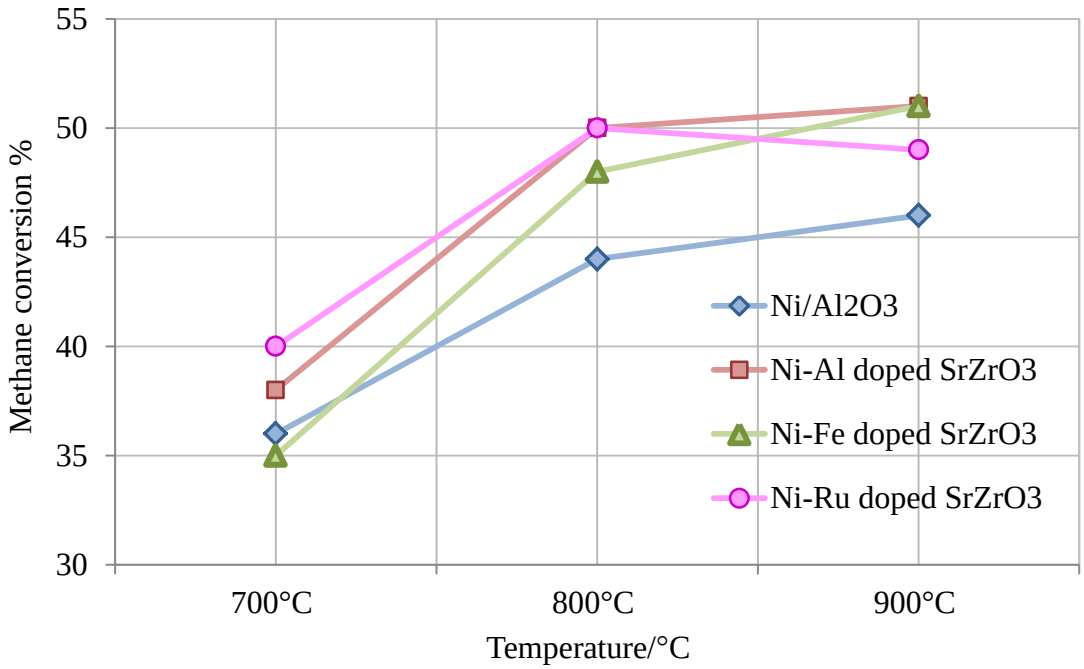

Figure 4.11: Average CH_4 conversions as a function of time for 20 h of 2:1 CH_4 /CO_2 mixture over four catalysts at three different temperatures.

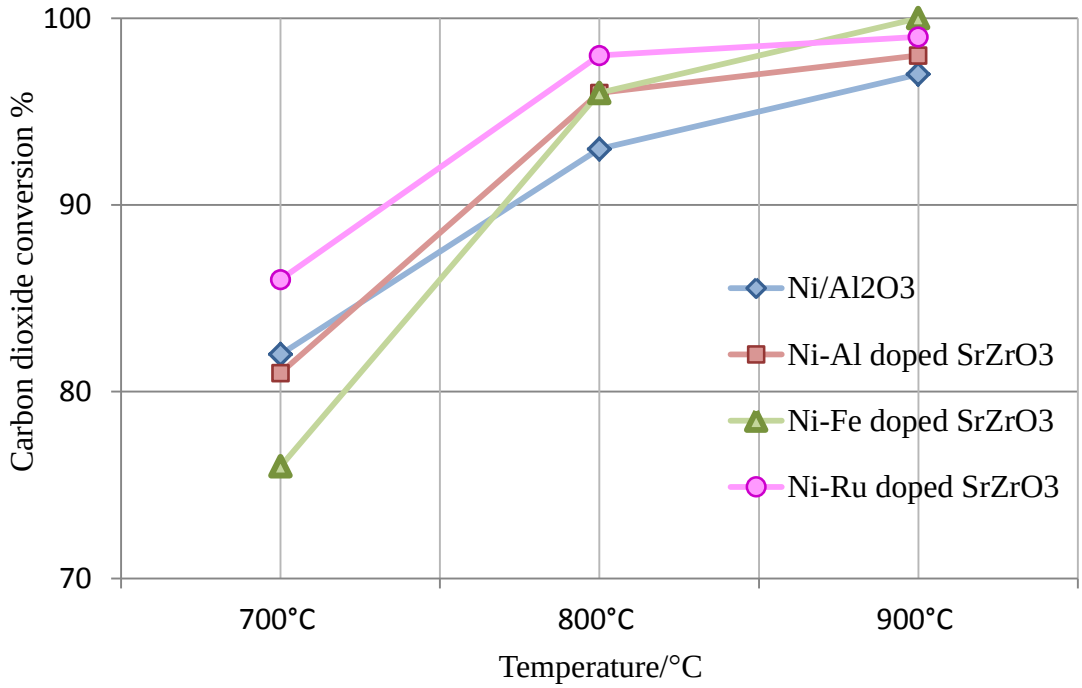

Figure 4.12: Average CO_2 conversion as a function of time for 20 hours of 2:1 CH_4 /CO_2 mixture over four catalysts at three different temperatures.

With methane rich conditions, CH_4 conversions of greater than 50% should not be possible without methane cracking. With the Ni-Ru doped perovskite a CH_4 conversion of 49% suggest that carbon dioxide reforming was occurring close to stoichiometrically, with no occurrence of side reactions such as methane decomposition. A greater reforming activity is reported for the co-doped perovskite samples than Ni supported alumina at high temperature. However, at low temperature the Ni-Fe doped $SrZrO_3$ perovskite displays a lower performance than that of any other catalysts in this study.

4.3.2.2 Syngas production

The differences in catalytic performance can be distinguished by product selectivity. Figures 4.13 and 4.14 show the hydrogen and carbon monoxide yield at different reaction temperatures for four catalysts. At 800 °C and 900 °C, the hydrogen yield for the co-

doped perovskite materials was higher than for the Ni supported material and reaches 99, 97% and 97, 94% by 900 °C and 800 °C for Ni-Al doped and Ni-Ru doped perovskite respectively. Whilst at 700 °C, it was either higher or lower than the yield for the supported catalyst. All catalysts gave the highest yield of H_2 and CO at 900 °C and the reaction profiles show that the co-doped materials are active towards the water gas shift reaction especially at 700 °C.

As we can see, a large increase in the amount of synthesis gas occurs for all catalysts on increasing the temperature from 700 °C to 800 °C, suggesting that there is an increase in adsorption-desorption processes with increasing temperature and hence the carbon dioxide is fully consumed to produce the main products.

Ni-Al doped perovskite catalyst gives a higher production of hydrogen at all reaction temperatures compared to all the other catalysts in this study, suggesting it has a higher activity under methane rich reaction conditions. At 900 °C the hydrogen and carbon monoxide yield for the co-doped perovskite catalyst exceeds the yield from the nickel supported material and the CO yield for the co-doped perovskite materials at all temperatures was higher than the yield for 10% Ni/Al_2O_3.

At 700 °C the H_2 /CO ratio was less than 1 for all catalysts, which is due to the occurrence of the RWGS. In contrast at 900 °C, the H_2 /CO ratio increased to greater than 1 in most of the catalysts partly because there was low level of methane decomposition and less occurrence of the RWGS. However, it remains close to the stoichiometrically predicted level for the biogas reforming reaction. Ni-Al doped perovskite shows a greater increase in H_2 /CO ratio (1.04) at 800 °C than the other catalysts and this is caused by the total consumption of carbon dioxide and a very low level of methane decomposition.

The Ni-Fe doped perovskite has a lower H_2 /CO ratio with an average of 0.81 at 700 °C and this increases steadily with temperature due to the decreasing occurrence of the RWGS reaction .This is attributed to the consumption of some hydrogen that is reflected by the production of water observed in the reforming reaction profile, which has a selectivity of 5% in the reaction.

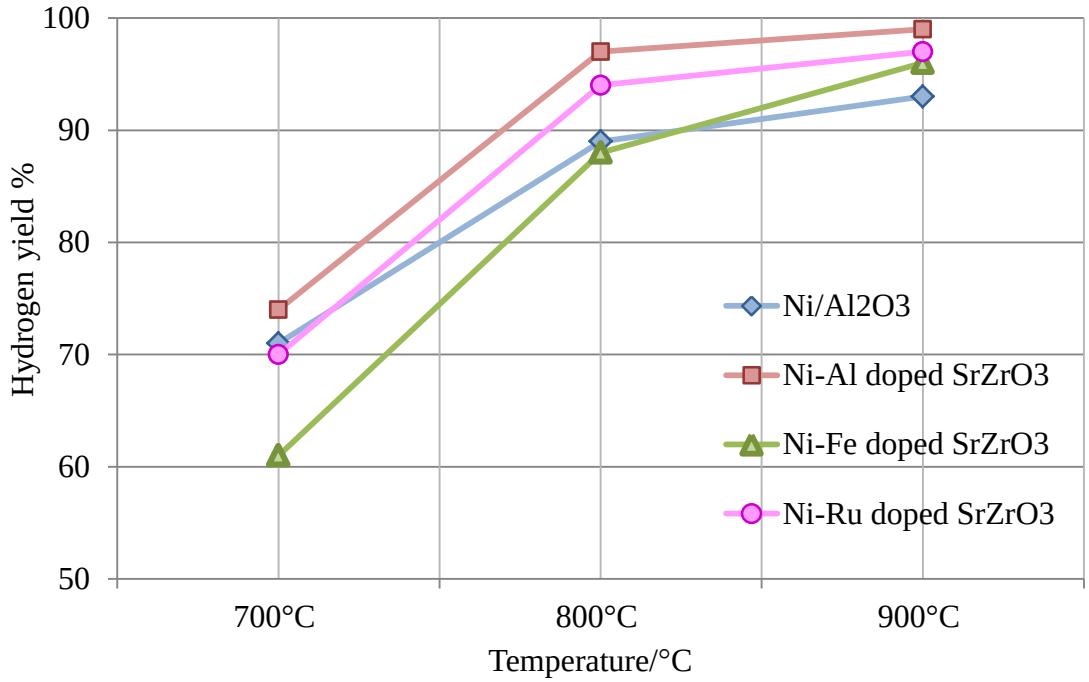

Figure 4.13: Average hydrogen yield as a function of time for 20 hours of 2:1 CH_4 /CO_2 mixture over four catalysts at three different temperatures.

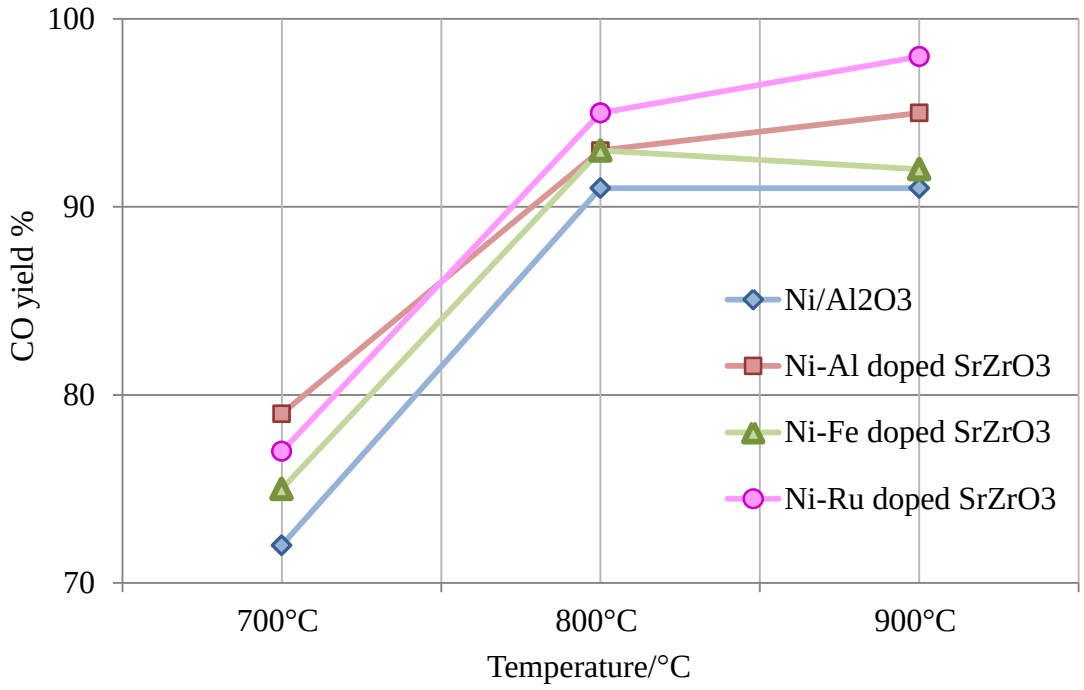

Figure 4.14: Average carbon monoxide yield as a function of time for 20 hours of 2:1 CH_4 /CO_2 mixture over four catalysts at three different temperatures.

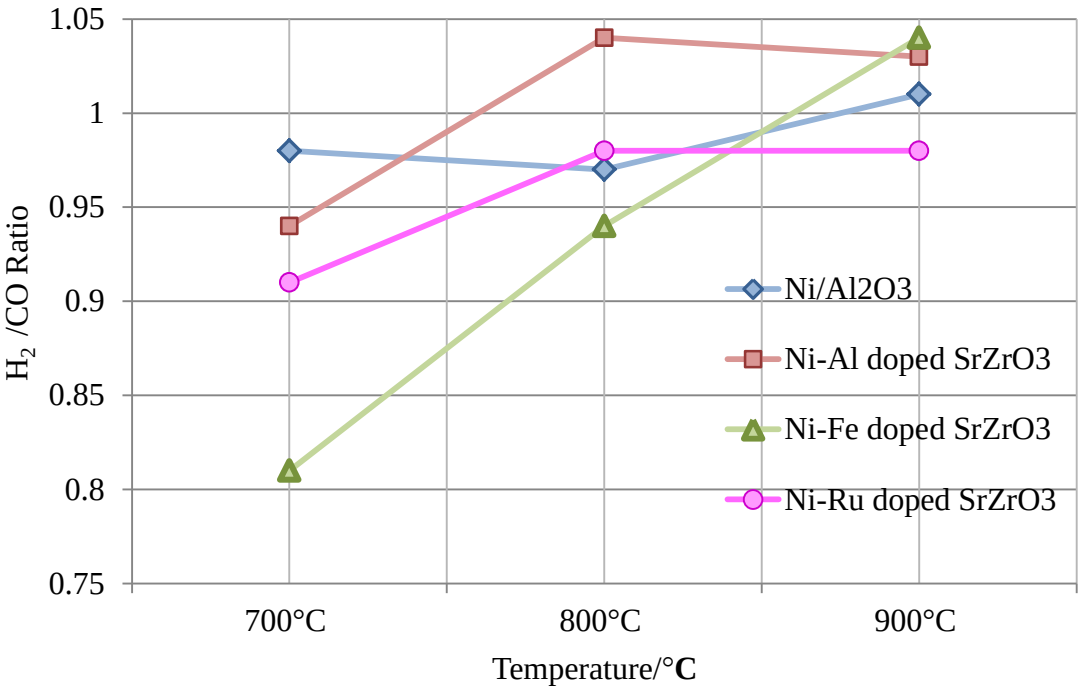

Figure 4.15: Average value of H_2 /CO Ratio as a function of time for 20 hours of 2:1 CH_4 /CO_2 mixture over four catalysts at three different temperatures.

Based on this study, the highest catalytic activity and stability for the biogas reaction was obtained over the Ni-Al doped perovskite at three determined temperatures in terms of both methane conversion and H_2 yield. The H_2 /CO ratio remains nearly 1 under all reaction condition even at elevated temperature due to the being less active towards the undesirable decomposition of methane and carbon formation reactions. These results show that the co-doped perovskite materials may be suitable for promoting biogas reforming on an industrial scale.

For comparison purposes the reaction profiles for the mono doped (4% Ni doped $SrZrO_3$) show that the consumption of methane continues to increase with temperature despite the carbon dioxide being fully consumed and the hydrogen yield exceeds 100% by the highest temperatures (900 °C) due to the decomposition of excess methane as reported by Evans et. al [13]. While, all three co-doped perovskites had lower propensity toward methane decomposition and carbon deposition due to the full consumption of carbon dioxide with ~50% methane conversions.

In general, the catalytic activity and selectivity for syngas production depended on the nature of the doping metals, as well as reaction temperature, which decreased in the order of Ni-Al doped > Ni-Ru doped > Ni-Fe doped at 700 °C. The low activity of the Ni-Fe doped catalyst is due to a weak metal-metal interaction at low temperature as confirmed by temperature programmed reaction (see figure 4.3).

4.3.3 Temperature programmed oxidation studies (TPO)

Temperature programmed oxidation was then carried out to quantify and compare the amount of carbon deposited on each catalyst. Deposition of carbon-containing species on

metal catalysts is inevitable in any reaction involving hydrocarbons and it is considered one of the main causes of catalyst deactivation. By far the most common technique utilized to characterize catalysts deactivated by carbon deposition is TPO.

Figures (4.16, 4.17, 4.18, and 4.19) show TPO profiles over four catalysts following biogas reforming reactions, While the amount of carbon produced over each catalyst differs, the TPO profiles from each reaction are similar to each other in terms of having one peak at approximately 600 °C, 615 °C, 665 °C and 715 °C, indicating similarities in the nature of the carbon. Moreover, it can be said that the carbon produced during 20 hours of operating at different temperatures was of a similar type in the sense that it did not appear to cause full deactivation of any of the catalysts.

Carbon quantification shows a trend of increasing carbon deposition with increasing reaction temperature. This trend may be attributed to the slight increase in the methane cracking reaction occurring at high temperatures. Figure 4.16 shows the TPO profiles following 20 h of methane-rich reactions at three specific temperatures 700 °C, 800 °C and 900 °C. These profiles suggest that the amount and nature of the carbon deposition was changing with reaction temperature. The size of the CO_2 desorption peak increases and shifts to higher temperatures relative to the reaction temperature at 900 °C, indicating that the carbon deposition was evolving to a slightly more stable form.

Low carbon deposition at 700 °C is strong evidence of the occurrence of the Boudouard reaction, which is an exothermic process and thus is prevalent at lower temperatures. There was an increase in carbon formation at higher operating temperature, which is indicative of methane decomposition occurring as shown in figure 4.16. While in figure 4.19, the reverse Boudouard reaction appears to dominate, causing a reduction in carbon deposition on increasing the temperature from 800 °C to 900 °C.

Suppression of methane decomposition has been observed clearly at 800 °C with the Ni-Al doped and Ni-Fe doped materials, resulting in less carbon deposition. The variation in the amount of carbon deposition with reaction temperature was also significant for the Ni-Ru doped catalyst. The ruthenium doped material exhibited low rates of carbon formation whilst maintaining a high reactant conversion and H_2 /CO ratio [14, 15]. The high CH_4 conversion over Ni-Al doped and Ni-Fe doped catalysts at 900 °C caused high levels of carbon formation and this is consistent with the increasing H_2 /CO ratios.

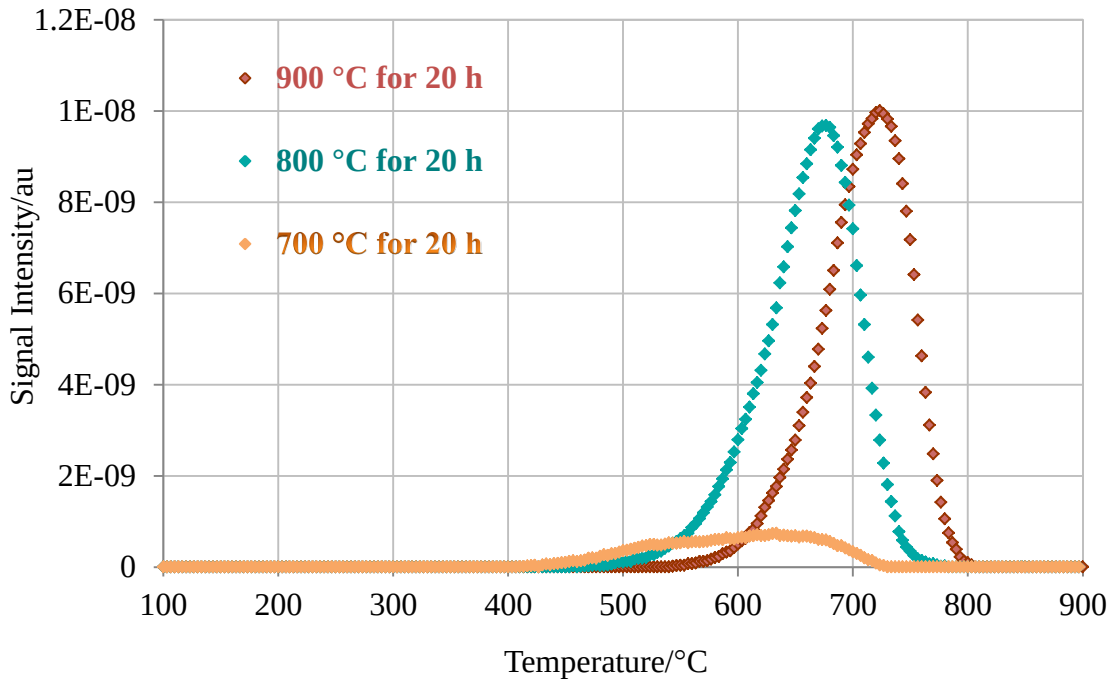

Figure 4.16: Carbon deposition profiles as a function of temperature after 20 hours of reforming reaction of a 2:1 CH_4 /CO_2 mixture over 10% Ni/Al_2O_3 catalyst at three specific temperatures.

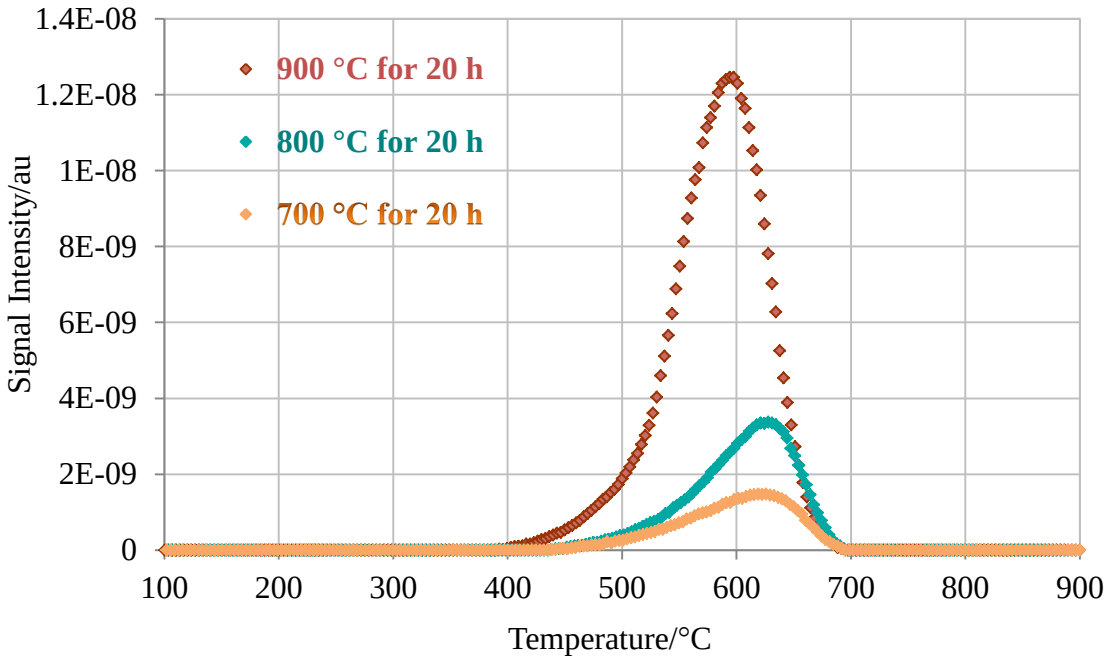

Figure 4.17: Carbon deposition profiles as a function of temperature after 20 hours of reforming reaction of a 2:1 CH_4 /CO_2 mixture over Ni-Al doped $SrZrO_3$ catalyst at three specific temperatures.

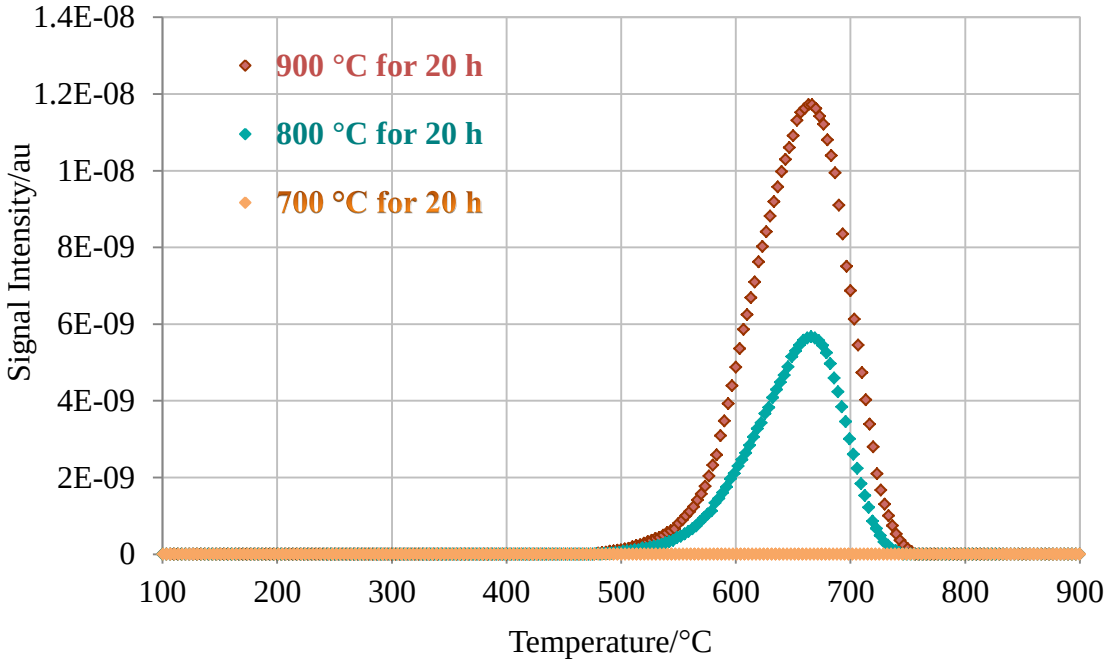

Figure 4.18: Carbon deposition profiles as a function of temperature after 20 hours of reforming reaction of a 2:1 CH_4 /CO_2 mixture over Ni-Fe doped $SrZrO_3$ catalyst at three specific temperatures.

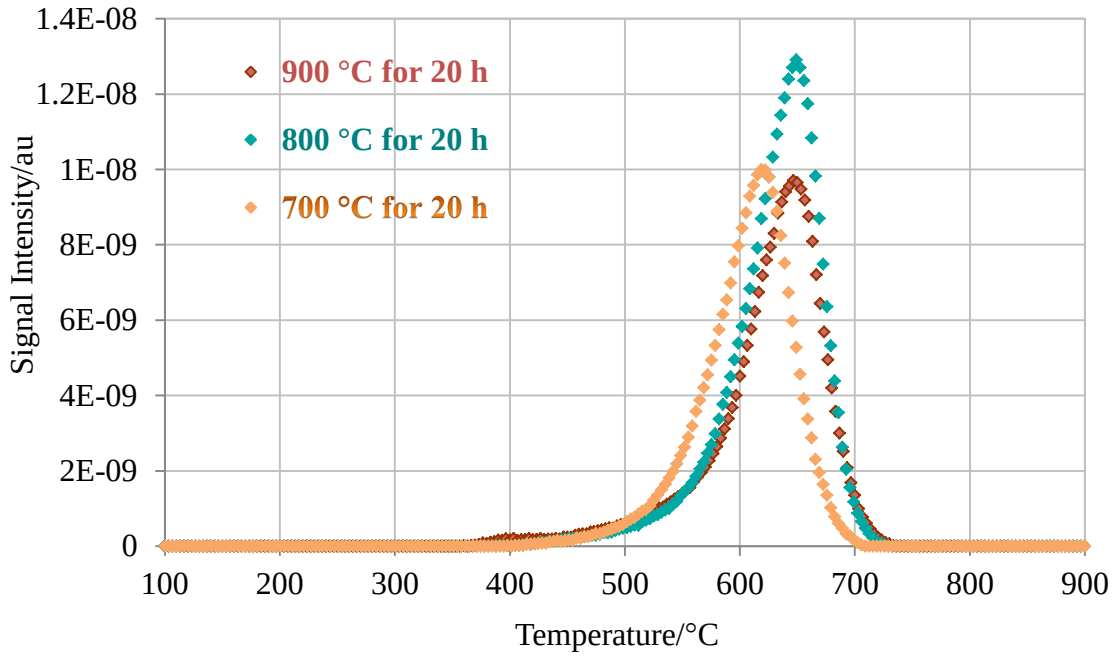

Figure 4.19: Carbon deposition profiles as a function of temperature after 20 hours of reforming reaction of a 2:1 CH_4 /CO_2 mixture over Ni-Ru doped $SrZrO_3$ catalyst at three specific temperatures.

Figures for the co-doped perovskites showed that altering the dopant metal did not alter the type of carbon formed during the reaction as all profiles contain one distinct peak approximately at the same temperature. It is likely that the catalytic dissociative adsorption of CH_4 caused the formation of graphitic carbon [16]. However, the different amounts of carbon produced indicate that the rate of carbon production is a function of reaction temperature, but does not act as a catalytic poison or prevent access of the reactants to the active sites of the catalyst surface. According to the evidence from reaction profiles for 20 h, there is no loss in reforming activity, indicating that the carbon formed is unlikely to be deactivating in nature.

A comparison of the amount of carbon deposited on each catalyst under reaction conditions after 20 hours is presented in figure 4.20. It shows a trend that is in agreement with the profiles that are presented in the figures above. The lowest level of carbon

deposited of the four catalysts was at 700 °C over the Ni-Fe doped perovskite. Whereas the Ni-Al doped shows the highest amount of carbon accumulation at 900 °C.

The formation of carbon was higher upon the Ni-Ru doped sample than any of the other catalysts at 800 °C. However the co-doped materials were shown to be more resistant to carbon deposition than 10% Ni/Al_2O_3 at specific temperatures. For example the Ni-Fe doped, Ni-Al doped and Ni-Ru doped perovskites have less carbon at 700 °C, 800 °C, and 900 °C respectively.

Figure 4.20 shows high levels of carbon formation at 900 °C compared with the levels at 700 °C that would limit the formation of CO and thereby increase the value of H_2 /CO ratios which is favoured at lower temperatures. The decrease in coke accumulation at lower temperatures was due to the simultaneous occurrence of the RWGS reaction and thus the H_2 /CO molar ratio drops below the equilibrium value.

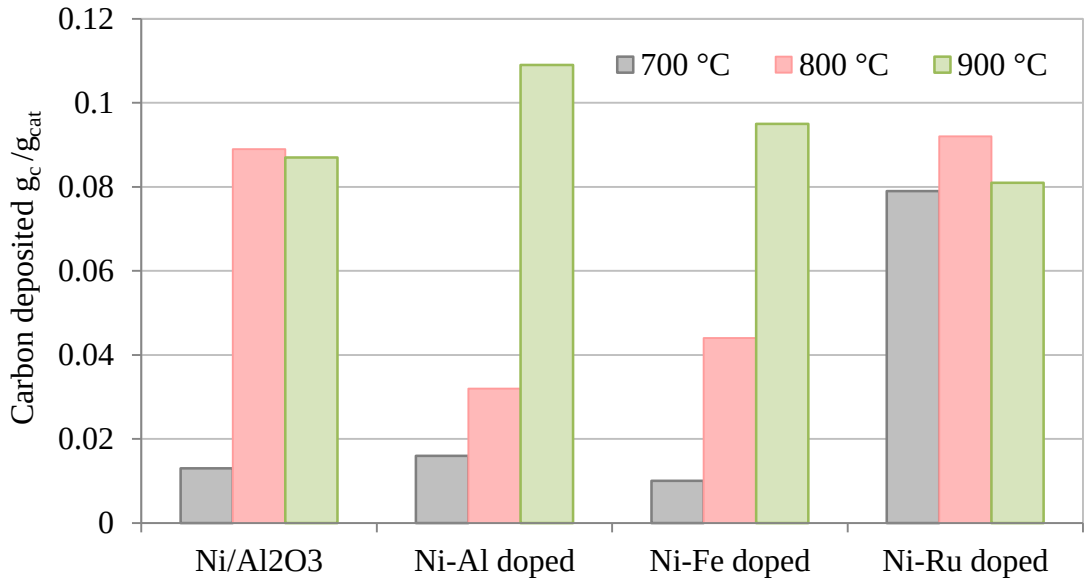

Figure 4.20: Comparison of carbon deposited on 10% Ni/Al_2O_3, Ni-Al doped $SrZrO_3$, Ni-Fe doped $SrZrO_3$ and Ni-Ru doped $SrZrO_3$ for 20 h at various temperatures in gram of carbon per gram of catalysts.

4.4 Influence of contact time on CH_4 decomposition and carbon deposition

To gain more insight into the methane decomposition and carbon deposition during the dry reforming reaction, temperature programmed reactions were performed as a function of time on stream at 900 °C for 3 hours and 20 hours for the Ni-Ru doped $SrZrO_3$ and the Ni-Fe doped $SrZrO_3$ catalysts. TPR and TPO reactions were carried out to determine the relationships between reaction time, carbon formation and methane decomposition. The reforming characteristics are displayed in figures 4.21 and 4.22 show that all of the carbon dioxide is consumed and as a result are unavailable for the reverse water gas shift reaction to occur and the H_2 /CO ratio is ~1 as well as no sign of methane decomposition occurs. The catalysts did not deactivate for at least 20 hours on stream under reforming conditions.

At the beginning of the reaction the initial production of H_2 was much higher than for carbon monoxide and it is likely this was due to a high level of temporary methane pyrolysis occurring on the catalyst surface when the surface active sites were clean and in the most reduced state. This led to an initial rapid formation of carbon and it is likely that the largest levels of carbon were deposited in the first half an hour of the reaction. This is further evidence that the carbon was inert, and becomes less active with time on stream as seen in figures 4.23 and 4.24. The conversion of CO_2 began steadily and remained approximately constant throughout the reaction, resulting in steady CO production. A stable methane conversion and hydrogen production occurred after 30 and 20 minutes for the Ni-Fe doped and Ni-Ru doped respectively.

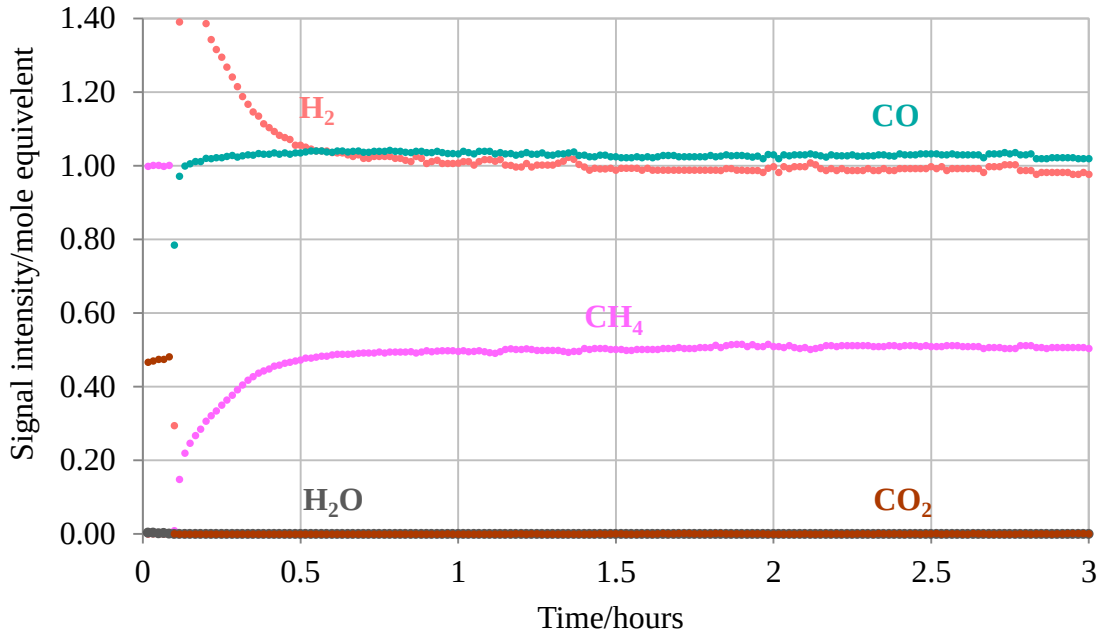

Figure 4.21: Biogas reforming profile of a 2:1 CH_4 /CO_2 mixture at 900 °C for 3 hours of conversion reaction over Ni-Fe doped $SrZrO_3$.

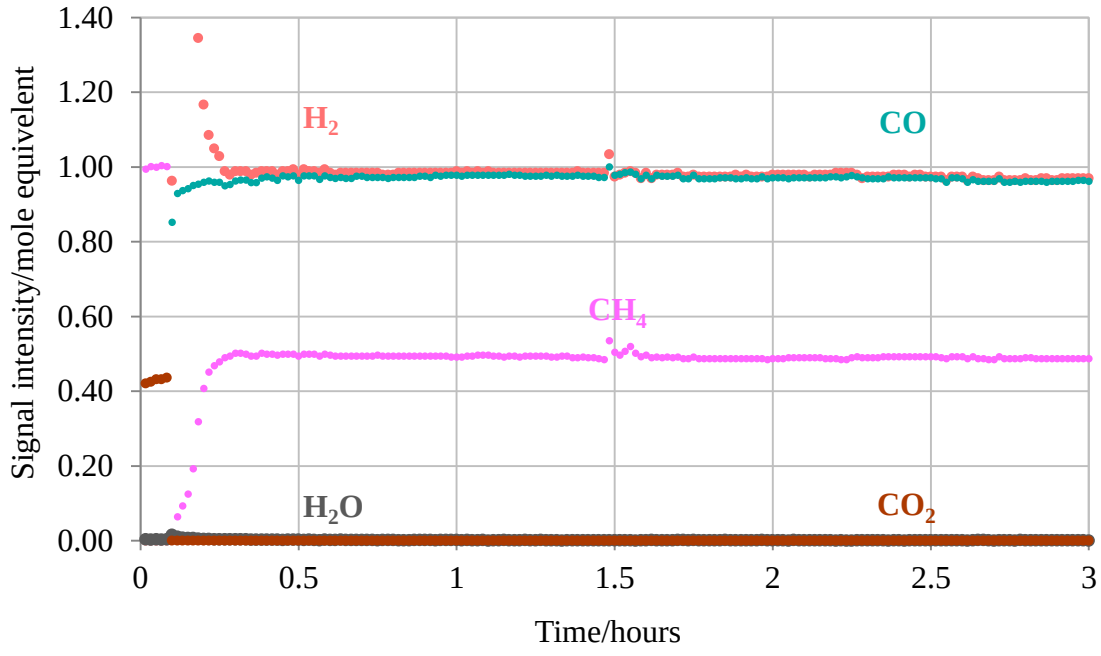

Figure 4.22: Biogas reforming profile of a 2:1 CH_4 /CO_2 mixture at 900 °C for 3 hours of conversion reaction over Ni-Ru doped $SrZrO_3$.

The profiles of carbon production as a function of reaction temperature after 3 and 20 hours of reforming reaction are shown in figures 4.23, 4.24. Ni-Fe doped perovskite gave a profile which proposes that the level of coke deposition was slightly greater over this sample compared to the Ni-Ru doped sample, due to the iron doped catalyst having a higher activity for carbon dioxide consumption than ruthenium doped under these reaction conditions. The interaction between nickel and ruthenium improved the stability of the catalysts and decreased coke formation [17].

Table 4.1 gives the values of CH_4 and CO_2 conversions, H_2 and CO yields and H_2 /CO molar ratios for each reaction temperature. As observed from the results in this table, the amount of H_2 and CO production was slightly decreased with increasing reforming time. It was clear that the high methane conversions caused small amounts of carbon formation on the surface of catalysts. As mentioned earlier, the origins of inactive carbon during dry reforming may occur via CH_4 cracking (endothermic reaction).

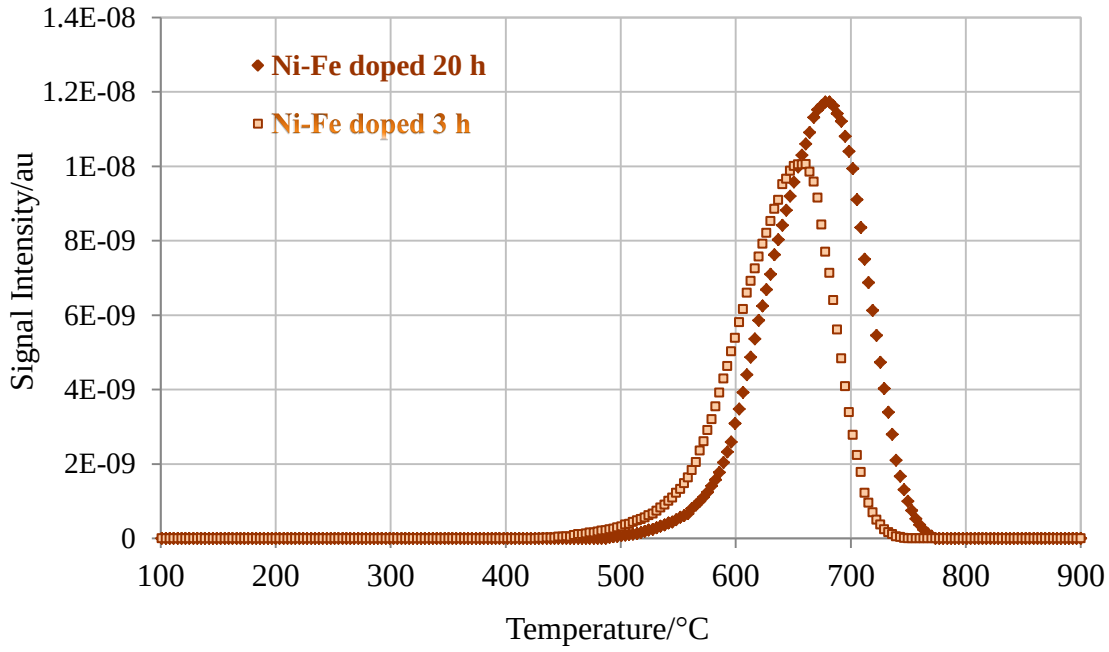

Figure 4.23 TPO profiles of isothermal reforming reactions for 2:1 CH_4 /CO_2 mixture over Ni-Fe doped $SrZrO_3$ perovskite catalyst at 900 °C after 3 and 20 hours of reactions.

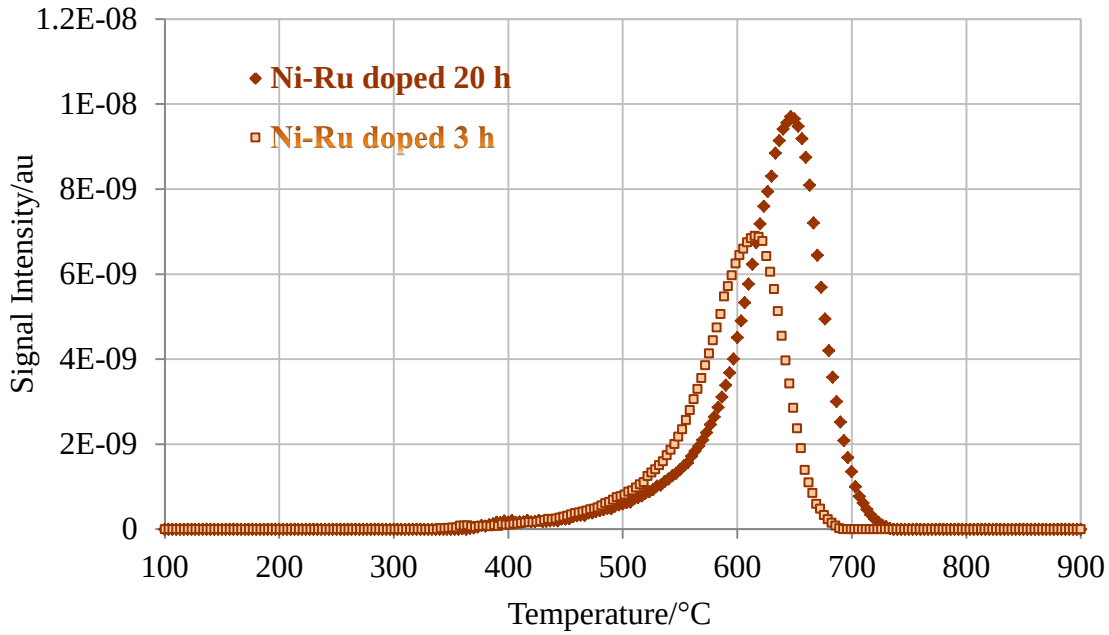

Figure 4.24 TPO profiles of isothermal reforming reactions for 2:1 CH_4 /CO_2 mixture over Ni-Ru doped $SrZrO_3$ perovskite catalyst at 900 °C after 3 and 20 hours of reactions.

As can be seen from post reaction profiles, different co-doped perovskites displayed a single carbon dioxide peak with a slight shift towards higher peak temperatures seen after 20 hours of reaction, suggesting that only one form of carbon is being formed over the co-doped perovskites. The amount of carbon gives an indication that the co-doped perovskites have a low propensity toward methane decomposition because the levels of carbon only increased by 0.006 g and 0.022 g for Ni-Fe doped and Ni-Ru doped respectively going from 3 to 20 hours of reformation reaction.

Table: 4.1 Average CH_4, CO_2 conversions and H_2, CO production as well as carbon formation over Ni-Fe doped $SrZrO_3$, and Ni-Ru doped $SrZrO_3$ at 900 °C after 3 hours and 20 hours of reaction.

Biogas reforming reaction results at 900 °C						
3 hours						
Samples	CH_4%	CO_2%	H_2%	CO%	H_2/CO	Carb. g_c/g_{cat}
Ni-Fe doped $SrZrO_3$	51	99	99	99	0.97	0.090
Ni-Ru doped $SrZrO_3$	51	99	99	96	1	0.059
20 hours						
Samples	CH_4%	CO_2%	H_2%	CO%	H_2/CO	Carb. g_c/g_{cat}
Ni-Fe doped $SrZrO_3$	51	100	96	92	1.04	0.096
Ni-Ru doped $SrZrO_3$	49	99	97	98	0.98	0.081

4.5 Conclusion

The main problems found by most studies in methane rich conditions are related to coke deposition and deactivation. Reaction temperatures have a significant influence on biogas reforming and can be observed by the increasing reactant conversion with increasing temperature. In addition numerous side reactions such as methane decomposition, Bouduard reaction and RWGS also affect the H_2 /CO ratio and carbon deposition.

The effect of co-doped metal ions into the perovskite catalysts was found to play a major role in the catalytic biogas performance. Among all the catalysts, and in comparison with Ni supported alumina, Ni-Al doped $SrZrO_3$ perovskite possessed good performance as it has achieved higher methane conversion, H_2 production and thermal stability with a low level of carbon formation.

Isothermal studies showed that the co-doped $SrZrO_3$ perovskite materials were more stable than the Ni supported catalyst towards the formation of synthesis gas which decreased from 99% after 2 hours to 83% at the end of the reformation by 900 °C. Despite the variation in the amount of carbon deposition on the catalysts at different temperatures, Fe-Ni doped $SrZrO_3$ gave the lowest carbon formation at 700 °C. While Al-Ni doped $SrZrO_3$ and Ru-Ni doped $SrZrO_3$ proved to be the best at 800 °C and 900 °C respectively.

Generally, hydrothermally synthesised co-doped perovskite catalysts show promising results for industrial application in terms of having a stable activity, high selectivity towards the reforming reaction and syngas production with little or no evidence of any undesirable side reactions occurring and with very little carbon deposition.

Reaction profiles have shown that all catalysts maintain a H_2 /CO product ratio of ~1 at higher reaction temperatures. However, the co-doped catalysts are at least as active as nickel supported alumina catalyst but contain significantly less active metal and all show very low amounts of carbon.

4.6 Reference

[1] O.A. Bereketidou, and M.A. Goula, *Catal. Today*, 2012, **195**, 93–100.

[2] A. Moral, I. Reyero, C. Alfaro, Fernando Bimbela, and L. M. Gandí, *Catalysis Today*, 2018, **299**, 280–288.

[3] K. Tomishige, M. Nurunnabi, K. Maruyama, and K. Kunimori, *Fuel Processing Techno*., 2004, **85**, 1103 – 1120.

[4] S. Wang and G. Q. (Max) Lu, *Energy & Fuels*, 1996, **10**, 896-904.

[5] L. F. Bobadilla, V. Garcilaso, M. A. Centeno, and J. A. Odriozola, *ChemSusChem,* 2017, **10**, 1193-1201.

[6] Y. Schuurman, C. Marquez-Alvarez, V.C.H. Kroll, and C. Mirodatos, *Catal. Today*, 1998, **46**, 185-192.

[7] J. Staniforth and R. M. Ormerod, *Catalysis Letters*, 2002, **81**, 19-23.

[8] Z. Jiao, N. Shikazono and N. Kasagi, *J. Power Sources*, 2011, **196**, 8366–8376.

[9] D. Pakhare and J. Spivey, *Chem. Soc. Rev*., 2014, **43**, 7813-7837.

[10] C. J. Laycock, J. Z. Staniforth and R. M. Ormerod, *Dalt. Trans.*, 2011, **40**, 5494.

[11] D. J. Nixon, PhD Thesis, Keele University, 2013.

[12] S. M. de Lima and J. M. Assaf, *Catalysis Letters*, 2006, **108**, 63-70.

[13] S. E. Evans, PhD Thesis, Keele University, 2016.

[14] L. S. Gangurde, G. S. J. Sturm, M. J. V.Romero, R. Mallada, J. Santamaria, A. I. Stankiewicz and G. D. Stefanidis, *Chem. Eng.& Processing*, 2018, **127**, 178-190.

[15] G. S. Kim, B. Y. Lee, H. C. Ham, J. Han, S.W. Nam and J. Moon, S. P. Yoon, *Int. J. Hydrogen Energy*, 2018, 1-11.

[16] X. Junke, Z. Wei, W. Jihui, L. Zhaojing and M. Jianxin, *Chin J Catal*, 2009, **30**, 1076–1084.

[17] G. C. de Araujo, S. M. de Lima, J. M. Assaf, M. A. Pen˜a, J. L. G. Fierro and M. C. Rangel, *Catal. Today*, 2008, **133**, 129–135.

Chapter 5

Studies for Dry Reforming of Methane

5. Dry Reforming of Methane (DRM) over all Catalysts

5.1 Introduction

Dry reforming of methane has been widely researched, with most studies showing a quick formation of carbon. For dry reforming, carbon deposition induces deactivation of the catalyst. Carbon formation as an unavoidable side reaction can occur by methane decomposition at high temperature and by the Boudouard and CO reduction reactions at low temperatures. Therefore, there is no operation temperature that is thermodynamically free of carbon formation.

However, another reversible slightly endothermic side reaction usually accompanies dry reforming (reverse water-gas shift reaction), which is driven by the presence of a high concentration of CO_2 at a temperature range of approximately 400 °C- 800 °C, leading to the production of water and reducing the H_2 /CO molar ratio to slightly less than unity. This H_2 /CO mixture can be used to produce a range of products via Fischer-Tropsch synthesis processes such as diesel and alcohols [1, 2].

Because the dry reforming reaction is endothermic it requires operating temperatures of 800 °C –1000 °C to attain a high equilibrium conversion of CH_4 and CO_2 to H_2 and CO and it is usually accompanied by carbon forming side reactions [3]. At these high temperatures, traditional supported metal catalysts are not always stable and are prone to deactivation due to sintering and carbon formation [4]. The majority of catalysts used for the reforming process consist of supported nickel, mostly on aluminium oxides. However, these catalysts also catalyse carbon formation during the reaction [5].

Noble metals have received much attention by researchers and it has been reported that noble metal catalysts are extremely active for dry reforming and have a higher tolerance to carbon

accumulation compared to nickel. Therefore, it has been used to promote Ni based catalysts in order to increase their resistance to deactivation, but these are generally uneconomical because of their cost and availability [6]. These suggest that there is a requirement to develop catalysts that are useful for lowering the activation energy of the dry reforming reaction and increasing selectivity to H_2 and CO while resisting carbon formation as well as avoiding structural changes due to sintering at elevated temperatures.

It has been found that the addition of a low loading of ZrO_2 as promoter significantly improves the stability of Ni/Al_2O_3 catalyst for dry reforming in terms of increased coke resistance by enhancing the dissociation of oxygen intermediates, which then react with coke species that are formed over the metal [7].

In this study, the dry reforming of a 1:1 ratio (CH_4 /CO_2) has been performed over three perovskite catalysts: Ni-Al doped $SrZrO_3$, Ni-Fe doped $SrZrO_3$ and Ni-Ru doped $SrZrO_3$, in addition to the conventional 10% Ni/Al_2O_3. This was done to compare the effect of doping different active metals on the perovskite performance as well as to compare the activity of these catalysts to a conventional nickel supported catalyst.

5.2 Temperature programmed conversion reaction (TPCR)

After the reduction of the catalysts as a pre-treatment, temperature programmed reactions were performed to form CO and H_2 at about 440 °C, and the rate of product formation increased rapidly above 500 °C. TPCR was carried out to test the catalyst reactivity. Figures (5.1, 5.2, 4.3 and 5.4) show reforming reaction profiles of 1:1 CH_4 /CO_2 mixture over three co-doped perovskites and the Ni supported on alumina catalyst. It was found that the reaction profiles over all the catalyst samples exhibit a similar reaction progression

trend with a small variation in H_2 /CO ratio. A steady production of H_2 and CO started at approximately 440 °C until it reached above 800 °C where there is also a low-level production of water due to the reaction between hydrogen and unreacted carbon dioxide. The lowest levels of H_2 /CO ratio at the end of the reaction at 900 °C was by the Ni-Fe doped and Ni-Al doped (0.92 and 0.95) catalysts respectively. This was due to the greater occurrence of the RWGS reaction, while the Ni-Ru doped and Ni/Al_2O_3 have the highest ratio (1.02 and 1.01) respectively.

As can be seen from the figures, the thermodynamic equilibrium of reactants and products does not change significantly after ~800 °C. Although Ni-Fe doped perovskite has a higher light-off temperature than other catalysts, the conversion of reactants is complete at approximately 850 °C for all the catalysts. However, high temperatures, up to 900 °C are needed to fully convert the CH_4 and CO_2 into synthesis gas [8]. Over all the samples the reforming reaction begins at about 420 °C when the consumption of methane begins and syngas production rises linearly with an almost 1:1 ratio of H_2 /CO till 800 °C.

The reaction rate of methane conversion is enhanced by doping these co-active elements Ni-Fe or Ni-Ru or Ni-Al into the $SrZrO_3$ perovskite compared to the undoped $SrZrO_3$ that has limited catalytic activity as shown previously [9].

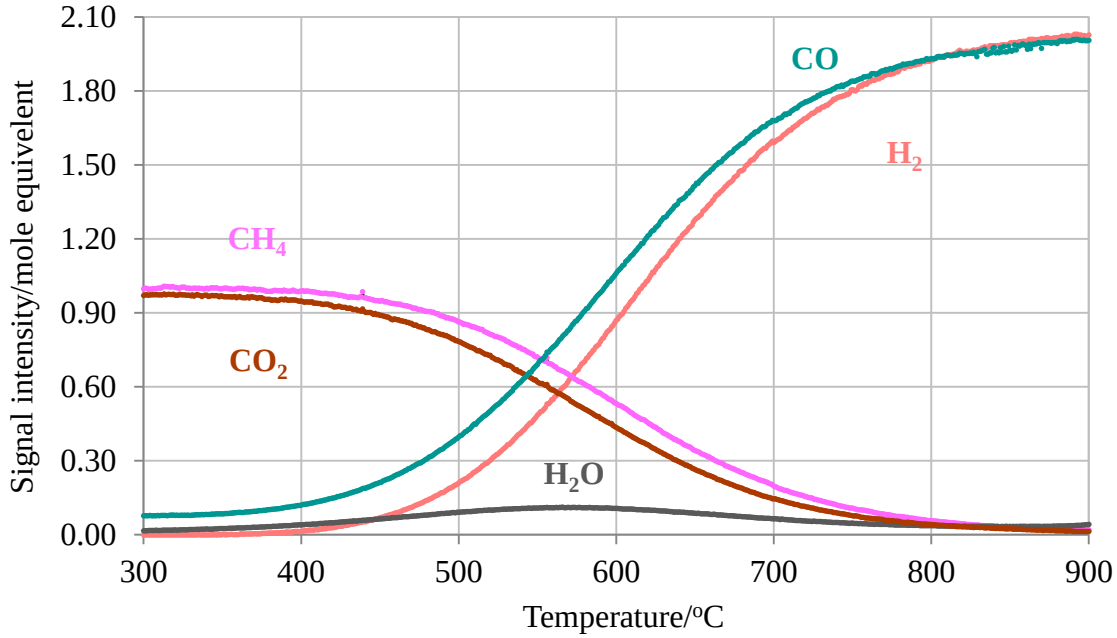

Figure 5.1: Reaction profile for a mixture of 1:1 CH_4 /CO_2 passed over 10% Ni/Al_2O_3 as a function of temperature.

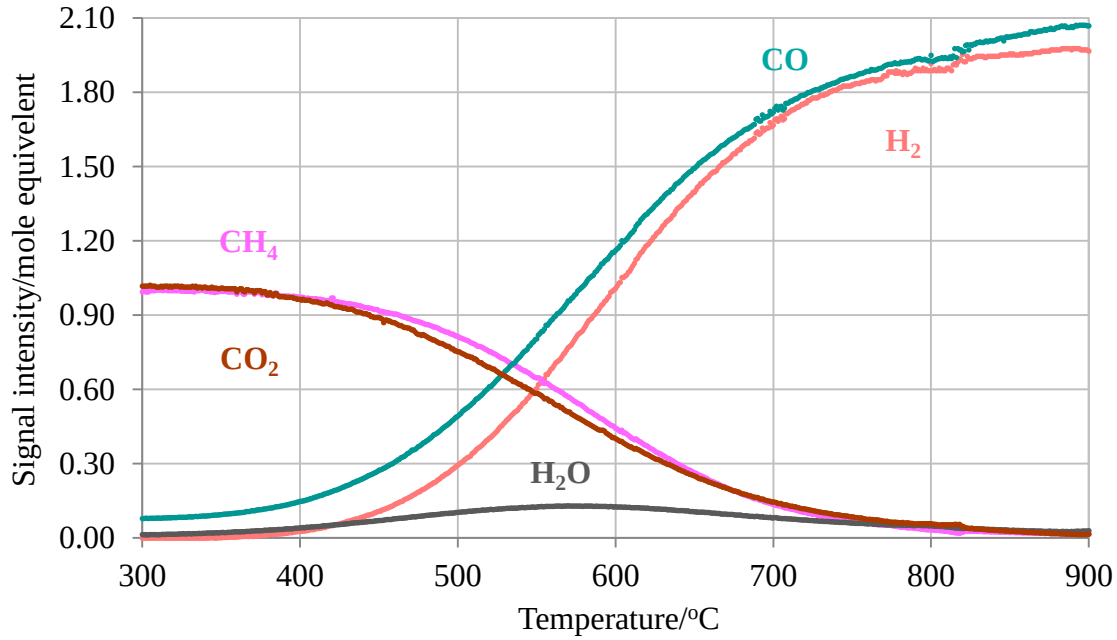

Figure 5.2: Reaction profile for a mixture of 1:1 CH_4 /CO_2 over Ni-Al doped $SrZrO_3$ as a function of temperature.

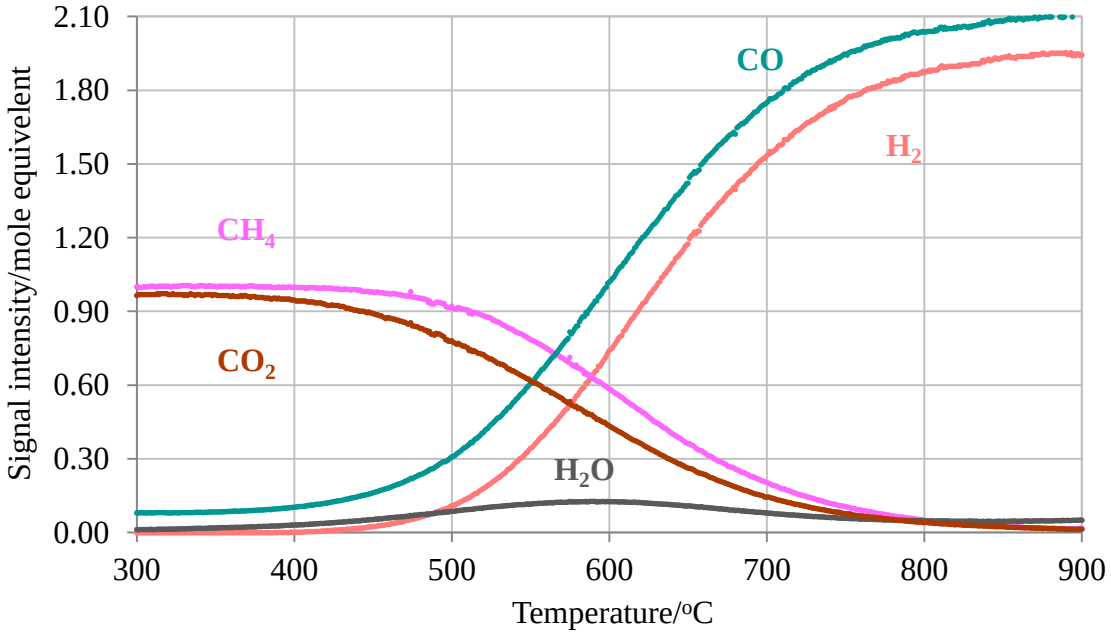

Figure 5.3 Reaction profile for a mixture of 1:1 CH_4 /CO_2 over Ni-Fe doped $SrZrO_3$ as a function of temperature.

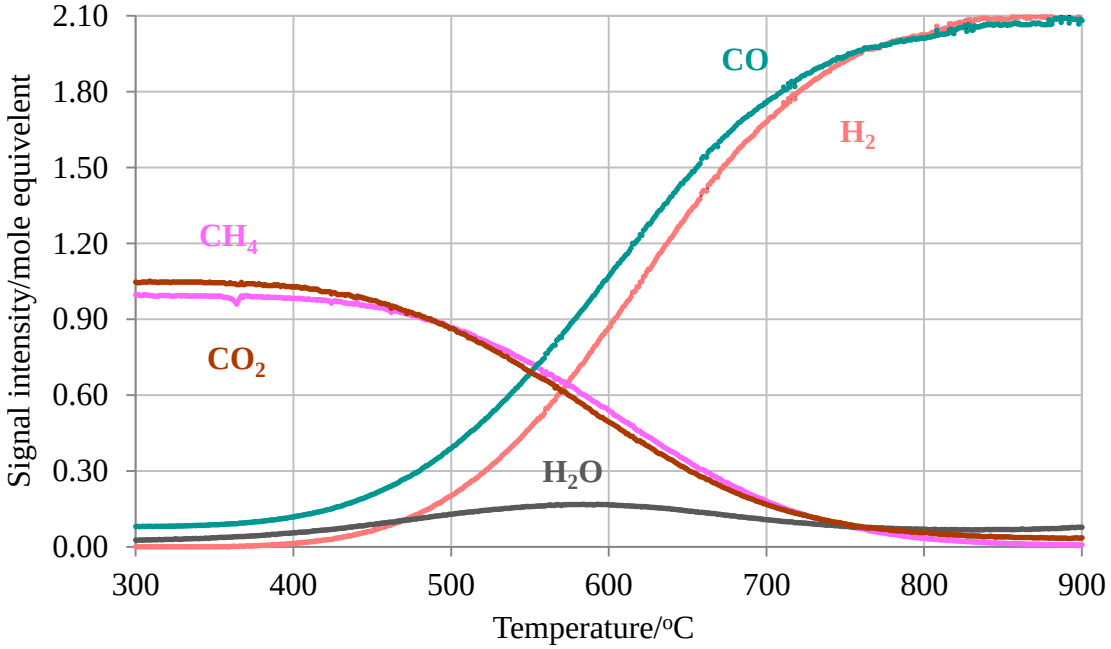

Figure 5.4: Reaction profile for a mixture of 1:1 CH_4 /CO_2 over Ni-Ru doped $SrZrO_3$ as a function of temperature.

The non-uniform conversion of CO_2 is strongly suggestive of the possibility that the addition of Fe within the perovskite increases the propensity of side reactions. In particular, an increase in the rate of the reverse water-gas shift reaction is inferred from the reaction profile obtained. This would explain the high CO /H_2 ratio. Once the reaction has begun methane conversion increases at roughly the same rate for all catalysts and reaches the maximum level by approximately 850 °C. Graphs show that the maximum reactant conversion and product yields was after 850 °C, this suggests that DRM should be performed at ~900 °C.

Methane conversion over each catalyst in this study is shown in figure [5.5]. Equilibrium conversions of CH_4 and CO_2 and the H_2 /CO ratio are typically influenced by the simultaneous occurrence of the side reactions, which results in the H_2 /CO ratios decreasing or increasing according to the type of side reaction. For example if the side reaction was RWGS as in the Ni-Fe doped sample, the H_2 /CO ratio will reduce and become less than 1 due to an increase in CO concentration as shown in equation 5.1.

$$CO_2 + H_2 \rightleftharpoons CO + H_2O \qquad \Delta H^{\circ}_{298K} = +41\ \text{kJ.mol}^{-1} \qquad [5.1]$$

Figure 5.5 shows that the activity is almost the same for all the catalysts. The only difference is the time to start the reforming reaction. The Ni-Fe co-doped catalyst takes slightly more time to begin the CH_4 conversion whereas the other perovskites and the Ni/Al_2O_3 started faster, which may be due to the Fe being more difficult to reduce [10].

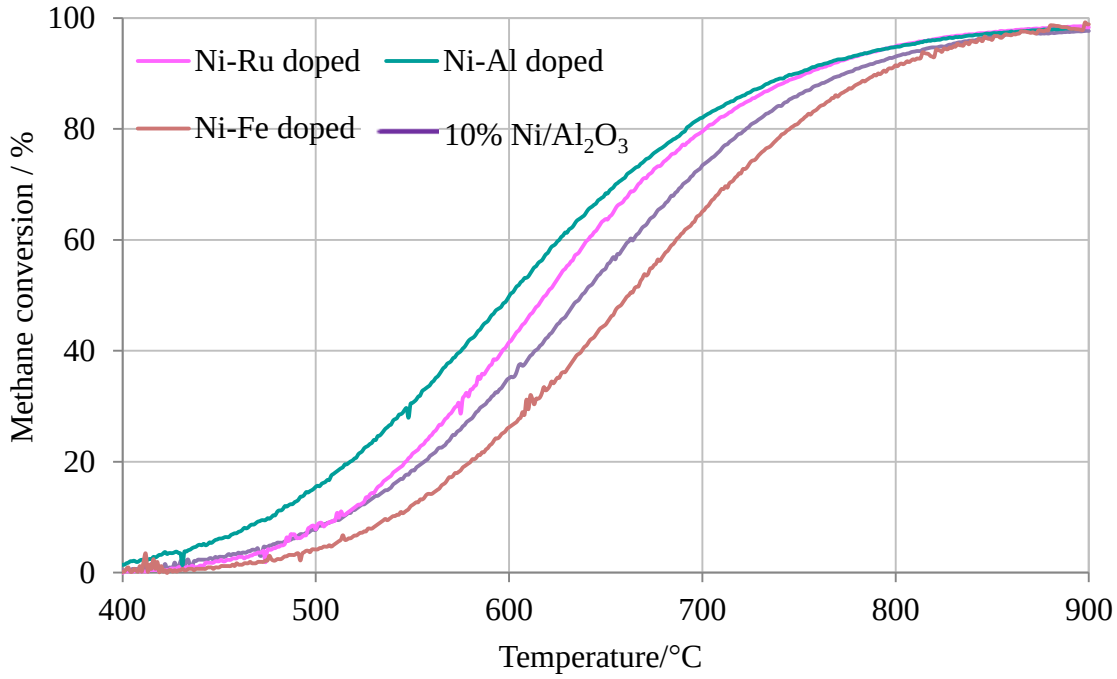

Figure 5.5: Methane conversion profiles during temperature programmed surface reaction of 1:1 CH_4 /CO_2 mixture over each catalysts material studied.

5.3 Isothermal testing and post reaction studies

5.3.1 Catalytic behaviour at different temperature towards dry reforming of methane

To gain more insight into the catalyst activity during the reaction, the profile of temperature programmed surface reaction as a function of reaction time was performed. Further investigation of the catalysts performance was performed by carrying out reactions at three different temperatures 700, 800 and 900 °C for 20 hours using an equimolar mixture of CH_4 and CO_2. These temperatures were chosen to determine the most appropriate temperature for full reaction conversion.

Long-term stability tests were performed with three of the synthesized perovskites and the Ni supported catalyst for 20 h to determine the effect of reaction temperature and time on stream on the conversion of reactants over the catalysts (shown in figures 5.6-5.9). Under methane rich conditions (biogas reforming), all reactions began with a brief 'burst' of hydrogen production due to methane decomposition occurring. Unlike the reaction with dry reforming no similar burst was seen and it is likely this is due to the presence of a higher level of CO_2 that prevents methane cracking. CH_4 and CO_2 conversion began steadily and remained roughly constant throughout the reaction, resulting in a steady H_2 and CO production especially at higher temperatures.

Isothermal reactions have shown selectivity towards the formation of synthesis gas with some evidence of the RWGS occurring due to the higher concentration of carbon monoxide than hydrogen in the products. DRM is a highly endothermic reaction, so when the temperature is increased and the conversion of the reactants also increases and consequently the yields of the products are increased [11].

Among all of the catalysts, nickel supported alumina displayed the highest initial CH_4 and CO_2 conversion, but these values dropped steadily because of the deactivation of the catalyst as shown in figure 5.6 C. At high temperature (900 °C) this could be due to the loss of active metallic sites because of sintering or carbon accumulation due to encapsulation rather than filament growth [12]. In contrast, the profiles of Ni-Al doped and Ni-Fe doped perovskites showed an initial decrease in CH_4 conversion and then an increase until the end of 20 hours of reaction which caused a lower yield of H_2.

While the Ni-Ru doped sample had a steady conversion of CH_4 and CO_2 and a higher yield of H_2 than Ni/Al_2O_3 without any deactivation, which indicates Ru is highly active for dry reforming. Ni-Ru doped $SrZrO_3$ has also achieved a high H_2 /CO ratio (1.01) at higher temperatures (800 and 900 °C), which is of great importance for the purpose of H_2 production by dry reforming and consequently it may be applicable to industrial use.

The conversion of reactants generally decreases with decreasing temperature to a given extent depending on the structure of the catalyst. For example, Ni-Al doped $SrZrO_3$ gave the lowest production of hydrogen due to having the lowest reactant conversion and consequently, a larger amount of water was produced as the H_2 /CO value is 0.87 and 0.88 at 800 °C and 900 °C respectively.

A higher amount of water produced with the lowest reactant conversion and product yields was observed at 700 °C due to the high level of CO_2 available to react with H_2 to produce water. Again as shown in profile A for all four catalysts, the occurrence of the RWGS is confirmed by the detection of water. At 700 °C, as was expected, the lowest performance was for Ni-Fe doped perovskite because iron often needs high temperatures to be more active and this was confirmed by temperature programmed reduction.

The higher activity exhibited by the Ni-Ru doped catalyst at 900 °C compared to other catalysts was attributed to the higher activity for CH_4 and CO_2 decomposition thereby higher yields of H_2 and CO which amounted to 96% and 94 % respectively, on which there is no observable CH_4 conversion decrease during the 20 h of reaction. The stability is due to the production of non-deactivating carbon and a negligible amount of coke formation was observed on this material as evidenced by an oxidation step (post reaction) after the temperature programmed reforming reaction.

It has been noted that although the same amount of active metals was used to promote the perovskite catalysts, the Ni-Al doped showed the lowest performance in terms of reactant conversion and product yields with the lowest H_2 /CO ratio at 800 °C and 900 °C. This suggests that there were side reactions predominating at the surface of this perovskite for dry reforming. Furthermore, the methanation reactions may be occurring (CO or CO_2 reacting with H_2 to form methane and water), both exothermic, in this case the water production will be limited when the temperature increases.

Although there was variation in catalytic performance among the three temperatures, the best overall performance was observed at all temperatures for dry reforming during 20 hours of reaction with Ni/Al_2O_3 in terms of reactant conversion. However, steady deactivation occurred due to sintering and carbon formation and this would limit the potential reaction time. As has been reported, coke accumulation is considered to be one of the aging factors for Ni-based catalysts [13].

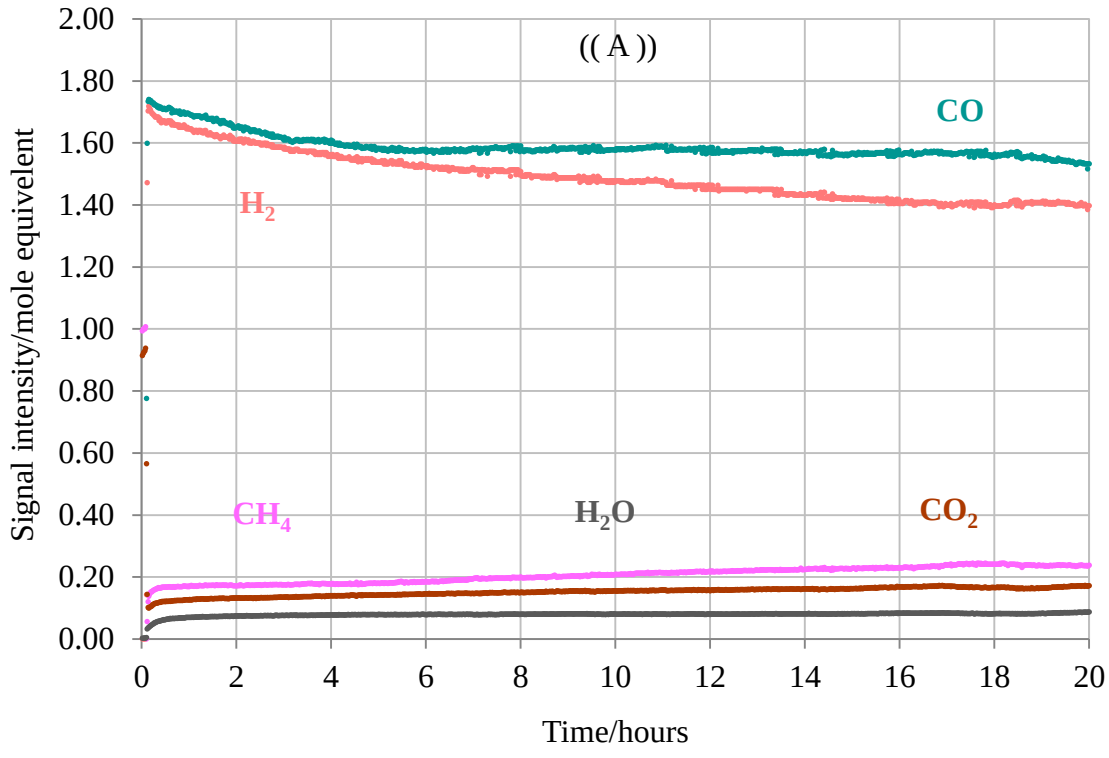

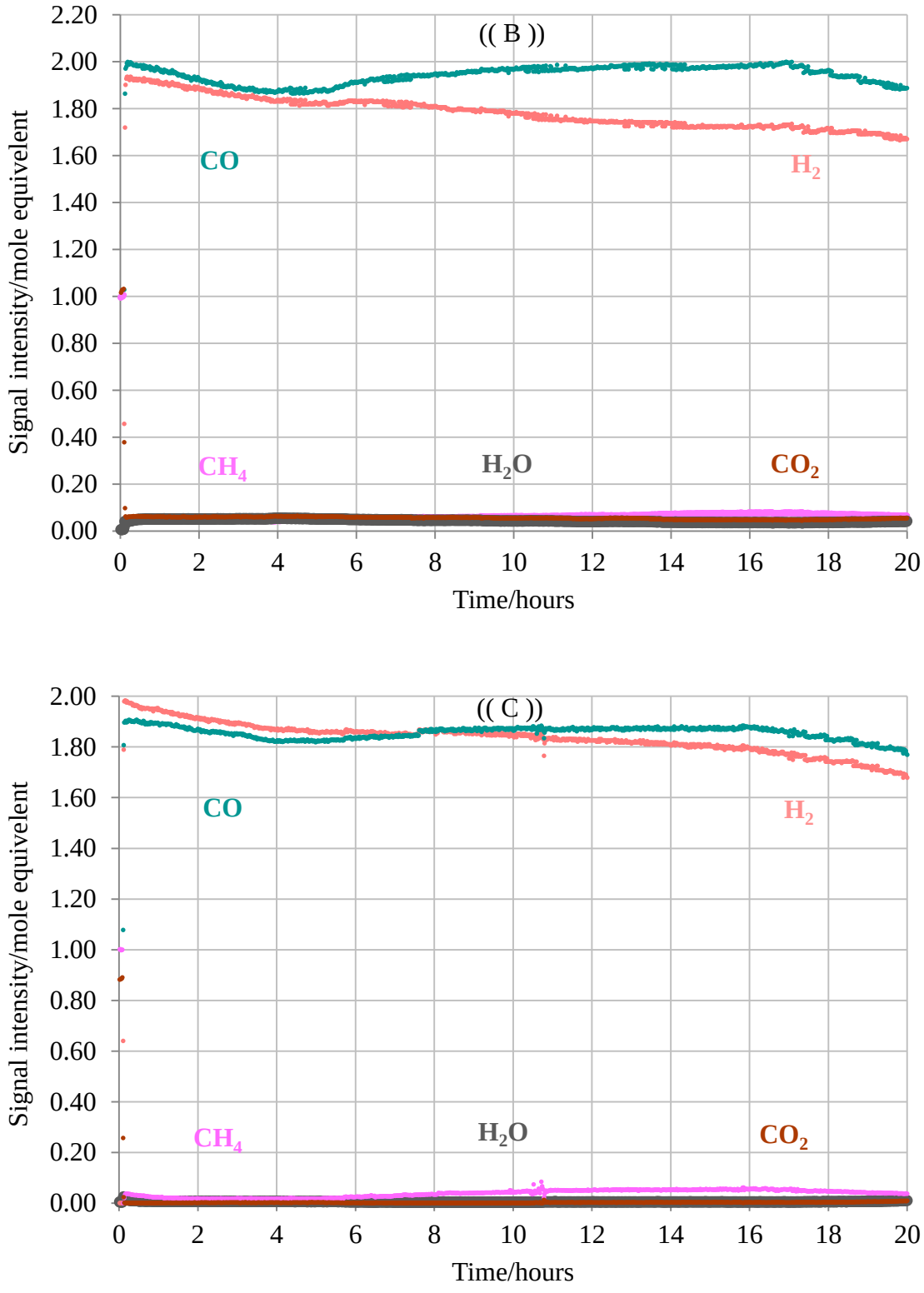

Figure 5.6: Dry reforming of methane profiles of a 1:1 CH_4 /CO_2 mixture over 10% Ni/Al_2O_3 catalyst for 20 hours at (A) 700 °C, (B) 800 °C and (C) 900 °C.

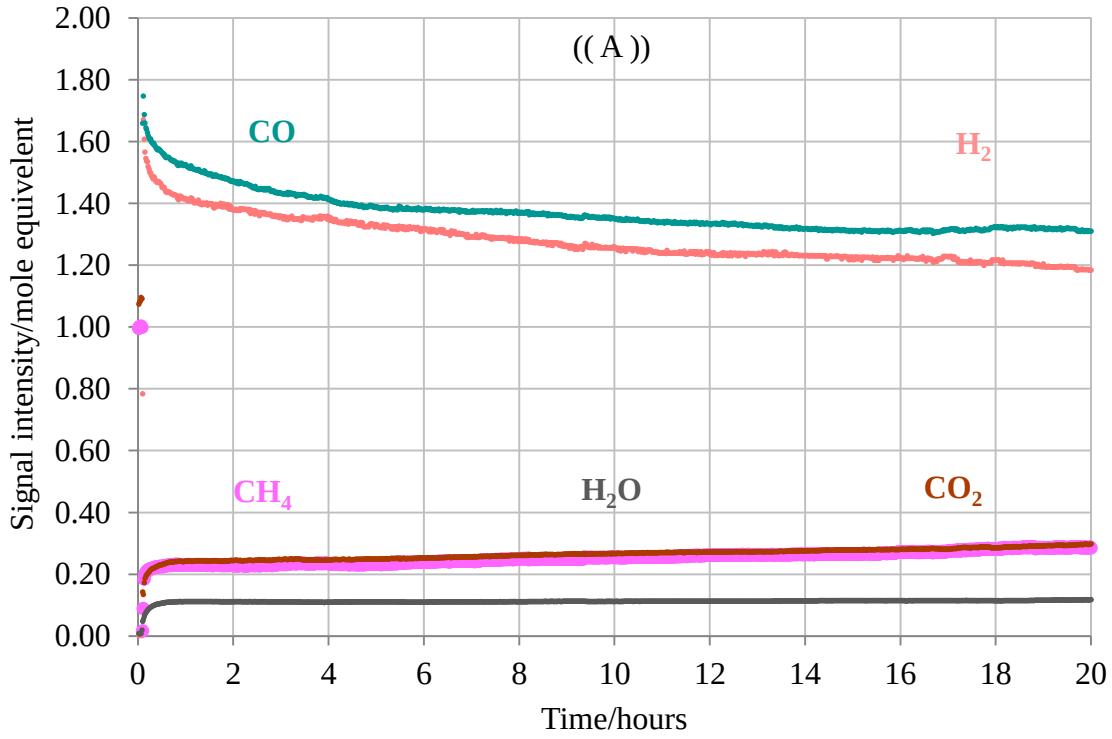
((A))
CO
H2
CH4
H2O
CO2
Signal intensity/mole equivelent
Time/hours
2.00
1.80
1.60
1.40
1.20
1.00
0.80
0.60
0.40
0.20
0.00
0
2
4
6
8
10
12
14
16
18
20

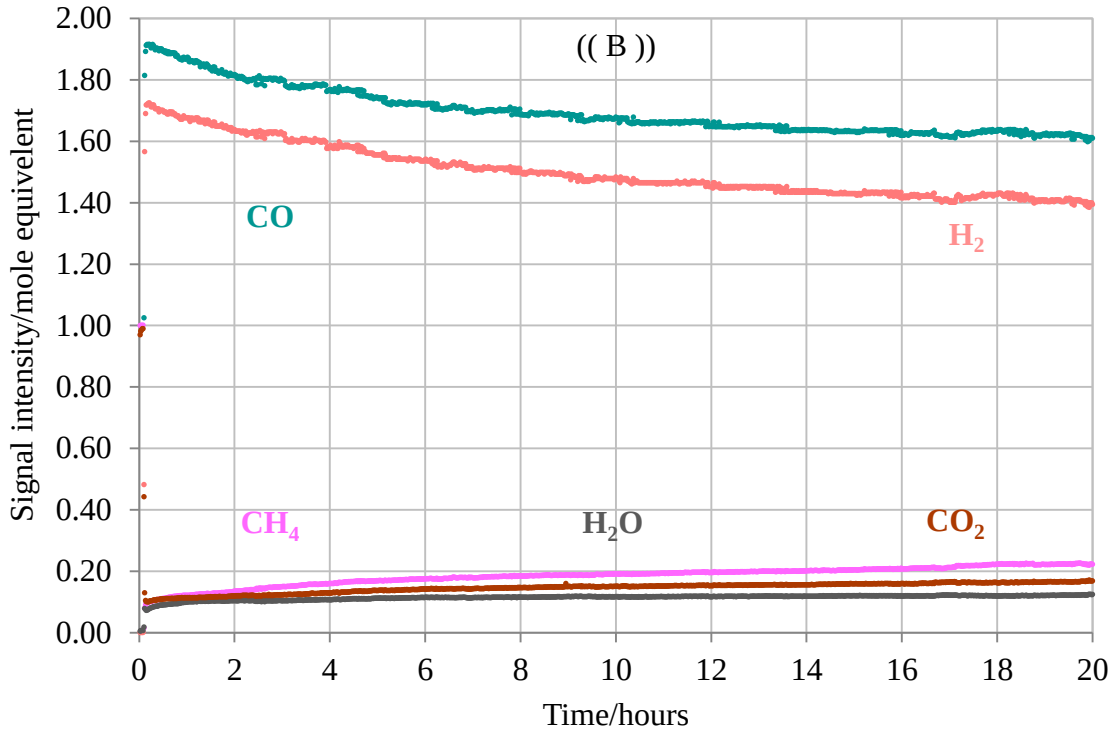
((B))
CO
H2
CH4
H2O
CO2
Signal intensity/mole equivelent
Time/hours
2.00
1.80
1.60
1.40
1.20
1.00
0.80
0.60
0.40
0.20
0.00
0
2
4
6
8
10
12
14
16
18
20

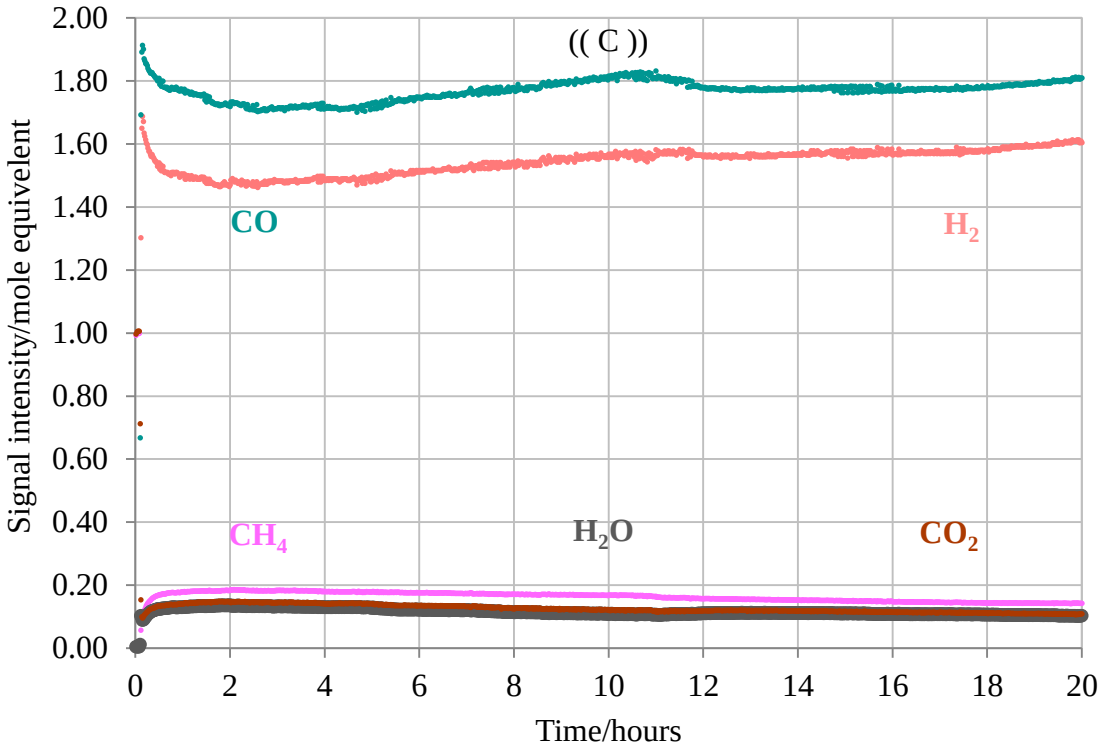

Figure 5.7: Dry reforming of methane profiles of a 1:1 CH_4 /CO_2 mixture over Ni- Al doped $SrZrO_3$ for 20 hours at (A) 700 °C, (B) 800 °C and (C) 900 °C.

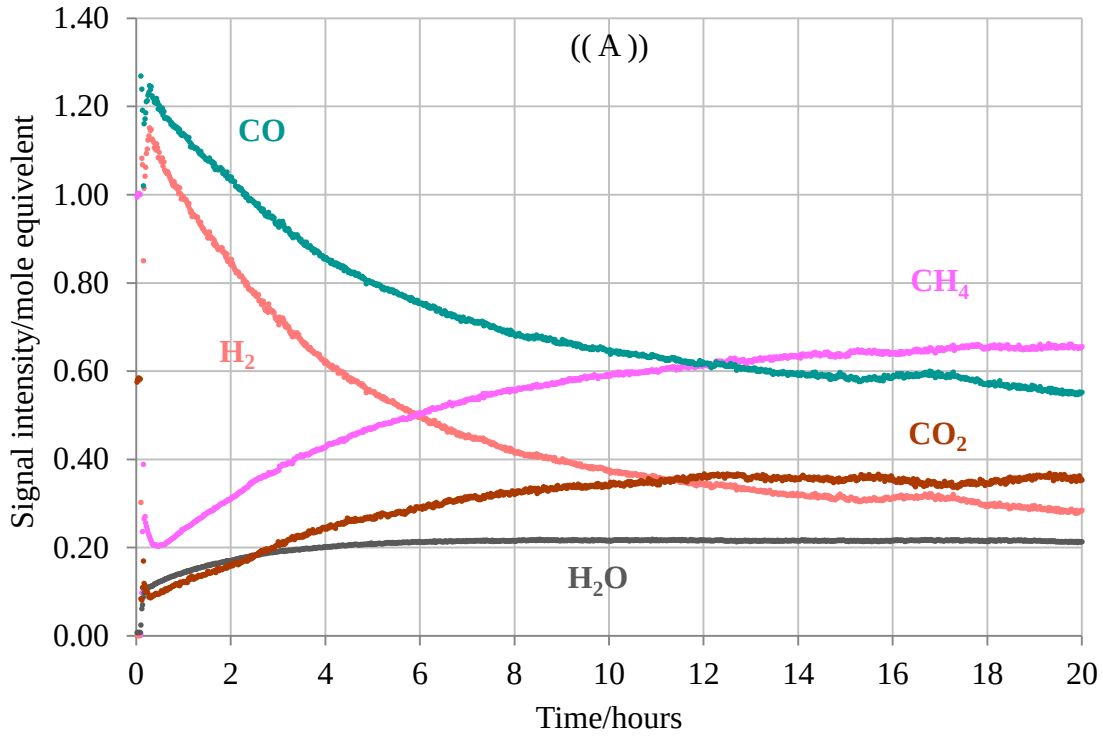

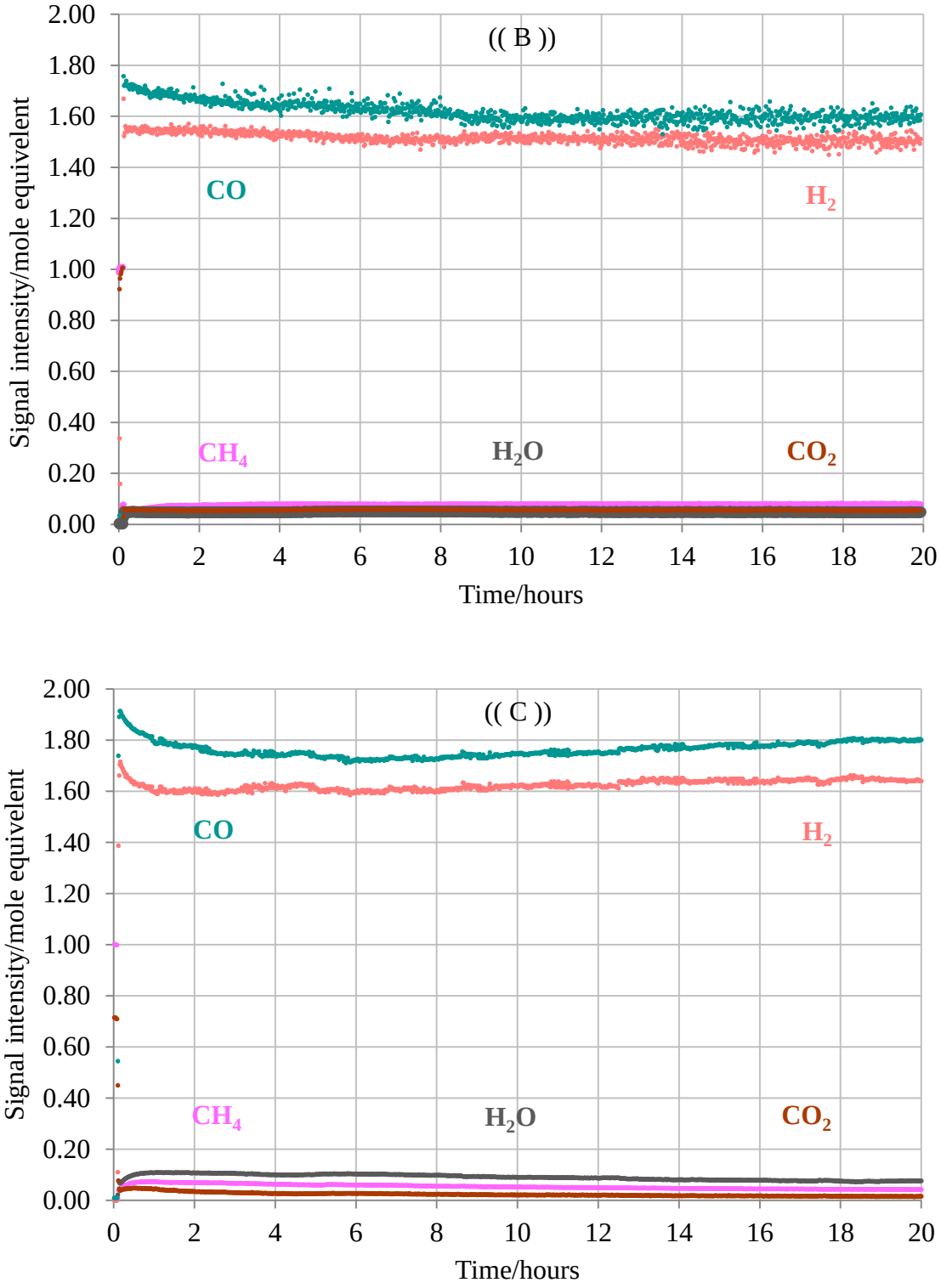

Figure 5.8: Dry reforming of methane profiles of a 1:1 CH_4 /CO_2 mixture over Ni-Fe doped $SrZrO_3$ for 20 hours at (A) 700 °C, (B) 800 °C and (C) 900 °C.

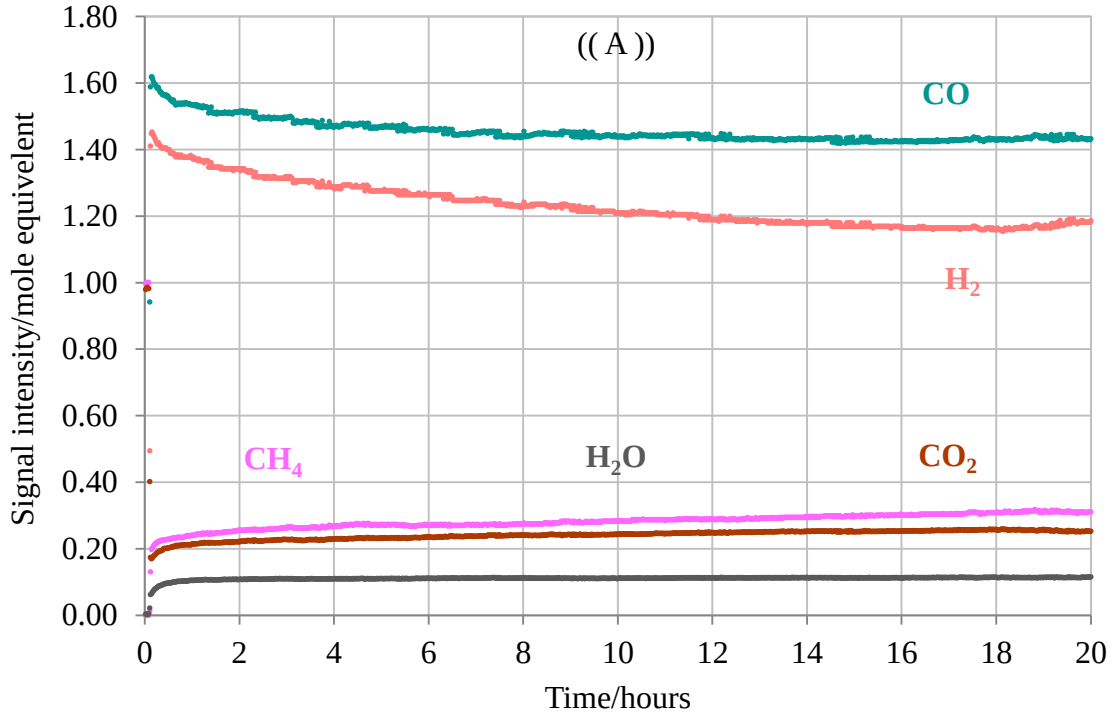
((A))
CO
H2
CH4
H2O
CO2
Signal intensity/mole equivelent
Time/hours
1.80
1.60
1.40
1.20
1.00
0.80
0.60
0.40
0.20
0.00
0
2
4
6
8
10
12
14
16
18
20

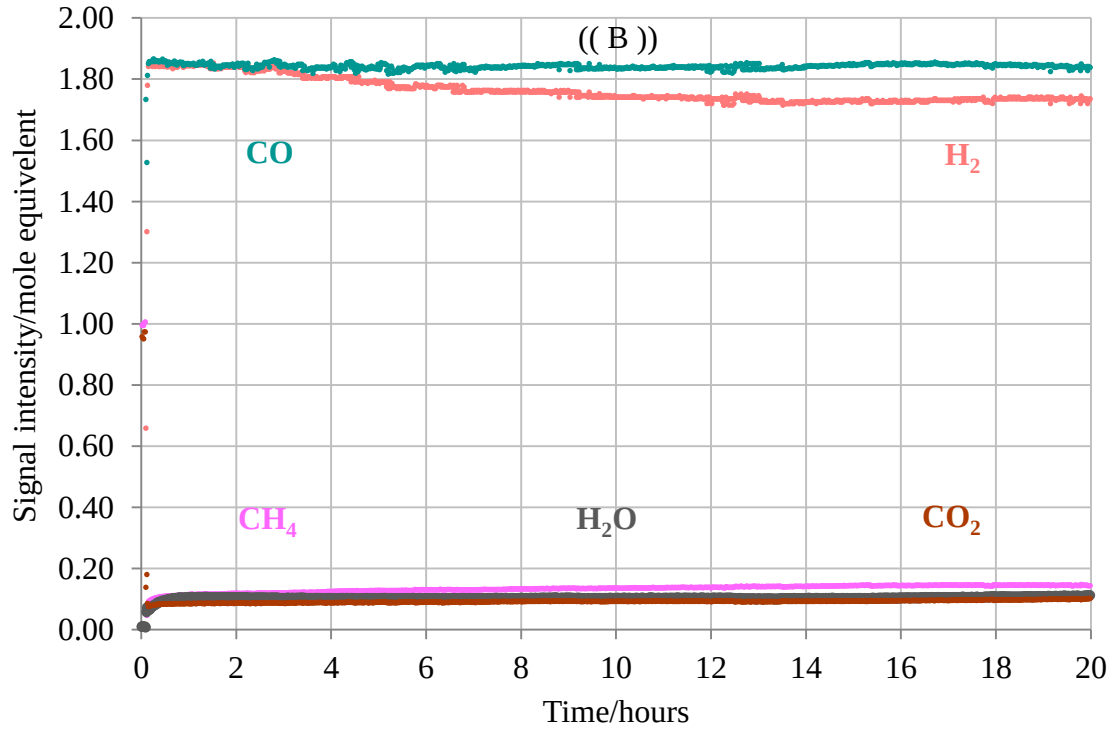
((B))
CO
H2
CH4
H2O
CO2
Signal intensity/mole equivelent
Time/hours
2.00
1.80
1.60
1.40
1.20
1.00
0.80
0.60
0.40
0.20
0.00
0
2
4
6
8
10
12
14
16
18
20

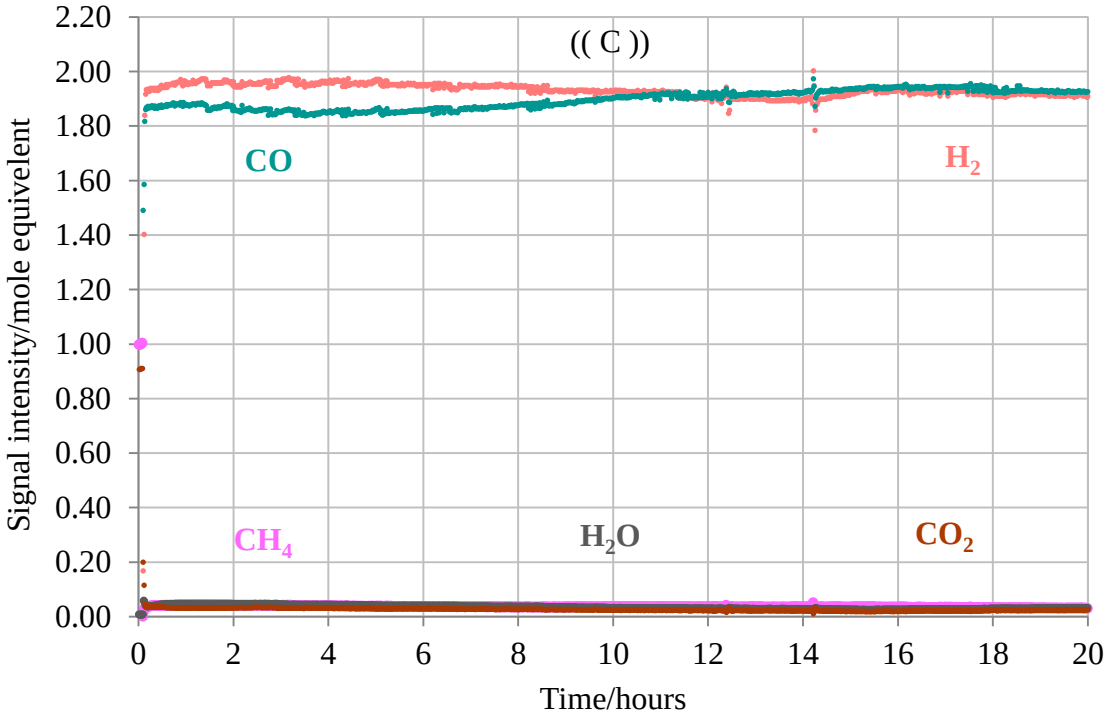

Figure 5.9: Dry reforming of methane profiles of a 1:1 CH_4 /CO_2 mixture over Ni-Ru doped $SrZrO_3$ for 20 hours at (A) 700 °C, (B) 800 °C and (C) 900 °C.

5.3.2 Activity evaluation of the catalysts

The reaction performance of the catalysts for dry reforming at different temperatures is shown in figures 5.10-5.14. The greater conversion of carbon dioxide than methane and the low value of H_2 /CO revealed the powerful contribution of the reverse water gas shift as well as other side reactions consuming H_2, such as the methnation reaction or hydrogenation of CO and CO_2 to methane as shown in equation 5.2.

$$CO_2 + 4H_2 \rightleftharpoons CH_4 + 2H_2O \qquad \Delta H^{\circ}_{298K} = -164 \text{ kJ.mol}^{-1} \qquad [5.2]$$

It has been observed in earlier studies, that the dry-reforming of methane reaction is highly endothermic and thus the high temperature can increase the rate of reactant conversion [14]. For the co-doped perovskites, CH_4 conversion on Ni-Ru doped perovskite increased

from 72% to 96% and the CO_2 conversion increased from 76% to 97% when the temperature increased from 700 °C to 900 °C. However, the higher coke deposited on Ni-Ru doped $SrZrO_3$, it indicates poor coke resistance ability compared to the other co-doped metal catalysts. Moreover, it seems that the coke was inert because it does not affect the catalyst activity. The sample showed good stability with no deactivation during 20 hours of reaction.

The H_2 /CO ratio for Ni-Al doped $SrZrO_3$ was found to be significantly lower than the other catalysts in this study at higher temperatures. This could be due to having lower CH_4 and CO_2 conversion which would limit the formation of hydrogen. Ni-Fe doped perovskite is also responsible for the high contribution of RWGS leading to very low values of H_2 /CO at 700 °C. In contrast, Ni-Ru doped $SrZrO_3$ catalytic behaviour was closer to what was expected, a high activity with a H_2 /CO ratio of 1.01, particularly at higher temperatures, meaning that it kinetically inhibited the RWGS to a greater extent compared to other catalysts in this study and the production of water becomes negligible.

At 900 °C, Ni-Ru doped perovskite shows a higher level of H_2 in the stream and there is no observable formation of water, which is stoichiometric for DRM it is assumed that no side reactions are taking place significantly. These results are confirmed by the H_2 /CO ratio values that approach 1.01 and 0.95 at temperatures of 900 °C and 800 °C respectively. For the Ni-Fe doped $SrZrO_3$, isothermal reaction results show a dramatic decrease in H_2 /CO ratio with a decrease in temperature from 900 °C to 700 °C due to the decline in H_2 yield by 58%, which was more significant than the decline in CO yield under the same conditions.

The conversions of methane and the H_2 /CO ratio obtained with the Ni-Ru doped catalyst were closer to the values that are claimed in literature for efficient catalysts [15]. At 700

°C, it is likely the Ni-Fe doped $SrZrO_3$ is also responsible for the high contribution of RWGS leading to poor activity and very low values of H_2 /CO ratio (0.62) because they would favour side reaction rather than hydrogen production at low temperatures [16]. The Ni-Ru doped $SrZrO_3$ sample also presented lower amounts of H_2 than expected, probably due to water formation.

The dry reforming equation shows that the reaction between reactants produces a syngas with a H_2 /CO ratio close to 1, but the simultaneous occurrence of side reaction like RWGS often causes a decrease in this ratio to less than 1 as shown in figures 5.14, 5.11 and 5.10. These results compare the average molar ratios of H_2 /CO, CO_2 and CH_4 converted for all catalysts. The profiles show that the four catalysts converted CO_2 at slightly higher rates than CH_4, and this is consistent with the product ratio, as the formation of CO was greater than that of H_2 which indicates the occurrence of the RWGS reaction and this is confirmed by the presence of traces of water.

The maximum conversion of CH_4 occurs over the Ni-Ru doped sample compared to the Ni-Fe doped and the Ni-Al doped at 900 °C. According to the results of the catalytic evaluation and temperature programmed reduction experiments, it is believed that the catalyst with a higher initial H_2 consumption rate in the range = 220 °C to 800 °C should exhibit a greater activity for CH_4 combustion.

The average value of the CH_4 and CO_2 conversions achieved under the same conditions for the four catalysts should in theory be the same. According to the test with Ni-Fe doped at 700 °C, the 23% H_2 and 36% CO yield was less than they should have been for a 46% CH_4 and 70% CO_2 conversion, giving a H_2 /CO ratio (0.62), which was far less than the theoretical equilibrium value. This suggested that dry reforming of methane on this catalyst

is also accompanied by several side reactions such as RWGS and Boudouard Reaction that determine the selectivity of the products.

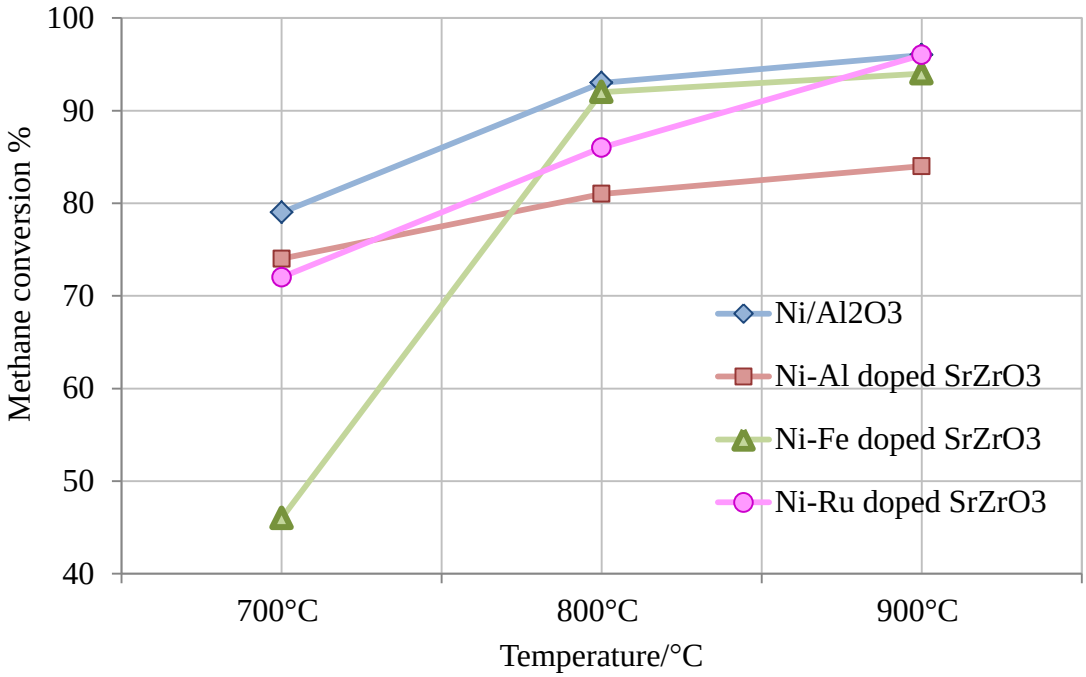

Figure 5.10: Average CH_4 conversion profiles of 1:1 CH_4 /CO_2 mixture over four catalysts at three different temperatures for 20 hours of reforming reaction.

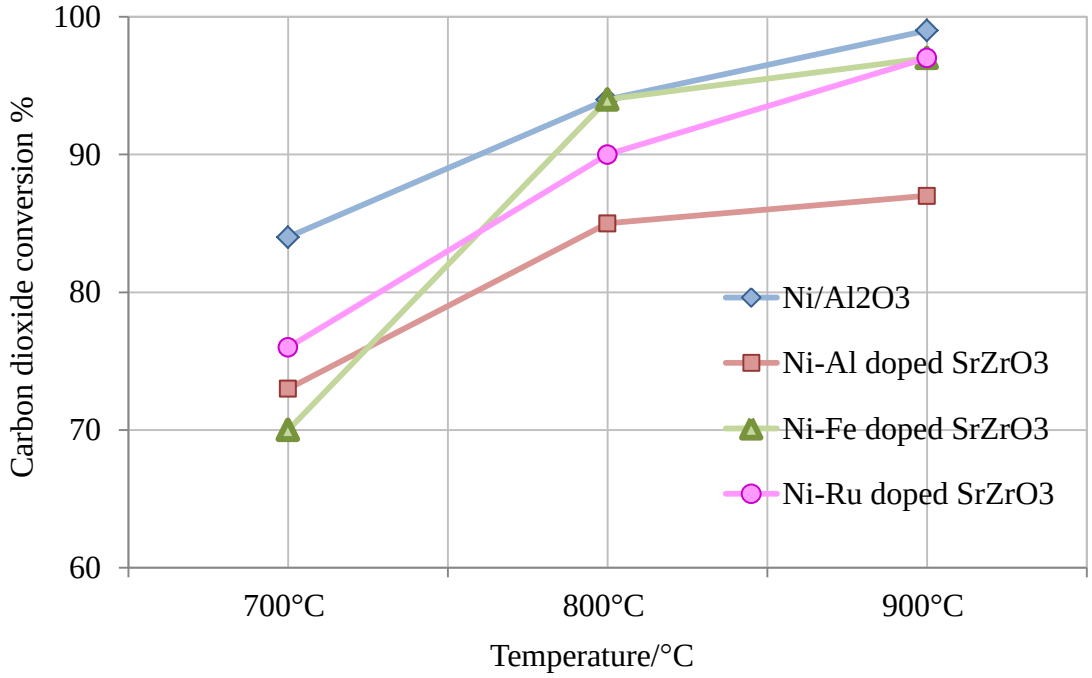

Figure 5.11: Average CO_2 conversion profiles of 1:1 CH_4 /CO_2 mixture over four catalysts at three different temperatures for 20 hours of reforming reaction.

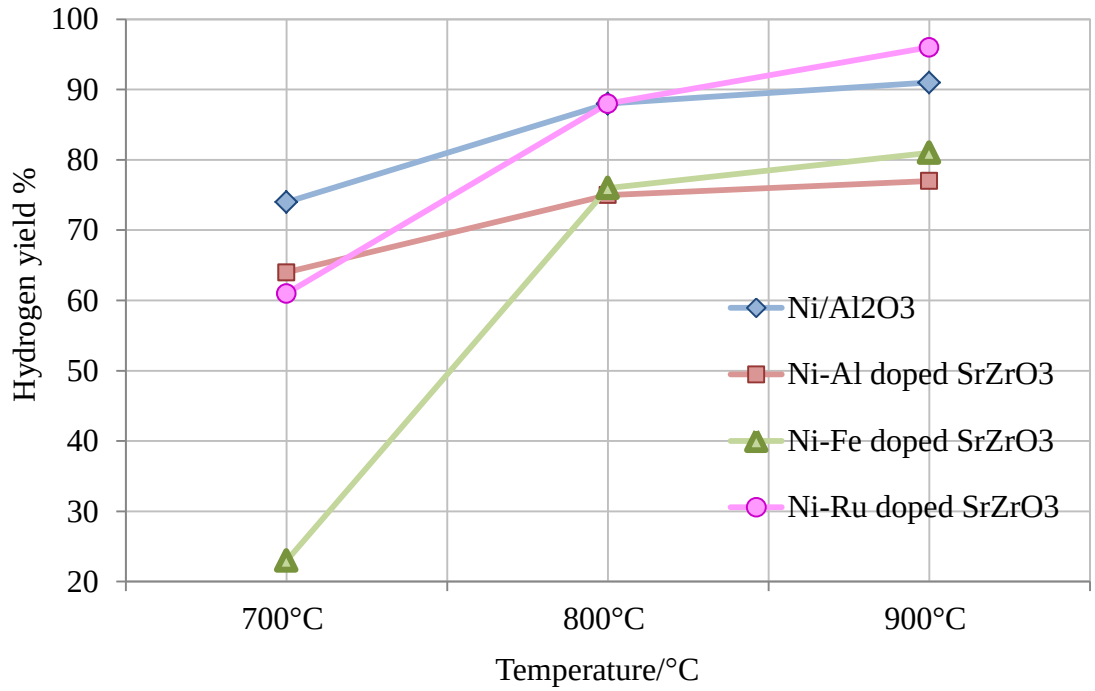

Figure 5.12: Average hydrogen yield over four catalyst of 1:1 CH_4 /CO_2 mixture after 20 hours of reforming reaction at particular temperature.

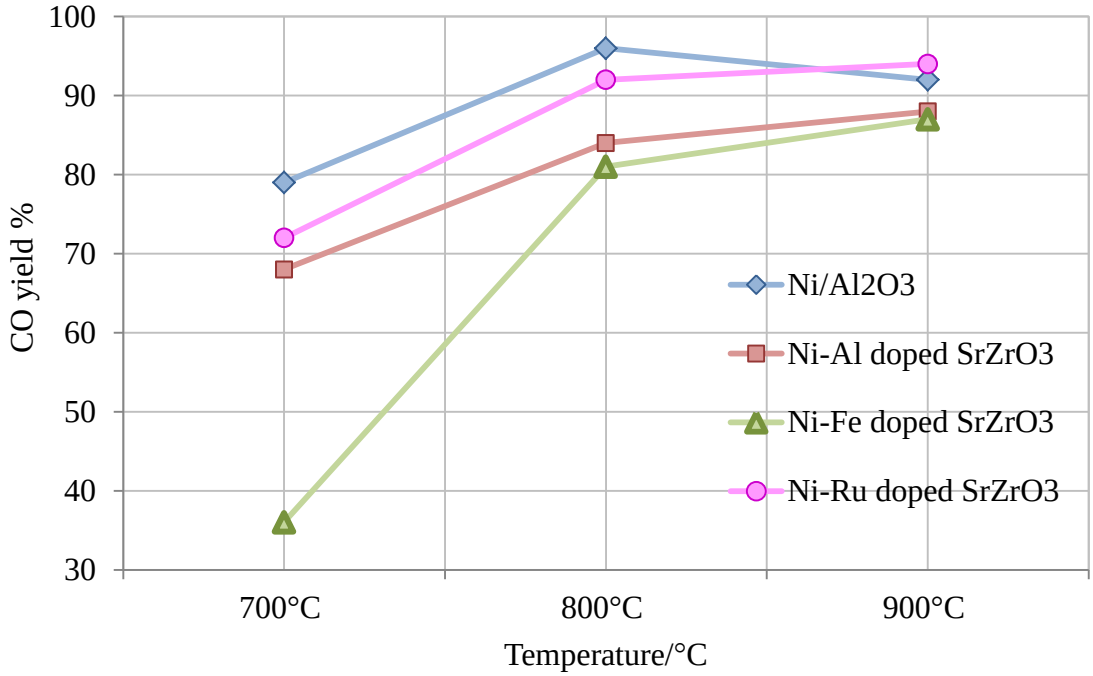

Figure 5.13: Average carbon monoxide yield over four catalyst of 1:1 CH_4 /CO_2 mixture after 20 hours of reforming reaction at particular temperature.

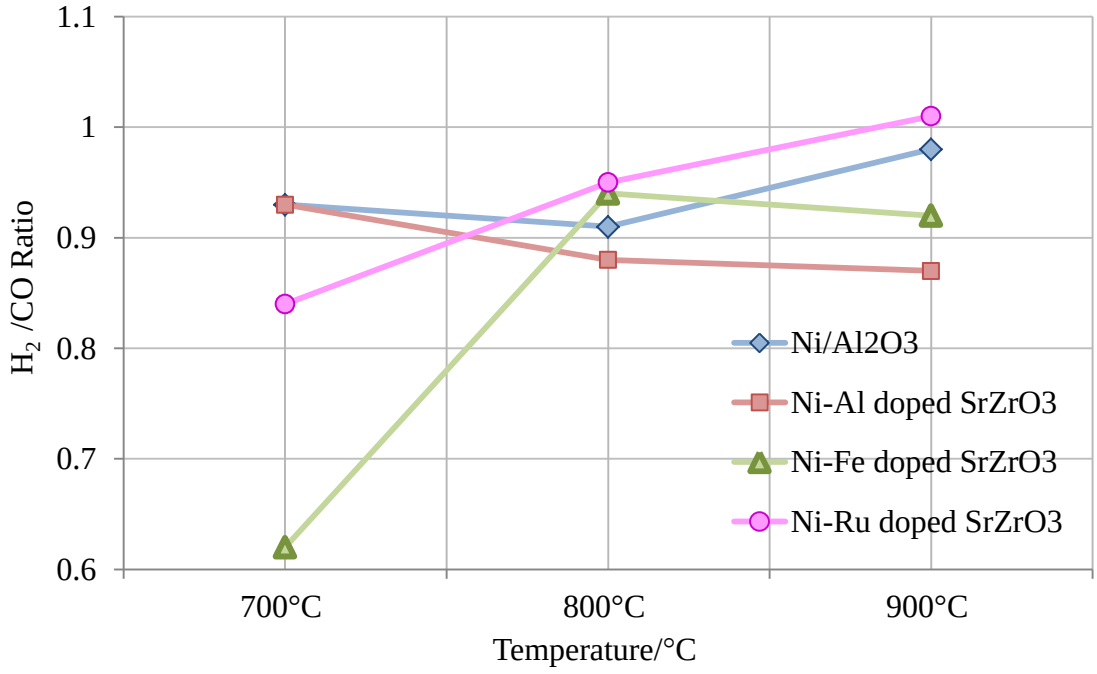

Figure 5.14: Average H_2 /CO Ratio over four catalyst of 1:1 CH_4 /CO_2 mixture after 20 hours of reforming reaction at particular temperature.

Generally, the catalytic activity and selectivity depended on the nature of the doping metals as well as temperature and decreased in the order of Ni-Ru doped $SrZrO_3$ > Ni-Fe doped $SrZrO_3$ > Ni-Al doped $SrZrO_3$ at 900 °C whilst at 700 °C the order is Ni-Al doped $SrZrO_3$ > Ni-Ru doped $SrZrO_3$ > Ni-Fe doped $SrZrO_3$. The low activity of the Ni-Fe catalyst was expected due to the reduction of iron not occurring at low temperature. Therefore, the activity for iron doped $SrZrO_3$ increases with increasing temperature.

The value of the H_2 /CO ratio for Ni-Al doped $SrZrO_3$ was considerably lower than for Ni-Fe doped $SrZrO_3$ and other catalysts in this study especially at higher temperature, suggesting increases in the CO production more than the H_2 production. Comparing these values with carbon accumulation, it appears that coke is kinetically limited on these catalysts, and increases with increasing H_2 /CO ratio.

The result showed that the actual reforming temperature should be maintained above 800 °C to minimize the coke formation and to achieve maximum reactant conversion and hydrogen concentration although the preferred operating temperatures is lower than 800 °C for cost purposes.

5.3.3 Temperature programmed oxidation (post reaction)

TPO post reaction was used to determine and compare the carbon deposited on each catalyst. Immediately after each reforming reaction run, the catalyst was cooled to room temperature under a He atmosphere. Temperature programmed oxidation was conducted to characterize the carbon formation as a function of temperature. TPO profiles for each catalyst at different temperatures are shown in figures 5.15-5.18 and the corresponding amount of oxidizible carbon is presented in figure 5.19.

It has been mentioned in the literature that the carbon accumulation decreases with increasing reforming temperature, as the higher temperature is a barrier for improving the exothermic side reactions such as CO disproportionation and hydrogenation of CO_2 [17]. During reforming reactions in previous studies, the formation of $SrCO_3$ and SrO phases were proposed to be responsible for the lack of carbon deposition [18, 19].

Concerning water production at lower temperatures, side reactions such as RWGS and Boudouard reaction were observed in this study leading to higher amount of carbon being deposited at 700 °C. It has also been reported that the hydrogenation of CO_2 and CO, both exothermic reactions, are attributed with coke accumulation at lower temperatures as shown in equations 4.6 and 4.7. However, considerable resistance to coke deposition was observed under the reaction conditions.

The chemical structure of the formed carbon depends on the reaction conditions and the type of catalyst. The appreciably higher conversion of CO_2 relative to CH_4 at higher temperatures could be due to the occurrence of the carbon gasification reaction (reverse Boudouard reaction) according to equation 5.3. At the lower temperature of 700 °C, it is likely that amorphous reactive forms of carbon are deposited and these convert to less reactive graphitic forms at high temperature [20].

$$C + CO_2 \rightleftharpoons 2CO \qquad \Delta H^{\circ}_{298K} = +172\ kJ.mol^{-1} \qquad [5.3]$$

Figure 5.19 shows that the highest level of carbon was formed at 700 °C, suggesting the carbon is formed via the CO disproportionation reaction which is favourable at lower temperatures. The propensity toward carbon formation was reduced on increasing the temperature to greater than 700 °C, although both CO_2 and CH_4 exhibited maximum conversion with respect to temperature. The peak area of the amorphous carbon below 640

°C is larger than that of the graphitic carbon at ~700 °C, suggesting that most of the accumulated carbon can be gasified at the lower reaction temperature [21].

Interestingly as observed in figures 5.16 and 5.17, there is only one carbon dioxide peak for Ni-Al doped and Ni-Fe doped perovskite at 700 °C and 800 °C respectively, with no carbon deposits evident on these catalysts at other temperatures under testing conditions. However, this variation in the amount of carbon formation seen is negligible, especially when compared to the literature.

Formation of carbon during dry reforming reaction is more favourable at the lower temperature of 700 °C. In addition, the occurrence of the RWGS reaction decreases the molar ratio of H_2 /CO in the product stream and enhances both the Boudouard reactions and CO hydrogenation. At high temperatures, greater than 800 °C, the RWGS reaction contributes to the slightly higher conversion of CO_2 than that of CH_4 and thus the presence of abundant CO_2 can easily oxidize carbon formed during reaction by reverse the Boudouard reaction. It can be concluded that coke is suppressed when the rate of gasification is equivalent or greater than the rate of coke formation.

Interestingly, figure 5.19 shows that after 20 hours reaction at 900 °C, the surface of the 10% Ni/Al_2O_3 is almost covered by a greater amount of carbon deposits compared with Ni-Fe doped and Ni-Ru doped perovskites, which show no detectable coke formation. In contrast at 800 °C, the greatest amount of carbon was found on the Ni-Ru doped sample. However, the highest amount of carbon deposition registered in this study for dry reforming was (0.11 g of carbon per gram of catalyst) and this is negligible.

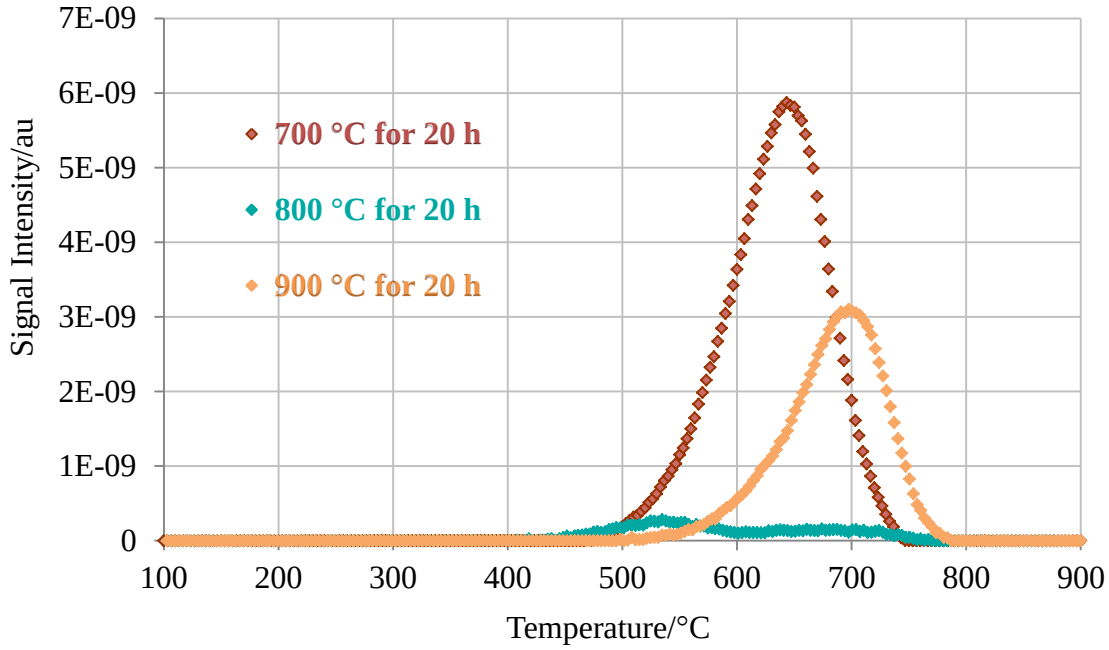

Figure 5.15: Carbon deposition as a function of temperature during 20 h of reaction of a 1:1 CH_4 /CO_2 mixture over 10% Ni/Al_2O_3 catalyst at three different temperatures.

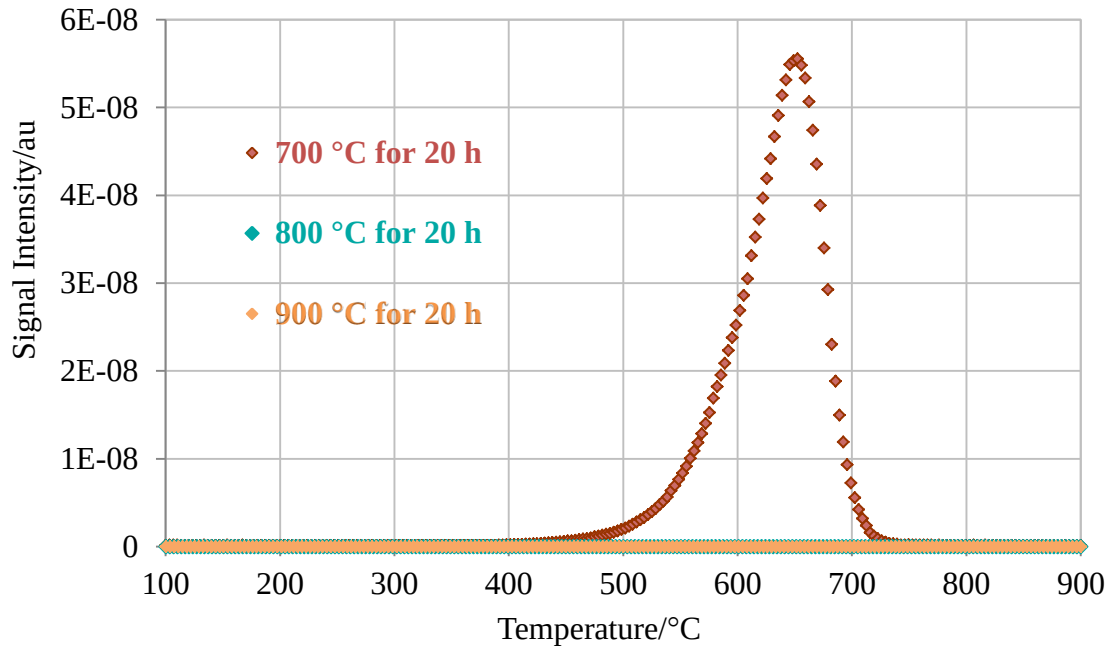

Figure 5.16: Carbon deposition as a function of temperature during 20 h of reaction of a 1:1 CH_4 /CO_2 mixture over Ni-Al doped $SrZrO_3$ catalyst at three different temperatures.

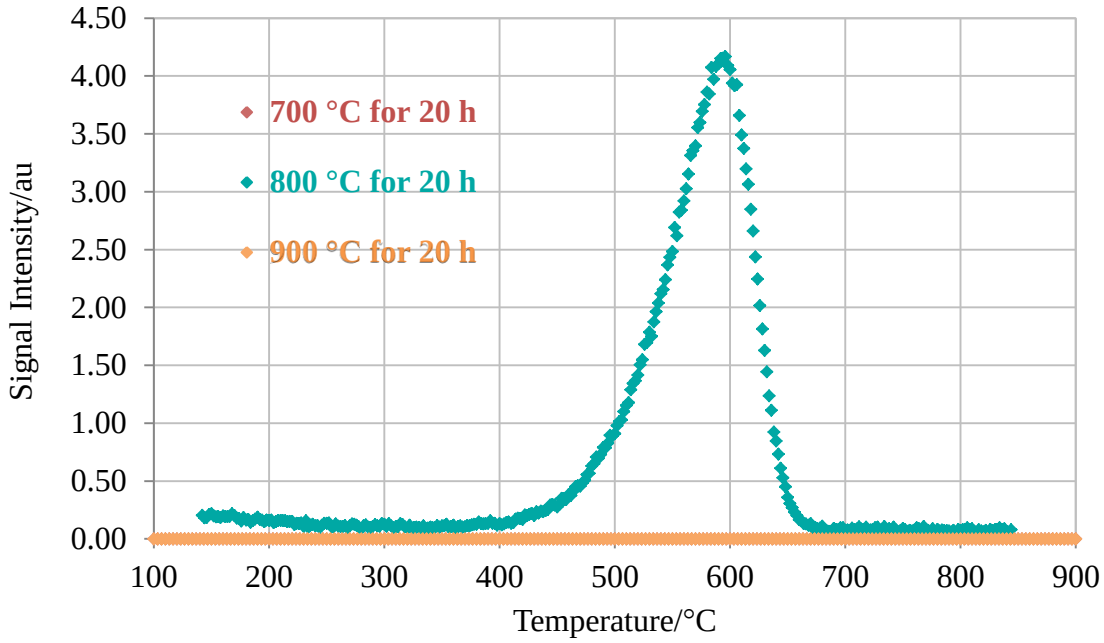

Figure 5.17: Carbon deposition as a function of temperature during 20 h of reaction of a 1:1 CH_4 /CO_2 mixture over Ni-Fe doped $SrZrO_3$ catalyst at three different temperatures.

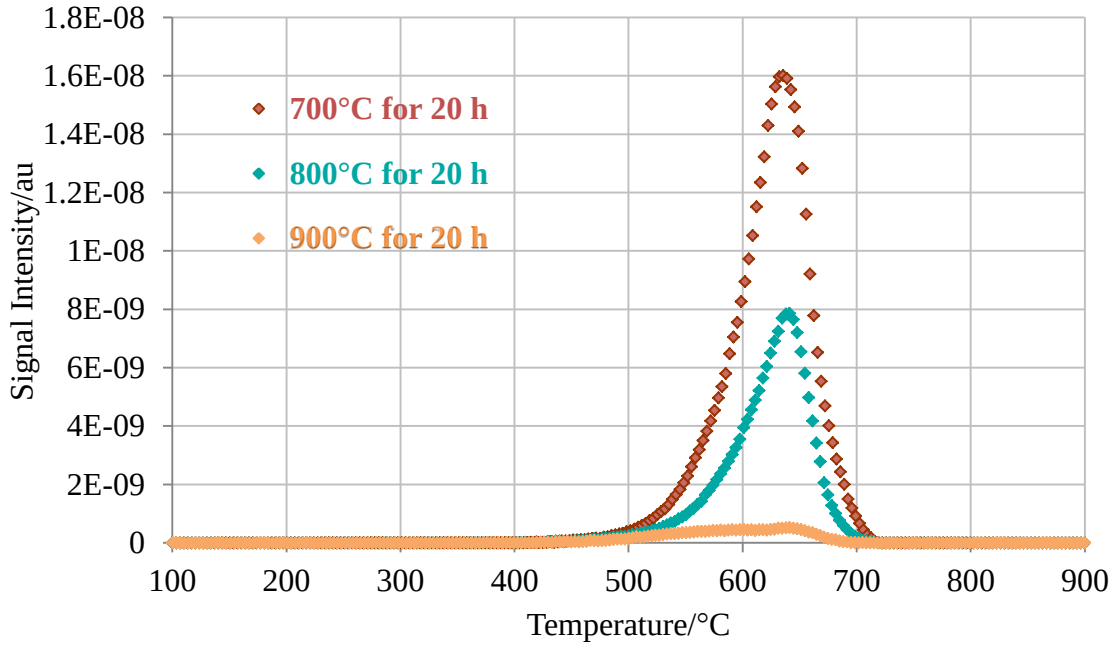

Figure 5.18: Carbon deposition as a function of temperature during 20 h of reaction of a 1:1 CH_4 /CO_2 mixture over Ni-Ru doped $SrZrO_3$ catalyst at three different temperatures.

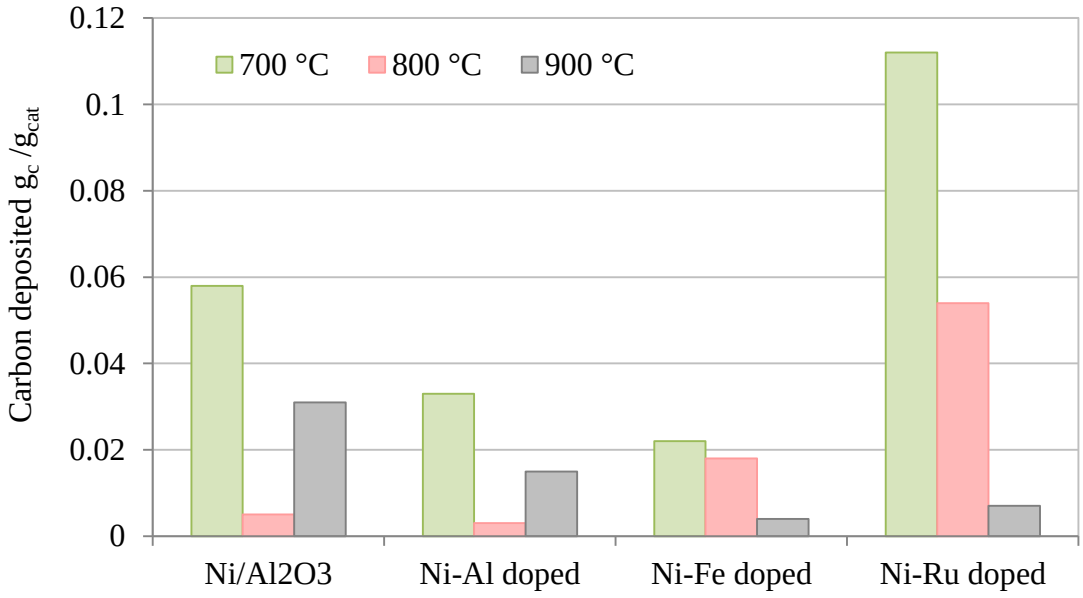

Figure 5.19: Comparison of carbon deposited on 10% Ni/Al_2O_3, Ni-Al doped $SrZrO_3$, Ni-Fe doped $SrZrO_3$ and Ni-Ru doped $SrZrO_3$ for 20 h at various temperatures in gram of carbon per gram of catalysts.

The carbon adsorbed on the smaller metal particles diffuses with more difficulty than that on the larger particles, providing the possibility for reducing net carbon accumulation as seen in the Ni-Fe doped material. Therefore, the modification of surface morphology is considered an effective strategy to avoid carbon formation on catalysts surface [22].

The amount of carbon deposited decreased with increasing reforming temperature, indicating that the reverse Boudouard reaction was dominant and responsible for carbon gasification under CO_2-rich conditions. TPOs following reactions at higher temperatures had a poorer resolution, especially with co-doped perovskite. Therefore, it is not possible to infer if the carbon was different at higher temperatures. However, there is no peak for CO_2 to suggest the nature of the carbon was different as perceived in figures 5.16 and 5.17 at temperatures (800, 900) °C and (700, 900) °C respectively.

5.4 Conclusion

Numerous studies and comprehensive research has been performed on DRM by metal or metal oxide-promoted catalysts as inhibitors for carbon formation. Most studies showed the positive effect of using different combinations of active metals with promoters. Comparison with the catalytic activity under such conditions can also be used to assess what temperatures give the best balance of high activity and low carbon deposition.

The results on the co-doped perovskite materials and supported metal alumina show that the activity increased and the amount of carbon formed decreased with increasing reaction temperature and thus deserve more attention from an economic point of view. However, Ni-based catalysts impregnated on alumina supports also show high catalytic activity with low level of coking as well as steady deactivation that was clear at the end of reaction.

The doping of other active metal ions into the perovskite catalyst precursors was found to significantly affect the catalytic performance for DRM reaction as shown for the three different doping metals. Based on this study, the highest catalytic activity and stability for DRM reaction was obtained over Ni-Ru doped $SrZrO_3$. This leads to an interesting phenomenon of three different types of metal-doped perovskite oxides which warrant further investigations due to their different but valuable properties in terms of both activity and stability.

During temperature programmed reaction tests, syngas with a H_2 /CO ratio between 0.62 and 1.01 was produced. Growth of carbon over the co-doped perovskite catalysts did not lead to deactivation. The amount of reactant conversion and temperature had a significant influence on the H_2 /CO ratio, deleterious carbon formation and the behaviour of the RWGS reaction. The use of excess CO_2 concentration under dry reforming conditions is effective in inhibiting carbon deposition.

In the dry reforming reaction, a significant contribution of RWGS accounted for the low values of H_2 /CO molar ratio. TPO results showed that co-doped perovskite catalysts have high resistance to carbon deposition and showed no increase in the amount of carbon deposition occurring with increasing reforming temperature and no observable deactivation over 20 h. The highest amount of carbon deposition was 0.11 g_{carbon} /$g_{catalyst}$ at 700 °C, however, carbon deposition at both high and low reaction temperatures was negligible.

Ni-Ru doped perovskite at 900 °C showed the highest activity for dry reforming of methane whilst the Ni-Al doped one the lowest. No deactivation of the catalysts was perceived meaning that the perovskite structure is stable in the course of testing and showed minimal coke formation and sintering, which are mainly responsible for catalyst deactivation. The study of the catalytic activity under different temperatures (700, 800, and 900 °C) for each catalyst showed that the H_2 /CO ratios are significantly lower than the theoretical equilibrium values except for Ni-Ru doped at 900 °C, this may be due to the relative rate of RWGS being greater than the competing reactions such as steam reforming that consume CO_2 to make the level of H_2 increase and hence the H_2 /CO molar ratios decrease.

Co-doped perovskite materials have high stability under reaction conditions as compared to Ni/Al_2O_3. Some improvement of the catalytic performance was obtained by adding Ru as a co-dopant within the perovskite structure. These results demonstrate that Ni-Ru doped $SrZrO_3$ is a promising catalyst for industrial use for dry reforming at 800 °C and 900 °C, since it has a strong resistance to deactivation and coke deposition with a high amount of H_2 yield. CH_4 conversion of each catalyst drops with decreasing the reaction temperature from 800 °C to 700 °C. Ni-Fe doped has only negligible reactivity at less than 750 °C.

5.5 References

[1] B. H. Davis, *Catal. Today*, 2003, **84**, 83–98.

[2] K. W. Jun, H. S. Roh, K. S. Kim, J. S. Ryu and K. W. Lee, *Appl. Catal*., A, 2004, **259**, 221–226.

[3] D. Pakhare and J. Spivey, *Chem. Soc. Rev.***,** 2014, **43**, 7813-7837.

[4] M. Rezaei, S. M. Alavi, S.Sahebdelfar, P. Bai, X. Liu and Z. F. Yan, *Appl. Catal. B: Environmental*, 2008, **77**, 346-354.

[5] Y. Chen and J. Ren, *Catal. Letters*, 1994, **29**, 39-48.

[6] Y. Jeon, H. Kim, C. Lee, S. Lee, S. Song, and Y. Shul, *Fuel*, 2017, **207**, 493–502.

[7] S. Therdthianwong, A. Therdthianwong, C.Siangchin, and S. Yongprapat, *Int. J. Hydrogen Energy*, 2008, **33**, 991-999.

[8] D. Pakhare, H. Wu, S. Narendra, V. Abdelsayed, D. Haynes, D. Shekhawat, and D. Berry, J. Spivey, *Appl. Petrochem Res*, 2013, **3**, 117–129.

[9] S. E. Evans, PhD Thesis, *Keele University*, 2016.

[10] M. H. Khazaal, J. Z. Staniforth, Z. A. Alfatlawi, R. M. Ormerod, and R. J. Darton, *Energy Fuels*, 2018, **32**, 12826–12832.

[11] D. Pakhare, C. Shaw, D. Haynes, D. Shekhawat, and J. Spivey, *J. CO_2 Utilization*, 2013, **1**, 37-42.

[12] S. Gaur, D. Pakhare, H. Wu, D. J. Haynes, and J. J. Spivey, *Energy Fuels*, 2012, **26**, 1989–1998.

[13] S. Kawi, Y. Kathiraser, J. Ni, U. Oemar, Z. Li, and E. T. Saw, *ChemSusChem*., 2015, **8**, 3556 – 3575.

[14] B. Nematollahi, M. Rezaei, and M. Khajenoori, *Int. J. Hyd. Energy*, 2011, **36**, 2969-2978.

[15] A.I.Tsyganok, M. Inaba, T.Tsunoda, S. Hamakawa, K. Suzuki, and T. Hayakawa, *Catal. Communications*, 2003, **4**, 493-498.

[16] R. Benrabaa, A. Löfberg, A. Rubbens, E. B. Richard, R.N. Vannier, and A. Barama, *Catal. Today*, 2013, **203**, 188– 195.

[17] M. K. Nikoo and N.A.S.Amin, *Fuel Proce. Techn*., 2011, **92**, 678-691.

[18] G. Valderrama, A. Kiennemann and M. R.Goldwasser, *J. Power Sources*, 2010, **195**, 1765–1771.

[19] M. M. Naira and S. Kaliaguine, *New J. Chem*., 2016, **40**, 4049-4060.

[20] V. Pawar, S. Appari, D. Monder, and V. M. Janardhanan, *Ind. Eng. Chem. Res.*, 2017, **56**, 8448–8455.

[21] Z. Hao, Q. Zhu, Z. Jiang, and B. Hou, H. Li, *Fuel Proc. Techno*, 2009, **90**, 113-121.

[22] J. H. Kima, D. J. Suh, T. J. Park, and K. L. Kim, *Appl. Catal. A Gen*., 2000, 197, 191–200.

Chapter 6

Studies for Partial oxidation of Methane

6. Simulation of the catalytic partial oxidation of methane to syngas over three co-doped perovskite and nickel supported catalysts

6.1 Introduction

This chapter presents a detailed description of the experimental results for catalyst materials that have been tested for activity for the partial oxidation of methane, which is a catalytic process producing synthesis gas with a H_2 /CO ratio of approximately 2:1. In this kind of reforming, oxygen is considered the limiting reactant at a stoichiometric feed ratio. The main reactions for partial oxidation are listed here again for convenience.

$CH_4 + ½O_2 \rightleftharpoons CO + 2H_2$ $\quad \Delta H^{\circ}_{298K} = -36\ kJ.mol^{-1}$ [6.1]

$CH_4 + O_2 \rightleftharpoons CO + H_2 + H_2O$ $\quad \Delta H^{\circ}_{298K} = -278\ kJ.mol^{-1}$ [6.2]

$CH_4 + 1\ ½O_2 \rightleftharpoons CO + 2H_2O$ $\quad \Delta H^{\circ}_{298K} = -520\ kJ.mol^{-1}$ [6.3]

$CH_4 + 2O_2 \rightleftharpoons CO_2 + 2H_2O$ $\quad \Delta H^{\circ}_{298K} = -880\ kJ.mol^{-1}$ [6.4]

Other reactions that are important in methane partial oxidation:

$H_2 + ½O_2 \rightleftharpoons H_2O$ $\quad \Delta H^{\circ}_{298K} = +41\ kJ.mol^{-1}$ [6.5]

$CO + ½O_2 \rightleftharpoons CO_2$ $\quad \Delta H^{\circ}_{298K} = -283\ kJ.mol^{-1}$ [6.6]

Synthesis gas production at atmospheric pressure requires temperatures between 700 °C and 900 °C to ensure complete reactant conversion to give a H_2 /CO ratio close to 2 as shown in the following figures 6.1- 6.4. However, a decrease in CO selectivity often leads to the formation of CO_2 due to complete combustion of methane with oxygen (total oxidation).

Comparison of the catalytic activity under such conditions can also be used to assess which metals give the best balance of high activity and low carbon deposition. A conventional

catalyst 10% Ni/Al_2O_3 was chosen for comparison purposes. However, nickel-based on alumina catalysts are reported to be deactivated because of the formation of nickel alumina spinel phases $NiAl_2O_4$ at high temperatures, which seems to influence the whole process such as sintering and coking problems [1, 2].

In recent years, there has been a great deal of attention by researchers in to improving the catalyst performance in terms of reactant conversions and hydrogen production utilizing bi-metallic catalysts [3]. It was reported that the combination of two metals can be more effective than a single metal-based catalysts in enhancing conversions and hydrogen selectivity, besides resistance to carbon accumulation.

Transition metals like Fe and Ni have been extensively studied due to their availability and cost in comparison with noble metals catalysts. Superior advantages of carbon deposition resistance have been shown by noble metals compared to nickel metal catalysts; nevertheless, the cost is very high. Therefore, developing new alternative catalysts by using a combination of a small amount of noble metal with non-noble metals may be a good way to lower the catalyst cost as well as improve catalytic performance. A study has mentioned that 1% Ru promoted 2.5% Ni supported on CeO_2 modified Al_2O_3 catalysts exhibit larger nickel surface areas compared to other catalysts and show excellent performances for steam reforming. In these, Ru plays an important role since it promotes the reducibility of Ni species to a metallic state [4].

POM reaction releases a large amount of heat due to the combustion of methane. This can lead to partial melting of the supported metal and separation from the support. Because nickel has a lower melting point than other active metals like ruthenium metal or iron, this makes it easier to deactivate [5]. Therefore, doping metals in to the crystal structure is better than the supported metals, as this reduces deactivation. In this chapter, catalytic

performance of all catalysts concerning the partial oxidation of methane was studied in order to investigate the effect of reaction temperature, CH_4 and CO_2 conversion, H_2 and CO yield, the selectivity for partial or total oxidation, carbon deposition and H_2 /CO ratio.

6.2 Catalytic conversion of methane to synthesis gas by partial oxidation

Temperature programed reaction of methane partial oxidation was carried out over Ni-Al doped $SrZrO_3$, Ni-Fe doped $SrZrO_3$, Ni-Ru doped $SrZrO_3$ and 10% Ni/Al_2O_3 catalysts. The partial oxidation reforming characteristics of catalysts were investigated by analysing the reforming reaction profiles as shown in Figures (6.1, 6.2, 6.3, and 6.4). The reaction over nickel supported alumina changes from predominantly total oxidation to partial oxidation at ~530 °C with a sharp drop in methane and oxygen coinciding with the production of a 2:1 ratio of H_2 and CO, reaching a maximum at ~800 °C (shown in figure 6.1).

The perovskite catalysts show a similar profile but with the switch over between total and partial oxidation occurring over Ni-Fe doped $SrZrO_3$ at ~630 °C and reaching a maximum at ~900 °C, whereas, over Ni-Al doped $SrZrO_3$ and Ni-Ru doped $SrZrO_3$ the switch over between total and partial oxidation occurs at ~475 °C and 450 °C respectively. At lower reaction temperatures, the greater exothermic nature of the total oxidation of methane reaction favours the selectivity of total oxidation (equation 6.4) over partial oxidation (equation 6.1) and then this begins to drop away above 600 °C.

All reactions displayed a sharp increase in synthesis gas with increasing temperature, and virtually complete conversion of the methane feed can be achieved at temperatures >750 °C, this is due to the adsorbed and desorbed processes becoming much faster when the temperature is increased, In all catalysts, the combustion of methane increased at around

700 °C, suggesting that decomposition of methane was happening and became more thermodynamically advantageous with the increasing temperature.

At lower reaction temperature less than 550 °C, the total oxidation combustion reaction becomes more favoured over partial oxidation and leading to the production of CO_2 and H_2O instead of H_2 and CO. Between 600 °C and 700 °C, the conditions for partial oxidation become advantageous as well as other side reactions such as steam reforming and dry reforming to generate more CO. Therefore, the yield of CO increased to approximately 80%. Above 700 °C, the product yields and CH_4 conversion reach more than 90%.

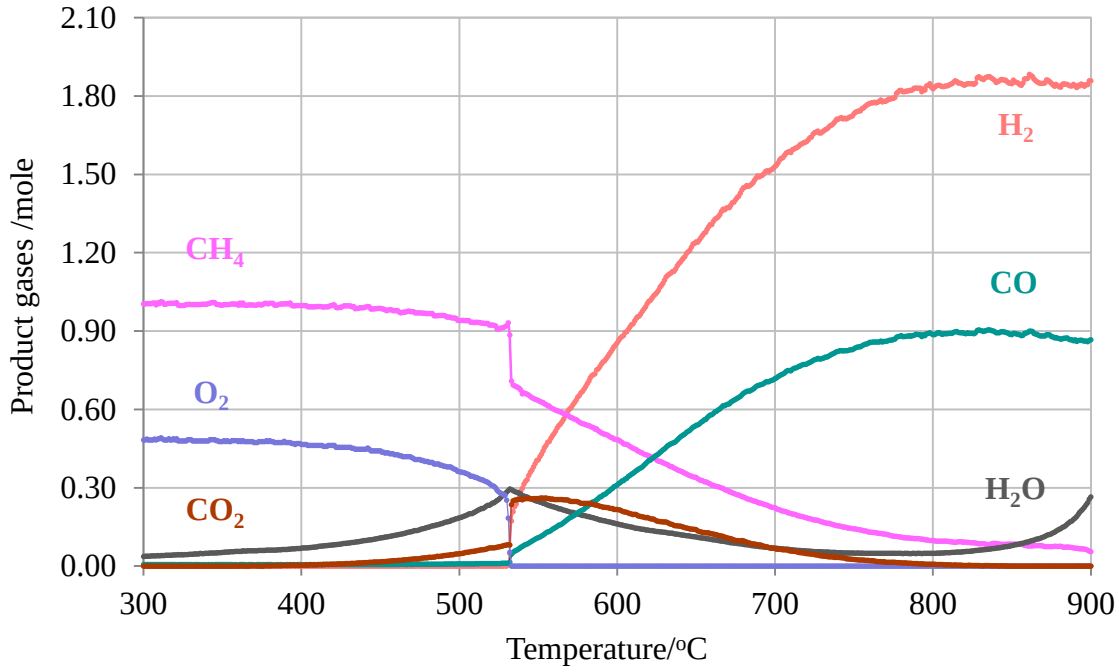

Figure 6.1: Temperature programmed reaction profile as a function of temperature for mixture of 1:0.5 CH_4 /O_2 over 10% Ni/Al_2O_3.

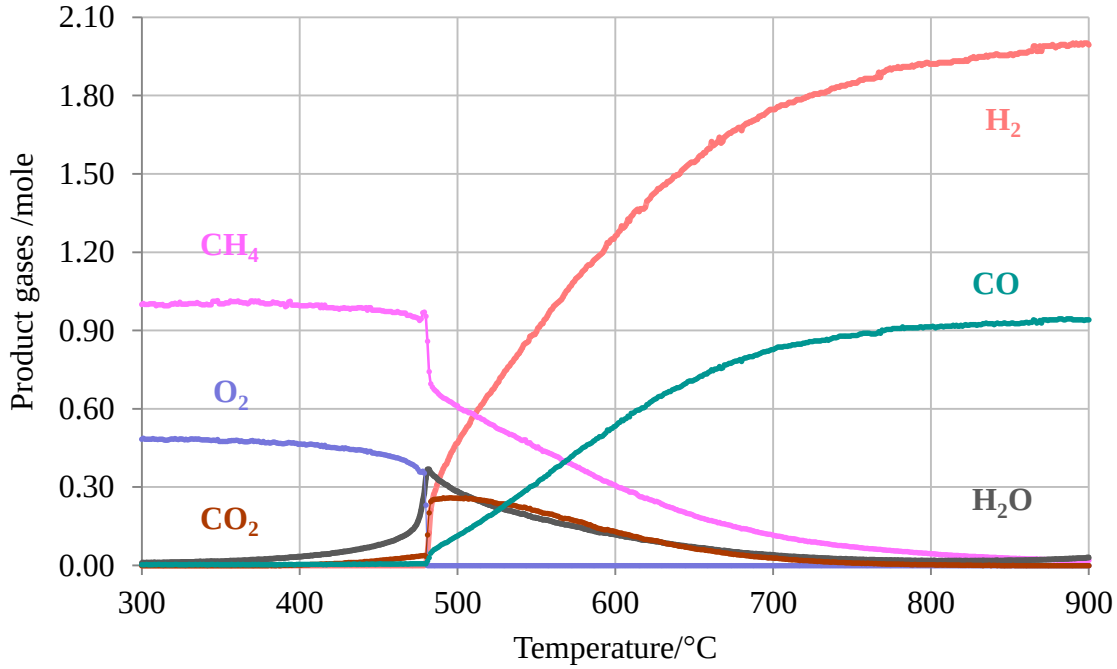

Figure 6.2: Temperature programmed reaction profile as a function of temperature for mixture of 1: 0.5 CH_4 /O_2 over Ni-Al doped $SrZrO_3$.

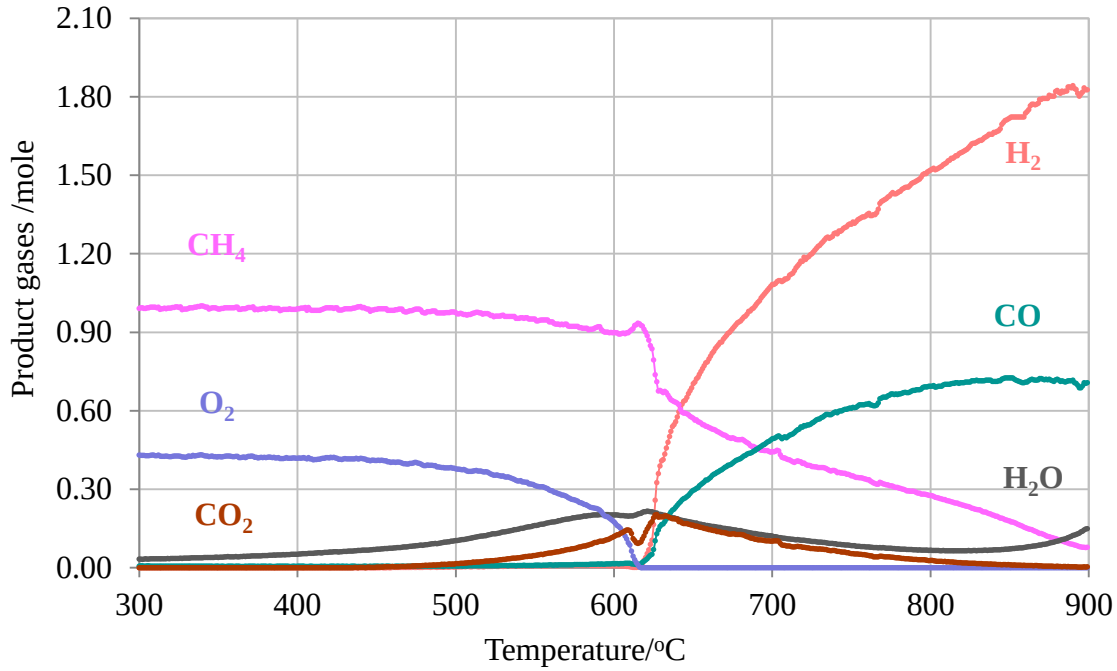

Figure 6.3: Temperature programmed reaction profile as a function of temperature for mixture of 1: 0.5 CH_4 /O_2 over Ni-Fe doped $SrZrO_3$.

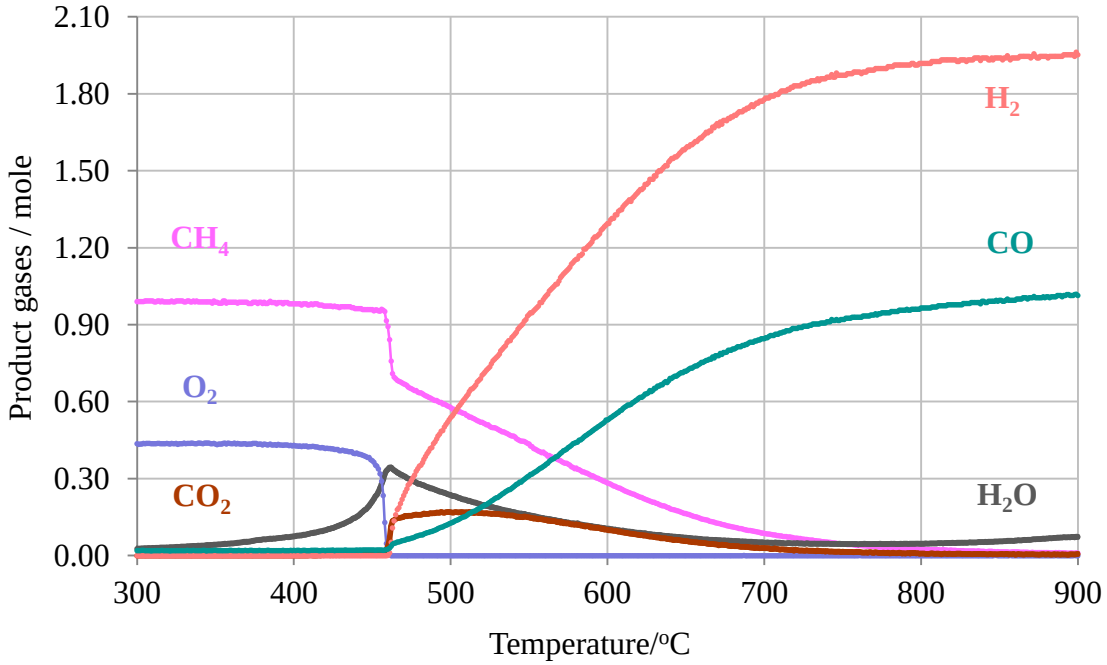

Figure 6.4: Temperature programmed reaction profile as a function of temperature for mixture of 1: 0.5 CH_4 /O_2 over Ni-Ru doped $SrZrO_3$.

Figure 6.5 shows the percentage of methane conversions over Ni-Ru doped $SrZrO_3$ and Ni-Al doped $SrZrO_3$ perovskites was much greater than that for 10% Ni/Al_2O_3 and Ni-Fe doped $SrZrO_3$, suggesting that Ru and Al doping increased the activity of the perovskite more than Fe doped under methane partial oxidation conditions. Among the four catalysts, Ni-Ru doped displayed the highest initial CH_4 conversion with greatest H_2 yield. In contrast, Ni-Fe doped $SrZrO_3$ showed the lowest initial reactant conversion and product yield.

Figures 6.5-6.7 show that exchanging the active metal Ru for Al as a co-dopant within the perovskite structure has an only minimal effect on the perovskite performance toward the partial oxidation of methane. Both catalysts display good catalytic activity in terms of methane conversion and selectivity to synthesis gas production at more than 750 °C. However, a significant decrease in activity was observed when exchanging Ru for Fe

especially at low temperatures. Therefore, higher temperatures are required to obtain a great conversion, and high selectivity to synthesis gas.

To start the reoxidation reaction requires electron transfer from the lattice to activate and dissociate the O_2 before incorporation into the vacancies. The reoxidation will be very fast when the oxygen vacancy location was near the surface. In contrast, subsurface reoxidation vacancies are much slower and depend on the catalyst ability to transport the oxygen from the surface sites to subsurface vacancies [6]. This means, incorporation of bi metallic Ni-Ru into strontium zirconate structure, decreases the activation energy for the reoxidation process more than the Ni-Fe incorporated catalyst, therefore, Ni-Fe $SrZrO_3$ doped has higher light-off temperature than the Ni-Ru doped $SrZrO_3$. The presence of mobile lattice oxygen species help to activate the C-H bond leading to significant enhancement in the activity of the catalysts even at the initial reaction stage. Ni-Fe doped has less initial activity due to lower reducibility of iron and low mobility of oxygen species.

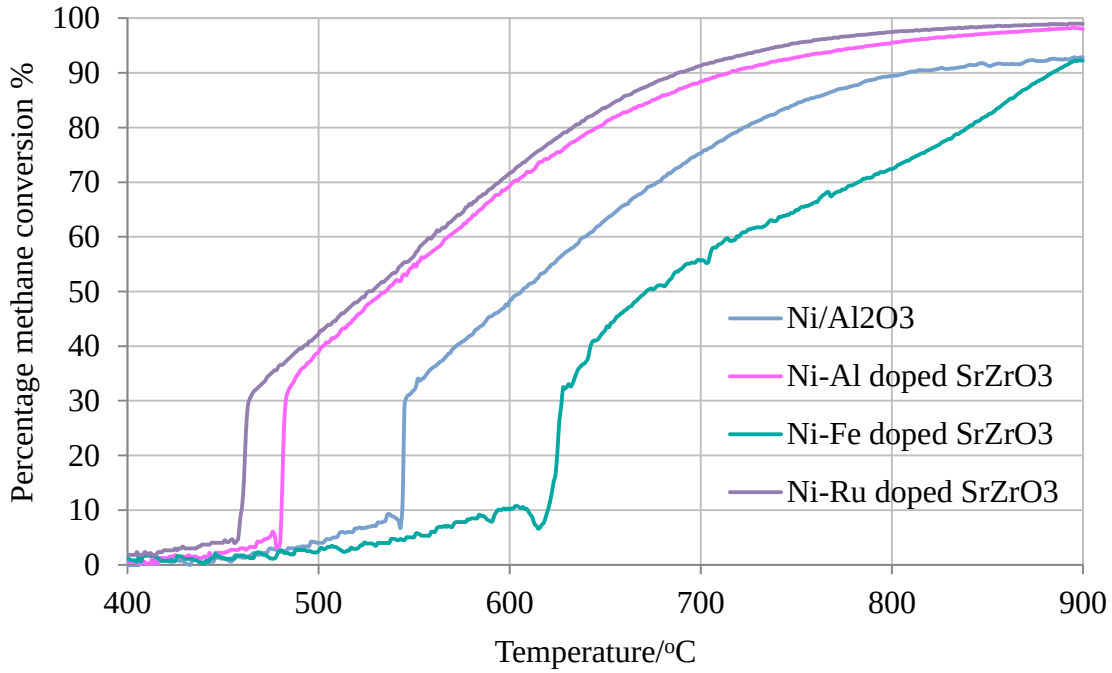

Figure 6.5: Methane conversion profiles of 1: 0.5 CH_4 /O_2 mixture over each catalyst material under study at temperatures between 400 °C to 900 °C.

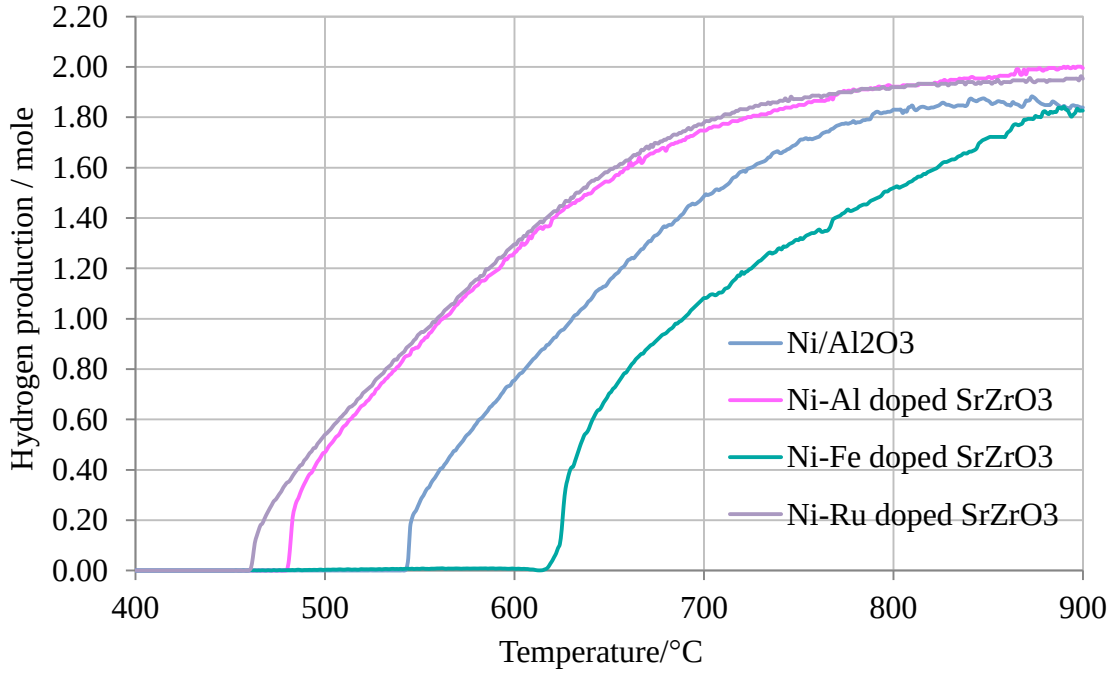

Figure 6.6: Hydrogen production profiles of 1: 0.5 CH_4 /O_2 mixture over each catalyst material under study at temperatures between 400 °C to 900 °C.

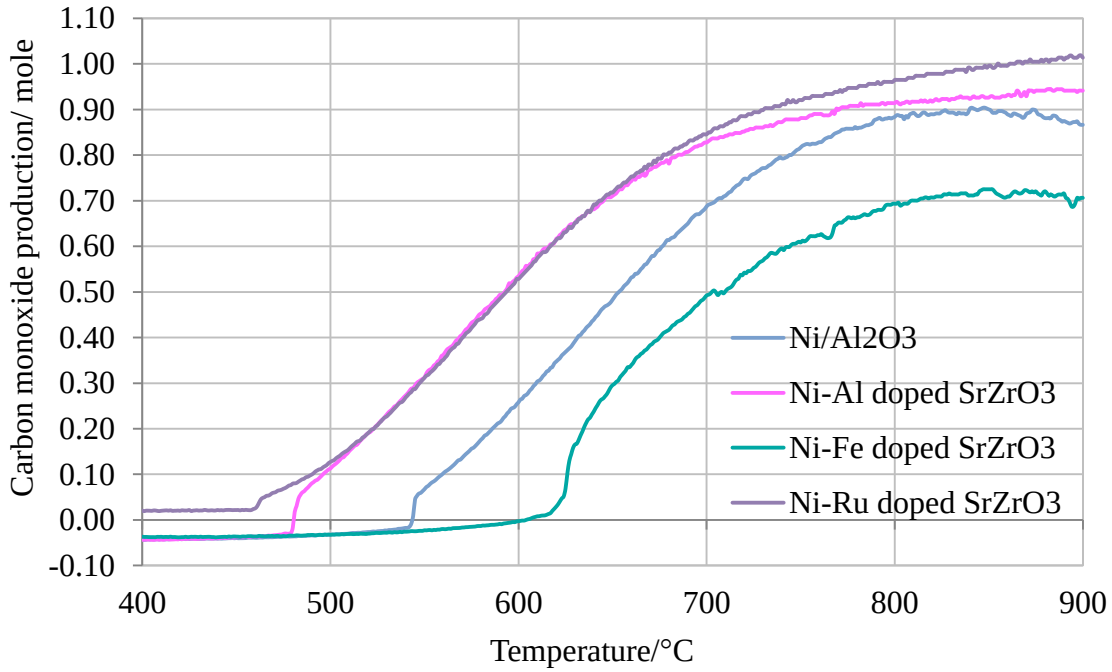

Figure 6.7: CO production profiles of 1: 0.5 CH_4 /O_2 mixture over each catalyst material under study at temperatures between 400 °C to 900 °C.

6.3 Isothermal testing and post reaction studies

6.3.1 Catalytic performance at different temperatures for partial oxidation of methane (POX)

Conventional reactions (POX) were investigated under varying temperatures 700 °C, 800 °C and 900 °C over three co-doped perovskites and 10% Ni/Al_2O_3 catalysts. Selection of the temperatures at which the isothermal partial oxidation of methane reforming reactions would be implemented was based on the temperature programmed reaction data. For all catalysts the influences of temperature on the conversion of reactant and product synthesis gas yields are given in figures 6.8-6.11 were determined over 20 hours of reaction. For

most of the catalysts in this study, CH_4 conversion began steadily and remained approximately constant throughout the reaction, resulting in a steady H_2 production.

The long duration tests at 900 °C are shown in part C of the figures. It can be seen that the perovskite catalysts do not deactivate whilst the 10% Ni/Al_2O_3 catalyst presents a slight loss of activity that is shown clearly by the hydrogen profile and calculated to be ~ 13% after 20 h of reforming reaction. These results were expected looking at the XRD and SEM analysis of the co-doped perovskite samples before and after the tests (in chapter 7) where no difference in the peak shape and surface morphology were detected, unlike nickel supported alumina which shows some signs of particle sintering that indicated by the sharper peaks for NiO crystallite at 36.5° and 62.4°.

It has been suggested in the literature that synthesis gas production by partial oxidation of methane proceeds in two steps, methane is combusted by O_2 to produce CO_2 and H_2O. The remaining methane is reformed with the H_2O and CO_2 to produce synthesis gas. H_2 and CO were formed, since the reforming reaction is endothermic with an increase seen with increasing reaction temperature improving the selectivity of both H_2 and CO [7]. From the temperature programmed reaction profiles observed in figure 6.10 C, it can be seen that there is an activity drop within the initial reaction as observed for both hydrogen and carbon monoxide production that was most likely due to some instability in the methane decomposition.

High stability was seen with Ni-Al doped and Ni-Ru doped perovskites in the H_2 and CO yields over the 20 hours at 900 °C, whereas with 10% Ni/Al_2O_3 there is a significant reduction in H_2 yield and this continues over the time of the reforming reaction. The presence of Ni and Fe dopants is known to be active for methane activation which can lead

to improved synthesis gas selectivity [8] and this is consistent with Ni-Fe doped perovskite result.

A typical partial oxidation temperature is 900 °C. At this temperature CH_4 conversion over Ni-Fe doped perovskite increases throughout the duration of the reaction, reaching a maximum of around 90% at the end of the isothermal reaction with 89% H_2 yield, 39% CO yield and 2.3 H_2 /CO molar ratio. For this sample, the H_2 /CO ratio was higher than that expected for thermodynamic equilibrium, indicating a favouring of H_2 formation. This may indicate oxidation of CO to CO_2.

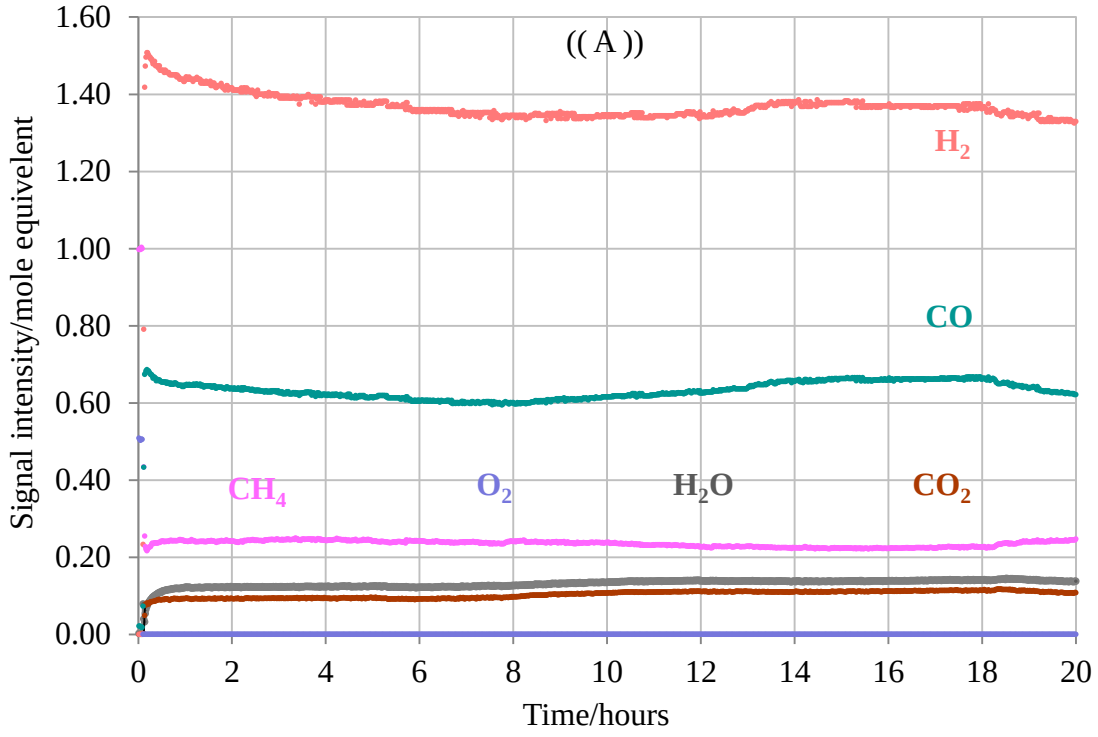

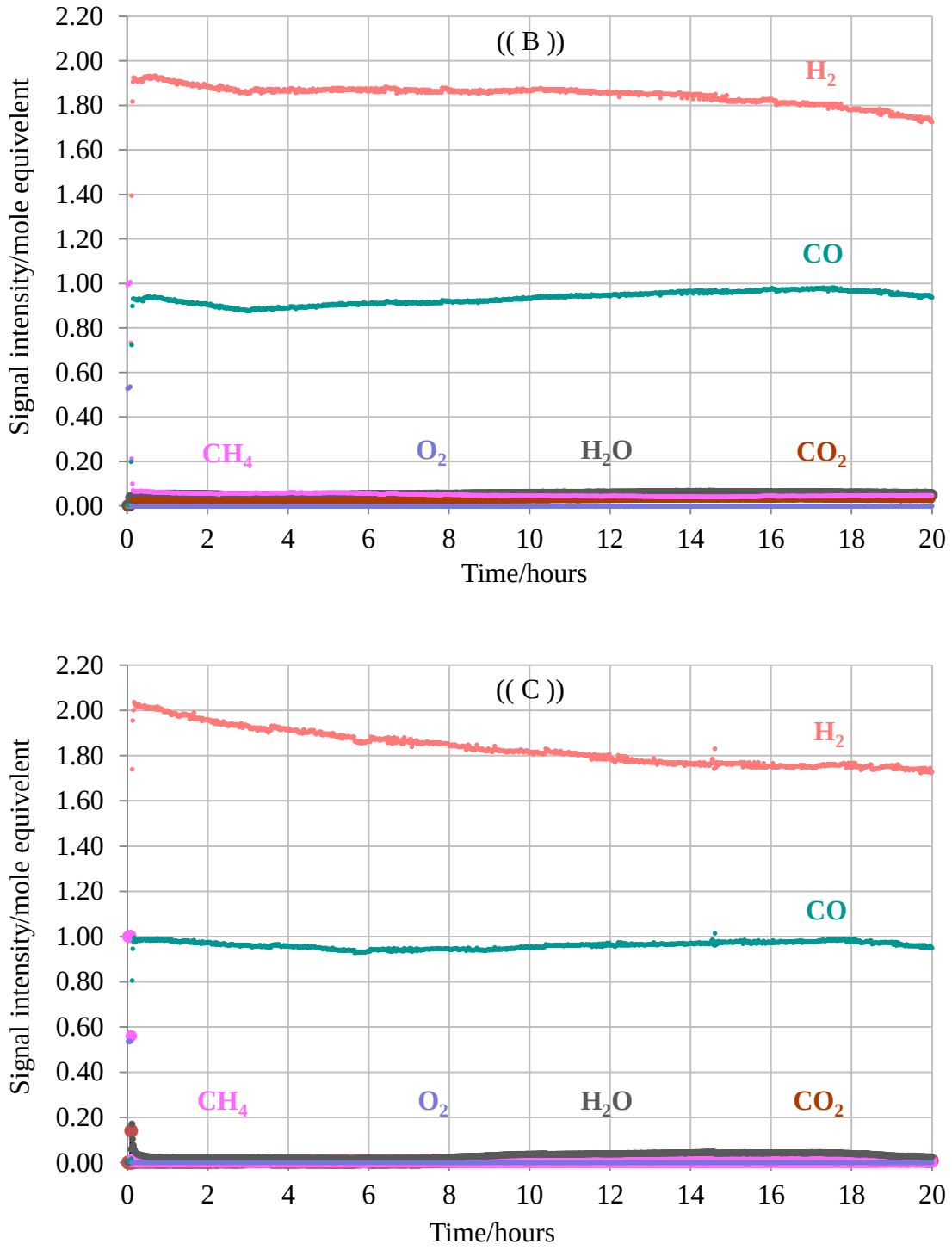

Figure 6.8: Partial oxidation of methane profiles of a 1: 0.5 CH_4 /O_2 mixture over 10% Ni/Al_2O_3 catalyst for 20 h at three temperatures (A) 700 °C, (B) 800 °C and (C) 900 °C.

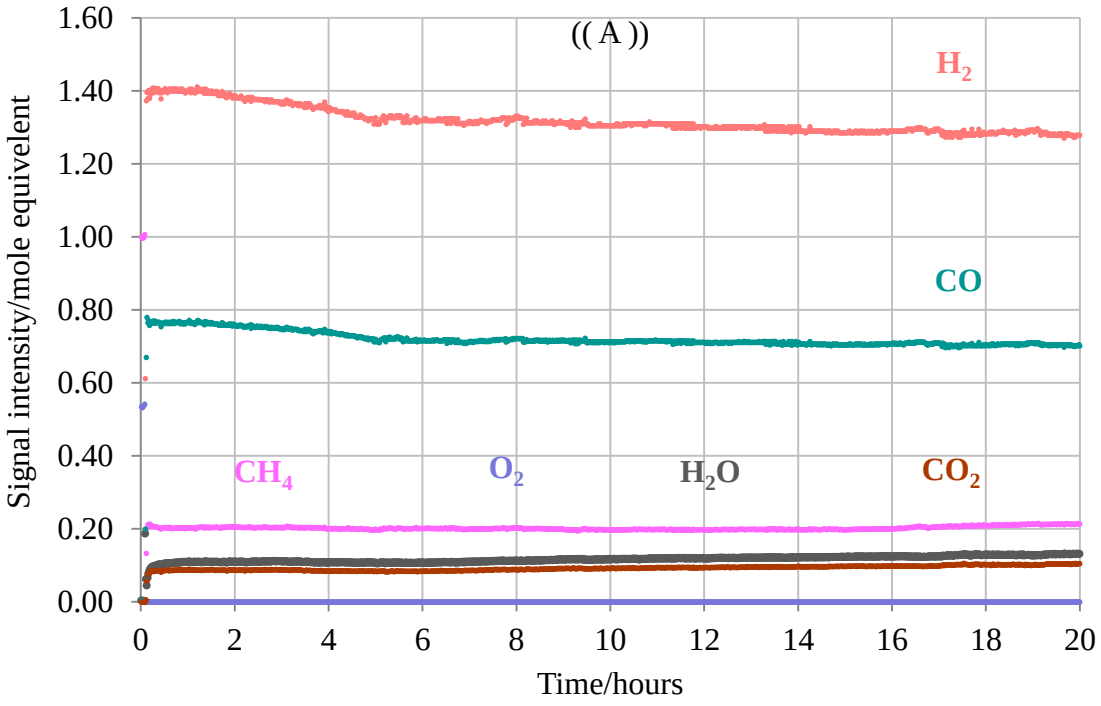
((A))
Signal intensity/mole equivelent
Time/hours
H2
CO
CH4
O2
H2O
CO2
1.60
1.40
1.20
1.00
0.80
0.60
0.40
0.20
0.00
0
2
4
6
8
10
12
14
16
18
20

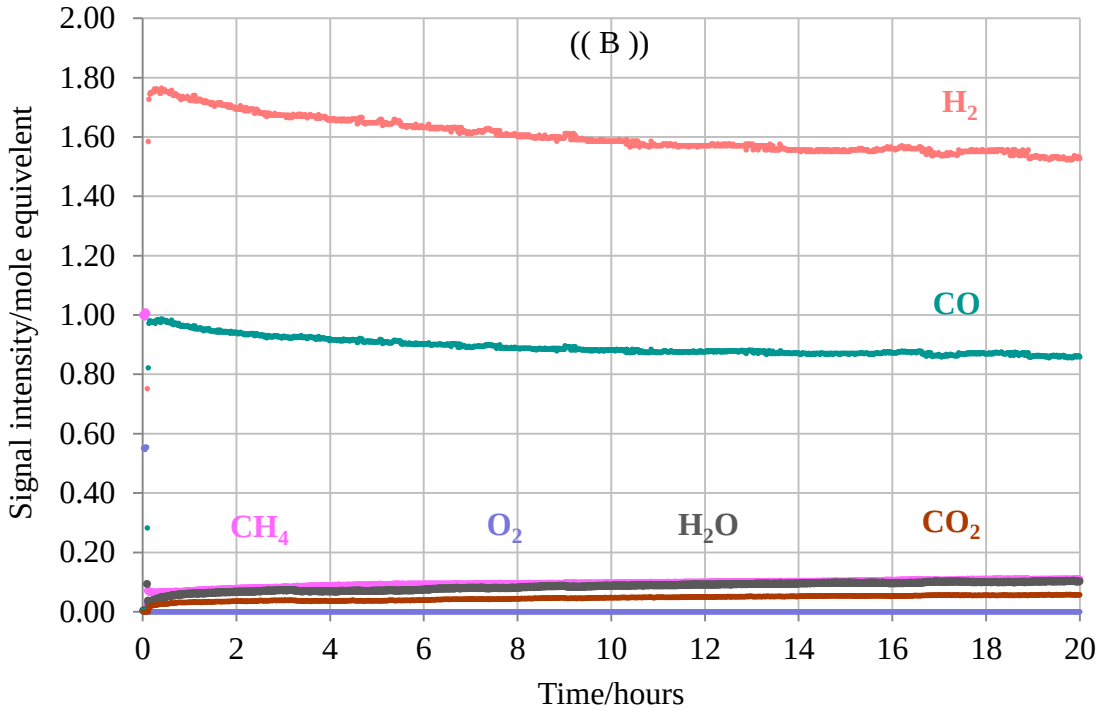
((B))
Signal intensity/mole equivelent
Time/hours
H2
CO
CH4
O2
H2O
CO2
2.00
1.80
1.60
1.40
1.20
1.00
0.80
0.60
0.40
0.20
0.00
0
2
4
6
8
10
12
14
16
18
20

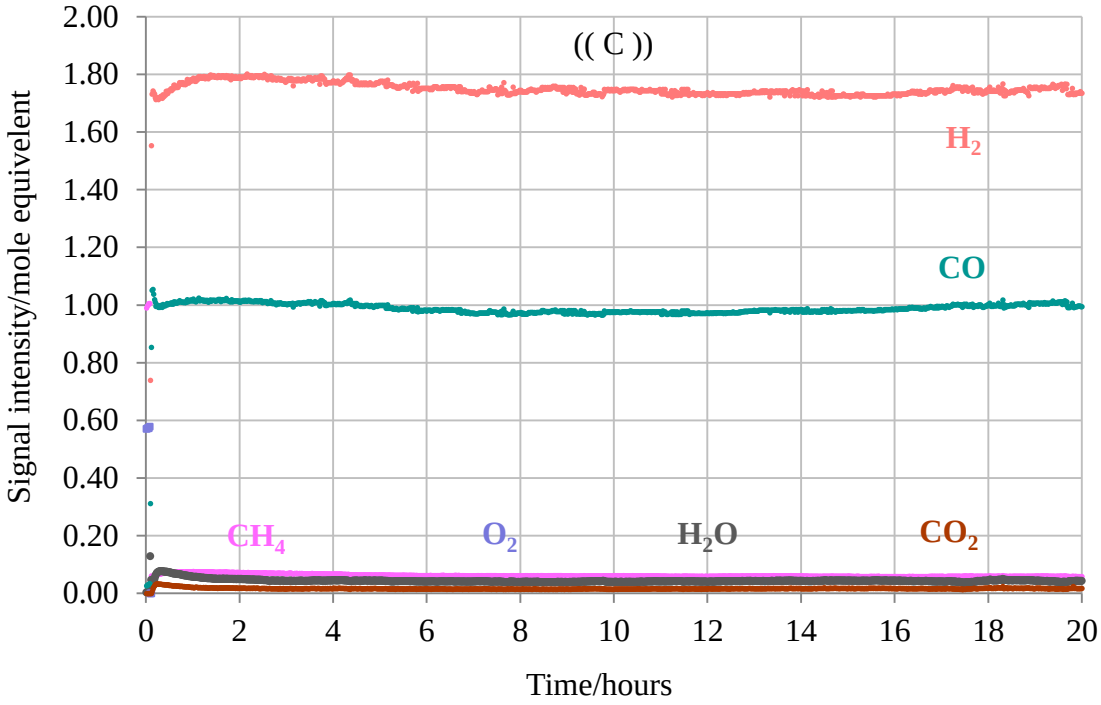

Figure 6.9: Partial oxidation of methane profiles of a 1: 0.5 CH_4 /O_2 mixture over Ni- Al doped $SrZrO_3$for 20 hours at three temperatures (A) 700 °C, (B) 800 °C and (C) 900 °C.

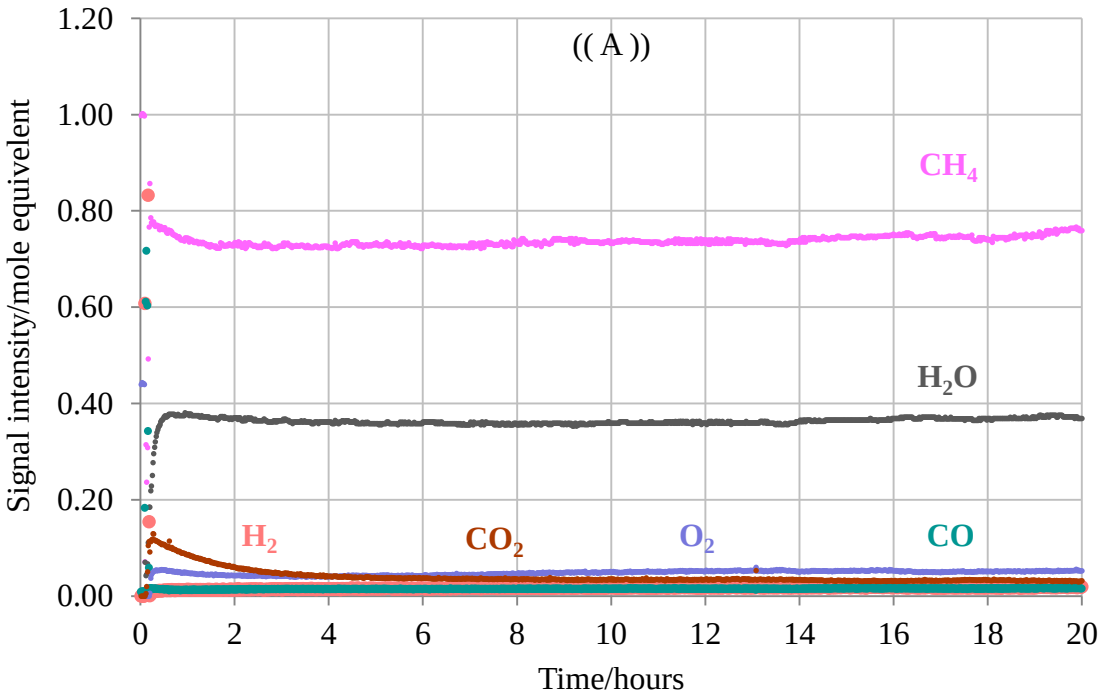

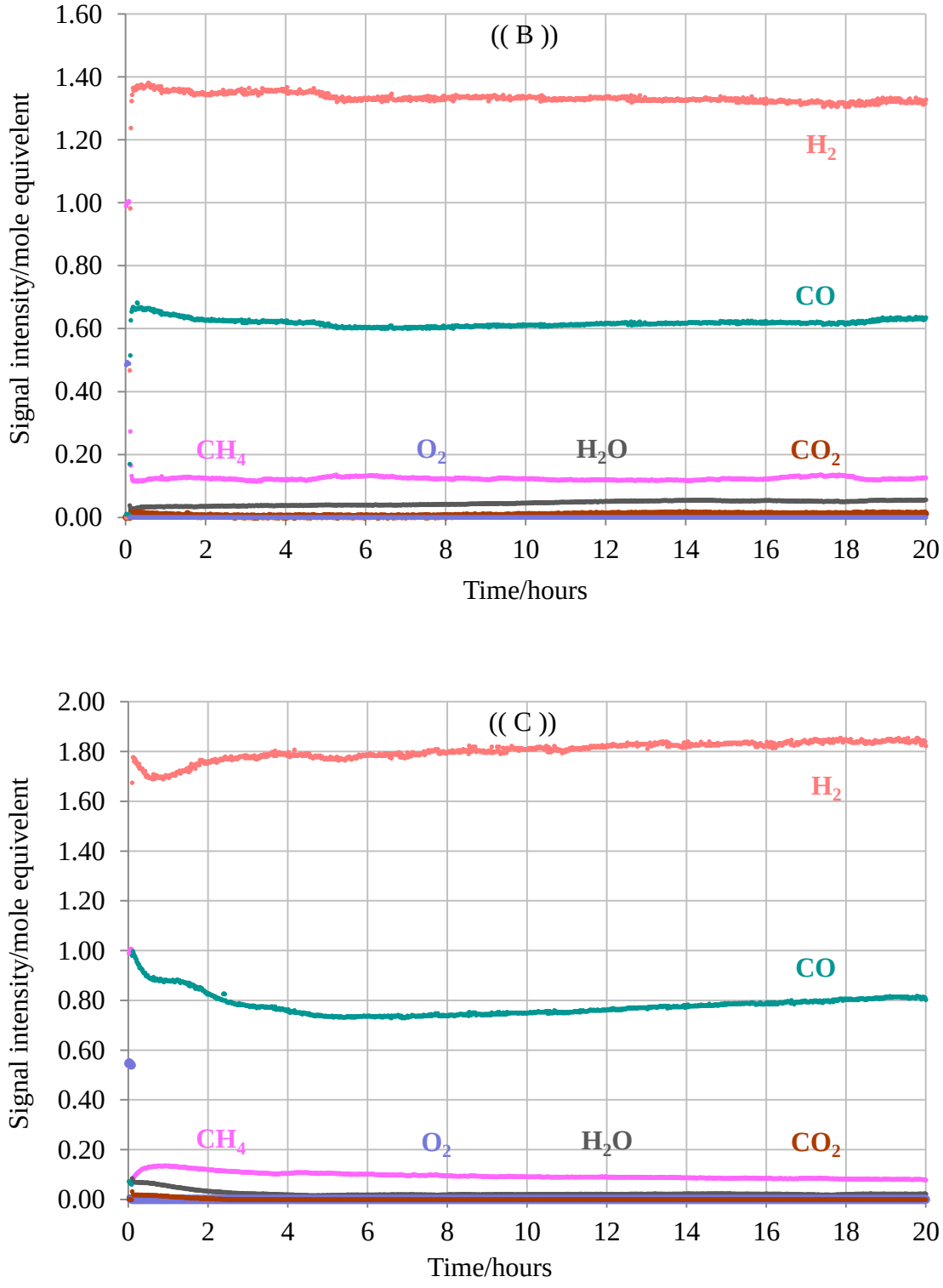

Figure 6.10: Partial oxidation of methane profiles of a 1: 0.5 CH_4 /O_2 mixture over Ni-Fe doped $SrZrO_3$ for 20 hours at three temperatures (A) 700 °C, (B) 800 °C and (C) 900 °C.

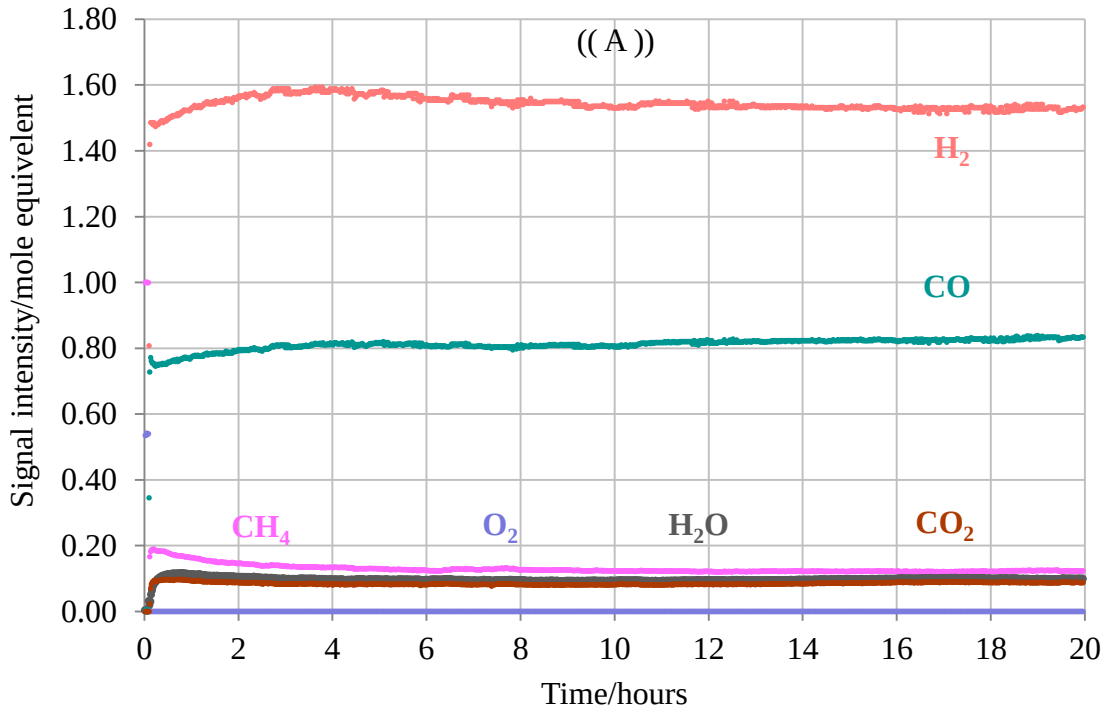
((A))
Signal intensity/mole equivelent
Time/hours
H2
CO
CH4
O2
H2O
CO2
1.80
1.60
1.40
1.20
1.00
0.80
0.60
0.40
0.20
0.00
0
2
4
6
8
10
12
14
16
18
20

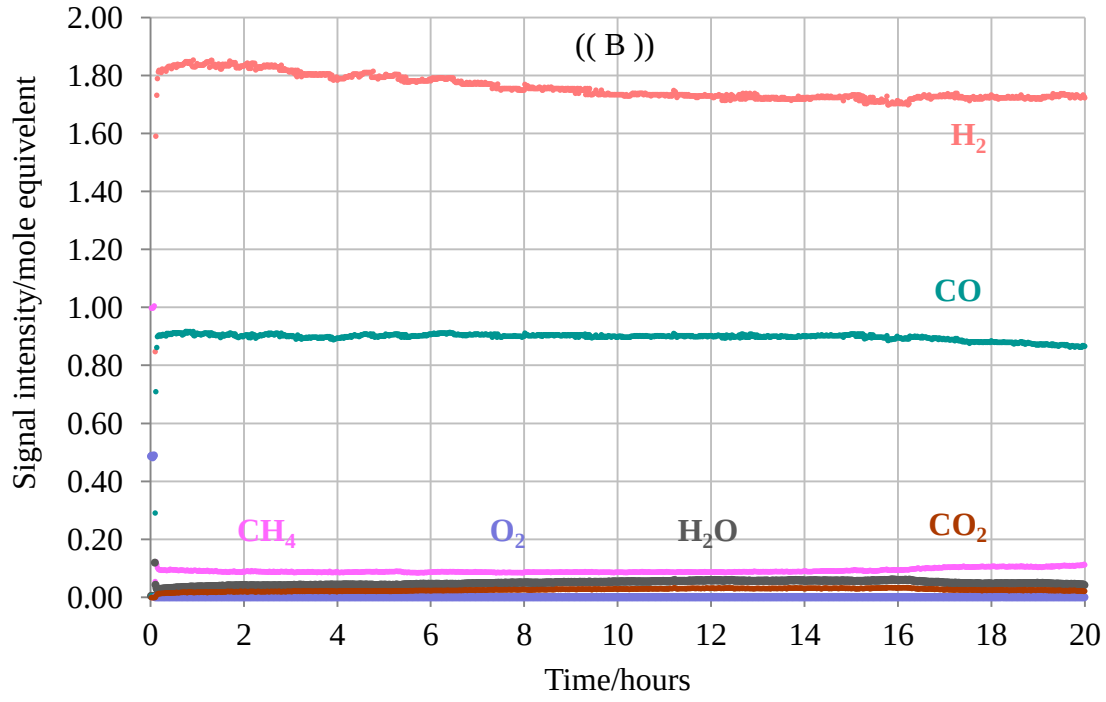
((B))
Signal intensity/mole equivelent
Time/hours
H2
CO
CH4
O2
H2O
CO2
2.00
1.80
1.60
1.40
1.20
1.00
0.80
0.60
0.40
0.20
0.00
0
2
4
6
8
10
12
14
16
18
20

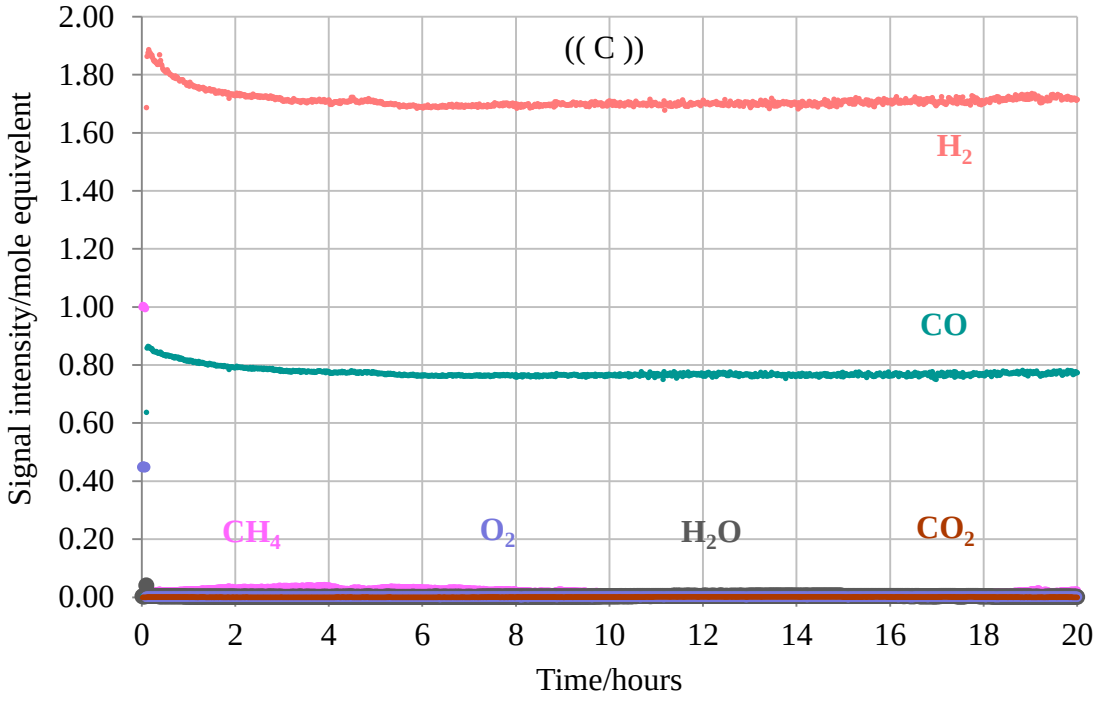

Figure 6.11: Partial oxidation of methane profiles of a 1: 0.5 CH_4 /O_2 mixture over Ni-Ru doped $SrZrO_3$ for 20 hours at three temperatures (A) 700 °C, (B) 800 °C and (C) 900 °C.

As can be seen from all the above figures of isothermal partial oxidation of methane reactions, the general trend was that H_2 production increased with temperature and a high yield of synthesis gas was only obtained when the temperature was greater than 800 °C. The Ni-Ru doped sample is the most active and stable catalyst among the three co-doped samples, on which there is no observable H_2 production decrease during the 20 h test at elevated temperature. However, the H_2 production over Ni/Al_2O_3 exhibits a high initial yield during the first 2 hours, and then H_2 production decreases from 100% to ~87% after 20 h of reaction, indicating this catalyst still deactivates. It looks like the water quantity is also increasing and this suggest that the catalyst is selectively oxidising the H_2 to H_2O.

CH_4 conversion of each catalyst drops substantially with decreasing the reaction temperature from 800 °C to 700 °C. The Ni-Fe doped sample has only negligible reactivity

at less than 750 °C, this is confirmed by the reaction values and profile at 750 °C shown in table 6.1 and appendix (figure 8.3).

Table 6.1: Average reactants conversion and products yield over Ni-Fe doped $SrZrO_3$ after 20 hours of partial oxidation of methane reaction at 750 °C.

Samples	20 hours at 750 °C					
	CH_4%	O_2%	H_2%	CO%	H_2/CO	Carbon $g_c/g_{cat.}$
Ni-Fe doped $SrZrO_3$	72	100	44	21	2.1	0.096

6.3.2 Catalytic activity evaluation studies

The experimental CH_4 conversions and synthesis gas production values over the four catalysts at various temperatures are shown in figures 6.12-6.15. The yield of hydrogen gas and methane conversion increases due to the enhancement of the rate of the POX reaction with increasing temperatures. There were differences in the yields of H_2 and CO between the catalysts and therefore the syngas ratios (H_2 /CO) fluctuated (see figure 6.15). Ni-Ru doped $SrZrO_3$ exhibited the highest CH_4 conversion among the three co-doped samples, which is close to the theoretical equilibrium conversion that is ~98%, 90%, and 87% at 900 $^{\circ}$C, 800 $^{\circ}$C, and 700 $^{\circ}$C respectively.

From the data presented in the figures below it can be seen that among the four catalysts the higher activity over 20 h at 700 $^{\circ}$C with the highest reactant conversion and product yields was obtained with the Ni-Ru doped perovskite. This catalyst had excellent stability with a high H_2 /CO product ratio (1.89), and achieved a good average methane conversion,

H_2 and CO yields of about 87% and 77% and 40% respectively. In contrast, very low activity was observed for the Ni-Fe doped perovskite.

The isothermal POX reactions over the four catalysts showed the general trend of CH_4 conversion increasing with temperature, with the highest conversion rate observed at 900 °C and the lowest observed at 700 °C as shown in figure 6.12. Interestingly, according to the test with Ni-Fe doped at 700 °C, the conversion of methane was 26% while the product yields were 1% H_2 and 1% CO with a H_2 /CO ratio (1.1), as it was in dry reforming. This suggests that partial oxidation of methane is accompanied by other side reactions such as RWGS which was confirmed by the high amount of water produced as observed in figure 6.10 A.

The syngas values (H_2 /CO ratios) often fluctuated due to the differences in the yields of H_2 and CO between the catalysts and the presence of the reverse water-gas-shift reaction. The trend for the syngas ratios was similar on Ni-Ru doped and Ni-Fe doped perovskites, which increased with temperature. In contrast on 10% Ni/Al_2O_3 and Ni-Al doped $SrZrO_3$ the syngas ratios decreased with temperature. It is likely that the RWGS reaction is more favoured on these catalysts. All catalysts have a ratio close to the equilibrium value (~2) at 900 °C. However, the Ni-Al doped catalyst showed a slightly decreasing trend in the syngas ratio, due to the greater increase in CO yield than other catalysts.

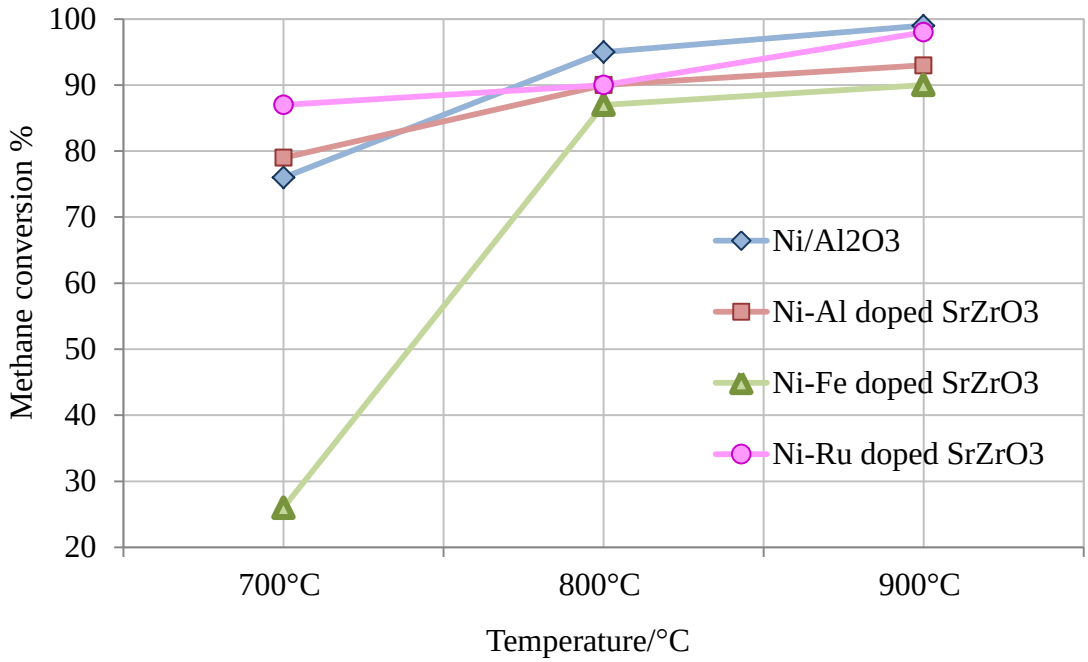

Figure 6.12: Average CH_4 conversion profiles of 1: 0.5 CH_4 /O_2 mixture over four catalysts at three different temperatures for 20 hours.

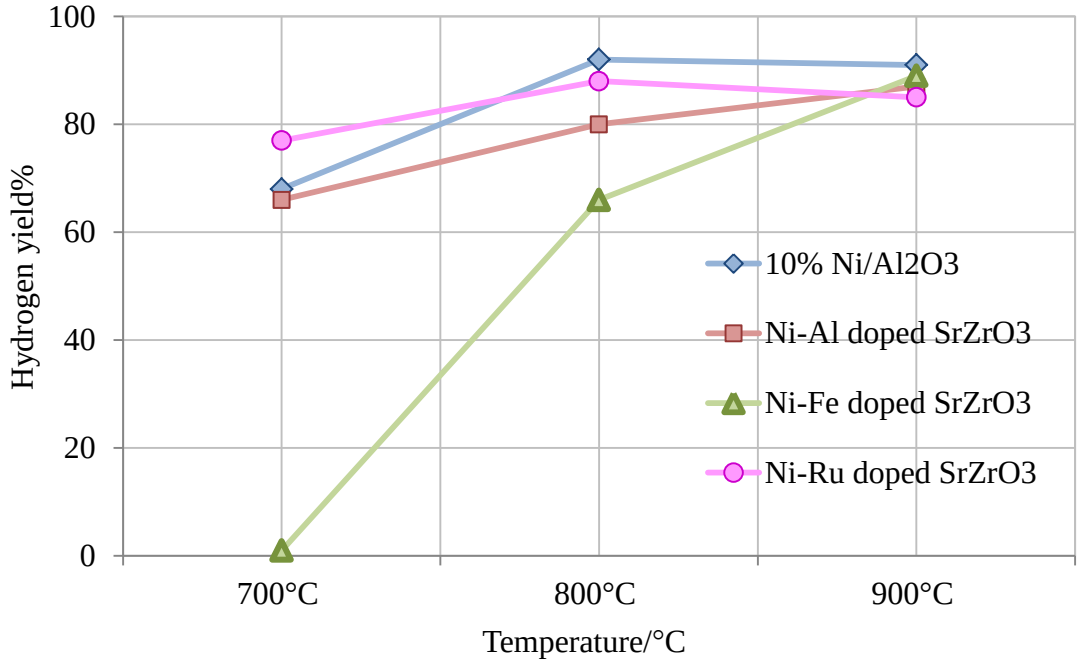

Figure 6.13: Average hydrogen yields over four catalysts of 1: 0.5 CH_4 /O_2 mixture at three different temperatures for 20 hours.

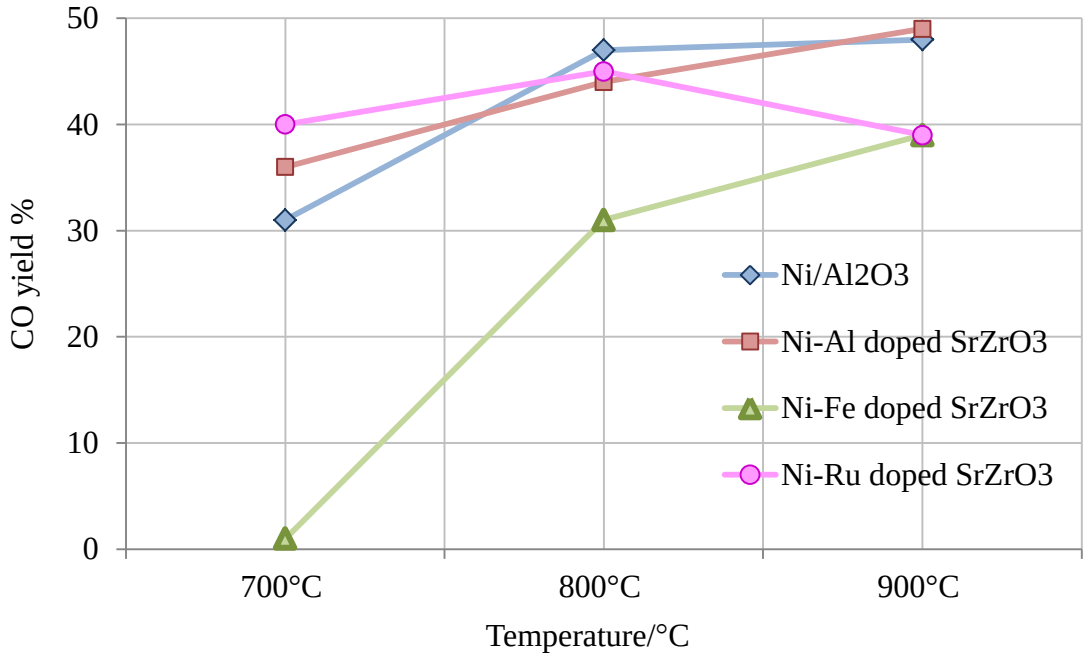

Figure 6.14: Average carbon monoxide yields over four catalysts of 1: 0.5 CH_4 /O_2 mixture at three different temperatures for 20 hours.

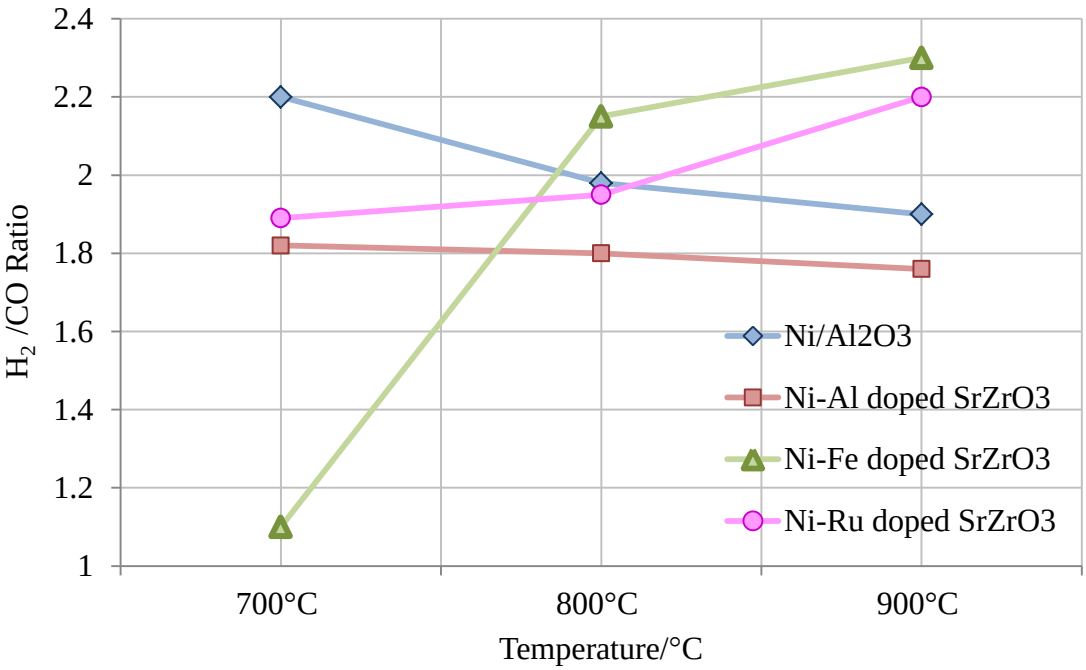

Figure 6.15: Average H_2 /CO Ratio over four catalysts of 1: 0.5 CH_4 /O_2 mixture at three different temperatures for 20 hours.

A comparison of noble (Ru) and non-noble (Fe and Al) a metal Ni-based catalyst towards partial oxidation of methane was investigated in this study. It was found that the Ni-Ru doped catalyst has a higher catalytic activity compared to the other catalysts and that is consistent with previous studies [9]. This indicates that the addition of noble metals to Ni catalyst leads to an increase in the activity and selectivity to syngas production with very low levels of inert carbon formation, which does not lead to catalyst deactivation.

6.3.3 Surface carbon analysis (post reaction)

Post reaction profiles can be used to get some insight into the nature of carbon formed on each catalyst during reforming reactions as well as allowing quantification of the amount of coke deposited during reformation reaction. The temperature at which carbon burn-off of the spent catalysts occurs during TPO depends on the sort of carbon and its stability on the active surface sites of the catalyst. Figure 6.16 shows the variation in the amount of carbon deposition with reaction temperature over 10% Ni/Al_2O_3 and the three co-doped perovskites (Ni-Al doped $SrZrO_3$, Ni-Fe doped $SrZrO_3$ and Ni-Ru doped $SrZrO_3$). It was found that there are no strong differences in the amount of carbon among the four catalysts after 20 hours of catalytic partial oxidation of methane reactions.

Negligible levels of coke were detected in post reaction test for all four catalysts and the catalytic activity remained high under reaction conditions. The highest amount of carbon formation per one gram of catalyst reached 0.046 g over Ni-Ru doped $SrZrO_3$ at 900 °C.

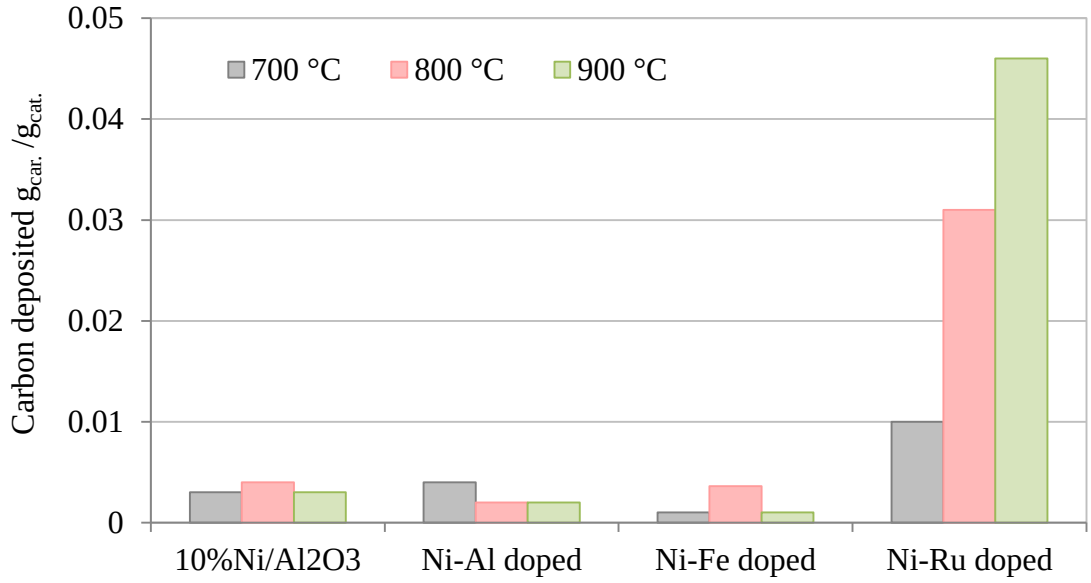

Figure 6.16: Comparison of carbon deposited on 10% Ni/Al_2O_3, Ni-Al doped $SrZrO_3$, Ni-Fe doped $SrZrO_3$ and Ni-Ru doped $SrZrO_3$ for 20 h at various temperatures in grams of carbon per grams of catalysts.

6.4 Conclusion

The partial oxidation of methane to synthesis gas over different co-doped catalysts (Ni-Al doped $SrZrO_3$, Ni-Fe doped $SrZrO_3$ and Ni-Ru doped $SrZrO_3$) showed that the catalyst performance during the reforming reaction is also affected by the type of active metal that is incorporated within the perovskite structure, either by influencing catalyst properties or by probably affecting the interaction between different doping metals. From these results, it was concluded that the use of a small amount of nickel and ruthenium is more beneficial in terms of the activity, stability and cost. Therefore, this type of catalyst deserves further attention and investigation.

In general, reforming reactions over heterogeneous catalysts lead to coke deposits, methane cracking, and the Boudouard reaction. The catalysts can handle these reactions as

long as the coke gasifying rates are higher than the coking rates. Thermodynamic results for methane partial oxidation to syngas suggest temperatures in access of 850 °C are required for high methane conversion and selectivity to carbon monoxide and hydrogen. Superior coking resistance, high stability and activity was observed for the co-doped perovskite materials. The nickel supported alumina catalyst also showed generally greater reforming activity indicated by higher the reactant conversion with low levels of carbon formation.

During 20 hours' time on stream of partial oxidation of CH_4, all co-doped catalysts showed ~90% methane conversion and had no significant sintering or deactivation. These levels of reactivity were much closer to the expected conversion levels of methane. However, only the standard nickel supported alumina catalyst showed slight deactivation due to sintering and coke accumulation. When the CO yield decreased more than the H_2 yield that means the combustion of CH_4 might be more favourable than partial oxidation.

It was possible to examine and characterize the deactivation of catalyst due to change in morphology by using SEM and XRD analysis of each catalyst as well as by the isothermal temperature programmed reaction profiles shape. Even though all the prepared catalysts showed good performances, the only catalyst able to present the highest activity with no deactivation was Ni-Ru doped $SrZrO_3$. The Ni-Fe doped catalyst showed a higher resistance to carbon deposition than the other catalysts. The level of coke formed on the four catalysts is extremely low and shows no effect on the activity and selectivity of the catalysts. Even if there was some amount of carbon on the surface of catalysts it would take a substantial period of time before this becomes a problem.

Interestingly, the Ni-Ru doped $SrZrO_3$ catalyst gave a higher deposition of carbon than the other co-doped and conventional supported catalysts under reaction conditions. However, it displays good reforming activity, stability as well as resistance to particle agglomeration and fouling caused by deposits of solid carbon.

6.5 Reference

[1] M. A. Goula, N. D. Charisiou, K. N. Papageridis, A. Delimitis, E. Pachatouridou and E. Iliopoulou, *Int. J. Hydrogen Energy*., 2015, **40**, 9183–9200.

[2] K. Sutthiumporn, T. Maneerung, Y. Kathiraser, and S. Kawi, *Int. J. Hydrogen Energy*, 2012, **37**, 11195-11207.

[3] C. Wang, N. Sun, N. Zhao, W. Wei, Y. Zhao, *Catalysis Today*, 2017, **281**, 268-275.

[4] V.S. Guggilla, J. Akyurtlu, A. Akyurtlu, and I. Blankson, *Ind. Eng. Chem. Res*., 2010, **49**, 8164–8173.

[5] A. P.E. York, T. Xiao, and M. L.H. *Green, Topics in Catal.,* 2003, **22**, 345-458.

[6] A. Gervasini, *Calorimetry & Thermal Methods in Catalysis*, chapter 5, 2013, **154**, 175-195.

[7] M. Peymani , S. M. Alavi and M. Rezaei, *Int. J. Hydrogen Energy*, 2016, **41**, 6316-6325.

[8] A. Mishra, N. Galinsky, F. He, E. Santiso and F. Li, *Catal. Sci. Technol.*, 2016, **6**, 4535-4544.

[9] A. I. Tsyganok, M. Inaba, T. Tsunoda, S. Hamakawa, K. Suzuki, T. Hayakawa, *Catal. Commun.,* 2003, **4**, 493–498.

Chapter 7

Overall Conclusions and outlook

7. Overall Conclusions and Outlook

7.1 Comparison of catalytic activity for different reforming methods

The catalytic performance for the biogas (2:1 CH_4 /CO_2), dry (1:1 CH_4 /CO_2) reforming and partial oxidation reactions have been studied concerning reactant conversion, synthesis gas yields and the produced gas mixtures H_2 /CO molar ratio. After approximately one hour of the start of each reaction, the temperature trends of dry reforming reactions were similar to those observed for biogas reforming as follows. Methane and carbon dioxide conversion increased with increasing reaction temperature and the side RWGS reaction was reduced due to increasing methane decomposition at higher temperatures.

According to the temperature programmed reaction shown in figures (4.1- 4.4 and 5.1- 5.4 and 6.1-6.4) for biogas reforming, dry reforming and partial oxidation respectively, the conversion of methane for all catalysts for dry reforming began at a temperature approximately 60 °C lower than that for the methane-rich mixture and the partial oxidation of methane (shown in figure 7.1).

In both dry and biogas reforming reactions, all catalysts have the same trend in terms of H_2 and CO production that increased roughly linearly over a temperature range of 500 °C to 850 °C with a higher level of carbon monoxide than hydrogen production. The higher amount of CO_2 in the dry reforming reaction increased the methane conversion, causing a sharp increase in reactant conversion and syngas production above 500 °C.

Over 95% methane was converted at 850 °C under CO_2-rich environments in the dry reforming compared with 95% methane converted at 900 °C under CH_4-rich environments in the biogas reforming. Despite the higher methane conversion, the relatively low H_2 /CO ratio suggests there was less methane decomposition for DRM. From the high levels of

carbon monoxide, the origin of any carbon deposition under CO_2- rich conditions would likely be the Boudouard reaction.

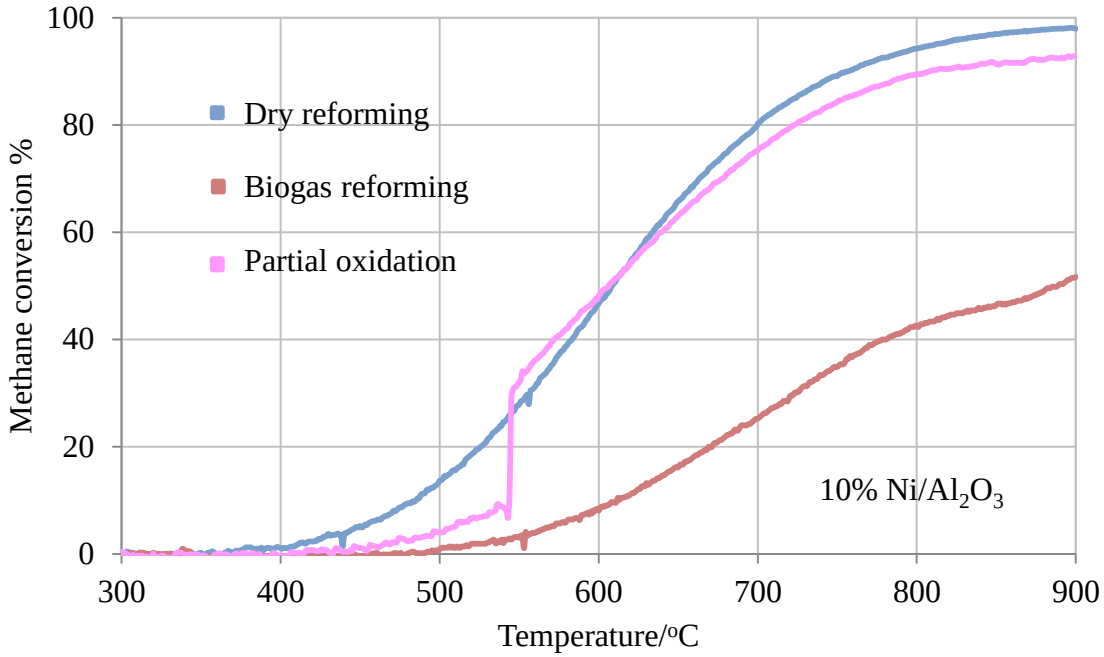

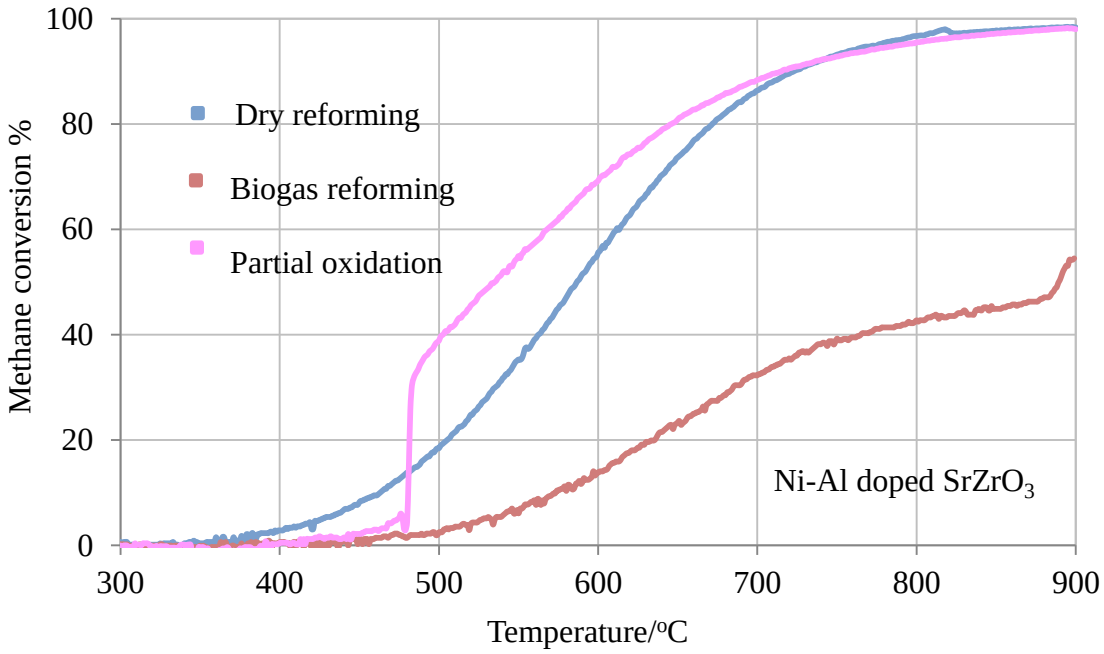

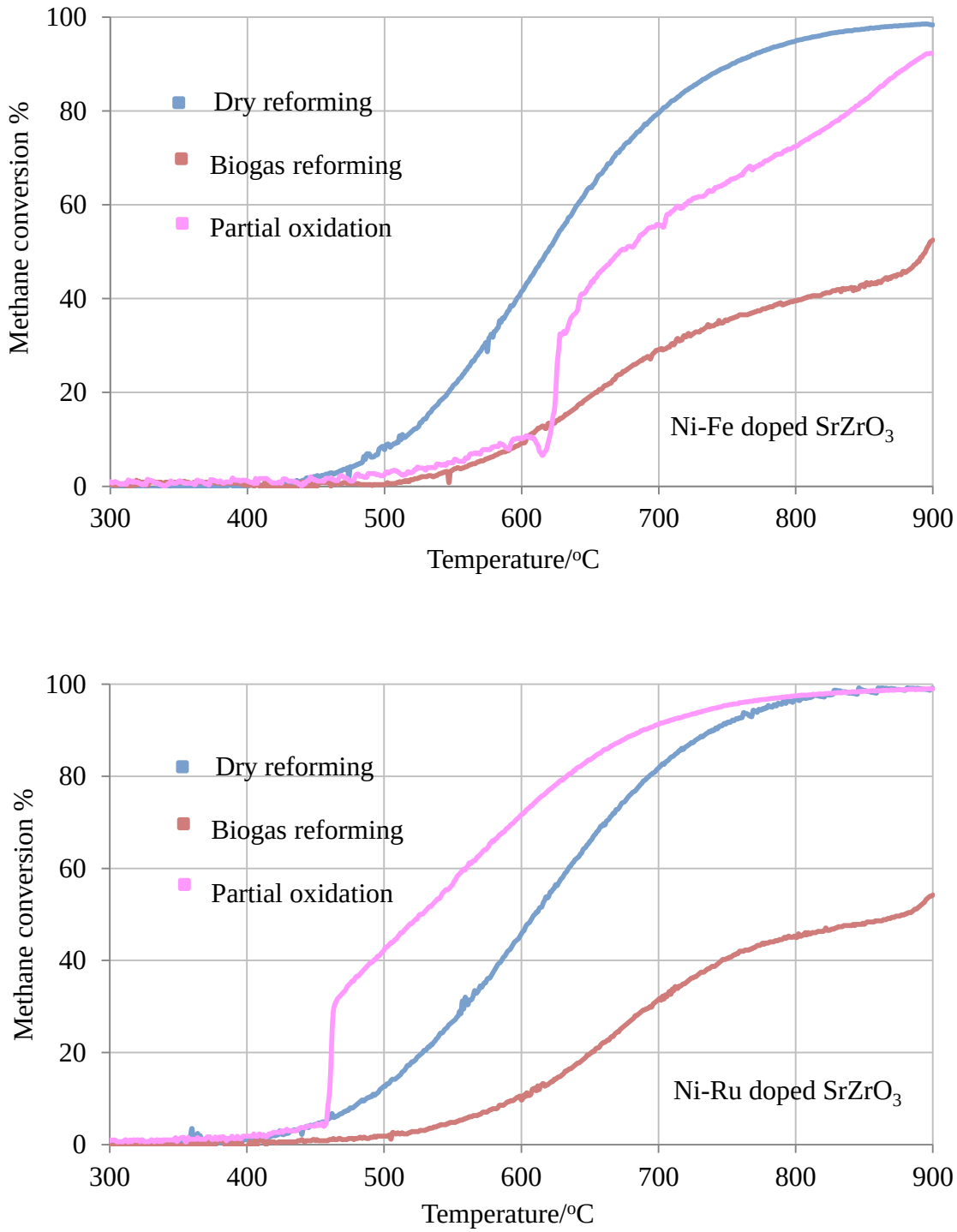

Figure 7.1: Percentage CH_4 conversion during temperature programmed reactions of dry and biogas reforming and partial oxidation over 10% Ni/Al_2O_3, Ni-Al doped $SrZrO_3$, Ni-Fe doped $SrZrO_3$ and Ni-Ru doped $SrZrO_3$ catalysts.

The higher level of CO_2 for the ratio of 1:1CH_4 /CO_2 had significantly reduced methane cracking compared with the ratio of 2:1 CH_4 /CO_2. Hydrogen production was also greater than carbon monoxide between 800 °C to 900 °C for biogas reforming and significantly increased with temperature (as shown in figure 7.2) with a H_2 /CO molar ratio greater than that observed for the dry reforming with a ratio of 1:1CH_4 /CO_2 (shown in figures7.3 and 7.4). This was due to a greater occurrence of the RWGS reaction in dry reforming, which caused greater levels of water production and CO content, as shown in figure 7.5.

As can be seen from this figure, there was a negative correlation between the reforming temperature and the production of water. Formation of water dropped after 600 °C due to a decreased occurrence of the RWGS reaction as the temperature increased and methane decomposition becoming more dominant for the biogas reforming process, which caused in increase in H_2 formation. This meant that the H_2 /CO ratio was higher than the dry reforming reaction, indicating that the presence of a high level of CO_2 reduces methane decomposition.

The perovskite materials show the same trend as observed for the nickel supported material in terms of synthesis gas production and the H_2 /CO ratio. This is a result of the very high selectivity of all four catalysts towards the formation of H_2 and CO rather than towards the formation of CO_2 and H_2O. Over the temperature range 800 °C to 900 °C, the H_2 production was greater and significantly became more H_2-rich with increasing temperature for biogas reforming, while for dry reforming, the H_2 production remained approximately constant. This suggests that the presence of a higher level of CO_2 within the ambient reaction led significantly to reduce methane cracking, consequently reducing H_2 as a product.

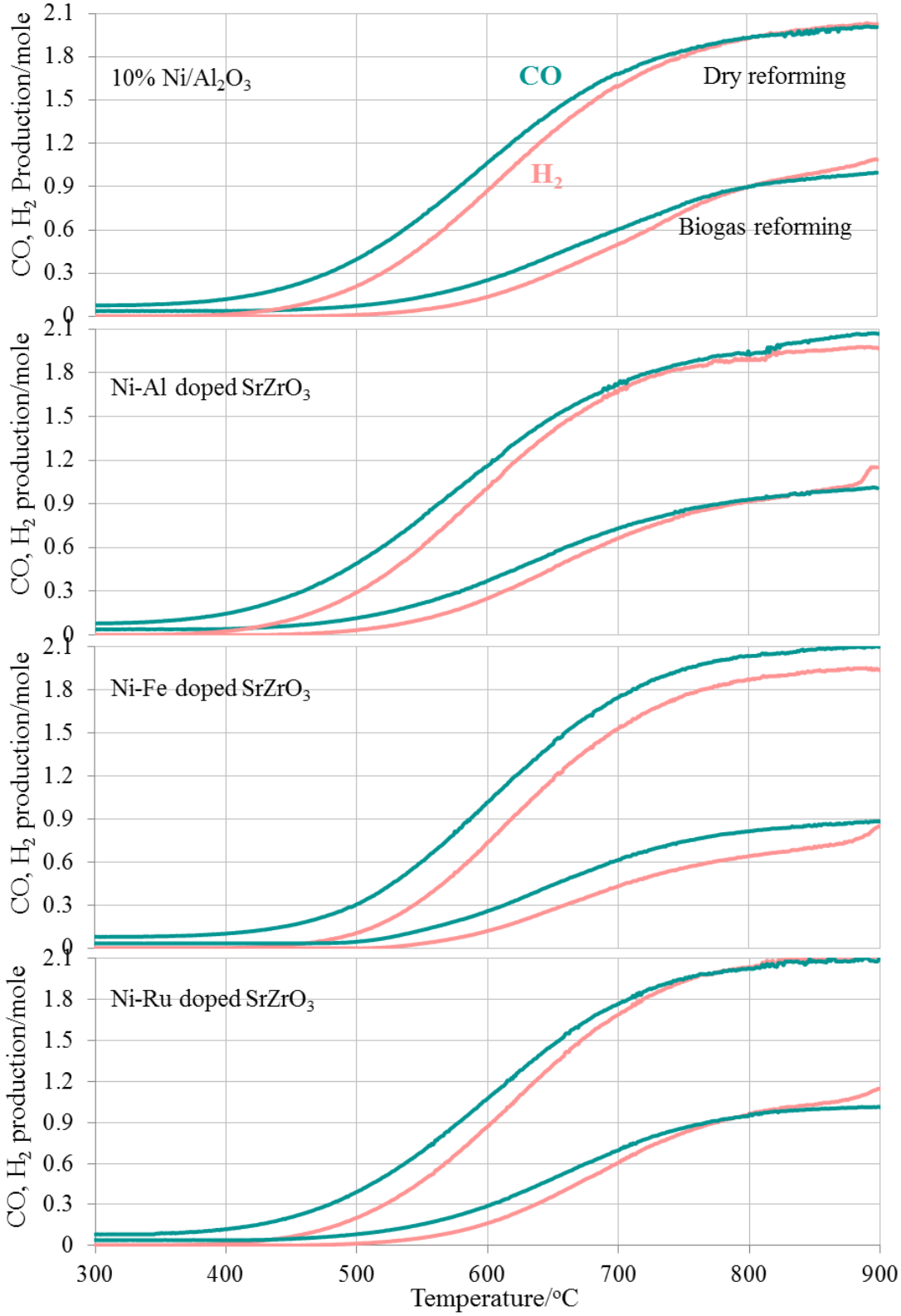

Figure 7.2: H_2 and CO production during temperature programmed reactions of dry and biogas reforming over 10% Ni/Al_2O_3, Ni-Al doped $SrZrO_3$, Ni-Fe doped $SrZrO_3$ and Ni-Ru doped $SrZrO_3$ catalysts.

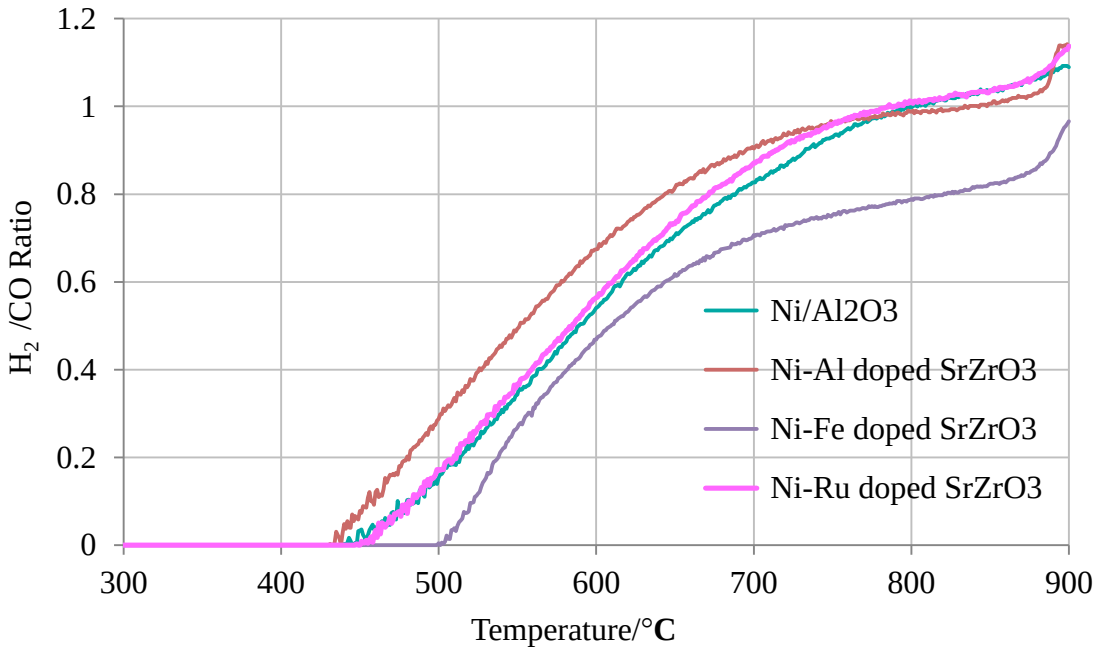

Figure 7.3: H_2 /CO molar ratio as a function of temperature over 10% Ni/Al_2O_3, Ni-Al doped $SrZrO_3$, Ni-Fe doped $SrZrO_3$ and Ni-Ru doped $SrZrO_3$ for 2:1 CH_4 /CO_2 mixture biogas reforming reaction.

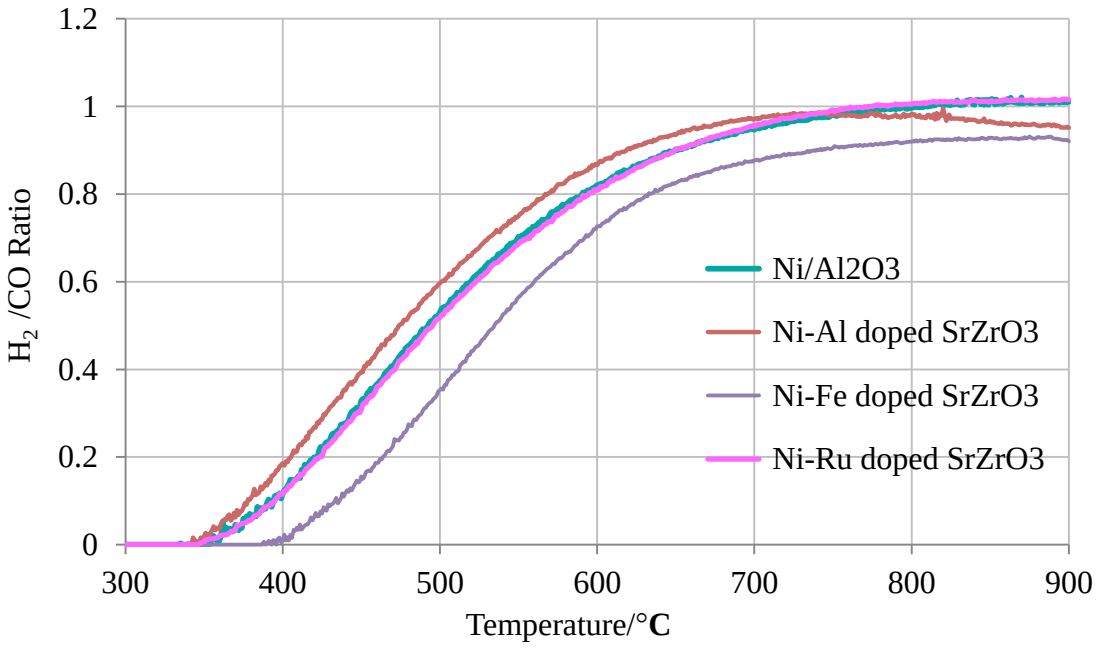

Figure 7.4: H_2 /CO molar ratio as a function of temperature over 10% Ni/Al_2O_3, Ni-Al doped $SrZrO_3$, Ni-Fe doped $SrZrO_3$ and Ni-Ru doped $SrZrO_3$ for 1:1 CH_4 /CO_2 mixture dry reforming reaction.

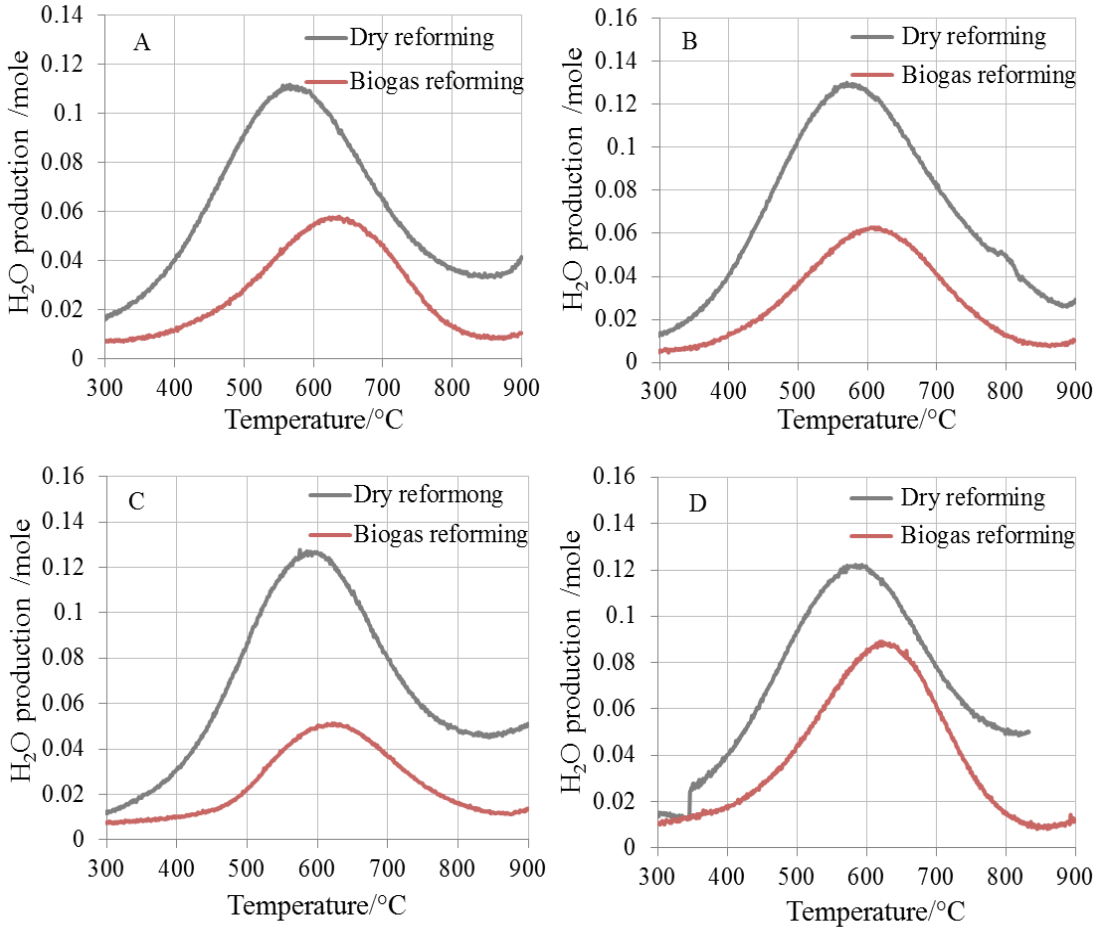

Figure 7.5: Water production during temperature programmed reactions over (A) 10% Ni/Al_2O_3, (B) Ni-Al doped $SrZrO_3$, (C) Ni-Fe doped $SrZrO_3$ and (D) Ni-Ru doped $SrZrO_3$ of 2:1 and 1:1 CH_4 /CO_2 mixtures (biogas and dry reforming).

Regarding the isothermal temperature programmed reaction at 700, 800 and 900 °C; a general trend of increasing reactant conversion with temperature is seen for all catalysts with the three reforming methods. High levels of methane conversion appear to occur only if there is a sufficient quantity of unreacted carbon dioxide available, as shown for biogas reforming in figure 7.6 for three reforming temperatures.

In the dry reforming reactions the conversion of methane is expected to be 100%, but it did not always show this result, suggesting that there is another factor limiting the conversion reaction. This may be due to some of the hydrogen being produced being simultaneously

consumed by reaction with carbon dioxide which leads to a higher level of water formation than that for biogas reforming under the same conditions. However, CO is also formed therefore, as the CO increases, the tendency for coke deposition by CO disproportionation increases too [l].

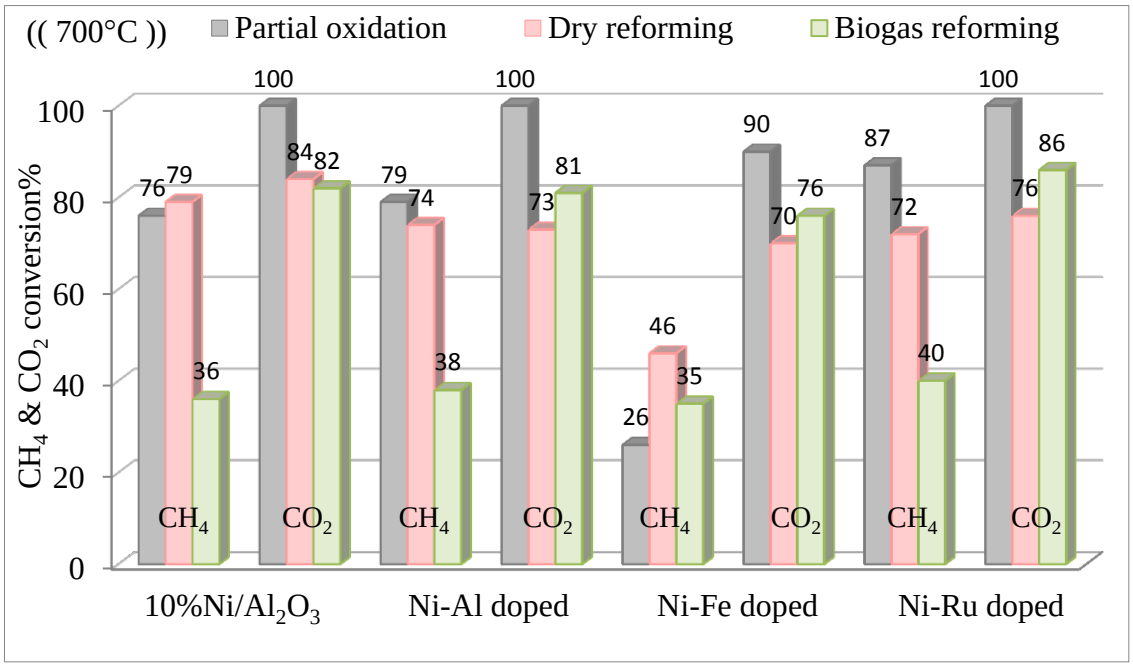

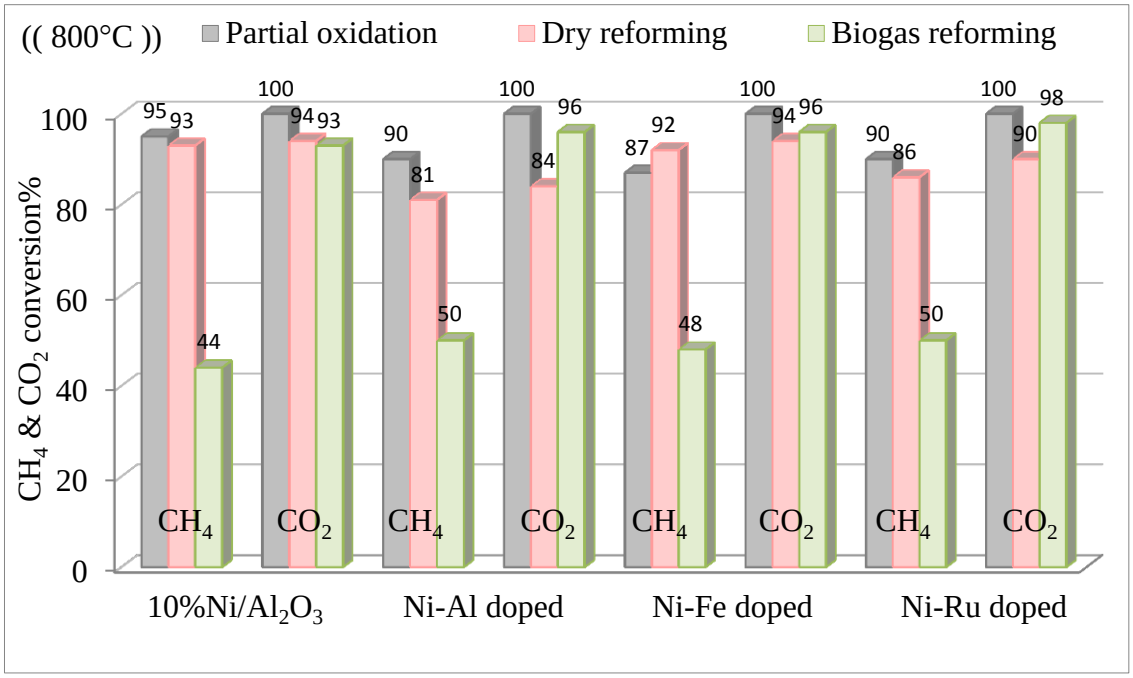

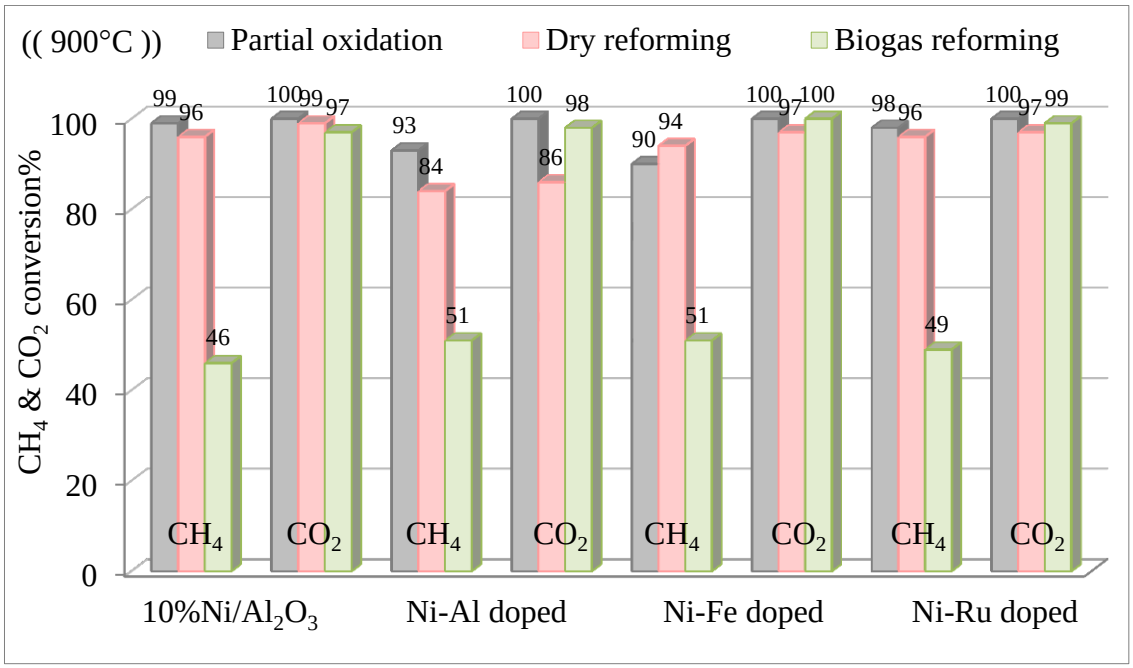

Figure 7.6: Comparison of the average CH_4 and oxidants conversions for BIO, DRM and POX at different temperatures (700 °C, 800 °C and 900 °C) for 20 h of reforming reaction.

Limited water production was observed at high temperature especially with a CH_4- rich environment. Figure 7.7 shows that the formation of water declines with increasing temperature for both biogas and dry reforming due to the decreased occurrence of the RWGS reaction and methane decomposition is becoming more favourable for biogas reforming. On increasing the temperature to 900 °C, the exothermic Boudouard reaction becomes less favourable and leads to stabilise the H_2 /CO molar ratio.

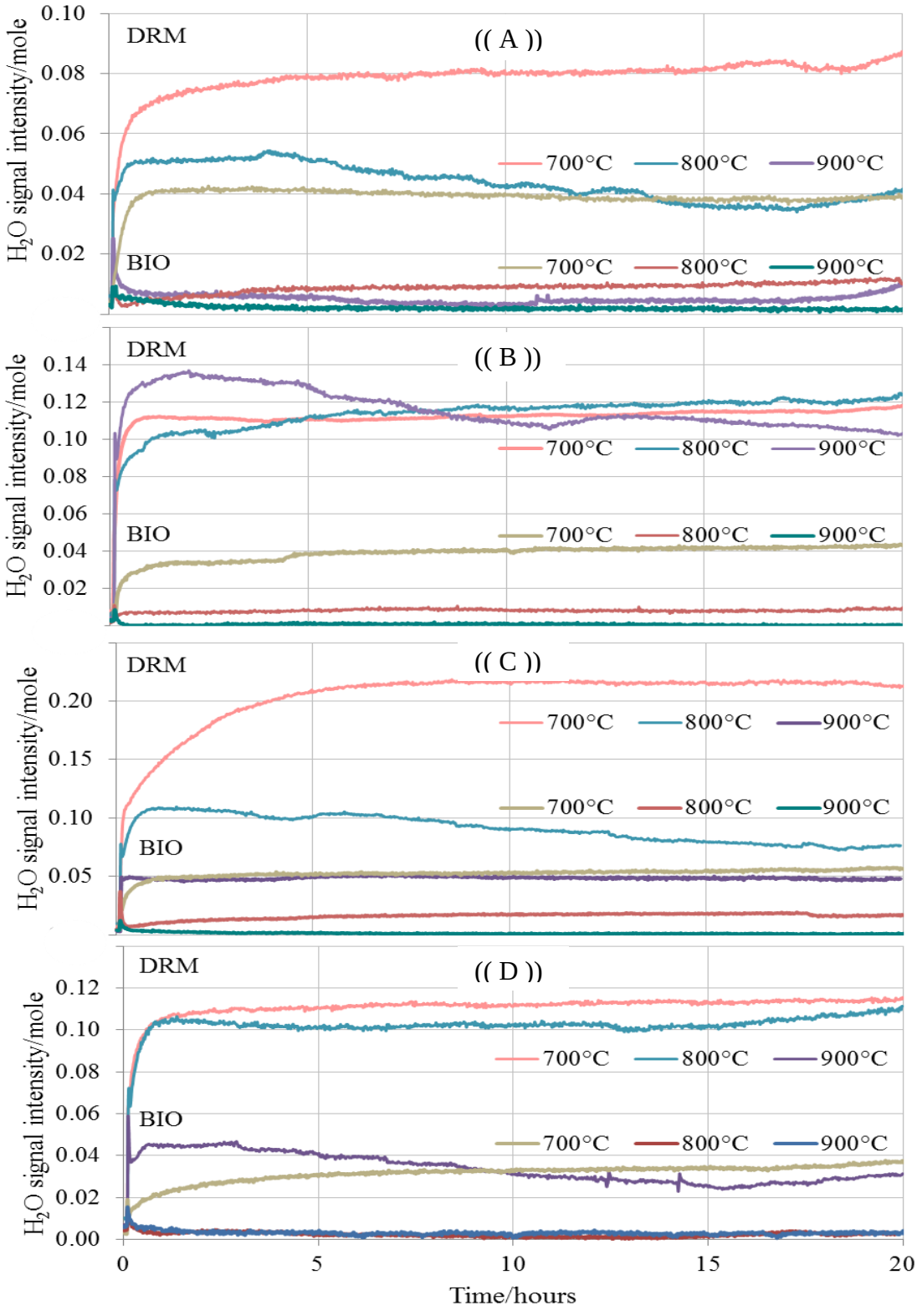

Figure 7.7: Comparison of H_2O production in reactions of 2:1 CH_4 /CO_2 (BIO) and 1:1 CH_4 /CO_2 (DRM) at 700 °C, 800 °C and 900 °C during 20 h over (A) 10% Ni/Al_2O_3, (B) Ni-Al doped $SrZrO_3$, (C) Ni-Fe doped $SrZrO_3$ and (D) Ni-Ru doped $SrZrO_3$ catalysts.

Table 7.1 shows the variation in synthesis gas production and H_2 /CO molar ratio with temperature for the three reforming processes. In the dry reforming reaction, there is more CO_2 to react with hydrogen than in the biogas reforming (CH_4- rich). Therefore, the ratio of H_2 /CO was less than that observed for the biogas reforming at the same reaction temperature on the same catalyst. This was is due to the greater occurrence of the RWGS reaction, which causes higher levels of water production as shown in figure 7.7. However, lowering of the H_2 /CO ratio was also as a result of decreasing methane decomposition, which caused less hydrogen production. Moreover, with more CO_2 available the methane conversion increases as well, so dry reforming has a greater value than that for biogas reforming.

The same trend was observed with the three reforming methods in terms of methane conversion that increased with increasing temperature as the RWGS reaction was more prevalent at low temperatures and declined at high temperatures. The H_2 /CO molar ratio produced from the results of the H_2 and the CO production depends on the input gas composition, the type of oxidant and reforming temperature. For example in the case of dry reforming it has a lower value of H_2 /CO than in biogas reforming. The highest value was in partial oxidation of methane due to the higher yield of H_2.

Relative to all the catalyst and examined temperatures, the conversions of CO_2 were higher than those of CH_4 mostly at low than 800 °C because of the existence of the RWGS side reaction. The dissociation of CH_4 is also significantly enhanced and this coincides with reforming temperature, which causes a high H_2 production and enhanced the formation of coke. The decrease observed in water production at high temperatures under CH_4-rich content can be attributed to there being an inadequate level of CO_2 for the reverse water

gas shift reaction. However, under CO_2- rich content, there was enough CO_2 available for both reforming and the RWGS reaction.

Based on overall hydrogen gas production and methane conversion, Ni-Al doped $SrZrO_3$ achieved the highest activity for biogas reforming under reaction conditions in terms of methane conversion, H_2 yield as well as an acceptable H_2 /CO ratio followed by Ni-Ru doped and Ni/Al_2O_3. In dry reforming, both Ni-Ru doped $SrZrO_3$ and the conventional Ni/Al_2O_3 catalysts showed the highest catalytic activity at 800 °C and 900 °C. At the same temperature for partial oxidation of methane, the best catalytic performance was for nickel supported alumina followed by the Ni-Ru doped perovskite.

High-temperature operation requires the use of special catalytic materials that have high resistance to agglomeration or sintering for achieving the desired product. By operating in methane-rich environments (2:1CH_4 /CO_2 ratio), carbon deposition over the catalyst is strongly enhanced because of the presence a substantial fraction (50%) of methane still remaining unconverted and thereby decomposed into H_2 and solid carbon. Therefore, a possible solution lies in the incorporation of transition or noble metals (Ru) within the catalyst as active metals for carbon resistance [2].

The numbers of moles of H_2 produced depends on the CO_2 /CH_4 ratio; these are commonly decreased with increasing CO_2 /CH_4 ratio from 0.5 to 1 for all temperature ranges and attaining a maximum at 900 °C due to the fact that the main reaction is enhanced and suppresses methane decomposition to produce H_2. Moreover, this is expected since the side reverse water gas shift reaction is increased due to the CO_2 supply. The CO production is higher than the H_2 when the CO_2 /CH_4 ratio is in unity and thus the carbon formation is expected to decrease [3].

Table 7.1: Average H_2, CO and H_2 /CO ratios production for dry reforming, biogas reforming and partial oxidation of methane at 700 °C, 800 °C and 900 °C for 20 h of reaction.

Dry reforming reaction results									
Samples	700 °C			800 °C			900 °C		
	H_2%	CO%	H_2/CO	H_2%	CO%	H_2/CO	H_2%	CO%	H_2/CO
10% Ni/Al_2O_3	74	79	0.93	88	96	0.91	91	92	0.98
Ni-Al doped $SrZrO_3$	64	68	0.93	75	84	0.88	77	88	0.87
Ni-Fe doped $SrZrO_3$	23	36	0.62	76	81	0.94	81	87	0.92
Ni-Ru doped $SrZrO_3$	61	72	0.84	88	92	0.95	96	94	1.01
Biogas reforming reaction results									
Samples	700 °C			800 °C			900 °C		
	H_2%	CO%	H_2/CO	H_2%	CO%	H_2/CO	H_2%	CO%	H_2/CO
10% Ni/Al_2O_3	71	72	0.98	89	91	0.97	93	91	1.01
Ni-Al doped $SrZrO_3$	74	79	0.94	97	93	1.04	99	95	1.03
Ni-Fe doped $SrZrO_3$	61	75	0.81	88	93	0.94	96	92	1.04
Ni-Ru doped $SrZrO_3$	70	77	0.91	94	95	0.98	97	98	0.98
Partial oxidation of methane reaction results									
Samples	700 °C			800 °C			900 °C		
	H_2%	CO%	H_2/CO	H_2%	CO%	H_2/CO	H_2%	CO%	H_2/CO
10% Ni/Al_2O_3	68	31	2.2	92	47	1.98	91	48	1.9
Ni-Al doped $SrZrO_3$	66	36	1.82	80	44	1.8	87	49	1.76
Ni-Fe doped $SrZrO_3$	1	1	1.1	66	31	2.15	89	39	2.3
Ni-Ru doped $SrZrO_3$	77	40	1.89	88	45	1.95	85	39	2.2

As can be seen from the table, the increase of the H_2 /CO ratio under dry reforming reactions was not as great as that seen under CH_4- rich conditions at the same temperature and upon the same catalyst due to the increased concentration of CO_2 that reacts with methane at high temperatures and prohibits extreme methane decomposition, resulting in

the H_2 /CO ratio being smaller under dry reforming reaction conditions and significantly lowering the level of deposited carbon compared with methane-rich environments.

By using the Ni-Ru doped catalyst at 900 °C, the average conversion of CH_4 and CO_2 gases for the biogas reforming was 49 and 99% respectively, while the conversion of the gases for the dry reforming was 96 and 97% respectively. This catalyst also has a higher selectivity towards H_2 and CO production compared to other catalysts in this study that could be due to the better resistance to deactivation and this is consistent with what has been proposed previously, that substituting Ru within the structure of the catalyst limits deactivation due to having reactive lattice oxygen which helps in the oxidation of the surface carbon during the reforming reaction [4].

The performance of catalysts during the reforming of methane is affected by the type of active metal that is incorporated within the perovskite structure. Regarding the type of active doping metal Ni-Ru exhibited very good performances for the three different methane reforming processes (biogas reforming, dry reforming and partial oxidation of methane), followed by Ni-Al doped $SrZrO_3$ and Ni-Fe doped $SrZrO_3$ respectively with varying activity.

7.2 Comparison of carbon deposition under different conditions

Several strategies have been studied to determine tolerance to carbon deposition on the catalyst used in reforming reactions involving hydrocarbons. The lowest level of carbon deposition was observed for partial oxidation of methane (exothermic reaction), which could be due to the presence of oxygen in the reaction that is directly involved in carbon gasification on the catalyst surface. The formation of carbon is almost guaranteed as the

thermal decomposition of methane occurs at higher temperatures with methane-rich content for a 2:1 CH_4 /CO_2 mixture (endothermic reaction). Therefore, the highest amount of carbon formation was observed for biogas reforming than other reforming processes.

The propensity towards coke formation can be estimated by the ratio of O /C and H /C in the feed gas which decreases with increasing the O /C and H /C ratios. These ratios will be in the dry reforming and partial oxidation of methane H /C = 2 and H /C = 4 respectively with O /C = 1. It is clear that dry reforming of methane has a higher affinity to coke compared to partial oxidation of methane [5].

Carbon formed should be consumed by the reverse Boudouard reaction to reduce the amount of carbon present by using dry reforming reaction for a 1:1 CH_4 /CO_2 mixture. Otherwise, there will be huge carbon deposition that would lead to catalyst deactivation. Moreover, during the DRM reaction the accumulation of carbon is more favourable at low temperatures (700 °C) because the occurrence of the RWGS reaction leads to an increase in CO concentration in the product stream. This is improving Boudouard reaction. At high temperatures, more than 800 °C, The decrease of the RWGS partly caused the concentration of CO_2 to increase thus the presence of abundant CO_2 can easily oxidize carbon deposited during the DRM reaction by reverse Boudouard reaction.

By comparing the results in figure 7.8, it can be seen that in the presence of excess methane with a feed molar ratio of $2CH_4$ /$1CO_2$ the catalysts showed a similar behaviour at 800 °C and 900 °C, suggest a favouring of carbon deposition. While in the case of dry reforming with a feed molar ratio ($1CH_4$ /$1CO_2$), a larger amount of graphitic carbon is produced at 700 °C more than at 800 °C and 900 °C, which is indicative that the reverse

Boudouard reaction appears to be dominate, causing a reduction in carbon deposition with temperature.

The presence of O_2 in the feedstock in the case of methane partial oxidation had a beneficial effect on the rate of coke accumulation on the catalysts, suggesting that carbon species can be oxidised to CO. Importantly the amount of coke formed on the co-doped perovskites was shown to remain very low and not exceeding 0.12 g regardless of the reforming type.

Figure 7.8 shows that there is a significant trend of carbon formation at different temperatures over the four catalysts with the following order:

Biogas reforming > dry reforming > partial oxidation of methane

The presence of oxidizing agents such as O_2 or abundant CO_2 in the reaction mixture can minimize the surface coke build-up in reforming of methane, with the oxidant leading to the oxidation of carbon species as has been reported previously in the literature [6].

Although the level of coke accumulation over the four catalysts is more complex with no obvious trend seen for the three reforming methods. The perovskite materials show the same trend as observed for the nickel supported material, with carbon deposition decreasing with increasing temperature in dry reforming, in contrary to that observed in biogas reforming, resulting from methane decomposition at higher reaction temperatures, and a small amount of carbon as a result of low reforming activity at the lower reforming temperatures.

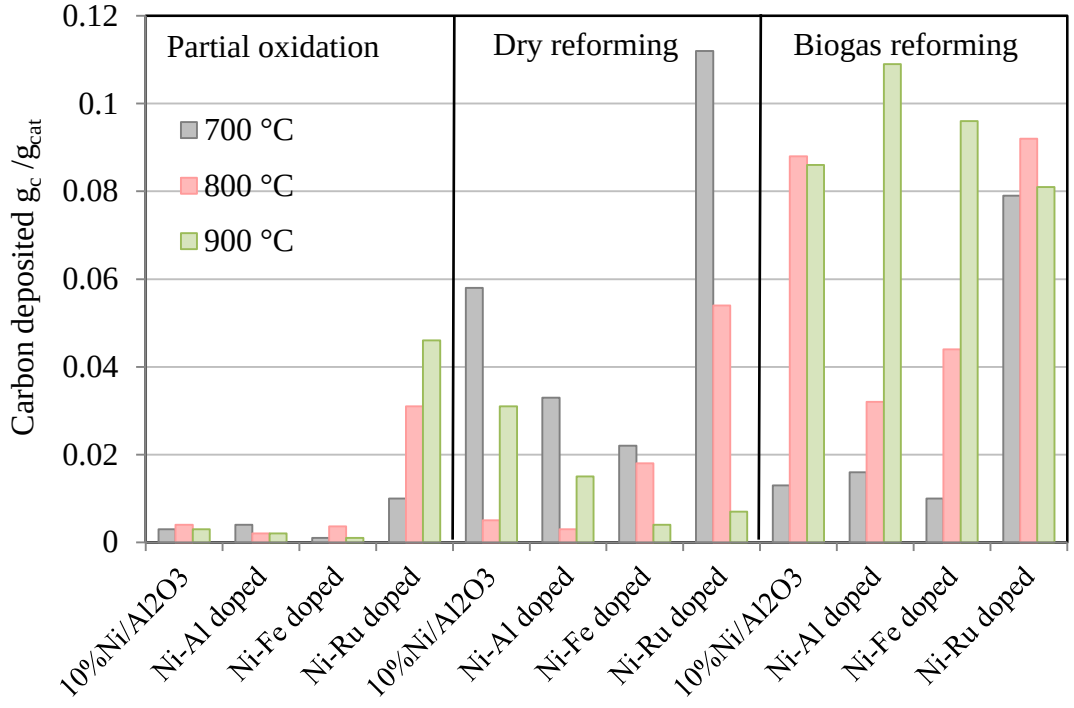

Figure 7.8: Effect of temperature and reforming reaction type on carbon deposition during reforming of methane reaction for 20 hours in gram of carbon per gram of catalysts.

The amount of carbon decreased steadily with reaction temperatures from 700 °C to 900 °C although there was a significant increase in methane conversion over Ni-Fe doped and Ni-Ru doped perovskite in the dry reforming reaction. A decrease in carbon accumulation with rising reaction temperature is characteristic of the endothermic reverse Boudouard reaction, which becomes more advantageous at elevated temperatures [7]. Overall, the Ni-Fe doped $SrZrO_3$ perovskite exhibited lower carbon formation than other catalysts during 20 h of reaction in partial oxidation and dry reforming at 900 °C. For biogas reforming it also exhibited low carbon formation at 700 °C.

The occurrence of the CH_4 decomposition reaction leads to generate reactive carbon at high temperature, and that can easily be oxidized in the presence of CO_2 during the dry reforming reaction. Therefore, lower levels of carbon were observed using the ratio of 1:1

CH_4 /CO_2 than 2:1. Deleterious solid carbon formation was significant at 900 °C and the conversion of CO_2 is limited for biogas reforming.

Although, the amount of carbon deposited on Ni-Ru doped was more than that deposited on the Ni/ supported alumina and other doped catalysts. The particular importance in carbon deposition results is that the amount of carbon accumulated on each catalyst was less than that observed when the inlet feed gas ratio was 1:1CH_4 /CO_2. This is due to the fact that, when a mole of methane reacts with a mole of CO_2 in the feed gases, the formation of carbon is thermodynamically limited.

The highest levels of carbon deposition were on Ni-Ru doped $SrZrO_3$ catalyst and figure 7.9 shows the TPO profiles following biogas reforming (2:1CH_4 /CO_2), and dry reforming (1:1CH_4 /CO_2) reactions at 700 °C, 800 °C, and 900 °C which reveal that the increased CO_2 levels changed only the amount of carbon formed and not the nature of the carbonaceous species. On comparison of the TPO profiles for the two types of reforming in this figure, there are three CO_2 peaks at approximately the same temperatures between 600 °C and 700 °C, suggesting the nature of the carbon deposited in each reforming reaction was similar. Moreover, it can be said that the coke formed was of a similar sort in terms of that it did not seem to act as a catalytic poison or cause any deactivation.

For dry reforming carbon deposition is not thermodynamically expected due to the presence of sufficient oxygen provided from the CO_2 to oxidize the carbon produced. However at biogas reforming (CH_4- rich), carbon formation can occur due to the presence of extra methane in reaction ambient. There are two temperature regimes in which carbon agglomeration likely occurs, a high-temperature range corresponds to the temperature at

which methane decomposition is favoured, the low-temperature range which corresponds to Boudouard and CO reduction reactions are taking place [8].

The lack of methane dissociation under dry reforming environments also caused significantly lower levels of solid carbon formation as determined by the post reaction oxidation and compared with the biogas results.

At high reaction temperatures, the high level of CO_2 concentration under dry reforming conditions leads to an increase in methane conversions, occurrence of RWGS and reverse Boudouard reaction. Carbon deposition was similar to that formed by partial oxidation and biogas reforming and did not cause any significant deactivation. Lower amounts were deposited with partial oxidation compared with dry and biogas reforming, particularly at reaction temperatures above 800 °C.

From these results it can be concluded that during biogas and dry reforming, the highest level of carbon was formed, while during partial oxidation of methane reforming no or very little carbonaceous deposits were observed. It is clear that the amount of carbon produced is limited by the type and amount of feed oxidant in addition to reaction temperature.

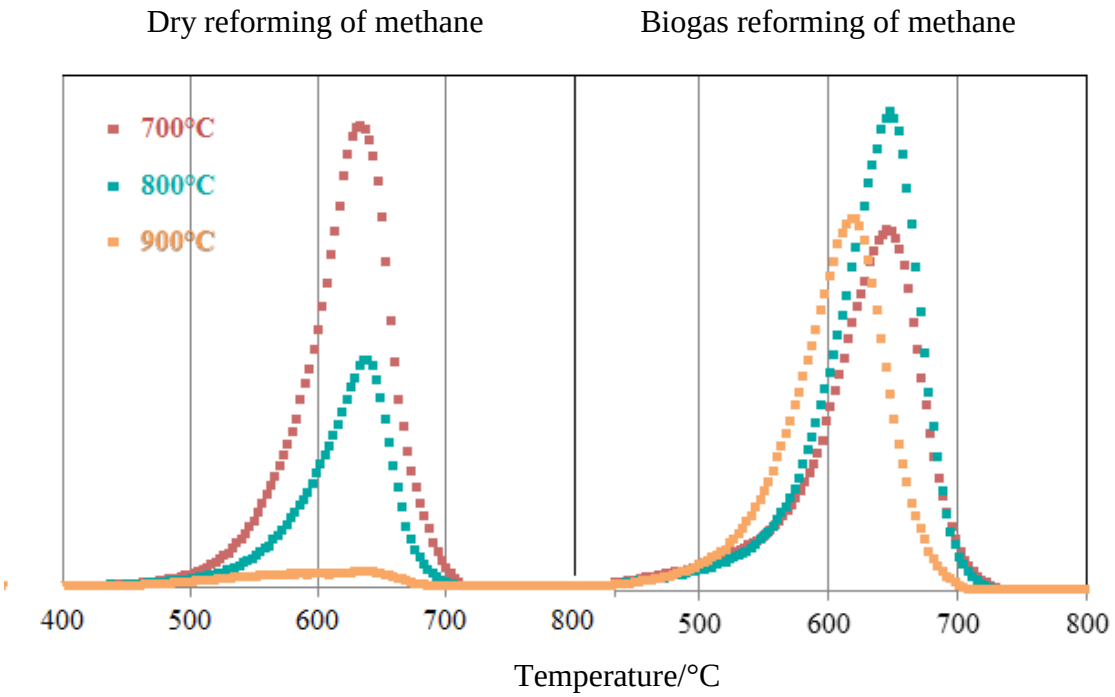

Figure 7.9: Comparison of TPO profiles following reactions of dry and biogas reforming over Ni-Ru doped $SrZrO_3$ catalyst for 20 hours of reaction at three different temperatures.

7.3 Stability Investigation

The comparison between the XRD analysis of all prepared co-doped perovskites and the conventional 10% Ni/Al_2O_3 catalyst before and after the experimental methane reforming tests are reported in figures (7.10-7.13). These patterns show no significant differences between the spent and the fresh catalyst, indicating that the co-doped perovskite structure is stable under the reaction conditions employed (900 $^{\circ}$C for 20 h). Whilst the conventional Ni/Al_2O_3 catalyst shows some signs of particle sintering that indicated by the peaks at 36.5° and 62.4° for NiO crystallites became sharper and reduced crystallinity. Preservation of the perovskite structure after such a reaction is a good indication that using the catalyst for multiple reaction cycles is an option to be considered in the future.

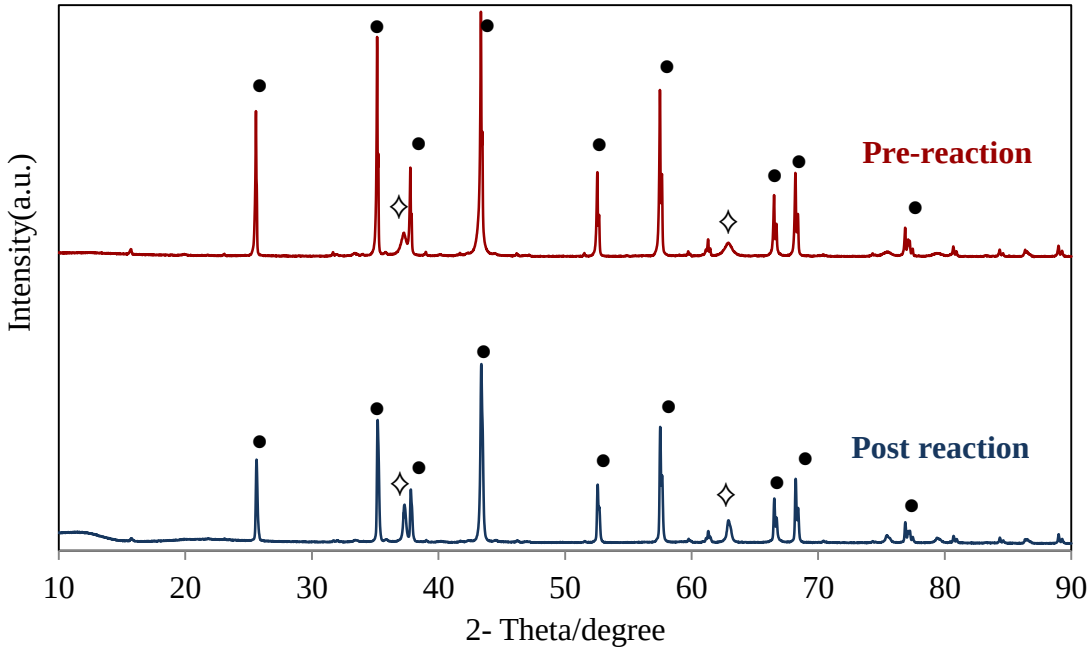

Figure 7.10: XRD pattern of 10% Ni/Al_2O_3 catalyst before and after reforming reaction. (✧) = NiO, (●) = Al_2O_3.

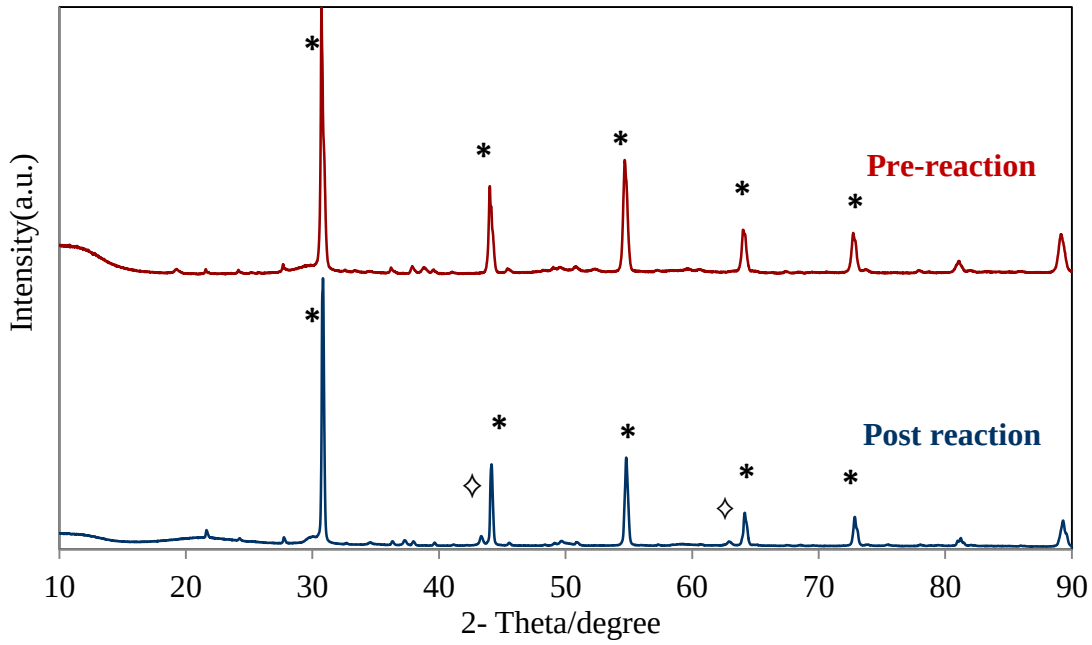

Figure 7.11: XRD pattern of Ni-Al doped $SrZrO_3$ before and after reforming reaction. (*) = $SrZrO_3$, (✧) = NiO.

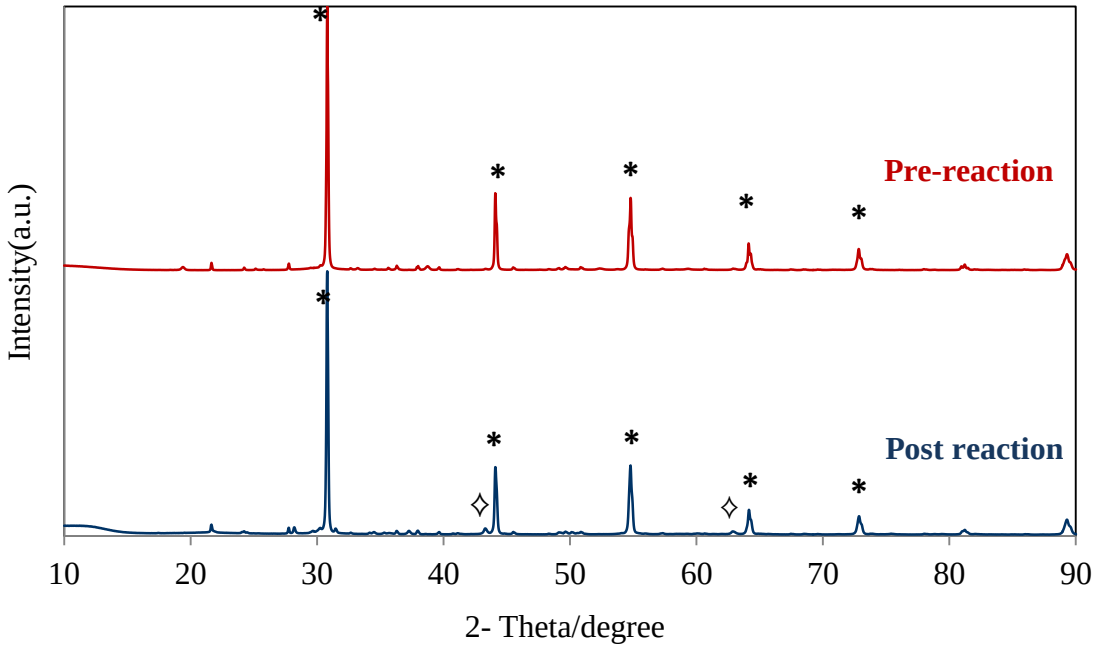

Figure 7.12: XRD pattern of Ni-Fe doped $SrZrO_3$ before and after reforming reaction. (*) = $SrZrO_3$, (◊) = NiO.

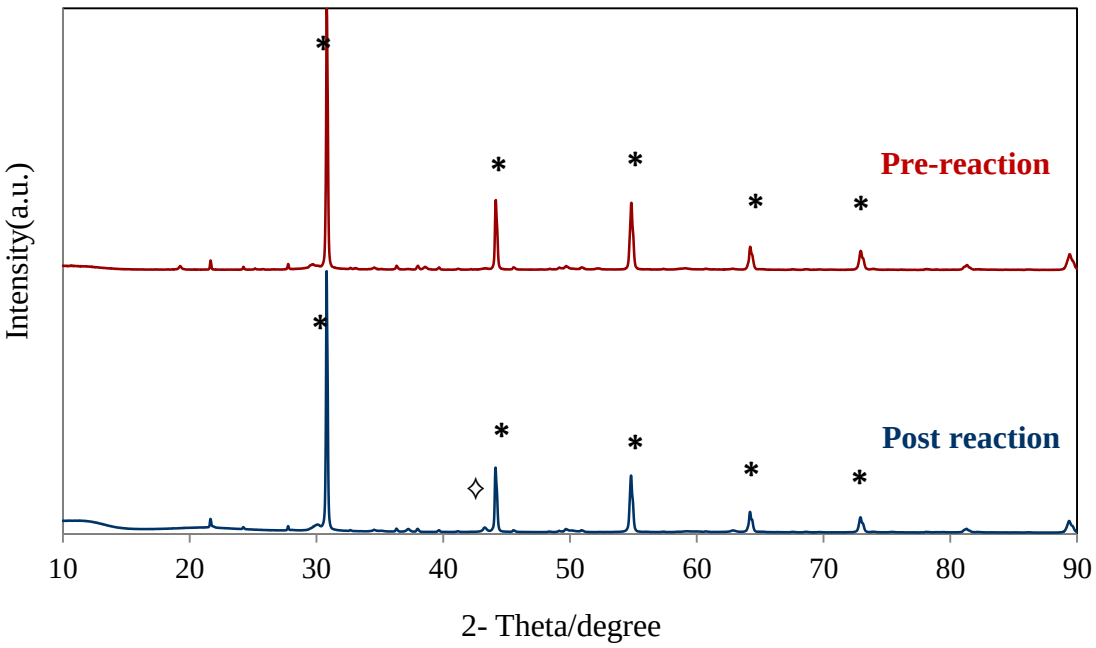

Figure 7.13: XRD pattern of Ni-Ru doped $SrZrO_3$ before and after reforming reaction. (*) = $SrZrO_3$, (◊) = NiO.

The perovskite structure for all of the doped catalysts did not show any change in the main peaks positions, with peaks corresponding to a $SrZrO_3$ type material and very small peaks corresponding to NiO at $2\theta = 42.3^{\circ}$ and 61.8° were observed after 20 h of the reaction at 900 °C. The results imply that the catalytic activity is excellent and fairly stable during the ageing tests for all samples prepared. However, that there is a slight change in catalyst morphology as shown in figures (7.14-7.17).

The morphologies and surface compositions of the samples were characterized by SEM and HR-SEM for all the catalysts before and after the reforming test. For the Ni-Al doped $SrZrO_3$ and Ni-Ru doped $SrZrO_3$ it is observed that there is a slight growth of perovskite grains through agglomeration of the particles during the ageing process. SEM images for Ni-Fe doped $SrZrO_3$ were hard to distinguish from each other due to their similar morphology and no signs of agglomeration or sintering of the spent particles, indicating a high degree of thermal resistance of this catalyst. Whereas, the spent of nickel supported catalyst shows less uniform and larger particle size with a less defined morphology than the fresh catalyst.

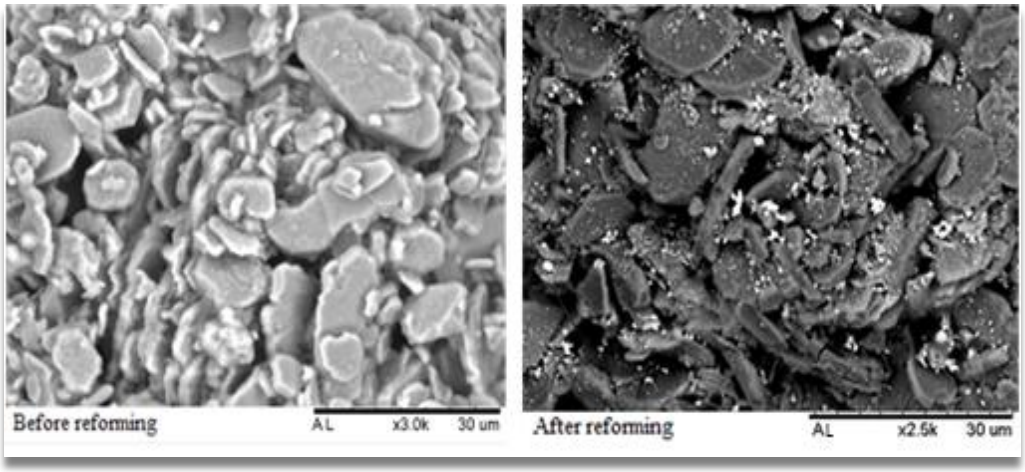

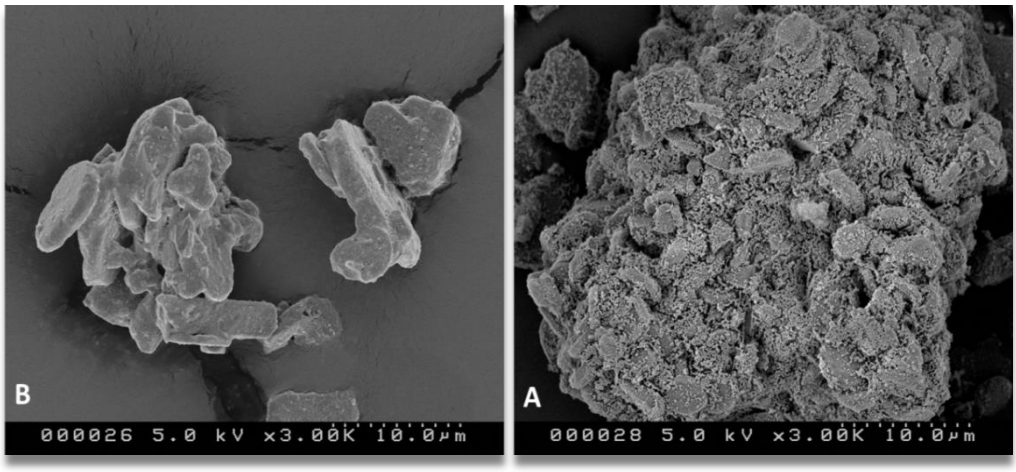

Figure 7.14: SEM and HR-SEM images of standard catalyst 10% Ni/Al_2O_3 (B) before and (A) after reformation reactions.

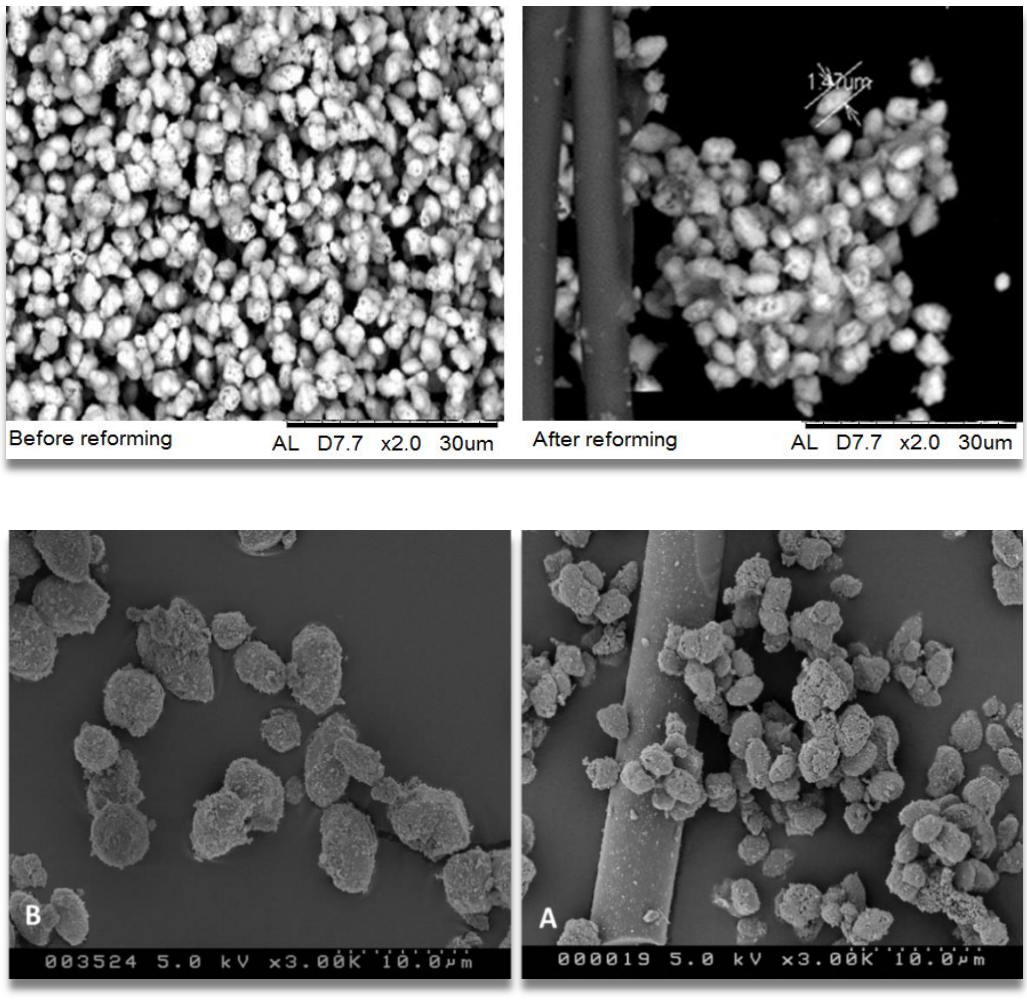

Figure 7.15: SEM and HR-SEM images of Ni-Fe doped $SrZrO_3$ perovskite (B) before and (A) after reformation reactions.

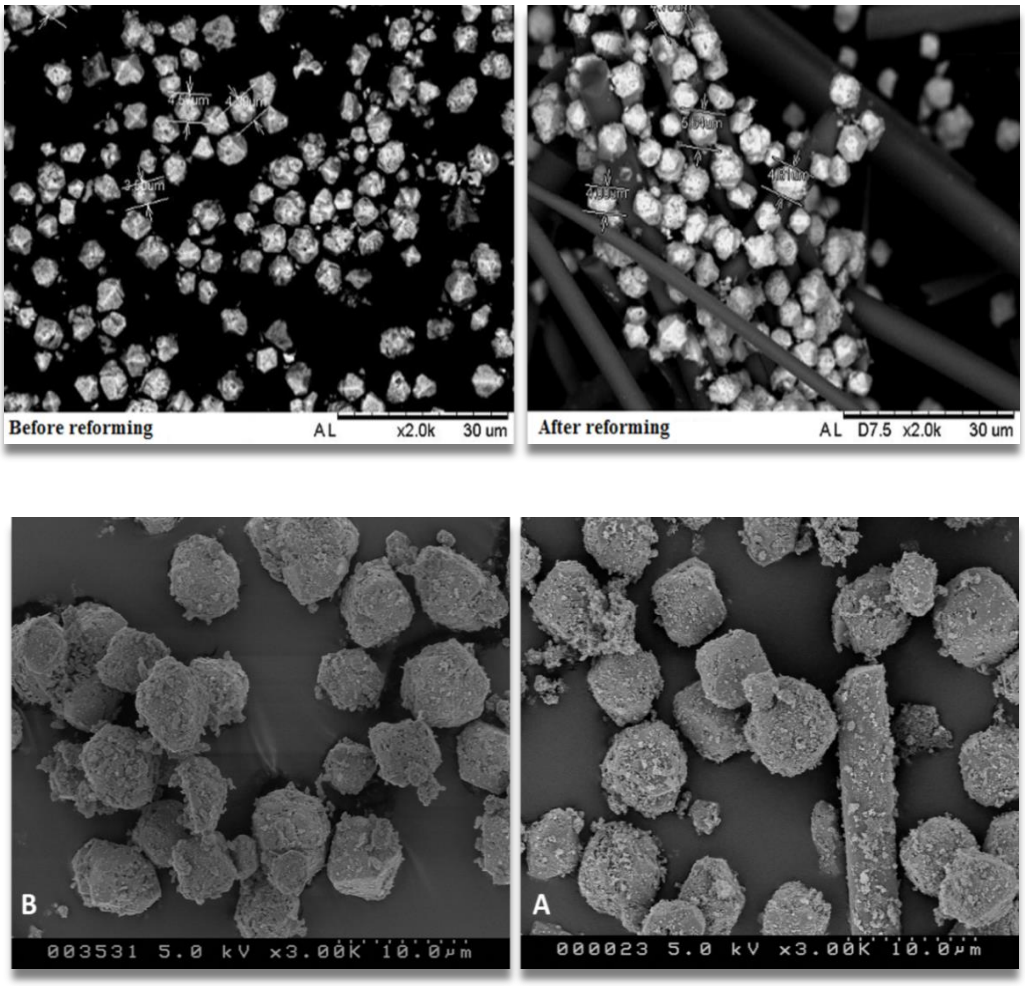

Figure 7.16: SEM and HR-SEM images of Ni-Al doped $SrZrO_3$ perovskite (B) before and (A) after reformation reactions.

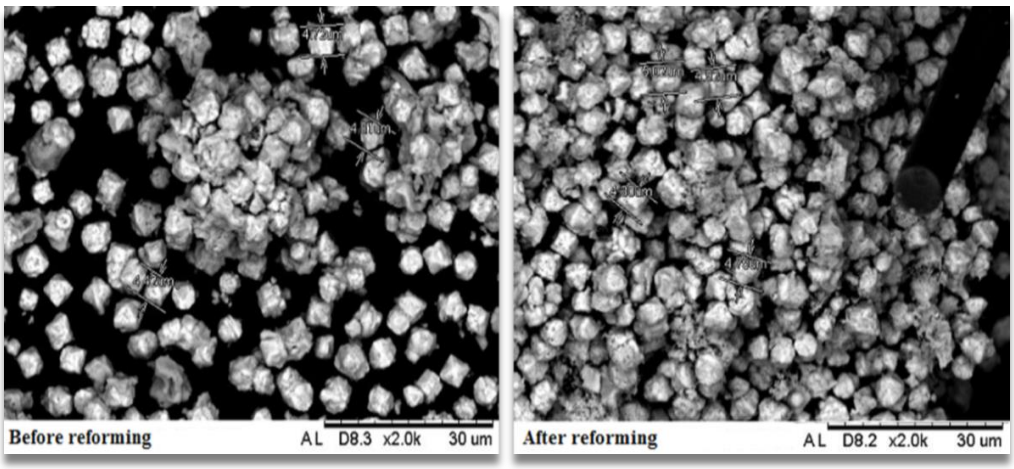

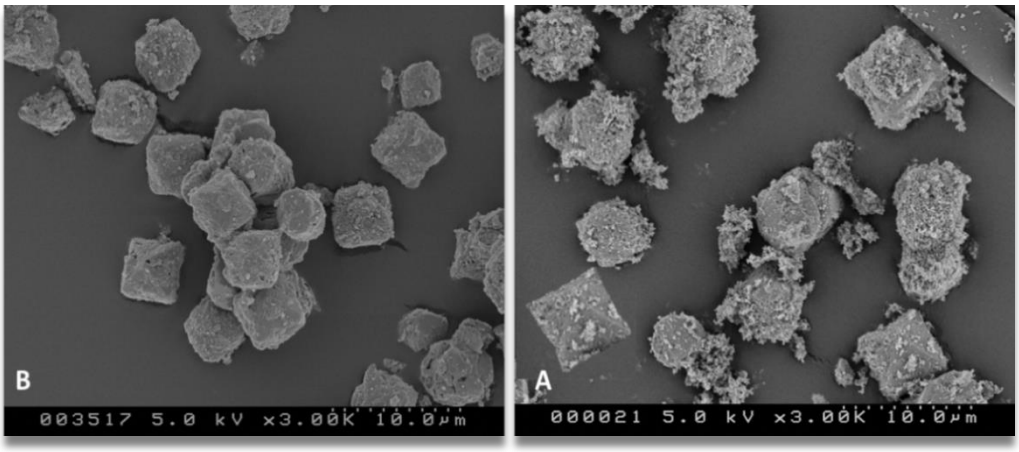

Figure 7.17: SEM and HR-SEM images of Ni-Ru doped $SrZrO_3$ perovskite (B) before and (A) after reformation reactions.

7.4 Summary of findings

The potential of using renewable energy has been growing fast recently, mainly due to the serious problems associated with fossil fuel usage, such as their depletion in the near future and effects on global warming. Although reforming reactions are capable of converting the natural components of biogas into usable products, it currently remains a nonviable option over large scales, as an effective catalyst has not been developed which shows a high enough activity and durability over long period time for economic and practical purposes. This thesis investigated the utility of several new co-doped materials for catalysing dry, and biogas reforming and partial oxidation of methane reactions. The following conclusions were drawn based on the results obtained from these investigations:

7.5 Conclusion

The lowest methane conversion was observed for biogas reforming due to insufficient CO_2 to react with all methane that presence in the reaction environments and that lead to producing the large level of carbon via decomposition of the excessive methane. At high reaction temperatures, methane conversion of approximately 50% was observed for biogas reforming compared with about 98% for dry reforming and partial oxidation. CO_2 rich environments enhanced reverse Boudouard reaction and thereby lowered the carbon accumulation significantly.

The form of carbon with dry reforming was similar to that produced by biogas reforming and did not cause any significant deactivation during 20 hours of reaction for all catalysts. This study has shown that the CH_4 /CO_2 ratio in dry and biogas reforming significantly influences synthesis gas production, reactant conversion and carbon accumulation on nickel catalysts whether the Ni be supported on the surface or incorporated within the perovskite structure. Partial oxidation of methane produces the highest H_2 /CO ratio and the least carbon deposition.

The hydrothermally synthesised perovskite materials showed excellent performance for the conversion of model biogas to syngas compared to the nickel supported material. The Ni-M co-doped containing materials exhibited high catalytic activity, which was maintained throughout 20 hours of reforming reaction. According to dry reforming stoichiometry, the H_2 /CO ratio is expected to be 1 in the product. However, RWGS side reactions occur and cause some decrease in H_2 and increase in CO yield, which is clearly observed in the results presented in section (5.3.2).

The co-doped Ni-Al catalyst showed the highest activity and stability of the modified perovskite catalysts in terms of feed gas conversion and synthesis gas production, followed by Ni-Ru and Ni-Fe for biogas reforming and partial oxidation of methane. On the other hand, the addition of co-doped Ni-Al resulted in a slight decrease in activity for the modified perovskite catalyst for dry reforming.

The relative ratio of CH_4 and CO_2 and reaction temperature had a significant effect on the reactant conversion, synthesis gas yields, H_2 /CO ratio, deleterious carbon formation and the behaviour of the RWGS reaction. Biogas with higher methane content had the lowest methane conversion and the highest carbon deposition due to the presence of excess methane causing methane decomposition that was prevalent at high temperatures. Despite the larger amounts deposited under methane-rich conditions, these did not deactivate the catalyst under these test conditions and this suggests that the carbon deposition with time appeared to be inert and negligible.

The greater occurrence of the RWGS reaction with dry reforming rather than biogas reforming caused greater levels of water production due to the presence of a higher concentration of CO_2 to react with H_2 and this caused a lower H_2 /CO ratio due to decreased methane decomposition.

In case of biogas reforming, the higher reactant conversion is observed for the doped perovskite samples than Ni supported alumina under reaction conditions, indicating that they have greater reforming activity. Overall reforming reaction applications can be enhanced by carrying out at high temperatures between 800 °C and 900 °C to obtain an almost complete conversion of methane. Higher temperatures and significant involvement of the reverse water gas shift reaction accounted for the low values of H_2 /CO ratio with

dry reforming not only leading to higher methane conversion rates but also lower deleterious carbon formation.

All catalysts in this study proved to have superior coking resistance, high stability and activity especially for higher temperature applications (> 800 °C). The XRD profiles of the fresh and spent catalysts show that co-doped perovskites maintained their crystalline structure after exposure to reforming conditions at temperatures of 900 °C for long time.

Using appropriate promoters and noble metals has helped in maintaining a balance between deposition and gasification of carbon that can lead to enhanced resistance to deactivation and thus results in an increase in the longevity of the catalyst with good performance. A variety of metals have been employed for the methane transformation using three types of reforming reaction, and it is confirmed that Ru-Ni containing catalyst is the most efficient to catalyse methane conversion to the desired synthesis gas product for all types of reforming reactions compared with other co-doped perovskites and Ni/Al_2O_3. While Fe-Ni, Al-Ni containing catalysts are efficient to convert methane to high concentration of hydrogen in biogas reforming more than in dry reforming and partial oxidation.

Generally, a catalyst with a larger surface area is favourable for better performance. However, taking into account of the fact that although Ni-Fe doped $SrZrO_3$ possesses the highest surface area, it does not have the highest activity and durability among all the catalysts with different reforming reactions, it is thus concluded that surface area is not the determining factor for the performance of the catalysts for reforming of methane in this study.

Perovskite catalysts show good promise as catalyst, since they showed high activity and stability for reforming of methane and produced low amounts of coke. Co-doped perovskite catalysts had nearly similar levels of activity which were close to the equilibrium levels, and showed no deactivation and the structure is maintained throughout the tests that indicated by XRD of fresh and spent catalysts.

It also confirmed that partial oxidation of CH_4 produced lower amounts of carbon than other methods. The higher tendency towards carbon deposition was observed in the lower ratio of O /C and H /C as expected. Considering the aforementioned ratios, biogas reforming of methane has a higher propensity towards carbon deposition compared to partial oxidation and dry reforming.

Furthermore, the H_2 /CO molar ratio can also be adjusted by controlling the feeding of gases, with the increase of CO_2 concentration as in dry reforming, the H_2 /CO ratio declines gradually and the carbon deposition also declines sequentially due to the enhancement of side reactions such as RWGS and reverse Boudouard reaction.

7.6 Recommendations for future studies

This work has shown that the co-doped perovskite catalysts are suitable materials for the formation of synthesis gas by reformation of methane. Further investigation is needed by carrying out reforming reactions for longer times-on-stream to evaluate the long-term stability of the perovskite catalyst under reaction conditions.

During biogas and dry reforming, the highest levels of carbon were formed, whilst during partial oxidation of methane reforming no or very little carbonaceous deposits were

observed. It is clear that the amount of carbon produced is limited by the type and amount of feed oxidant. These perovskite catalysts should be used as potential candidates for other hydrocarbon reforming processes such as steam reforming or auto thermal reforming or mixed reforming of biogas that uses an additional oxidant (O_2 or H_2O) in order to offset for the lack of oxidant usually found in biogas to control the ratio of the product H_2 /CO ratio as well as to reduce operating cost and thereby overcoming the practical challenges of employing biogas.

Investigation other perovskite materials that can be synthesised by a combination of various ions and possible concentration of ions to incorporate within the lattice structure to find the best additive that gives the highest syngas production and carbon resistance along with the cheapest price. This study has observed that doping different metals within the perovskite increases the selectivity to a particular reforming method. For example, Ni-Al doped $SrZrO_3$ has excellent performance under biogas reforming conditions, while Ni-Ru doped $SrZrO_3$ has better performance under dry reforming conditions.

In spite of the fact that the perovskite material preparation methodology is already well defined, a special concern is also carried out to the investigation of catalysts design and synthesis to gain the exact crystalline structure and morphology of the produced catalyst without any impurity.

Natural biogas fuel contains sulphur impurities, which often leads to a loss of reforming activity over time, an investigation should be held to study the effect of the addition of hydrogen sulphide on the resistance of perovskite materials to sulphur poisoning.

7.7 References

[1] S. Gaur, Master Thesis, Louisiana State University, 2011.

[2] P. Djinović, I. G. O. Črnivec, B. Erjavec, and A. Pintar, *Appl. Catal. B: Environ*., 2012, **125**, 259-270.

[3] A. Serrano-Lotina, and L. Daza, *Int. J. Hydro. Energy*, 2014, **39**, 4089-4094.

[4] D. Pakhare and J. Spivey, *Chem. Soc. Rev*., 2014, **43**, 7813-7837.

[5] M. Usman, W.M.A.W. Daud and H. F. Abbas, *Renew. Sustain. Energy Reviews*, 2015, **45**, 710-744.

[6] N. Kumar, Z. Wang, S. Kanitkar and J. Spivey, *Appl. Petrochem. Res*., 2016, **6**, 201–207.

[7] C. J. Laycock, J. Z. Staniforth and M. Ormerod, *Dalton Trans*., 2011, **40**, 5494 –5504.

[8] M. S. Fan, A. Z. Abdullah, and S. Bhatia, *ChemCatChem.*, 2009, **1**, 192 – 208.

The Appendix

8.1 Masses selected for detection on QMS

The quadruple mass spectrometer technique provides an on-line spectrum page that contains masses for each gas in different colour to allow the user to know what is passing through the system at any one time. So, the reaction products can be seen at any particular time or temperature and can produce product composition profiles along temperature programs or time periods.

Table 1: Appropriate gas Masses selected for detection on QMS

Mass	Appropriate gases
2	Hydrogen
4	Helium
15	Methane
18	Water
28	Carbon monoxide
32	Oxygen
44	Carbon dioxide

8.2 Sample of Gas Relative Ionisation

Table 2: The sensitivity for various mass fragments of gases is calculated by method shown in section 2.3.2.

(H_2) Hydrogen	1.00
(CH_4) Methane	2.00
(H_2O) Water	1.61
(CO) Carbon Monoxide	1.80
(O_2) Oxygen	1.00
(CO_2) Carbon Dioxide	1.40
(I) Helium	0.29

8.3 Calibration of Mass Flow Controllers

Calibration was performed for each mass flow used to attain the desired flow rate of gases on the mass flow controller. The gas diverted away from the reactor to a bubble flow meter and then the time for a bubble to move a set distance on the bubble flow meter was recorded. For example, the bubble moves from 0 ml to 10 ml during 60 seconds that means the flow rate is 10 ml min^{-1} and that was set on the mass flow controller.

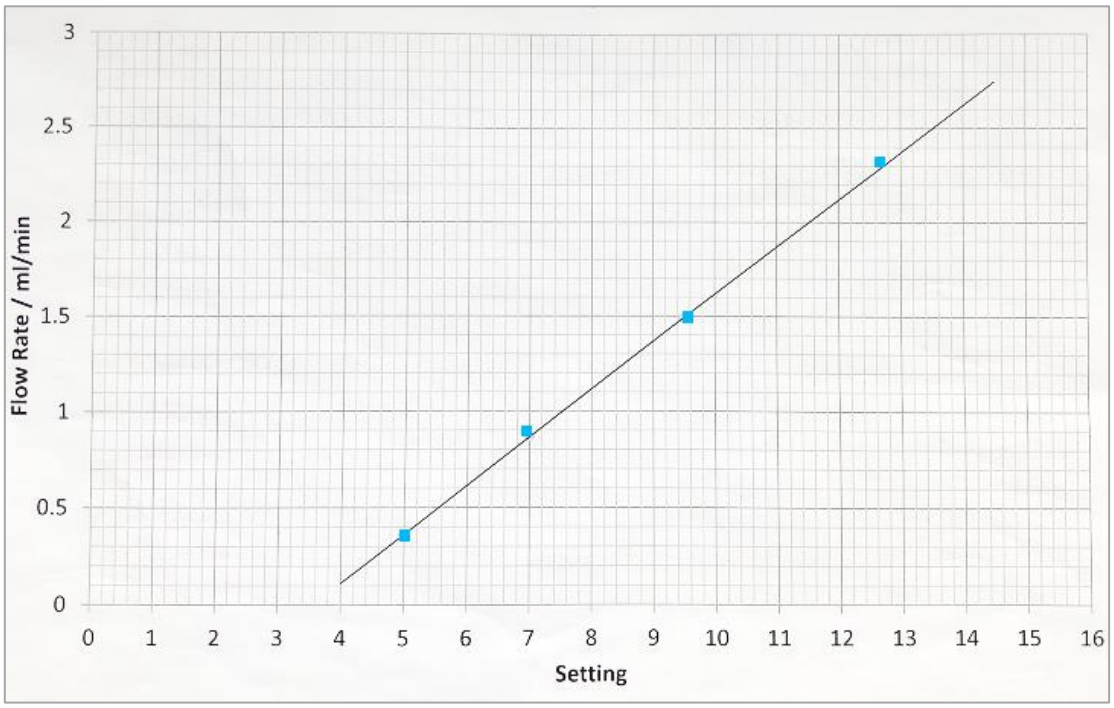

Figure 8.1: Example methane mass flow controller calibration.

8.4 Calibration for Quantification of Carbon deposited during catalytic reaction.

The calibration graph was established by passing 2 ml min^{-1} of oxygen in 18 ml min^{-1} of helium over a known mass of carbon into the quartz tube under a temperature program which up from room temperature and holding at 900 °C. The quantity of CO and CO_2 that produced from known amount of solid carbon and monitored using the QMS was summed. This process was repeated several times with different amount of carbon. The sum of CO_2 and CO produced during each reaction was tabulated to get a calibration graph with a straight line such as Figure 8.2. This used to estimate an accurate mass of deposited carbon during any reforming reaction. Thus, the peak of carbon dioxide and carbon monoxide that gained during TPO reaction was compared to the carbon calibration graph.

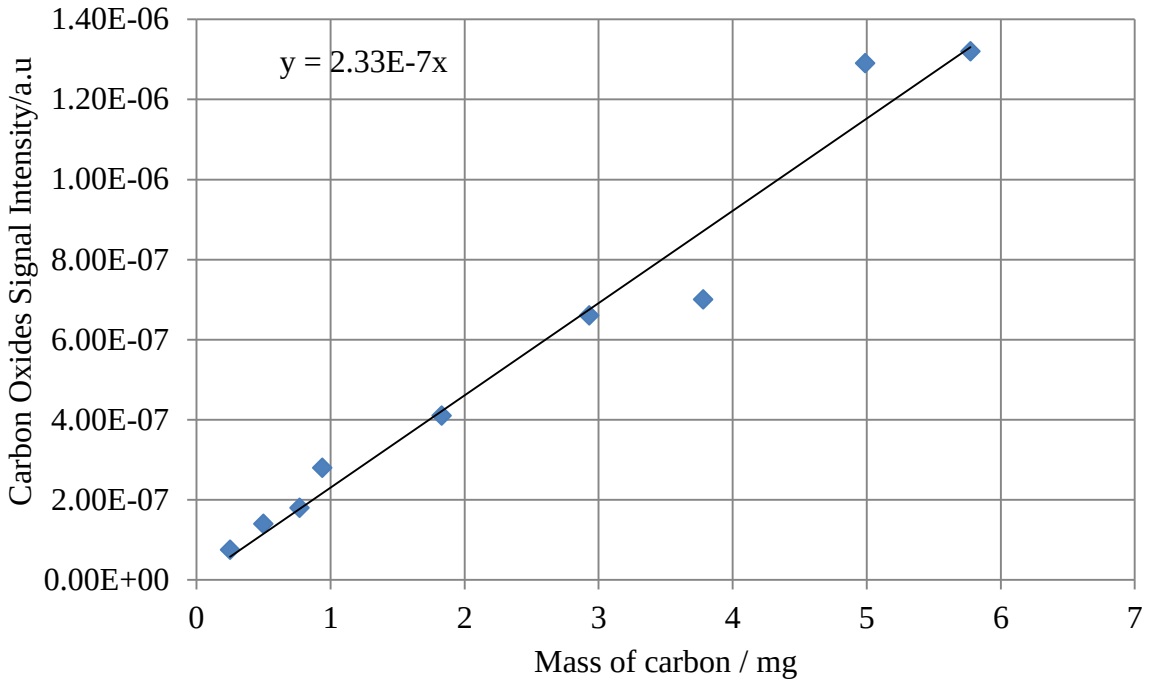

Figure 8.2: Example Carbon Calibration graph displaying the signal intensity for CO + CO_2 quantities produced due to oxidation known amounts of carbon.

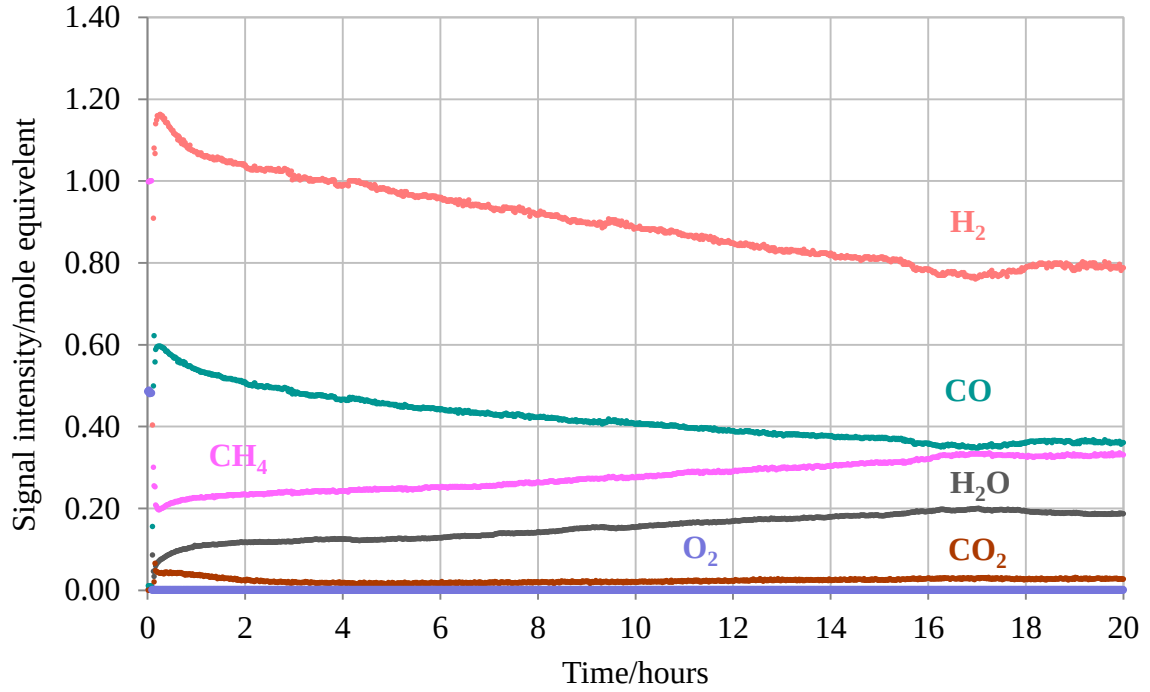

Figure 8.3: Partial oxidation of methane profiles of a 1:0.5 CH_4:O_2 mixture over Ni-Fe doped $SrZrO_3$ for 20 hours at 750 °C.

Surface area measurement for Ni-Fe doped $SrZrO_3$

Quantachrome Instruments
Quantachrome Autosorb Automated Gas Sorption System Report
Autosorb 1 for Windows 1.50

File name:	E:\Majida\MH2.raw				
Sample ID:	mh1	Description:			
Comments:					
Operator:	Majida	Sample weight:	0.2 g		
Analysis gas:	Nitrogen	X sect. area:	16.2 Å²/molec	Non-ideality:	6.58e-05
Adsbate (DRP):	Nitrogen	Bath Temp.:	77.30		
Outgas Temp:	350.0 °C	Outgas Time:	5 hrs	Analysis Time:	569.5 min
P/Po tolerance:	3	Equil. time:	1	End of run:	05/13/2016 19:07
Station #:	1	PC sw. version:	1.55	TempComp:	On

t-Method Micropore Ana ysis (de Boer)

P/Po	Thickness Å	Volume [cc/g] STP
3.6475e-02	3.08	9.342
6.1075e-02	3.35	10.114
8.5560e-02	3.56	10.796
1.1041e-01	3.76	11.416
1.3494e-01	3.93	11.963

Slope = 3.095E+00

Y - Intercept = -2.206E-01 cc/g

Micro-pore volume = 0.000E+00 cc/g

Micro-pore area = 0.000E+00 m²/g

External Surface Area = 4.740E+01 m²/g

Correlation Coefficient = 0.999830

Surface area measurement for Ni-Al doped $SrZrO_3$

Quantachrome Instruments
Quantachrome Autosorb Automated Gas Sorption System Report
Autosorb 1 for Windows 1.50

File name:	E:\h53Al.raw				
Sample ID:	h53	Description:			
Comments:					
Operator:	Majida	Sample weight:	0.2 g		
Analysis gas:	Nitrogen	X sect. area:	16.2 Å²/molec	Non-ideality:	6.58e-05
Adsbate (DRP):	Nitrogen	Bath Temp.:	77.30		
Outgas Temp:	350.0 °C	Outgas Time:	5 hrs	Analysis Time:	600.5 min
P/Po tolerance:	3	Equil. time:	1	End of run:	09/27/2016 20:37
Station #:	1	PC sw. version:	1.55	TempComp:	On

t-Method Micropore Analysis (de Boer)

P/Po	Thickness Å	Volume [cc/g] STP
3.6374e-02	3.08	8.462
6.1030e-02	3.35	9.136
8.5729e-02	3.56	9.678
1.1019e-01	3.76	10.250
1.3496e-01	3.93	10.730

Slope = 2.667E+00

Y - Intercept = 2.205E-01 cc/g

Micro-pore volume = 3.389E-04 cc/g

Micro-pore area = 1.330E+00 m²/g

External Surface Area = 4.099E+01 m²/g

Correlation Coefficient = 0.999433

Surface area measurement for Ni-Ru doped $SrZrO_3$

Quantachrome Instruments
Quantachrome Autosorb Automated Gas Sorption System Report
Autosorb 1 for Windows 1.50

File name:	E:\Majida\MH3.raw				
Sample ID:	mh3	Description:			
Comments:					
Operator:	Majida	Sample weight:	0.2 g		
Analysis gas:	Nitrogen	X sect. area:	16.2 Å²/molec	Non-ideality:	6.58e-05
Adsbate (DRP):	Nitrogen	Bath Temp.:	77.30		
Outgas Temp:	350.0 °C	Outgas Time:	5 hrs	Analysis Time:	514.2 min
P/Po tolerance:	3	Equil. time:	1	End of run:	05/17/2016 18:11
Station #:	1	PC sw. version:	1.55	TempComp:	On

t-Method Micropore Analysis (de Boer)

P/Po	Thickness Å	Volume [cc/g] STP
3.6577e-02	3.08	7.409
6.1070e-02	3.35	8.070
8.5975e-02	3.57	8.604
1.1066e-01	3.76	9.069
1.3532e-01	3.94	9.511

Slope = 2.460E+00

Y - Intercept = -1.714E-01 cc/g

Micro-pore volume = 0.000E+00 cc/g

Micro-pore area = 0.000E+00 m²/g

External Surface Area = 3.764E+01 m²/g

Correlation Coefficient = 0.999979